THE UNIVERSITY *of* EDINBURGH

EXPERIMENTAL STUDIES OF THE HYDRODYNAMIC CHARACTERISTICS OF A SLOPED WAVE ENERGY DEVICE

Chia-Po Lin

A Thesis Submitted for the
Degree of Doctor of Philosophy

The University of Edinburgh
1999

Abstract

Many wave energy convertors are designed to use either vertical (heave) or horizontal (surge) movements of waves. But the frequency response of small heaving buoys and oscillating water column devices shows that they are too stiff and so their resonance is at too short a period. A device moving in the horizontal (surge) direction has less restoring spring and so its resonance is at too long a period. It follows that a device that moved at some intermediate slope angle could have an intermediate value of hydrodynamic stiffness and so be resonant at a variable and desirable part of the wave spectrum.

There have been two series of model tests in this work. The first used a simple free-floating model with no power take-off apparatus and with constraint achieved by means of a large inertia plate lying in the slope plane. The second used a rig that constrained the slope movement of the buoy head by means of hydrostatic bearings running on a guide rod set to the chosen slope angle. An external power take-off system was used to simulate a linear damper for absorbing the incident wave energy and control the motion of the model.

This thesis firstly studies the potential of varying the slope angle as a way of tuning the natural period of the device to suit useful wave periods. Secondly, it studies the experimental and theoretical power capture ability of models with different slope angles in regular waves in the frequency domain. The hydrodynamic coefficients of the model were determined both experimentally and numerically based on linear hydrodynamic concepts. The power absorption of the models was calculated using the experimental data of the hydrodynamic coefficients and also measured directly.

Some control of power take-off was also investigated. Some irregular wave tests were carried out for the 45 degrees slope angle case.

The results show that it is feasible to alter the slope angle of the device as a way of tuning its natural period. However, in further studies of the power capture ability for different slope angles, the device shows a very wide bandwidth and high efficiency performance when it is set to 45 degrees slope angle. This suggests that to constrain the device to a 45 degrees slope angle is suitable for most of the sea states.

Declaration

This thesis has been composed by myself and,
except where stated,
the work contained is my own.

Chia-Po Lin
1999

Acknowledgments

The work presented in this thesis is a result of my research activities in the Edinburgh Wave Power Group and I would like to thank the following people for their help and advice during the work.

I am indebted to my supervisor Professor S. H. Salter, an engineering genius. Without his brilliant fundamental idea, determined motivation and efficient supervision, this thesis would not have occurred. Stephen has been very kind to allow me to use his workshop and to learn machining skills from him.

In particular, I would like to give my warmest thanks to Mr. J. R. M. Taylor, a remarkable teacher, for his wonderful guidance, kind assistance and warm friendship throughout this project. Without his directions, inspiration and experiences, none of this would have been possible. Jamie has also been very kindly helping me to digest some of the Scottish culture and history.

In addition, I would also like to give my sincere thanks to Dr. R. Yemm, who designed the external dynamometer for the second experimental rig, and Dr. D. Pizer, who performed numerical calculations of the radiation impedance for this work.

My thanks will also go to all the members of the Edinburgh Wave Power Group, Dr. Win Rampen, Mr. Jon Almond, Mr. Uwe Stein, Mr. Niall Caldwell and Mr. Carn Gibson, for advice, encouragement, and most of all friendship, over the last four years.

Finally and most importantly, I would like to thank my wonderful parents, brother, and sister for their constant support and encouragement. I would also give my sincerest thanks to my lovely wife, Maw-Shu, for her patience and love.

To all my friends, I express my earnest gratefulness.

Chia-Po Lin

August 1999

Contents

List of Figures

Chapter 1

Introduction

1.1 The background to wave energy

The idea of extracting useful energy from ocean waves has intrigued people for centuries. The first known patent for a wave energy device was granted to the Frenchman Girard and his son in 1799. Their idea was to use a 'ship of the line' attached by a gigantic lever to the shore, with the oscillatory motion of the lever driving machinery directly (Shaw, 1982). An early implementation of wave energy was at Royan, near Bordeaux, France in 1910. A turbine was driven from air compressed by the oscillations of sea water in a capped natural bore hole in a cliff (Pontes, 1998). This was probably the first oscillating water column (OWC).

In the early 1970s, the 'energy crisis', following large oil price increases by the Organisation of Petroleum-Exporting Countries (OPEC), promoted a popular awareness that fossil fuel resources were both finite and precious. A great amount of effort started to be put into the study and promotion of renewable energy, or 'alternative energy' as it was sometimes called. In the United Kingdom between 1974 and 1983 a large number of device concepts were studied within the framework of the government wave energy programme. This was initially run by the Department of Industry and later by the Department of Energy through the Energy Technology Support Unit (ETSU) at Harwell in Oxfordshire (Thorpe, 1992). At least seven different 'device teams' were thus directed to develop their own initial concepts, through analysis, model tests and industrial collaboration into

reasonably detailed and costed plans for gigawatt (GW) scale power stations. The officially supported UK research programme was halted in 1985 after the government concluded that wave energy was not currently economically viable. Research funding was almost completely curtailed, nevertheless some research was continued.

In 1991, Directorate-General XII (DG XII) of the European Union (EU) which deals with science, research and development inaugurated a new programme which included support for wave energy research. The programme has included major generic studies involving a large number of research groups throughout Europe (Russell and Diamantaras, 1995). The EU is currently supporting the construction, commissioning and testing of a large OWC of 500 kilowatts (KW) in the island at Pico in the Azores, by the Instituto Superior Técnico in Lisbon. Under a separate contract, an experimental high-speed stop-valve and variable-pitch air turbine is being built at the University of Edinburgh for the same OWC. These machines are in addition to a conventional turbine supplied by Applied Research and Technology Ltd. at Inverness. This programme is continuing. In the past six years, three European wave energy conferences were held: Edinburgh, Scotland (Elliot and Caratti, 1993), Lisbon, Portugal (Elliot and Diamantaras, 1995) and Patras, Greece (1998). Many teams from countries outside Europe, such as Japan, China, India and USA also presented their research. The Japanese have been continuously active in wave energy research since well before the start of the original UK programme. Recently, the Mighty Whale, a 110 KW floating OWC device, has been launched in Goyasho bay in central Japan (Edwards, 1998).

1.2 The demand for renewable energy

The UK Renewable Energy Advisory Group (REAG) defined renewable energy as, '*the term used to cover those energy flows that occur naturally and repeatedly in the environment and can be harnessed for human benefits. The ultimate sources of most of this energy are the sun, gravity and the earth's rotation.*' (Boyle, 1996). Sea waves are caused by the capture of wind energy at the ocean surface whilst

winds are convection currents due to solar heating. Therefore, wave energy is a renewable resource deriving from the sun's energy input to the earth.

In the 1970s renewable energy programmes were initiated by the 'energy crisis' brought on by seemingly very high oil prices rises by OPEC countries. People were simply afraid of running out of fossil fuel and started looking for alternative energy resources to substitute for oil. Later, in the early 1990s environmental problems, such as global warming, acid rain and radioactive waste became the main spurs to promote the study of renewable energy resources. In order to reduce the human-induced change of climate, an international environmental agreement was signed by 38 individual countries in Kyoto, Japan in 1997. The EU response was to set a target of an 8% cut in CO_2 emissions below 1990 levels by 2010 (Taylor, 1998). The EU has proposed a scheme to achieve the target that includes improving energy efficiency, reducing energy consumption and developing renewable energy resources. The UK government overall target of CO_2 emissions is a 20% reduction on 1990 levels by the year 2010, with renewables being hoped to supply up to 10% of UK electricity (Elliot, 1999). Clearly, the demand for renewable energy will be considerably greater in the future than at present.

1.3 The wave energy resource

A point of particular interest to the EU is the considerable wave energy potential along its coasts. The mean wave power off the Atlantic coasts varies from around 25 MW/km off the Portuguese coast to 65 MW/km off Ireland. In the North Sea the figure is 15 MW/km off the Danish coast (Randlov, 1993) and 30MW/km off the Norwegian coast. The western approaches to the UK have annual averages of 60 to 80 MW/km (Mollison, 1985). Recently, research has shown that wave heights in the North Atlantic have increased over the past 30 years or more at a rate of the order of 1% to 2% per annum (Hogben, 1995). The total wave energy resource of the world is thought to be roughly equal to world electricity consumption (around 1 TW, i.e. 10^6 MW) (Randlov, 1993). However, electricity is not the only possible use. Direct use of wave power may also be attractive for

desalination (Salter, 1986) or oxygenation of sea water, to extract nutrients for fish farms and for hydrogen production.

1.4 The classification of wave power devices

Very many different designs of wave power devices have been studied or proposed. Table 1.1 shows a number of prominent devices. Here, the devices are classified according to three basic characteristics:

- Mode of response to waves.
- Location and mooring system.
- Geometry and orientation.

1.4.1 Mode of response to waves

In order to capture energy from sea waves, it is necessary to intercept the waves with a structure which can respond in an appropriate manner to the wave forces. The motion response mode of a wave power device is one of the useful classifying parameters. The motion of a floating structure in waves can be described by the six components of motion shown at the centre of figure 1.1. There are three modes of *translation*: heave, surge and sway, and three modes of *rotation*: roll, pitch and yaw. In the figure the wave power devices are classified by their motion response modes. For instance, Salter's Duck (Salter, 1974) shown in figure 1.3 uses mainly pitch mode, whereas the IPS buoy (Bergdahl, 1992) shown in figure 1.7 and the Tethered buoy utilise heave mode. The SEA (Sea Energy Associates) Clam (Norman, 1982) and the Pendulor device (Watabe, 1986) use surge mode, but the PS Frog (Bracewell, 1990) uses both pitch and surge modes (hence the first part of its name). The Sloped IPS buoy was proposed by Salter (1993), with the idea of coupling heave and surge modes.

The above devices utilise wave generated buoyancy and inertial forces acting on some or all of their structure parts, moving according to the modes described, so as

to transfer wave energy to a power take-off system. Thus, the devices can absorb energy from the particular motion of response to the incident waves.

In contrast, the structures of OWC devices are generally designed to be static by attaching to seabed or huge structure, but to provide a suitable internal volume for the transfer of energy between water and air. The essence of an OWC is one or more partially submerged hollow structure open to the sea some distance below the water surface and extending well above the maximum wave height. The upper air-filled part of the chamber is connected to atmosphere by a duct which contains an air-turbine coupled to an electrical generator. In a sense these are "heaving air" devices, however it seems most appropriate to have a special, separate classification for OWC as shown at the bottom of figure 1.1. The first Britain's shoreline gully OWC was built at Islay by the Queen's University of Belfast (Whittaker, 1987). Figure 1.2 shows the schematic of the OWC.

Device name	*Inventor and country*	*Location*	*year*
Navigation buoy OWC	Masuda, Japan	offshore	1965
Duck	Salter, UK	offshore	1973
TapChan	Mehlum, Norway	shoreline	1975
NEL OWC	National Engineering Laboratory, UK	near shore	1975
Kaimei OWC ship	JAMSTEC, Japan	offshore	1978
Tethered buoy	Danish Wave Power, Denmark	offshore	1978
Bristol cylinder	Evans, UK	offshore	1978
Flexible bag	French, UK	near shore	1978
Point absorber	Budal, Norway	offshore	1978
IPS buoy	Sea Power Ltd., Sweden	offshore	1980
Pendulor	Watabe, Japan	shoreline	1980
SEA Clam	Bellamy, UK	offshore	1981
Backward Bent Duct Buoy (BBDB)	Masuda, Japan	offshore	1982
Kvaerner OWC	Kvaerner Burg, Norway	shoreline	1985
Islay OWC	Queen's University, Belfast, UK	shoreline	1985
PS Frog	French, UK	offshore	1985
Might Whale	JAMSTECH, Japan	offshore	1990
OSPREY OWC	ART, UK	near shore	1990
Mace	Salter, UK	offshore	1992
Sloped IPS buoy	Salter, UK	offshore	1995
Bending Spine	Yemm, UK	near shore	1998

Table 1.1. List of selected wave energy devices.

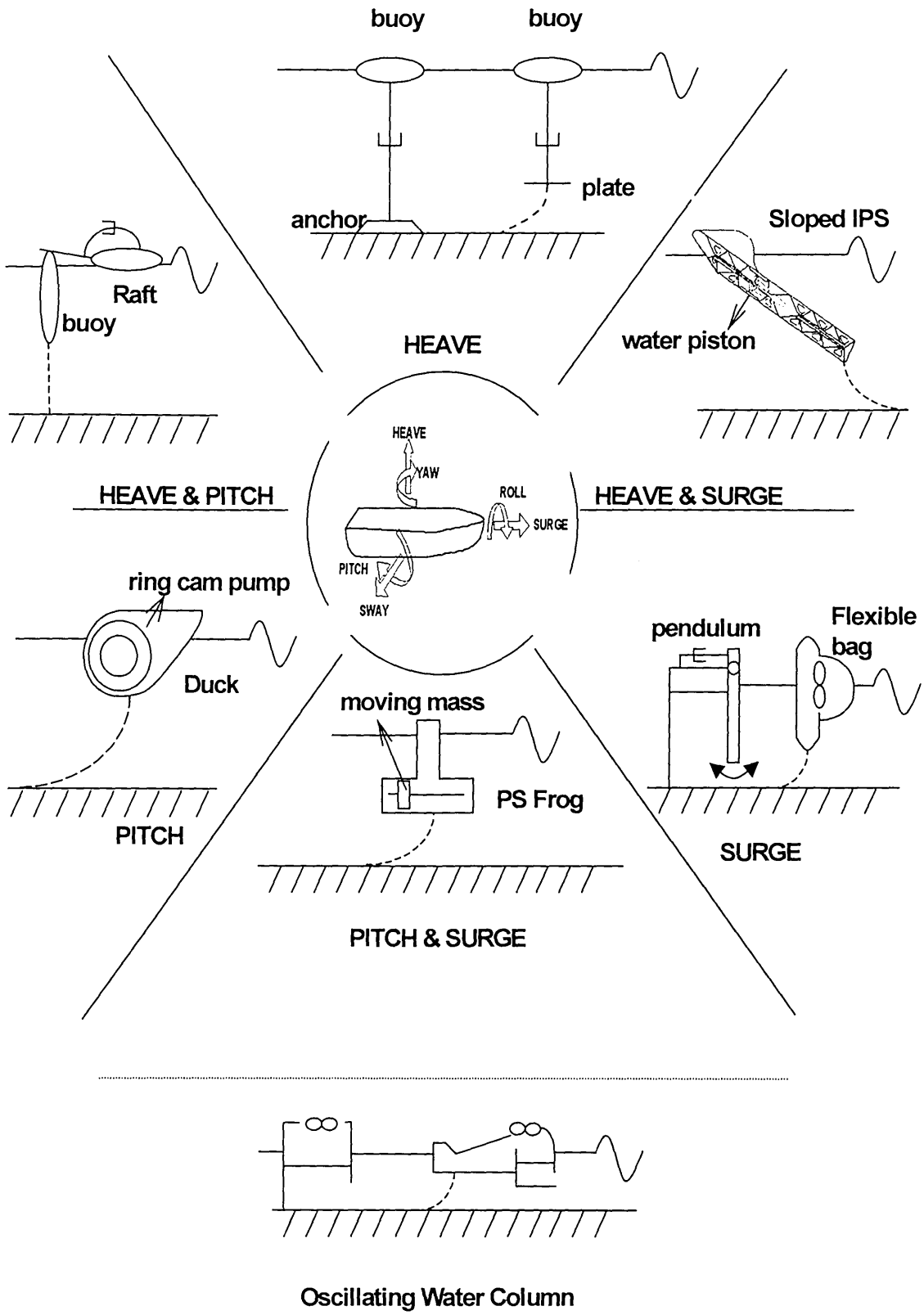

Figure 1.1. Wave Power devices classified according to their motion response to waves.(based on Falnes and Løvseth (1991).)

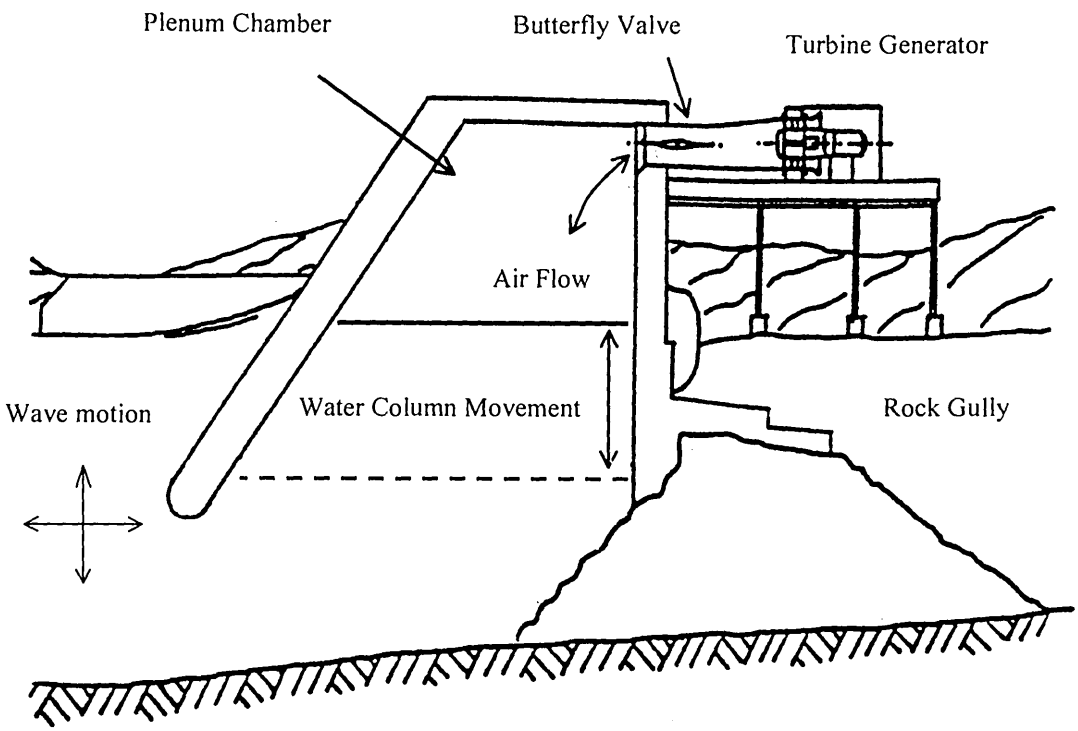

Figure 1.2. Outline of the Islay shoreline gully oscillating water column (Whittaker, 1987). The chamber contains partly air partly water and the water is adjusted in order to make the water column resonate at a given wave frequency. The contained air is forced out and then into the chamber by the wave crests and troughs. On its passage from and to the chamber, the air passes through an air turbine generator and so produces electricity. In case of emergency, the airflow can be shut off by a butterfly valve.

TapChan, which was invented by Even Mehlum in Norway (Mehlum, 1985; Bisio and Boots, 1995), is another exception. It does not response to waves, but modifies the waves by its inlet and ramp geometry and forces overtopping into a reservoir two to three metre above mean sea level. The width of the channel decreases in a shoreward direction, and its end is sealed off. As the waves travel along the ever-narrowing channel, they increase in height, spilling water over the sides and into the reservoir. Water then drains back to the sea through a low-head turbine.

1.4.2 Location and mooring system

It is necessary to provide devices with a source of reaction for capturing energy from sea waves. When devices are located on shore or near shore, the reaction can be obtained by attachment to land or sea bed. Submerged or floating deep-water devices also need a stable frame of reference. This can be achieved by taking advantage of the inertia of the structure, by reacting against an additional inertia or by making the structure so large that it can span several wave crests and usefully react one set of wave forces against another.

The wave power density is generally considerably higher for deep-water devices than for onshore and near-shore devices, since waves decrease power through breaking and bottom friction as they travel from deep water into shallow water.

For the generation of large amounts of power, the deep water floating type device is desirable. However, the advantage for floating systems of being exposed to more energetic wave environments is reduced by the need to provide moorings. Where the floating system is completely self-sufficient in terms of force reaction for power conversion, and also has some way of shedding the loads from extreme waves, then station keeping is all that is required of the mooring system. It is then possible to use a minimal 'slack mooring' that can cope with the worst-case mean drift forces. However, some floating wave energy systems require 'tight' moorings that can supply additional force reactions to cope with survival loading as well as forces associated with power conversion (Eidsmoen, 1995a).

1.4.3 Geometry and orientation

The general layout and orientation of wave energy converters must also be considered. They are often categorised into three groups: 'terminators'; 'attenuators' and 'point absorbers'.

Terminator

The term 'terminator' is used to refer to structures which lie parallel to the incident wave front and present to them a single stage power transfer interface. Examples might include a 'string' of Salter's Ducks, an array of Bristol Cylinders (Evans *et. al.*, 1979) and an array of floating or shore mounted OWCs. The description 'terminator' refers, by analogy with transmission line theory, to the ideal behaviour where all energy is absorbed. When the wave energy is within the design frequency band and power conversion range these systems are intended to reflect and transmit only small fractions of the incident energy. Outside this design range, the terminator moves in such a way as to increase the percentage of power transmitted past the device and thus off-load the power take-off system. An example is the flexing of the spine of a string of Ducks in large waves.

Attenuators

The term 'attenuator' is used to refer to structures which lie perpendicular to the incident wave front and absorb power through a sequence of conversion stages. Examples are the Lancaster Flexible Bag device and the Bending Spine (also called Pelamis) by Ocean Power Delivery Ltd., UK (Yemm *et. al.*, 1998). Such systems convert wave energy progressively along their lengths, perhaps through a linear series of articulations. In some cases the configuration and mooring may be such that in moderate waves, the system can lie at an angle to the perpendicular and thus increase exposure to waves.

Point absorbers

Isolated wave power devices that are relatively small compared to the incident wavelength can benefit from 'point absorption', whereby more energy is converted than would at first appear to be available within the sea width occupied by the device. The term 'capture width' is frequently used to quantify this ratio of device output power to the wave power apparently incident in the nominal width. Budal and Falnes (1978) showed that a small axisymmetric device, constrained to move vertically, has a theoretical maximum power absorption equivalent to having an effective exposure or wave frontage of $\lambda/2\pi$ (λ is wave length).

If instead of moving in the heave direction the axisymmetric device is only able to move in surge, the capture width increases to λ/π. This value also applies to a pitch only device. Furthermore, a device able to move independently in both heave and surge (i.e. with two degrees of freedom) has the still larger capture width of $3\lambda/2\pi$ (Budal and Falnes, 1977). The theoretical detail of the point absorber effect will be discussed in chapter 3. However, it is very important to note that point absorption generally requires device motions larger than the associated water motions and practical considerations generally impose limits on how much any device can benefit from it.

The term 'point absorbers' is used both for rotationally symmetrical devices such as Budal's Point Absorber and for 'solo' implementations of terminator type devices such as the Solo Duck. Groups of point absorber devices can also be arranged as open arrays. However, There are interaction effects between the neighbouring point absorbers. Budal (1977) and Evans (1980) assume that the interaction effects arise solely from radiated wave potentials due to the oscillations of neighbouring bodies and neglect the additional diffraction effect due to incident waves scattering off one device and thereby affecting its neighbours. The results show that for small devices the diffraction effect is not significant. Greenhow (1980) then examined the interactions of large device where the diffraction interaction is expected to be important.

1.5 The Edinburgh Wave Power Project

1.5.1 The Duck

In the early seventies, Salter demonstrated an asymmetric cam shaped device, which extracted energy through semi-rotary motion induced by incident waves. In the ocean, individual Ducks would be rotated about a long cylindrical 'spine' facing into the incident wave fronts. By averaging out surge, heave and pitch motions, the long spine configuration also would provide a relatively stable reference for individual Ducks.

A good wave absorbing shape when moved in still water generally makes good waves on the front side and little or no waves behind. The Duck evolved from a simple, vertical flap. The surging vertical flap makes waves on both sides, and the back wave represents energy lost as a transmitted wave. An improved flap would have a back profile which was a poor wave generator. Therefore, the flap evolved into a stubby airfoil, shown in figure 1.3, like section with the rear surface in the shape of a cylinder. The surging mode of motion was changed into a pitching mode. As the cylindrical rear surface rotated, it displaced no water and made no waves. The displacement due to the front surface was designed to match the fall off with depth of the orbital motions of water particles in the approaching wave. This enabled the Duck to have high efficiency characteristics.

Early Ducks achieved more than 80% (90% later) efficiency experimentally in a narrow test tank (Salter, 1974). In the early stages of development, the Duck was intended to operate on a rigid stable reference. Later, significant improvements in efficiency in long wave conditions were made by letting the Duck and spine move together with controlled compliance in surge and heave (Salter, 1980). The intuitive explanation for the improvement is as follows. In short waves the water movement is concentrated near the surface and very little energy passes beneath the Duck. In long waves however, there is movement well below the Duck's draught and it becomes more difficult for a surface device to extract the wave energy. If

the stern of the Duck can be moved in such a way to generate waves which are the inverse of those propagating below, then the water behind must be calm and the wave energy extracted. Figure 1.4 shows a long spine of Ducks in the Edinburgh wide tank.

1.5.2 The Solo Duck

During most of the 1980s work was directed towards a 'reference design' for a 2GW ocean going wave power plant. The resulting proposal consisted of a string of 896 Ducks constrained by articulating cylindrical spine units. It would be moored in water depths of from 80 to 100m, and approximately 40km in total length.

In the 1990s, interest in wave power has been renewed. A costing model of the 2GW reference design has been maintained but construction of such a large system is considered too ambitious as an initial target. It is hard to imagine such a large amount of investment without the clear success of a much smaller, confidence building or problem solving project. A more realistic approach was the development of a smaller scale plant. The idea was to reduce the funding requirement and provide a testing ground for ideas, paving the way for large-scale devices in the future.

The 'Solo Duck' concept addressed this new requirement (Skyner, 1987; Pizer, 1994; Nebel, 1994). The pro-rata costs of a full-scale Solo Duck project would be much higher than those of 2GW system. However it would usefully demonstrate related technology at full scale. Additionally the 'point absorber effects' discussed above might help to produce worthwhile amounts of energy. The individual Duck unit would be 20 metres in width and have 2 megawatts (MW) of rated electrical capacity. It would use tension legs attached to the sea bed to provide force reaction, rather than the spine of the original design. However it was found very difficult to design tension legs economically able to handle 'snatching' following reversing loads.

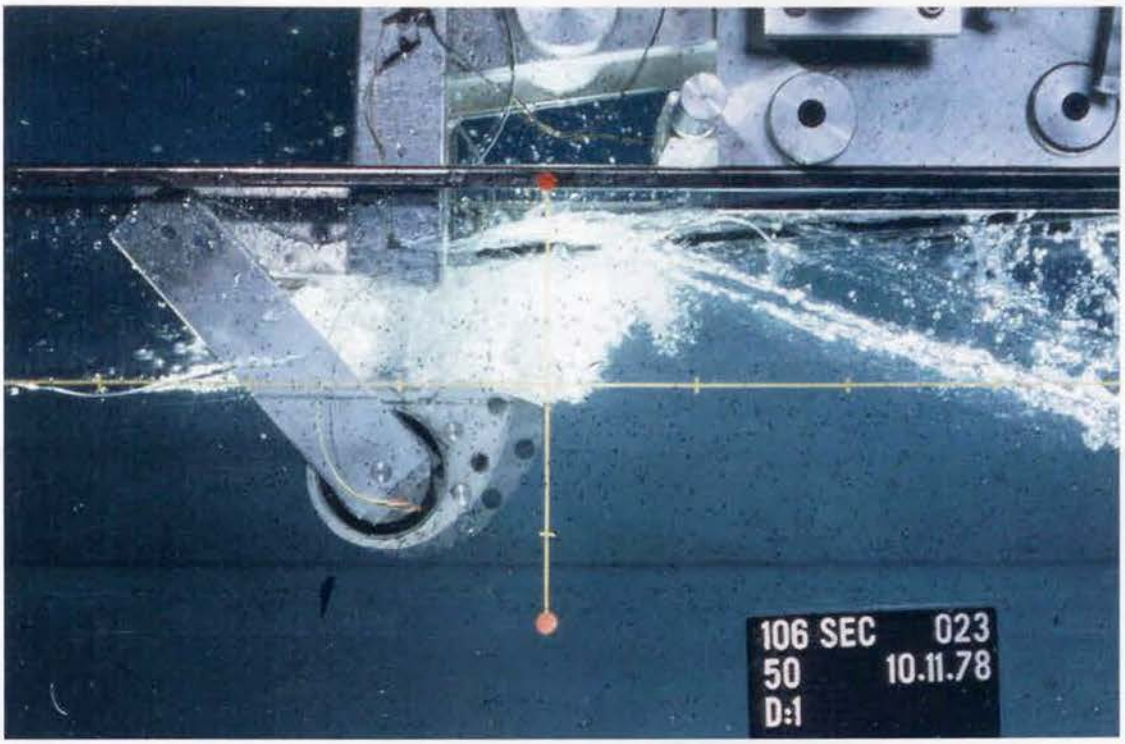

Figure 1.3. The duck model in narrow tank

Figure 1.4. The duck spine models in the Edinburgh wide tank.

1.5.3 The Mace

The wave-induced surge forces on deeply immersed bluff objects such as cylinders are greater than the heave ones. Salter proposed the 'Swinging Mace', shown in figure 1.5, in the early nineties, and this mainly used the surge mode (Salter, 1992b). The Mace is a buoyant cylindrical spar with the axis aligned vertically. It can swing in both surge and sway about a universal joint at the sea bed. The power take-off reaction to the seabed is via sets of cables wound several times around a winch drum leading both fore and aft in the prevailing wave direction. The drum contains a ring-cam pump, as originally designed for the Duck, to extract the power. Since the Mace has very low stiffness in surge mode, its natural frequency is very low and this may lessen its performance. Tank tests showed that it had a wide but rather low efficiency band and good survivability in large waves.

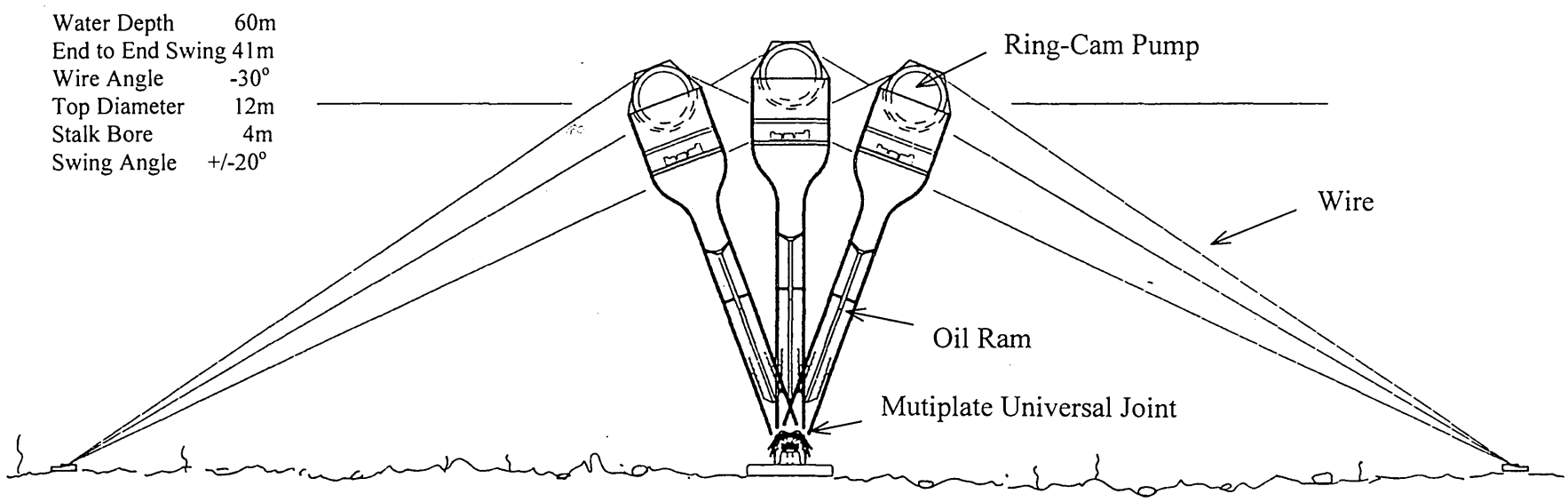

Figure 1.5. Sectional side view of the Swinging Mace. The safe range is greater than the trough-to-crest height of the mid-Atlantic100-year wave (Salter, 1992b).

1.6 The concept of the Sloped IPS buoy

After many years of work by the Edinburgh Wave Power Group, Salter concluded that an ideal 'first generation' device would have four indispensable characteristics (Salter and Lin 1995):

Physical Robustness

There should be no end stops in the power conversion mechanism and no rigid connections to the sea bed.

Productivity

The device should be able to benefit from the point absorber effect and should have a natural frequency appropriate to the local wave climate.

Maintenance

Inspection, repair and changing of components should be easy.

Mobility

The device should be easy and cheap to move between the sea testing area and a nearby harbour or yard for repair or adjustment.

The latter two requirements would speed up the iterative cycles of modification and improvement that are inherent to the development of new technologies. Associated with the mobility requirement is the need for low mooring forces and cheaply deployed mooring systems with rapid attachment and disconnection.

In 1995, Salter proposed an apparently suitable new device, the Sloped IPS Buoy. It was based on a Swedish design for a heaving buoy wave power device, but with a critically important change in the direction of movement.

1.6.1 The Swedish IPS Buoy

The IPS Wave Power Buoy was proposed in 1980 by a Swedish organization called Inter Project Service (IPS). It consisted of a floating buoy connected to a submerged vertical tube open to the sea at the bottom end, somewhat analogous to

a spar buoy. Inside the tube is a piston which acts as a reaction plate. Between the buoy structure and the piston there are attached two hydraulic rams which are part of a high pressure oil hydraulic energy conversion system. In waves the buoy heaves in response to the surface and near-surface wave motion whilst the piston remains relatively fixed by the massive volume of comparatively static water around it. The 'Mark I' IPS Buoy (Bergdahl, 1992) shown in figure 1.6, was first tested in a large lake, and then in the open sea outside Gothenburg during 1980 and 1981. At sea the piston plate in the tube was lost due to a failure of the power take-off system. The accident highlighted the need for an appropriate solution to the end stop problem. This was provided in a most interesting way by widening the tube at each end so as to provide bypasses, see figure 1.7: IPS buoy Mark IV (Fredrikson, 1992). The improved tube design enables the piston to operate within safe limits even in extreme waves. The advantage of the bypass concept is that when the pistons inside the hydraulic rams approach their own end stops, the main piston has already entered the bypass zone so that water can flow around it, thus reducing the pressure on it.

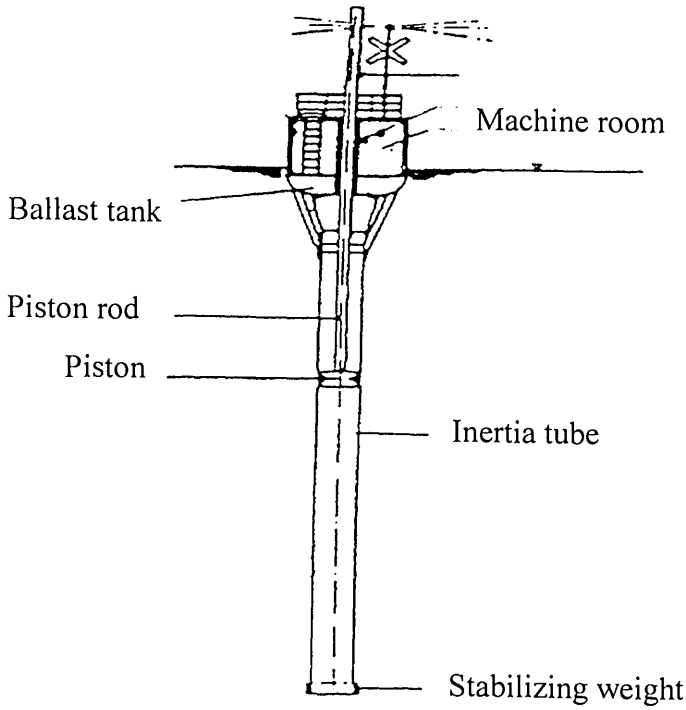

Figure 1.6. The IPS buoy, Mark I. (Bergdahl, 1992)

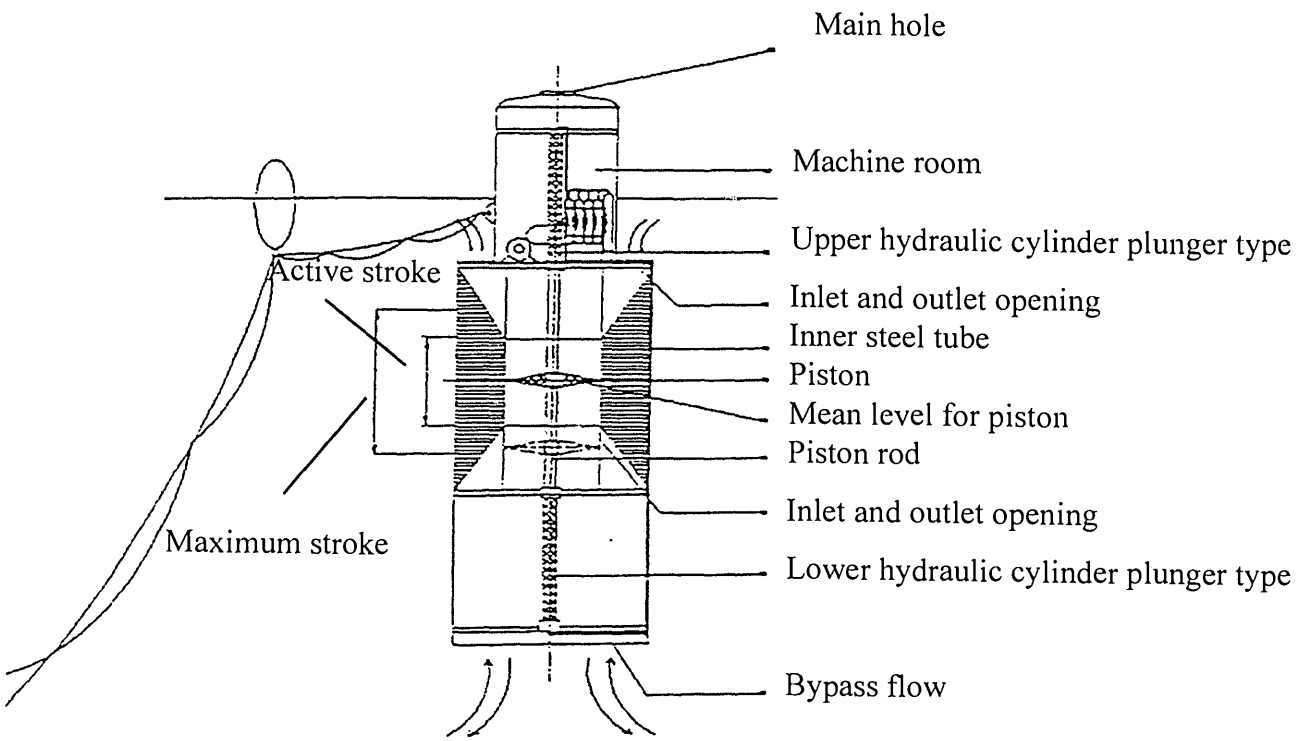

Figure 1.7. The IPS buoy, Mark IV (Fredrikson, 1992).

1.6.2 The effects of inclination of movement direction

A free-floating wave energy device, which is an oscillating system with frequency-dependent response, shows the phenomenon of resonance. Resonance occurs, when the wave period agrees with the natural period of the oscillating system, and the energy conversion will be maximum if the amplitude of oscillation is adjusted to the proper value. A wave energy device with longer natural period can capture more energy than one with a short period, since the power in waves is proportional to the period. Good long wave performance corresponds to a smaller and cheaper full-scale ocean installation. Hence, in the design of a wave power device, natural period is one of the important concerns. As the natural period of a device responding to waves is proportional to the square root of the inertia divided by its stiffness, there are two ways to make the natural period longer. One is to add more mass to the device itself or to increase the added mass by altering the shape of the device. This generally implies a larger and more expensive structure. The other way is to reduce the stiffness. The stiffness of a floating structure comes from its hydrostatic restoring force which known as buoyancy, and buoyancy is related to the body geometry which also determines the damping characteristics of the device.

French (1985) showed an alternative method of altering the natural frequency of a wave power device. A 'stiffness modulation' was used to change the natural frequency of a buoy which reacted against an internal mass. A spring modulation consists of a spring divided into two parts and connected in series giving two stiffness. At an intermediate frequency, the spring has a low stiffness at smaller displacements and changes to its high stiffness when the displacement exceeds a certain value.

As noted earlier many wave energy devices can be thought of primarily as 'heave' devices. The frequency-response of small heaving buoys and oscillating water columns shows that they are too stiff and so their resonance is at too short a period. A device like the Mace moving in the horizontal direction has very little restoring spring force, and so its resonance is at too long a period. An 'inclined' device might have movements which combined a particular ratio of surge and heave

motions. By choosing an appropriate angle, it might be possible to 'tune' the natural period. Accordingly, in 1995, Salter proposed the 'Sloped IPS Buoy'. By changing the axis of movement to reduce its hydrodynamic stiffness, the resonant period of a relatively small IPS Buoy could be brought into the more energetic long wave part of the spectrum.

The hydrostatic stiffness of an oscillating buoy is defined as the buoyancy force divided by the buoy displacement or stroke. Since the buoyancy force only acts at the direction normal to the water surface, the stiffness can be reduced when the buoy moves at inclined angles. Therefore, by changing the inclined angle the device can have an intermediate value of hydrodynamic stiffness and so be resonant at a chosen part of the wave spectrum.

Experimental results also show that changing the angle of the movement direction can vary the bandwidth (Salter and Lin, 1998). This advantage may apply to other wave power device, such as the Sloped OWC. Inclined angle effects will be discussed in detail in chapter 6.

1.6.3 Description of the Sloped IPS Buoy

Figure 1.8 shows the proposed shape for the Sloped IPS Buoy. In essence it is a combination of a surface piercing wedge type wave absorber with an under-sea motion constraint. Wedge type wave makers have better performance in long waves than paddle type wavemakers of similar size (Patel, 1980). The wedge geometry defines the response to waves and provides the hydrostatic stiffness. It then attaches to a long 'tail-plate'. The tail-plate is a long, comparatively thin, and open-ended box structure which reaches down into undisturbed water. This gives the buoy an enormous added mass for movements normal to the plate and no restraint in the plane of the plate. There are a number of 'inertia' tubes in the tail-plate. The central axial working section of each provides a snug fit for a piston. Beyond this working range, at top and bottom, the tube widens out. (See figure 1.9).

While the piston remains in the narrow section, it is effectively coupled to the large inertia of the water in the tube and so tends to stay with that water rather than move with the relative axial motions of the buoy. Therefore, the entire structure will tend to move along the axis of the inertia tube in response to wave action, leaving the water mass and the piston plate nearly stationary. Work can be done by a double-acting high-pressure oil hydraulic ram located between the buoy and the piston plate. When the movement of the piston plate exceeds the length of the narrow passage and it travels into the conically shaped area, a gap opens around the piston. The water in the tube can then flow through the gap, and release the pressure on the piston plate. The water tube then no longer provides a large inertia force to the piston plate. This reduces the end-stop forces in the high-pressure oil hydraulic rams, and by so doing allows more economical ratings and higher load factors in the power train. The piston slides on the outer body of a hydraulic ram and is coupled to it by push rods. It is rounded at its edges to reduce the pressure drops across it when in the open passage bypass zones.

Since the hydrostatic stiffness of a floating buoy is due to vertically acting buoyancy forces, the hydrostatic stiffness with regard to sloped buoy movements is modified by the sine of the angle of deviation from the horizontal. It was anticipated that the IPS design would use angles in the range from 30 to 45 degrees for most of time. By varying the angle of slope, the device could be tuned to an optimum for the prevailing wave spectrum. The concept for trimming the slope angle was to vary the proportion of oil and water in a ballast compartment at the submerged end of the tail-plate. Note however that the experimental results show that the device has unexpectedly wide bandwidth at a slope angle of 45 degrees. This suggests that it may be feasible to always deploy the device at 45 degrees and not vary the angle with wave spectrum. However, it would probably need continuous trim control to maintain the motion direction precisely. The whole IPS structure is envisaged as having a horizontal deployment mode for transportation in which it can float as a small ship and be either towed or propel itself with its own hydraulic motors, and vertical model for survival at extreme wave conditions.

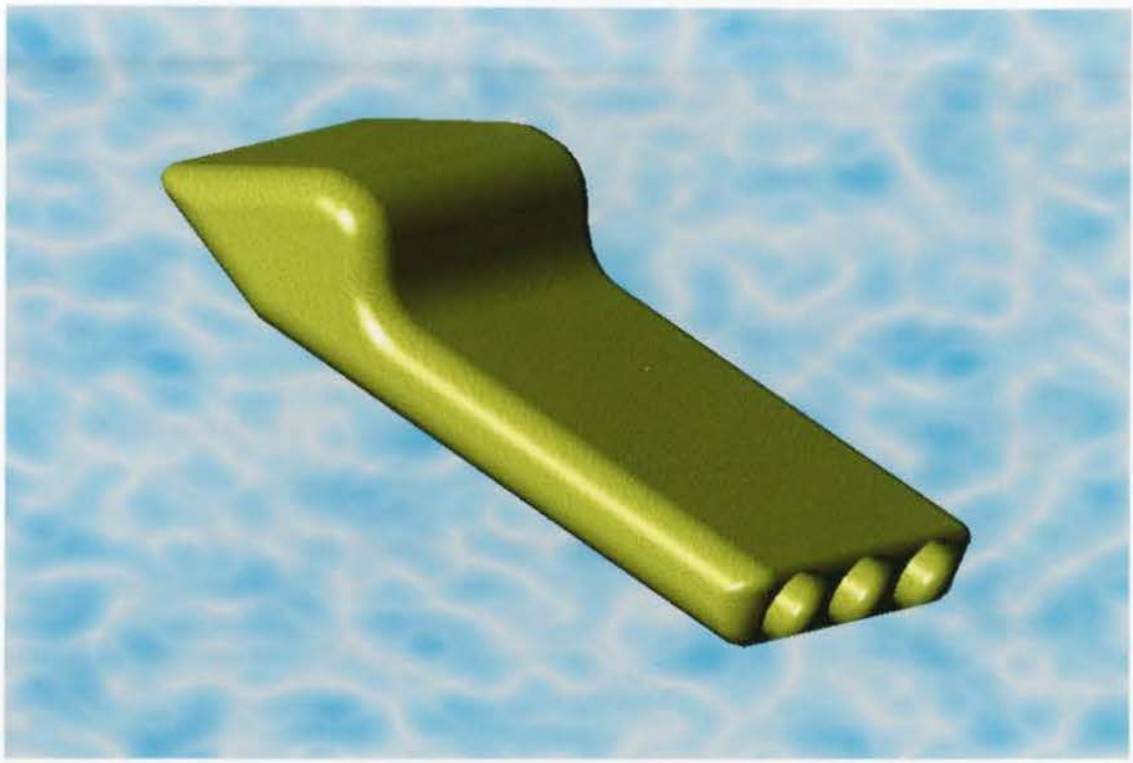

Figure 1.8. Simplified solid model of the Sloped IPS buoy.

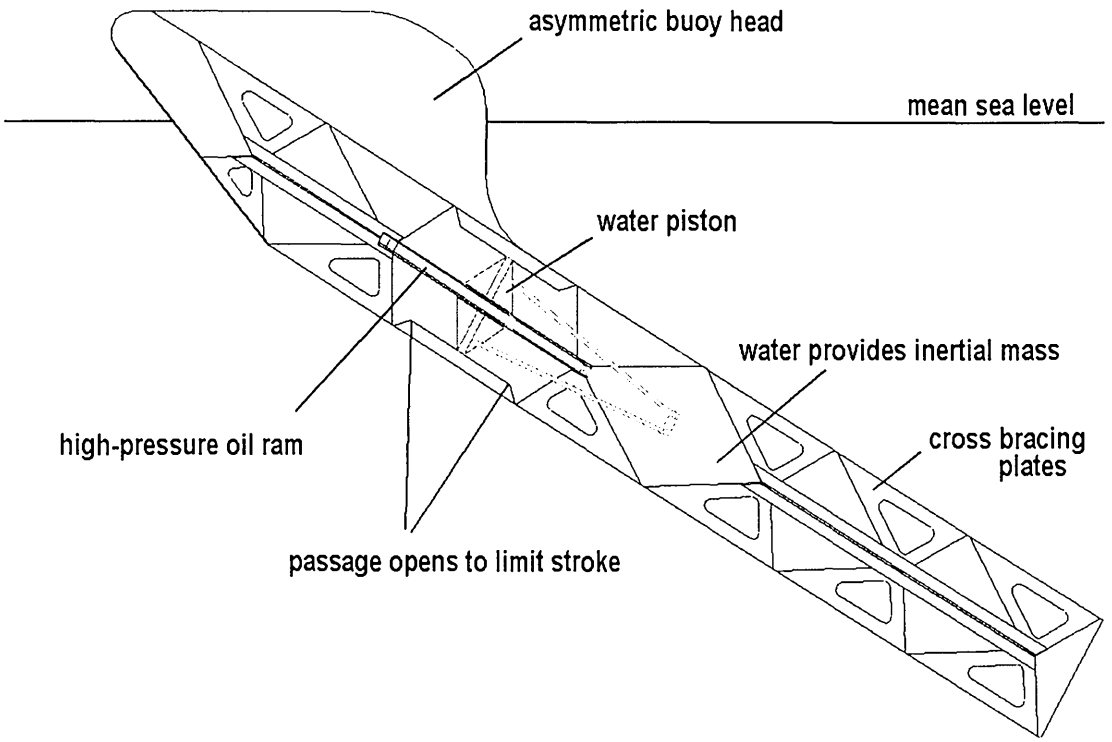

Figure 1.9. Sectional side view of the simplified Sloped IPS Buoy at a 45 degree angle of slope showing the water piston sliding on the outside of the high-pressure oil hydraulic cylinder. Thrust is reduced when the piston moves out of the narrow section so that end-stop dangers are minimised. The internal bracing plates are edge onto the flow and so should offer low resistance to flow.

1.7 Thesis content

The main topic in the present thesis is the experimental testing of a semi-submerged wave energy system working with a sloped angle of motion. Until now most ideas for wave power devices have used either vertical motion or horizontal motion or both individually. The present work focuses on the effect of intermediate slope angle motion between heave and surge. Firstly, the concept of changing the natural frequency through variation of the angle of motion is discussed. Secondly, the effect of slope angle variations on the performance of the wave power device is examined. It is found that at 45 degrees slope angle the model shows particularly promising behaviour. Thereafter, the study is restricted to the 45 degrees configuration and control strategies are investigated. Hydrodynamic coefficients are measured and compared with the numerical results.

1.8 Thesis outline

In chapter 2, the antecedents to the present work are presented through a brief review of literature which relates to wave power devices. More detailed aspects of prior research are included within the appropriate chapters.

In chapter 3, certain mathematical aspects of the hydrodynamics relevant to the Sloped IPS device are described. The equation of motion of the device is also described based on linear hydrodynamics. The calculations of power absorption and efficiency are also described. These equations are then used throughout the remainder of the work.

In chapter 4, the experimental environment and model preparation are presented. Two simple free-floating models without power take-off system and with constraint achieved by a large inertia plate lying in the slope plane was tested to observe the motion of the model. Further, a variable slope angle test rig constraining the slope movement of the buoy was built to perform most of the tests. An external power

take-off system with a feedback control loop was implemented. The full details of the test apparatus are described in this section.

Chapter 5 describes the experimental work in regular waves. In order to establish the equation of the motion, the hydrodynamic coefficients were required. The radiation impedance was determined by forced oscillation of the model in still water and the wave exciting forces were measured on a model which was held locked. Hydrodynamic coefficients calculated independently from a numerical model are also presented. The components that contribute to the model's hydrodynamic behaviour such as added inertia, added damping and spring rate are identified. Values for power capture were obtained both experimentally and numerically using experimental determined hydrodynamic coefficients. Efficiency curves were obtained to describe the overall performance in the frequency domain.

In chapter 6, the results of the power absorption for the model at different angles of inclination are plotted together and discussed. The results show that at 45 degrees slope angle, the device has a particularly wide bandwidth and high efficiency. The point absorber effect and a 'double peak' effect are also investigated. In present work, the power take-off system is assumed as a simple linear damper. Calculations are shown for the optimal damping constants corresponding to different wave periods. Some consideration is also given the possibility of enhancing performance by use of the well-established 'reactive' power take-off concept. A wave energy device needs a reaction source. The Sloped IPS buoy uses the inertia of an internal water instead of the sea bed or a heavy structure. A simple mathematical model of a finite reaction mass is presented to enable calculation of the volume of water in the inertia tube.

In chapter 7, some tests in irregular waves are presented with predictions of full-scale device performance in the reference 'South Uist 399' sea climate.

Finally in chapter 8, discussions and general conclusions are drawn.

Chapter 2

Literature review

2.1 Introduction

This chapter presents a general review of previous published work relating to bodies oscillating in water. The mathematical modelling of the hydrodynamics of wave energy devices and methods for determining the hydrodynamic coefficients such as exciting force and radiation impedance are reviewed. Control strategies to achieve optimum power absorption are also surveyed. Because the Sloped IPS buoy at 90 degrees slope angle has much in common with floating OWC devices, some research work on the OWC is reviewed. The descriptions are necessarily brief and where relevant more details are given in later chapters

2.2 Mathematical modeling of hydrodynamics

Devices for extracting energy from ocean waves generally involve large motions on or close to the water surface. The solutions to the problem of ocean wave interaction with wave power devices on the one hand and with ships or offshore structures on the other have some similarities. In some aspects the theory of wave power devices is simpler than that of ships, since there is no net forward speed. They share the extreme wave conditions which ship and offshore structures are exposed to. However, their movements are usually more complex than either of these.

Theoretical studies of the interaction of ships with waves have been developed over a number of years, largely based on pioneering work by Ursell (1949). He described the vertical forcing of a cylinder in simple harmonic motion of small amplitude about its initial position. A surface disturbance is set up in which waves travel away from the cylinder. He takes the Laplace equation for the velocity potential with a boundary condition that the pressure on the free surface of the fluid is constant. The normal velocity of the cylinder must also be equal to the normal velocity of the fluid adjacent to it. By satisfying these boundary conditions, expressions are obtained for the diverging wave train at infinity and for the increase in the inertia (added mass) of the cylinder due to the presence of the fluid.

After Salter achieved high performance experimental results in 1974, many researchers became interested in the theory of maximum power absorption of various kinds of wave power devices and in many different modes. The pioneering work on the mathematical modelling of wave power devices expanded the existing work in the fields of hydrodynamics of marine and offshore structures and began in the 1970s.

Newman (1976), Evans (1976) and Mei (1976) independently established a good basis for the theory of wave energy absorbers. Newman (1976) began with linear hydrodynamics theory and then applied Green's theorem to derive the damping coefficients relating to the far-field asymptotic form of the radiation potentials. He calculated the wave force coefficient on a stationary vessel from the damping coefficient, both for two-dimensional and for vertical axisymmetric three-dimensional bodies. An analysis of the extracting of wave energy by a floating body was illustrated by using these diverse relationships.

Evans (1976) derived a general expression for the efficiency of wave absorption in a sinusoidal wave train by a body oscillating in one or two modes. The results showed that a cylinder able to move independently in both surge and heave could achieve 100 percent efficiency. For a vertically axisymmetric device or a hinged plate (neither of which can respond to an incident wave without making a new

wave to the rear) the maximum efficiency is only 50 percent. Mei (1976) and Newman (1976) also presented similar results independently.

By analogy with electrical engineering theory, Falnes (1979) introduced the idea of mechanical impedance to the study of oscillating bodies in water.

Most early experimental work was carried out in narrow tanks with the model width the same as the tank width. An important theoretical result showing the point absorber effect in a three-dimensional sea was observed by Evans (1976) and Falnes (1978) independently. Point absorption occurs when a small device absorbs energy from an effective frontage that is greater than its geometric width. For vertical axisymmetric oscillating bodies, the efficiency is independent of the diameter of the bodies, but for terminators or attenuators the picture is still not clear. However for small structures the predicted amplitudes are large and linear theory will cease to be valid.

Mei (1989) gives a complete reference of floating body hydrodynamics including wave power devices. Evans (1985) and Count (1980) also edited useful conference proceedings including much work on the modeling of wave power devices.

2.3 Determination of the hydrodynamic coefficients

Linear hydrodynamics, which assumed that the waves were of small amplitude, relative to both the wavelength and the water depth, and of permanent regular form, was used to predict the performance of wave energy devices in the frequency domain. This enabled important global results, such as the maximum power which a device could extract in one or more modes of motion, to be established at a very early stage.

According to the results of Evans (1993), it is possible to obtain maximum power without knowing the motion of the device. Only the hydrodynamic coefficients such as radiation impedance and wave excitation force coefficients are needed to

predict the performance of the devices. The radiation measurements benefited from early work on ship design. Most of this work concentrated on simplified shapes, and in particular on cylindrical bodies with different cross-sections.

Haskind (1946) investigated the forces acting on an oscillating body excited by progressive waves, with the assumption of zero forward speed, and decomposed the forces into inertial force, damping force, restoring force and disturbing force. Inertia force depends linearly on acceleration of the body. The coefficients of inertia force may be considered as added mass.

Newman (1962) further applied the Haskind relations to compute the exciting forces on a submerged ellipsoid and on floating two-dimensional ellipses. He also derived a relation between exciting force and added damping for a vertical axisymmetric body. This allows the measurement of damping coefficients to determine the amplitude of exciting forces, and vice versa.

Vugts (1968) used Laplace's equation for velocity potential in two dimensions to compute the added mass and added damping coefficients for some simple shapes, such as circles, rectangles and triangular cylinders.

Greenhow and Simon (1985) developed a method for calculating the added damping of an axisymmetric body by replacing the body generating the waves by an equivalent wavemaker with its normal velocity distribution. The added damping can be calculated from the energy dissipation of the equivalent wavemaker. The variation in added mass can be calculated from the frequency integral of the added damping by applying the Kramers-Kronig relations. Although the errors involved in using this approximation are difficult to estimate, the method could be particularly useful for extrapolating known results in a finite frequency range into high or low frequency regions where numerical methods often experience difficulties.

Pizer (1993) has taken the numerical studies of the Solo Duck into three dimensions. He generated a multi-faceted approximation to the shape of the Solo

Duck, then computed the fluid flow around the body produced by an approaching wave field of a specified frequency, approach angle and water depth. The forces and torques on the body are then evaluated directly from the hydrodynamic pressure at each facet.

2.4 Control of wave power devices

In order to absorb the maximum energy from waves, the device needs to properly respond to the incident waves. Therefore, the motion of the device should be controlled. In most wave power devices, the power take-off system provides this reaction force. In initial studies of wave power devices, the power take-off system is often ideally treated as a simple linear damper having a resistance to motion which is proportional to velocity only.

Evans (1976) and Mei (1976) presented a theory for predicting the absorption of the power in an incident wave train by means of a damped, oscillating, partly or completely submerged body. Evans also varied the spring rate and device inertia for tuning the device to the desired wave period and calculated the maximum efficiency. The Edinburgh Wave Power Group (Salter, 1975) also experimentally varied the spring and inertia rate to investigate the effect on efficiency. This later led to the idea of "reactive control" which used the power take-off to provide not only damping force but also virtual spring and inertia forces.

Evans (1976), Falnes (1978) and Mei (1976) concluded that wave power devices could absorb the maximum power when the velocity is in phase with the exciting force. When the device is driven at its natural period, the effects of stiffness and inertia are cancelled and the device velocity is in phase with exciting force. The response then is solely determined by damping. If the damping value is correct, the best conversion can be achieved. At periods above and below resonance the forces due to stiffness and inertia cause phase differences between the device velocity and the wave exciting force with a consequent reduction in efficiency. To obtain the

maximum power absorption, the phase and damping need to be properly controlled. Some control strategies were proposed to obtain optimum phase.

Salter *et. al.* (1976) introduced a "reactive control" strategy into the power take-off. A control unit processed the velocity signals in a network and produced different gain and phase changes at different frequencies. This cancelled to some extent the reactive forces of the device and produced a substantial widening of the efficiency band. Since the power take-off device was no longer passive with power only flowing into it but could also provide a reactive force to change the phase difference, a hydraulic system which combined a pump and a motor was developed (Salter, 1992). Skyner (1987) and Nebel (1992, 1994) applied "complex conjugate control" to the Solo Duck which takes the reactive control concept to the limit. All the spring and all the inertia terms at all useful frequencies are cancelled and the damping coefficient is set to the best value for each of the frequency components of the incident spectrum. Edismoen (1995b) has proposed a mathematical model of phase control in the time domain. However, advance information of waves is necessary to apply this control method.

Instead of continuously controlling the phase, Budal and Falnes (1981) proposed a discrete control – "latching" (or locked) method to obtain approximate optimum phase control. The buoy is latched when it reaches the top or bottom position of its stroke then unlatched again a short time before the exciting force reaches its next extreme. In this way the maxima of the wave exciting force and the velocity of the buoy can be kept in phase, thereby increasing the power absorption. Experimental results showed that it improved power absorption by 20%. However, a short-term prediction of the incoming wave is still necessary to perform this control strategy. Greenhow et al. (1984) has applied the latching control strategy to the Clam wave power device. Recently a high-speed stop-valve for the latching control of an oscillating water column has been built (Salter and Taylor, 1995).

French proposed a quasi-resonance control strategy called "Stiffness Modulation" (SM). Instead of latching the device stationary, a stiffness modulation is applied to provide a higher stiffness when the displacement exceeds a certain value and a

lower stiffness when it returns back to the smaller displacement. The higher stiffness causes the device to slow down and allows the wave to "catch up" without the problem of suddenly trying to restrain the huge moving mass. There are no discontinuities in the force on the mass, only in the rate of change of force. The advantage of this control method is that it reduces the radiation of energy back into sea at higher frequencies (French, 1985; Bracewell, 1990).

In the above control strategies, the excursion of the devices is unconstrained to obtain their optimum absorption. In practice most wave energy devices have physical limitations placed on their excursions due to restraints such as ram stroke or mooring lines. Whereas there exists a significant band of wave periods and wave heights for which the device does not reach these limits, in long waves a relatively small device would need to make large excursions to achieve optimum power absorption. Also larger amplitude waves require larger device excursions for optimum absorption. At some point either engineering constraints are reached, or the assumptions of linear theory are invalidated. Evans (1981) presented an expression for the maximum power absorption of a multi-degree of freedom system when its velocities are constrained such that their magnitude never exceeds a given multiple of the incident wave amplitude, and introduced a "global constraint" to allow for different weightings for each degree of freedom. This method has recently been applied to the Solo Duck by Pizer (1993).

2.5 Research work on oscillating water column devices

The Sloped IPS buoy is inherent to be an asymmetrical wave power device. However, when the Sloped IPS buoy is set at an angle of 90 degrees, it presents as a heaving oscillating buoy. There are some similarities between a 90 degrees sloped IPS buoy and a heaving OWC buoy. For example, Both use mainly the heave motion responded to waves and contain water column in the tail tubes. The Sloped IPS buoy is designed to have a large inertia of water in the tube and the tube is long enough to keep the water column motionless. The body of the buoy then moves along the axis of the inertia tube in response to the incident waves. Though,

the heaving OWC buoy has more complex motion than the heaving Sloped IPS buoy, since the motions of OWC buoy can be divided into two parts, one part being the motion of the outer body and the other the inner water column (McCormick, 1975; Whittaker and McPeake, 1985).

In early 1970s, Masuda (1971) first applied the oscillating water column principle to a navigation buoy. The buoy consisted of a float structure with a long tail tube attached to it. The wave motion induced vertical, cyclic motion of the water column in the tail tube to trap the air in a plenum chamber above water surface and then vent it through an axial flow turbine-generator. However, the airflow needed to be rectified for the axial flow turbine by an arrangement of valves. Later, a self-rectifying air turbine, was invented by Wells and is known by his name. The Wells turbine can provide unidirectional rotation in reciprocating flow (Raghunathan and Ombaka, 1985; Gato and Falcao, 1988). It is widely used for navigation buoys (Whittaker and McPeake, 1985; Whittaker *et. al.*, 1985a) and larger OWC devices (Whittaker *et. al.*, 1985b; Inoue *et. al.*, 1988). Research work has also been carried out to improve the performance of the Wells turbine in the past two decades.

There are two resonant frequencies for an OWC type navigation buoy in heave. One responds to the buoy dynamics, the other to the water column dynamics. Whittaker *et. al.* (1985a) conducted experiments on the response of water columns in a fixed buoy and in a floating buoy. The results show two peaks in the frequency domain efficiency curve for floating buoy, but a single peak for the fixed buoy. The bandwidth of the floating buoy is also wider than that of the fixed buoy.

The OWC device is widely regarded as one of the most attractive "first generation" concepts for wave energy converters. Workers in many countries have built such devices. For example, the UK's first demonstration prototype was the 75KW shoreline wave power device on the island of Islay. The project commenced in 1985, led by a group at Queen's University, Belfast (Whittaker, 1991). In Norway the Kvaerner OWC had a concrete chamber built onto a rocky edge with a hollow steel tower on top and was in operation during 1986-1987. Unfortunately, a storm

washed the steel tower into the sea. There are also shoreline OWC projects in progress in Portugal (Falcao *et. al.*, 1995), India (Ravindran *et. al.*, 1995) and China (Yu *et.al.*, 1993). In Japan, near-shore floating OWC devices were developed. The Japan Marine Science and Technology Center (JAMSTEC) commissioned the ship-type floating OWC, called Kaimei, in open sea tests in 1978 (Miyazaki and Masuda, 1978). Recently a floating OWC device, called Mighty Whale, has been launched (Kato and Miyazaki, 1991; Edwards, 1998). Masuda (1993) developed a floating OWC device, called Backward Bend Duct Buoy (BBDB), to continue his early work on the light buoy and on Kaimei. The BBDB is based on the OWC concept but the enclosed water mass is increased by using a bent duct under the hull. The entrance of the duct is at the stern and under the water line. The waves induce relative motions between water column and the body of the buoy.

Much work has been carried out on the control of OWC devices, such as latching control of OWC (Jefferys and Whittaker, 1985; Salter and Taylor, 1995), OWC with blade-pitch controlled air turbine (Sarmento *et.al.*, 1987; Taylor and Salter, 1995) and twin OWC with phase control (Brendmo *et. al.*,1995).

Chapter 3

The linear hydrodynamics of wave energy devices

3.1 Introduction

Most of the theoretical work on wave power devices in the past two decades has concentrated on *linear hydrodynamic* theory and the *frequency* domain. Despite the apparent randomness of the real sea surface it is usually reasonable to analyse a wave energy device in incident regular sinusoidal waves with limited wave height and wave steepness. Such assumptions enable the advantages of linearity to be exploited so that it is possible to predict performance of a wave power device in irregular seas by linearly superposing results from tests in discrete wave components at different frequencies. In addition, the motion of the device and its power take-off system are usually regarded as operating in a linear manner. However, such assumptions are clearly not valid in the case of severe sea states where survivability is more important, and a non-linear model may need to be used. The frequency domain analysis, which describes the interaction between the waves and the oscillating bodies, is used to perform the fundamental analysis on wave energy devices. On this basis the device's energy output and efficiency versus the incident wave frequency can be predicted.

The frequency domain model is restricted to linear hydrodynamic theory. However, this approach is computationally compact and is adequate for many of the problems in wave power, failing only when the device dynamics contain significant non-

linearity in the presence of non-harmonic external forces, large motions of the device or large waves (Jefferys, 1979).

Jefferys has also pointed out that most of the wave energy devices proposed have used non-linear power conversion systems such as air turbines. These components generate non-harmonic forces when they undergo harmonic motions and cannot be described by a conventional frequency domain model. Moreover, in order to achieve high performance from wave power devices, latching and reaction control techniques may be implemented. *Time* domain models are better at representing the transient, non-linear forces in the power take-off system and also amplitude constraints. However, these models usually require the complex and difficult convolution integral model which describes the continuing influence of previous body motion on the present motion.

There are good reasons for applying the frequency domain approach in the early study of a new wave power device. The equations describing the device's motion and energy absorption can be solved easily and require very little computing time. Moreover, the agreement between theory and experiments is usually good, despite the mathematical model being relatively simple. Frequency domain models can also give overall prediction of device responses to spectra. Although the results from linear theory and the frequency domain are not applicable to fully realistic sea conditions, it still provides some help in understanding the physical processes and in the prediction and optimisation of some of the full-scale characteristics of such structures.

In section 3.2, the variables such as the appropriate coordinate system and the Fourier transform are defined and discussed. Section 3.3 describes the hydrodynamics on which the linear theory of wave power devices is based. Since power is a function of velocity and force, section 3.4 gives the equation of the device's motion based on the interaction of its motion and incident wave loads. The interaction of the device motion and the waves is represented by a *radiation impedance* which is proportional to the velocity. The restraining forces from the

power take-off system are also modelled as an impedance parameter proportional to velocity. This simplifies the force and velocity equation of wave energy devices as a function of four parameters. These are radiation impedance, the damping coefficients of the power take-off system, the force coefficient in the incident wave and the incident wave amplitude. The maximum power absorption capability of wave energy devices is described in section 3.5. Control of power take-off coefficients is also discussed.

The overall performance of a wave power device can be best shown in graphs of efficiency versus frequencies and section 3.6 discusses the concept of efficiency in a multi-directional wave tank. In three-dimensional seas, a wave energy device benefits from the point absorber effect which enables the device to absorb energy from beyond its physical dimensions. The theory of the point absorber effect is described in section 3.7.

Most equations described in this chapter are based on Evans' work (Evans, 1980; Evans and Linton, 1993).

3.2 Definition of the variables

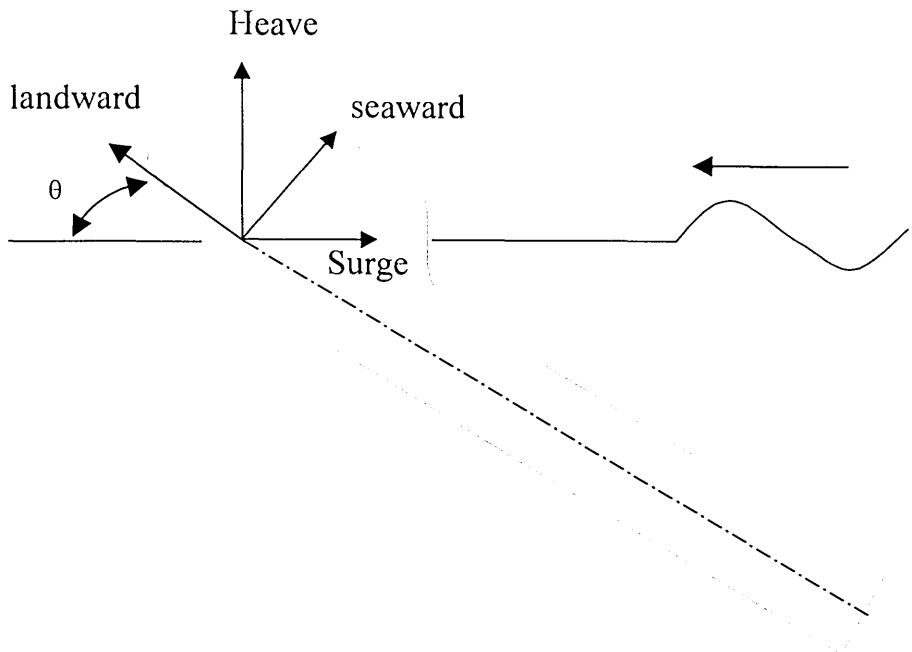

Figure 3.1. The coordinate system of the sloped IPS buoy

A rigid body in three dimensions can move with six degrees of freedom, which comprise a *rotational* and a *translational* mode for each dimension. However, in order to concentrate on the sloped angle idea in this early stage, the Sloped IPS model is assumed to be constrained to move in a plane intermediate between heave and surge with a single degree of freedom as shown in figure 3.1.

The state of the Sloped IPS buoy may be represented by two functions of time t, one being a force and one a velocity, both measured with reference to the *landward* axis. The arrow shows the direction of the incoming wave train. The slope angle θ is defined between the horizon and the landward axis.

The same symbols are used to represent the variable in both time domain and frequency domain. If the dependence of a variable is not explicitly stated, it may be assumed to be a function of frequency. The time domain function indicates how a signal's amplitude changes over time, the frequency domain function tells how often

such changes take place. The bridge between them is the Fourier transform. The standard definition of a Fourier transform of a periodic function $f(t)$ is

$$f(\omega) = \frac{2}{T}\int_0^T f(t)e^{-i\omega t}dt \qquad (3.1)$$

and its inverse is:

$$f(t) = \frac{1}{2}\sum_{n=-\infty}^{\infty} f(\omega_n)e^{i\omega_n t} \qquad (3.2)$$

where

T is the sampling period and is always a whole number of cycles.

ω is the angular frequency and $\omega_n = 2\pi n/T$.

3.3 Linear theory of hydrodynamics

In the present work all the equations for calculating the maximum power absorption and the hydrodynamic coefficients are based on the linear theory of hydrodynamics. A brief description is given below.

The frame of reference for the linear hydrodynamic analysis of free floating bodies is the water. The device and its motions are considered only through the boundary conditions that they impose on the fluid. The behaviour of the body can be understood as being due to the superposition of three idealised and isolated interactions. The first of these is the water motion of the incident wave in the absence of the body. The second is the effect that the body if held static would have on the water motion of the wave. The third is the effect that the moving body would have on the water in the absence of the wave.

In fluid dynamics, the velocity of flow is usefully expressed in terms of a single-valued function, namely *velocity potential* $\Phi(x,y,z,t)$. Velocity potential can be thought of as *gravity potential energy (P.E.)* which relates to force F times distance l, shown as $F=-\delta P.E./\delta l$. Thus, Velocity potential Φ relates to velocity U times distance l, shown as $U=-\delta\Phi/\delta l$ *(Barber, 1969)*.

The velocity potential can be expressed as:

$$u = \frac{\partial \Phi}{\partial x}, \quad v = \frac{\partial \Phi}{\partial y}, \quad w = \frac{\partial \Phi}{\partial z} \tag{3.3}$$

Thus, the fluid velocity U can be expressed as:

$$U = -\nabla \Phi \tag{3.4}$$

In linear theory, the water is assumed as incompressible and to have continuity of flow. The *continuity equation* states that the mass of the fluid is conserved. Since incompressibility is assumed, it is equivalent to expressing the conservation of the volume, which can be stated in terms of fluid velocity as:

$$\frac{\partial u}{\partial x} + \frac{\partial v}{\partial y} + \frac{\partial w}{\partial z} = 0 \tag{3.5}$$

If the equation (3.3) is substituted in the continuity equation (3.5), then the Laplace equation can be obtained.

$$\nabla^2 \Phi = \frac{\partial^2 \Phi}{\partial x^2} + \frac{\partial^2 \Phi}{\partial y^2} + \frac{\partial^2 \Phi}{\partial z^2} = 0 \tag{3.6}$$

As a consequence of the linearisation, the time dependence of the solution may be factored out for steady monochromatic solutions as

$$\Phi(x, y, z, t) = \phi(x, y, z) e^{-i\omega t} \tag{3.7}$$

where

$\phi(x,y,z)$ is the time independent velocity potential.

ω is the angular frequency of the wave.

The time independent velocity potential can be divided into three parts, say ϕ_o, ϕ_d and ϕ_r. The potential ϕ_o corresponded to an incident wave alone in the absence of the device. ϕ_d is known as the *diffraction* potential experienced if the device were held fixed in the incident waves. ϕ_r is known as the *radiation* potential which would be caused by the forced movement of the device in calm water.

$$\phi = \phi_o + \phi_d + \phi_r \tag{3.8}$$

The concept of separate potentials is convenient since Newman (1977) showed that the pressure forces acting on the body due to ϕ_d can be determined from ϕ_r and ϕ_o. This will be discussed in section 3.7. From an experimental point of view this insight is valuable because velocity potentials though convenient for analytical purposes are neither easy to visualise nor to quantify. Forces on the other hand can be easily measured and can be used as the key practical understanding of a wave energy device.

3.4 Equation of motion of the device

In linear theory, the equation of motion modeling the hydrodynamic system can be described by the external force loads on a floating body. These can be separated into two parts: *wave excitation* loads and *device radiation* loads.

Wave excitation loads

The forces and moments on the device when it is restrained from movement and exposed to incident regular waves.

Device radiation loads

The forces and moments on the device when it is forced to oscillate at the wave excitation frequency in any rigid-body motion mode in still water. With no incident waves, the corresponding hydrodynamic loads are identified as added inertia (sometimes called added mass), damping and hydrodynamic restoring terms.

Because the system is assumed linear, the forces obtained as wave excitation loads and device radiation loads can be added to give the total hydrodynamic forces.

The hydrodynamic forces F on an oscillating body in waves can then be represented as:

$$F(t) = F_e(t) + F_r(t)$$

or

$$F(\omega) = F_e(\omega) + F_r(\omega) \qquad (3.9)$$

where

$F_e(t)$ and $F_e(\omega)$ are the forces acting on the body when it is held fixed in the presence of the incident waves.

$F_r(t)$ and $F_r(\omega)$ are the forces due to the oscillation of the body in the absence of the incident waves.

The wave excitation force is a function of the incident wave amplitude, therefore. It can be expressed as

$$F_e(\omega) = W(\omega) \cdot a(\omega) \qquad (3.10)$$

where

W is the excitation force coefficient.

a is the wave amplitude

W gives the excitation forces on the stationary model when a wave of unit amplitude is incident.

The device radiation force can be expressed as a function of device velocity.

$$F_r(\omega) = Z(\omega) \cdot U(\omega) \qquad (3.11)$$

where

Z is the radiation impedance.

U is the velocity of the device.

Hence the equation of motion 3.9 in the presence of incident waves can be expressed as:

$$F(\omega) = W(\omega) \cdot a(\omega) + Z(\omega) \cdot U(\omega) \qquad (3.12)$$

The equation of motion gives the device velocities U resulting from the external forces and the wave forces.

$$U(\omega) = \frac{F(\omega) - W(\omega) \cdot a(\omega)}{Z(\omega)}$$

Radiation Impedance

The radiation impedance Z is related to the geometry of the buoy and its oscillating frequency. It can be decomposed into added inertia, damping and hydrodynamic restoring terms. The real part of the radiation impedance is known as the added damping, because energy is radiated from the device when there is a component of force in phase with the velocity. The imaginary part is due to the effects of hydrostatic spring, the device inertia and the added inertia of the water around the device. Added inertia is due to hydrodynamic pressure from the surrounding water which is affected by the acceleration of the device.

Using the equivalence $d/dt = i\omega$, the radiation equation can thus be split up into these three parts

$$Z(\omega) = D_a(\omega) + i\omega \cdot \mu + i\omega \cdot M_a(\omega) + \frac{1}{i\omega}\sigma \qquad (3.13)$$

where

D_a is the real, frequency dependent added damping.

μ is the device inertia.

M_a is the real, frequency dependent added inertia.

σ is the hydrostatic spring.

Power take-off system forces

The power take-off system typically couples wave induced device motions to an electrical generator. Most proposed wave power devices use air turbines, high-pressure hydraulics or water turbines for this purpose. Here, a damper is assumed to represent the power take-off system with force proportional to the velocity only. Therefore, the force F acting on the buoy from the power take-off system can be expressed as

$$F(\omega) = -B(\omega) \cdot U(\omega) \qquad (3.14)$$

where

B is the complex damping coefficient of the power take-off system.

B will be real and positive for a simplified linear hydraulic ram. Other power take-off systems including air turbines might be quite hard to model.

Combining equations 3.12 and 3.14 gives the device velocity and force:

$$-B \cdot U = W \cdot a + Z \cdot U \qquad (3.15)$$

$$U = -(B + Z)^{-1} \cdot W \cdot a \qquad (3.16)$$

Substituting for U in equation 3.15:

$$F = -B \cdot (B + Z)^{-1} \cdot W \cdot a \tag{3.17}$$

Thus, the forces on the device can be expressed as a function of the damping impedance of the power take-off system, the radiation impedance, and the wave excitation forces on the device.

3.5 Power absorption

The instantaneous power P extracted from the device is the scalar product of the reaction force of the power take-off system and device velocity:

$$P(t) = F(t) \cdot U(t) \tag{3.18}$$

The mean power the time domain passing through the buoy is given in by:

$$P = \frac{1}{T} \int_0^T F(t) \cdot U(t) \cdot dt \tag{3.19}$$

Note that the definitions of F and U lead to P being negative when power is extracted.

By taking the Fourier transform of equation 3.19 in the frequency domain (see Appendix A):

$$P = \frac{1}{4} \{ \sum_{n=1}^{\infty} F(\omega_n) \cdot U^*(\omega_n) + \sum_{n=1}^{\infty} F^*(\omega_n) \cdot U(\omega_n) \} \tag{3.20}$$

where

$\omega_n = 2\pi n/T$ and * denotes *complex conjugate*.

For a specific frequency $\omega = \omega_n$.

$$P = \frac{1}{4} (F \cdot U^* + F^* \cdot U) \tag{3.21}$$

Substituting F from equation 3.18

$$P = \frac{1}{4}(B \cdot U \cdot U^* + B^* \cdot U^* \cdot U)$$

$$= \frac{1}{4}(B + B^*) \cdot |U|^2 \qquad (3.22)$$

Substituting equation 3.16 into 3.22 and re-arranging (see Appendix B):

$$P = \frac{1}{4}(B + B^*) \cdot \left| \frac{F_e}{B + Z} \right|^2$$

$$= \frac{|F_e|^2}{8 \cdot D_a} \cdot \left(1 - \frac{|B - Z^*|^2}{|B + Z|^2}\right) \qquad (3.23)$$

In this form, it is clear that the maximum power:

$$P_{\max} = \frac{|F_e|^2}{8 \cdot D_a} \qquad (3.24)$$

Occurs when

$$B = Z^*$$

$$= D_a - i\omega(\mu + M_a - \omega^{-2}\sigma) \qquad (3.25)$$

Implementation of this idea has been called *complex conjugate control* (Skyner, 1987). In addition to the pure damping forces associated with electricity generation, the power take-off system provides additional forces equal to the complex conjugate of the radiation impedance of the device at all useful frequencies. In effect, the resulting combination of external and hydrodynamic forces reduces the combined inertial and stiffness term to zero, equivalent to forcing resonance throughout the frequency band. An implementation of this idea with the Solo Duck is described by Nebel (1992,1994). However, it must be noted that the realisation of complex conjugate control requires accurate knowledge of incident wave spectra and phases.

More typically in a simplified power take-off system the damping coefficient of the power take-off system will be real and positive. This corresponds to the control force being pure damping only. The equation 3.23 can be rearranged as:

$$P = \frac{|F_e|^2}{4(D_a + |Z|)} \cdot (1 - \frac{(B - |Z|)^2}{|B + Z|^2}) \tag{3.26}$$

Showing that in this case the maximum power achieved

$$P_{\max} = \frac{|F_e|^2}{4(D_a + |Z|)} \tag{3.27}$$

when

$$B = |Z|$$

$$= (D_a{}^2 + (\omega\mu + \omega M_a - \omega^{-2}\sigma)^2)^{\frac{1}{2}} \tag{3.28}$$

When the device is at resonance, B is equal to D_a and P_{max} is in agreement with equation 3.24.

Wave Power

The energy E in a regular wave of unit width can be written as (Taylor, 1984):

$$E = \rho g H_{rms}{}^2 \lambda \tag{3.29}$$

where

ρ is water density.

g is gravitational acceleration.

H_{rms} is root mean square wave height

λ is wavelength.

The power density can be calculated by dividing the energy by the time taken for it to cross a line perpendicular to its direction of travel. If the energy travelled at the phase velocity, the time would be the wave period, but in fact it travels more slowly at the group velocity. Denoting the ratio of group to phase velocity as n which is related to the water depth, power density can be written as:

$$P_w = n \cdot \frac{E}{T} \tag{3.30}$$

where

P_w is the power of the incident wave in unit width.

E is the energy in unit width.

T is wave period

n is the ratio of group to phase velocity, and can be expressed as a function of water depth h:

$$n = \frac{1}{2}\left(1 + \frac{2kh}{\sinh(2kh)}\right) \tag{3.31}$$

The wave length can also be expressed as a function of water depth h.

where

$$\lambda = \frac{gT^2}{2\pi}\tanh(kh) \tag{3.32}$$

k is the wavenumber $=2\pi/\lambda$.

Rearranging equations 3.29 to 3.32, the power density of the incident wave can be rewritten as:

$$P_w = \frac{\rho g^2 H^2 T}{32\pi} \cdot \tanh(kh) \cdot \left(1 + \frac{2kh}{\sinh(2kh)}\right) \tag{3.33}$$

where H is the wave height.

3.6 Efficiency

For multi-directional wave tests in the open sea or in a wide wave tank, we further define the *capture width* l as the ratio of the absorbed power to the incident power per unit width, that is:

$$l = \frac{Power\ absorbed}{Power\ incident\ per\ metre} = \frac{P}{P_w} \tag{3.34}$$

The efficiency of a three-dimensional device is expressed in term of its relative width. This is defined as the capture width divided by the device width:

$$\eta = \frac{Capture\ width}{device\ width} = \frac{l}{W} \qquad (3.35)$$

where

W is the device width.

3.7 Point absorber effect

With reference to section 3.3 the idea of decomposing the velocity potential into three parts associated with the incident wave (ϕ_o), the diffraction potential (ϕ_d), and the radiation potential (ϕ_r). Newman (1977) demonstrated that the pressure forces acting on the body due to the diffraction potential ϕ_d can be determined from knowledge of potentials ϕ_o and ϕ_r alone.

The relation between damping and excitation force can be expressed as

$$D_a = \frac{\omega k}{4\pi\rho g^2 a^2} \int_0^{2\pi} |F_e(\theta)|^2 d\theta \qquad (3.36)$$

where

θ is the direction of the incident wave.

a is the wave amplitude.

The wave power in deep water can be re-expressed equation 3.33 as:

$$P_w = \frac{\rho g^2 a^2 T}{8\pi} \qquad (3.37)$$

Combining equations 3.36 and 3.37:

$$P_w = \frac{1}{8\lambda D_a} \int_0^{2\pi} |F_e(\theta)|^2 d\theta \qquad (3.38)$$

The maximum capture width then can be expressed as:

$$l_{\max} = \frac{P_{\max}}{P_w} = \frac{\lambda |F_e|^2}{\int_0^{2\pi} |F_e(\theta)|^2 d\theta} \qquad (3.39)$$

For a vertical body of revolution making heave oscillations, the heave excitation force is independent of the direction of incident wave. Equation 3.39 then reduces to $\lambda/2\pi$. For horizontal motions the corresponding excitation force can be shown to be proportional to $cos\theta$ (Evans, 1980). The equation 3.39 then reduces to λ/π. This shows the maximum capture width is independent of the physical size of the device but dependent on the wavelength. Furthermore, it is possible to absorb energy from a wave front considerably wider than the physical width of the device.

The advantage of this *point absorber effect* is that the device absorbs a large amount of energy compared to its physical size. The disadvantage is that the device movement may have to be very large in order to achieve the maximum power. These results are well established and were first discovered independently by Evans (1976), Newman (1976) and Budal (1977).

Chapter 4

The experimental system

4.1 Introduction

The aim of this study was to use small-scale models to simulate full-scale conditions realistically and to obtain systematic data representative of the full-scale Sloped IPS buoy, including power, efficiency and structural loads. To achieve this aim, tank tests with a model and dynamometer test rig were required. Most programmes of study to develop wave energy devices initially start from two-dimensional tank tests and then extend to three-dimensional tanks. For example tests on the Salter Duck were conducted in a *narrow tank* (2-D) which had the same width as the model and then in a *wide tank* (3-D) which allowed directional seas to be used. In the early work on the Duck, the narrow tank tests produced large amounts of useful data and fundamental insights into the design of full-scale wave energy devices. Later, the Duck models were tested in the Edinburgh wide tank, which is a multi-directional wave tank (Salter, 1981). The wide tank tests gave more information of the devices in real sea conditions. The details of wide tank will be described in section 4.5.

Working in a narrow tank has advantages such as cost efficiency, well-controlled boundary conditions, easy operation and measurement, and quick modification of models. Moving to a wide tank introduces a number of difficulties, which are not present in a narrow tank, such as power measurements, boundary reflections, harder working environment and high running costs. Although the wide tank work is more difficult than the narrow tank, there are advantages such as more realistic sea

conditions, point absorber effect and multi-directional wave effect. In this study, the experimental work was conducted in the Edinburgh wide tank, since it is freely available to the Edinburgh Wave Power Group and previous experience (Skyner, 1987) also encourages us to go into the wide tank directly. Moreover, the wide tank gives us more freedom to test the model in different sea states and to study three-dimensional effects.

After deciding to use the wide tank, four generations of model were built. The first two were free-floating models for demonstrating the concept of keeping the motion of the device to a slope plane by using a thin plate. The motions of these models were recorded by video, and showed that the slope-plate concept works well in short and medium wave lengths. The details will be discussed in section 4.2. The free-floating models were tested with no power being extracted from the waves. For small-scale models it is neither appropriate nor easy to apply a realistic power take-off system such as hydraulic ram or air turbine. A dynamometer was designed and built to simulate the power take-off system using a servo motor with feedback control. In Section 4.4, the control system of this simulated power take-off system will be discussed.

In the early study stage, it is reasonable to reduce the degrees of freedom of the model's motions and concentrate on the effect of the slope angle. A two-degree of freedom rig was built to allow model movement in the plane of the slope angle as well as in roll. This rig was later abandoned, since its low stiffness made it hard to implement a high gain for the feedback loop. A second rig was built with high stiffness and low friction to achieve a high gain for the control loop. However, the roll motion of the model needed to be sacrificed, because of the re-arragement of the simulated power take-off system. The final model then has only one degree of freedom. Details of these systems are given in section 4.4. In a three-dimensional tank, the efficiency cannot be obtained by direct accounting of the energy of the incident, reflected and transmitted waves. Power absorption was measured directly by the dynamometer and power of the incident wave was calculated from the

measured wave heights in the absence of the model. Wave generation and wave measurement are discussed in section 4.6.

4.2 Free-floating models

Before the study began, the first simple free-floating model was built to verify the concept of the Sloped IPS buoy. The model had a wooden block as a float head with a thin folding aluminium plate. A schematic diagram and dimensions are shown in appendix C. Two small polystyrene floats were attached via strings to the tail edges of the plate to help the model float at a sloped angle. This arrangement verified that the model could move at a slope angle. However, it was not convenient to use floats to adjust the slope angle. The sloped IPS buoy should be able to float at a slope angle by careful control of its own gravity and buoyancy centres.

The second free-floating model, shown in figure 4.1, was built to demonstrate movement at a slope angle without the assistance of external floats. The float part of the model was made with a trapezoidal section from expanded polystyrene with a number of embedded aluminium tubes to carry ballast weights. It was attached to a long flat aluminium plate. A schematic diagram and dimensions of the model are shown in appendix D. Figure 4.2 shows the experimental set up for the free-floating model. This simple model did not contain or use any power take-off device. The model was slack moored to prevent it from drifting away. The mooring was attached to the centre of the lower edge of the flat plate and consisted of a string with a sinker, a float and then a heavy concrete block as anchor. Such an arrangement gives a spring like restoring force on the model. All tests of this model were made in regular waves and video was used to record the motions. The records showed that the slope-plate constraint works well in waves between 0.7 to 1.5 Hz. When the wave frequency is lower than 0.7 Hz, the buoy begins an ellipse motion, which may be because the effective wave motion is deeper than the buoy tail. When the wave frequency is higher than 1.5 Hz, the buoy will tile forward to the horizontal direction, which may be because the effective wave motion is only near to the wave surface. Nevertheless, the results confirm that it is possible to achieve a stable-floating angle

despite the rather short water line. Figure 4.3 and 4.4 show the models at 1 and 0.6 Hz regular waves.

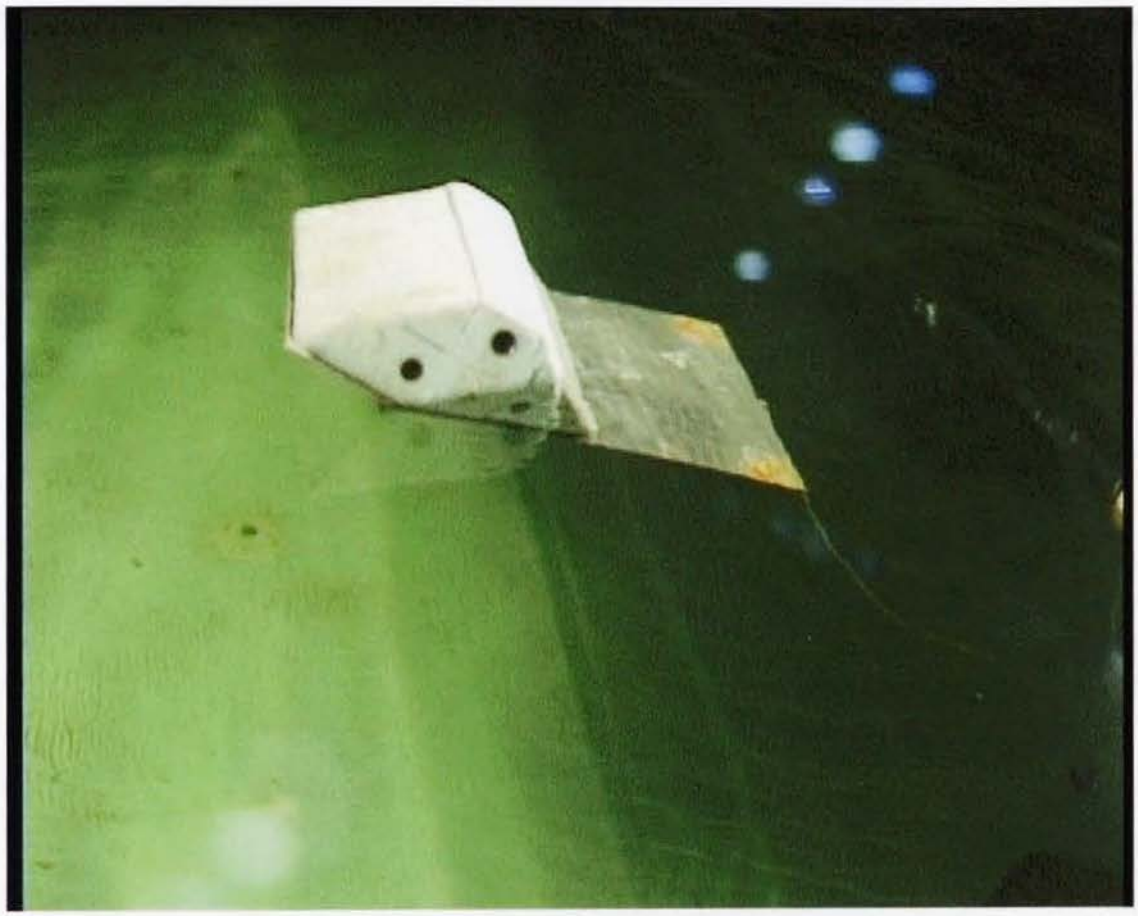

Figure 4.1. The simple free-floating model of the Sloped IPS buoy with no power take-off system. The model was slack moored. Movement was mainly in the tail plane of the plate except for long waves. ($\lambda > 3$ m, six times the length of the model tail plate).

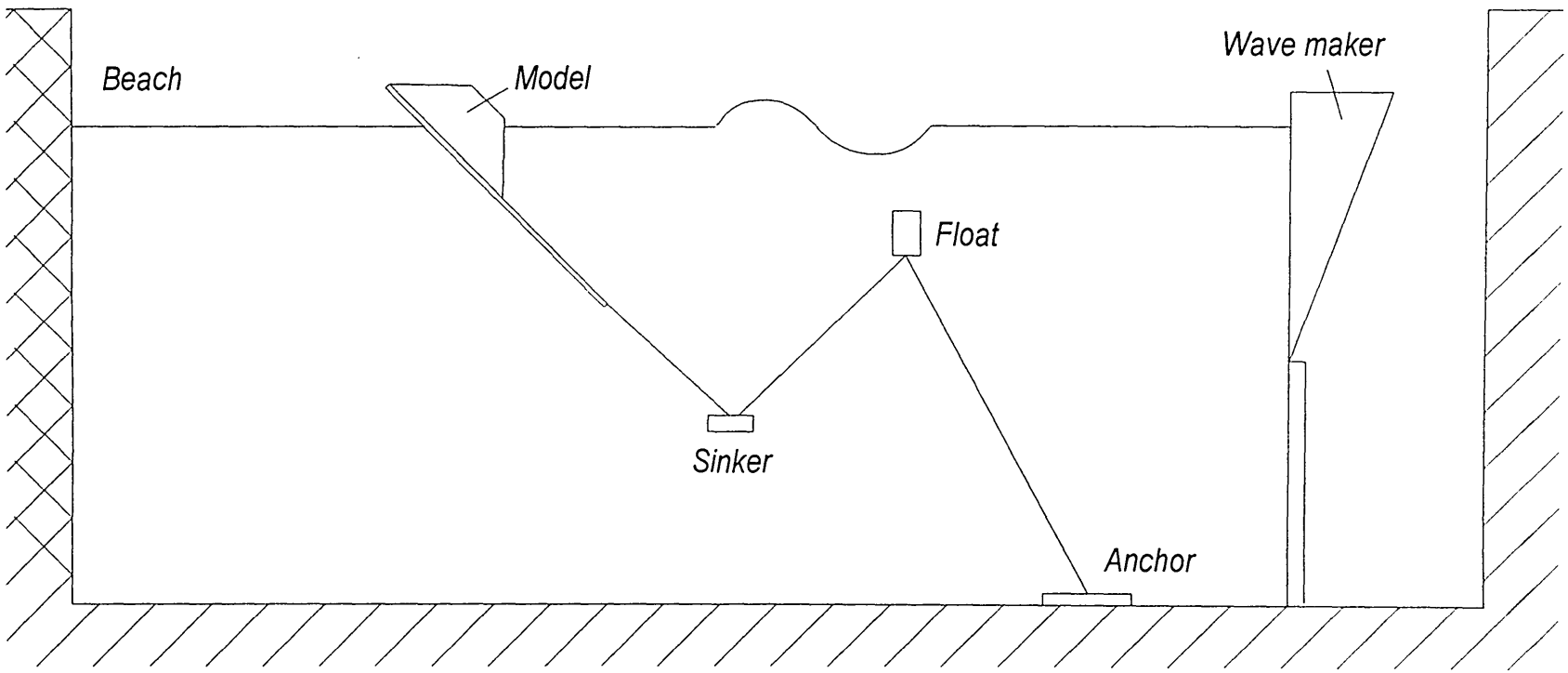

Figure 4.2. The experimental set-up of the free-floating model in wave tank

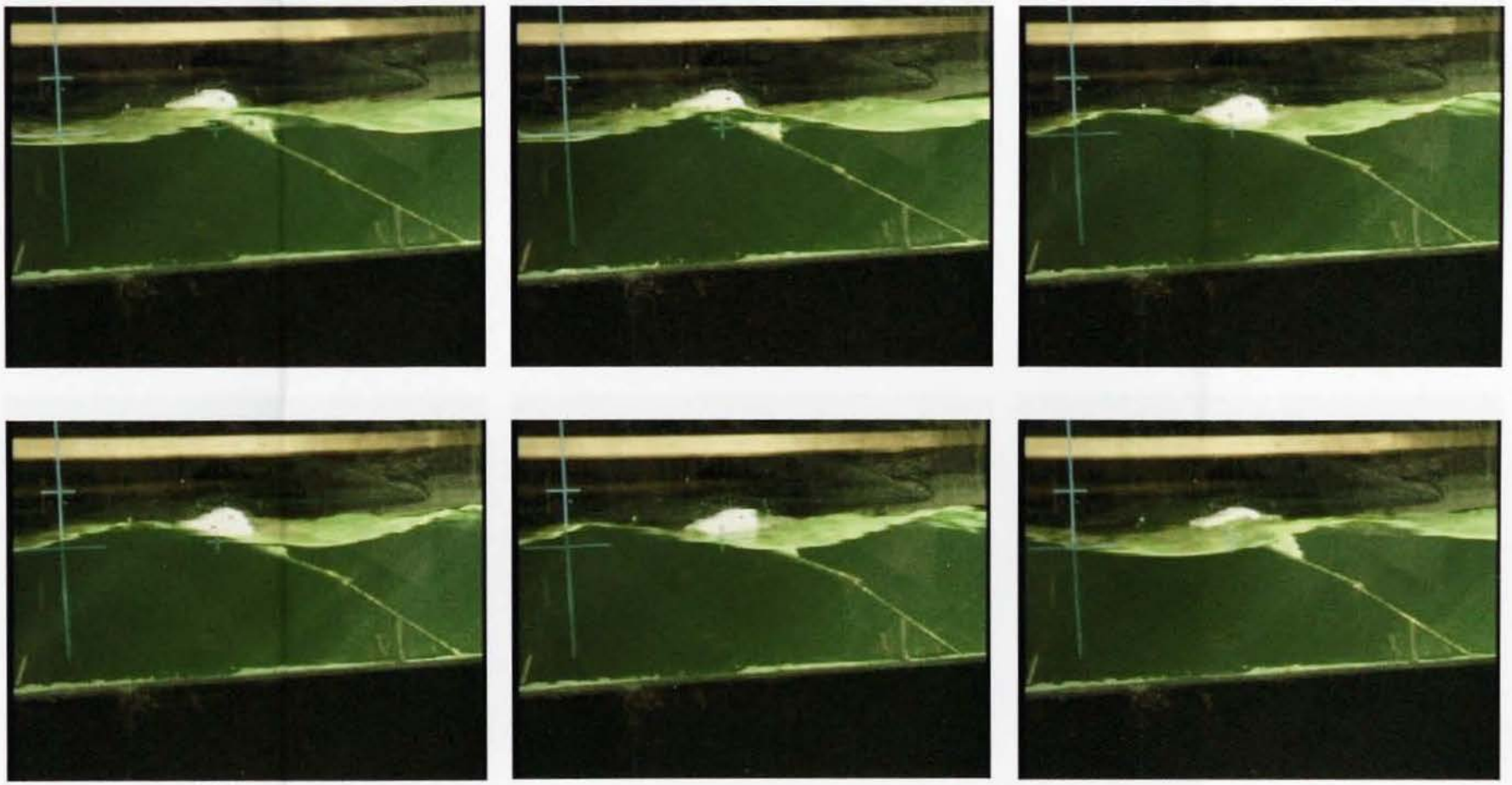

Figure 4.3. The free-floating model at 1 Hz regular waves. Wave height is about 10 cm. The Model is able to keep its angle quite well.

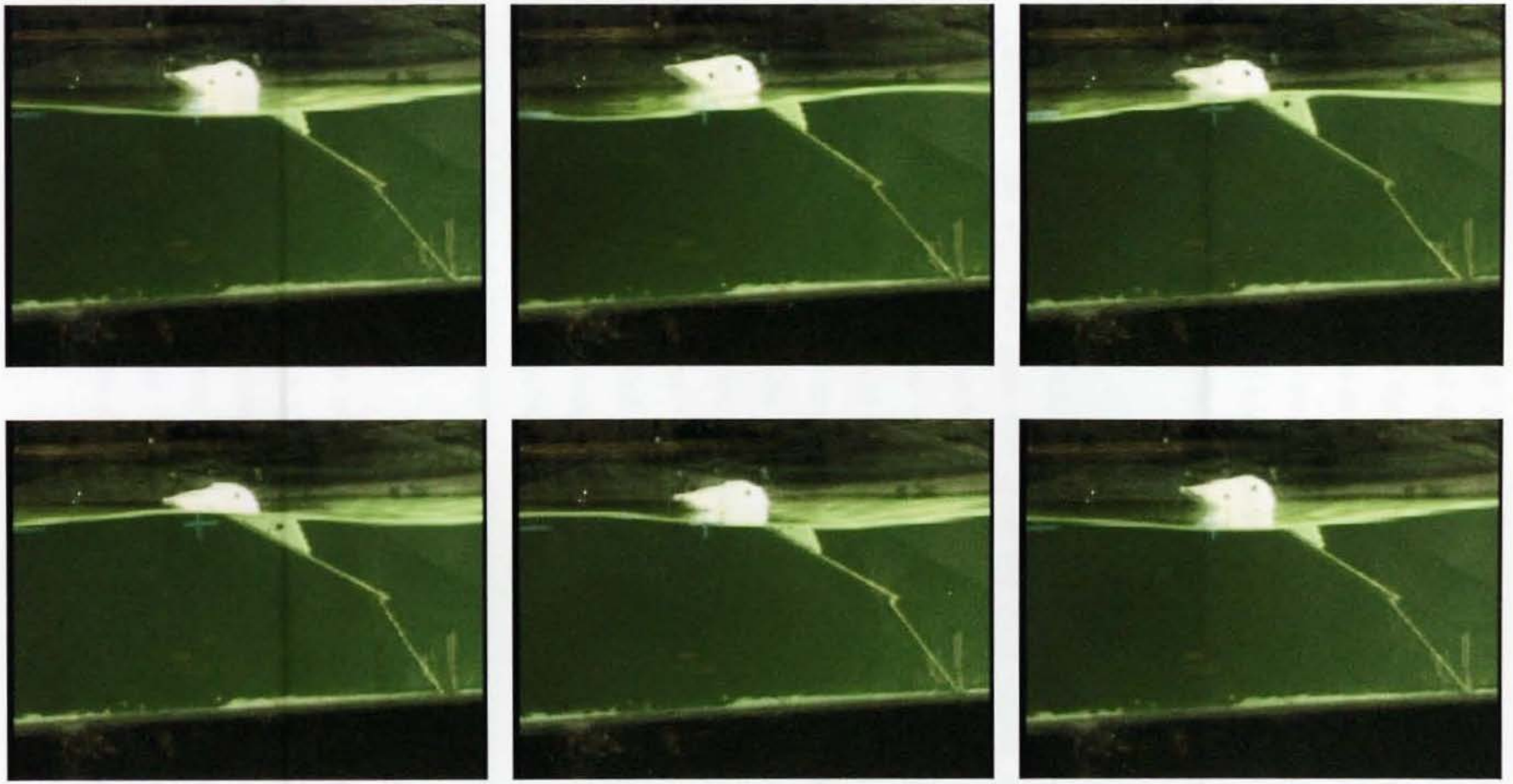

Figure 4.4 The free-floating model at 0.6 Hz regular waves. Wave height is about 10 cm. The Model begins the ellipse motion.

4.3 Motion constraint rigs and dynamometer systems

The original idea of the Sloped IPS buoy envisages it as a deep water free floating device. In order to understand the effects of inclination angle, it is reasonable in the early stages to assume that the plate will be able to provide a stable reference at the desired angle of movement and to therefore reduce the degrees of freedom. An experimental rig is required to constraint the motion of the buoy to only the sloped direction. For controlling the loading to the device so as to simulate a full-scale power take-off system, there must be an accurate dynamometer.

The first rig

A rig with two degrees of freedom, roll and landward, was built with an inclined cantilever tube supported from well above the water surface and with another bigger tube sliding on it as a carrier. The bottom of the bigger tube was sealed and attached to a force transducer via two angular contact bearings, face to face, allowing it to take the thrust and the model to roll. The force transducer was then connected to a steel rod, 12.7 mm in diameter and 1.2 m in length. The steel rod was inserted through the middle of the cantilevered tube and grasped by a pinch roller on the shaft of a DC motor. The motor was driven by a power amplifier, and formed part of a servo system. The schematic diagram of the rig is shown in appendix E. The servo feedback circuit will be described in detail in section 4.4. Closing the feedback loop revealed serious low frequency oscillations in the rig at about 10 Hz, caused by low stiffness in the push-pull rod. 10 Hz was too near the range of wave frequencies of interest and so a major re-trial was required.

The second rig

From this experience, it was clear that the push-pull rod should have higher stiffness and lower weight to avoid its vibration coupling into the control loop. A new rig was built. The mechanism of this power take-off system is shown in appendix F. A 12.7 mm diameter and 0.6 m long hollow carbon-fibre rod was used for lightness and high stiffness. The rod was shifted from the inside of the inner rail tube to the outside, thereby preventing roll motion in the model. The system

was thus reduced to only one degree of freedom. Figure 4.5 shows the photo of this rig and model in the wave tank. Figure 4.6 shows the schematic of experiment set-up in wave tank.

The buoy head of the model was a semi-circular cylinder 0.5m in width and 0.3m in diameter, made from high-density expanded polystyrene (Divinycell) pierced by tubes to carry ballast weights. The surface was coated with epoxy paint for waterproofing. The buoy head was attached to an aluminium tail plate which could freely slide on a dinghy mast tube 0.65m in diameter and 3m in length via a pair of hydrostatic bearings energised by tap water. The mast tube was connected to a vacuum suction pad, which rigidly attached to the tank floor and was maintained by a small pump. The other side of the mast tube was fixed to a scaffolding frame well above the water. The water fed hydrostatic bearing was developed because it had no corrosion, lubrication or tank pollution problems and gave very low friction. Two in line hydrostatic journal bearings were made from aluminium outer tube inserted with inner PVC tubes to avoid damage to the mast surface when the system was unpressurised. A thin wall aluminium tube connected the two bearings to make sure that they were concentric. The hydrostatic bearings needed very small clearances and any eccentricity would cause the bearings to jam and fail. Each bearing had six pockets, each 20mm in width and 30 mm in length, and fed tap water with four bars nominal pressure. 0.8mm holes between each pocket and the water-manifold acted as impedances. The aluminium tail plate was then connected via a force sensor to a hollow carbon-fibre thrust-rod and then through a pinch roller drive to a printed-armature motor controlled by a force feedback loop.

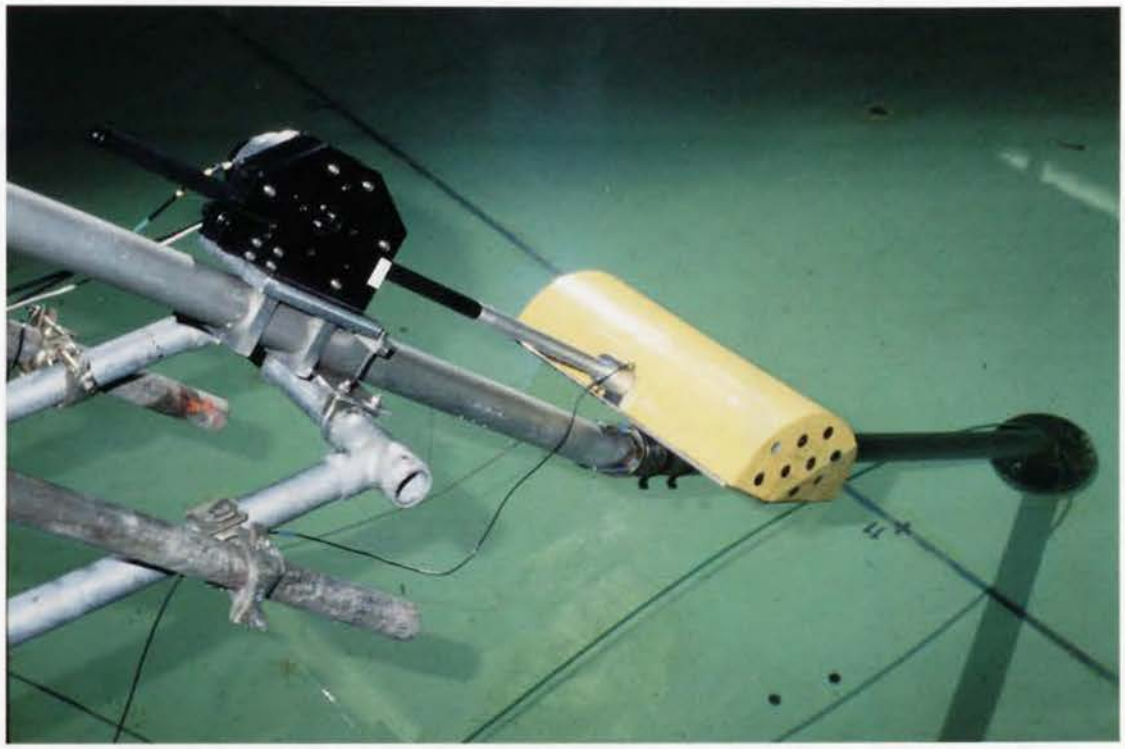

Figure 4.5. The experimental model set-up using the second rig in the Edinburgh wide tank. The model (yellow) slides on an aluminium dinghy mast via a pair of hydrostatic bearings fed by tap water. At the bottom end of the mast is a suction pad. The hollow rod of an external dynamometer (black anodised apparatus at the top left) is connected to the model via a force transducer housed inside the aluminium cup in the centre of the model.

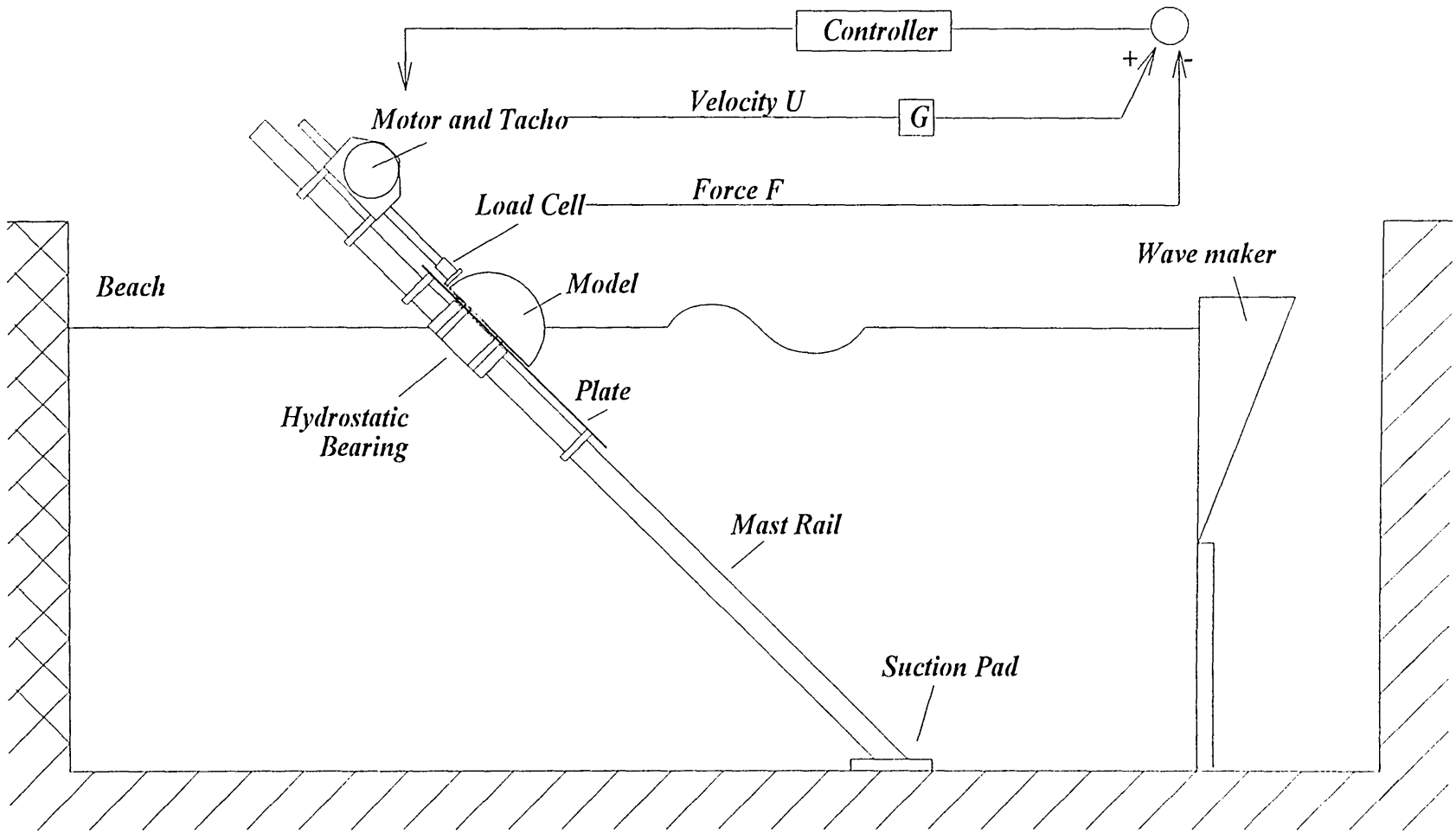

Figure 4.6. Schematic of experimental set-up in wave tank and the control loop of the power take-off system

4.4 Control system

In order to extract power from waves and to measure the hydrodynamic coefficients, a motion control system is required. This system should be able to provide a force to simulate a full-scale power take-off system and to drive the model in calm water to obtain the hydrodynamic characteristics. There is no linear hydraulic ram at the model scale size available. Hence, a simulated power take-off system was applied to the model. The first step in commissioning the mechanically complete model is to close a force feedback loop around the model and the external power take-off mechanism, which provides the linear constraint for the model motion. There are two very important aims.

The first reason for the force feedback loop is to reduce parasitic frictional loading on the model by its power take-off and motion constraint systems. Unavoidably, in a small-scale wave energy model the detailing will be different from the full-scale equivalent and will tend to exhibit relatively high levels of friction and inertia. It is desirable to reduce these effects as far as possible to be proportionally consistent with their effects in a full-scale device.

The second reason is to implement force as the command variable to the model. If we then pre-set a command signal to the power take-off command input, which is proportional to model velocity and of the correct polarity, the model motion will be damped. If we present a command proportional to the displacement from its still water position, this will be seen by the model as stiffness additional to its own inherent hydrostatic or buoyancy stiffness. Similarly an acceleration fed into command input should force the motor to modify the apparent inertia of the model. A mixed signal of displacement, velocity and acceleration can produce a complex command, which simultaneously modifies the stiffness, damping and inertia of the model.

The extent to which parasitic loading of the model by motor brush and bearing friction can be reduced is dependent on the loop gain of the force feedback system.

The feedback system takes the difference between the command input to the system and the signal from the force transducer. This difference is amplified with a finite gain, passed through filters, and sent via the power amplifier to the motor.

Figure 4.7 shows the schematic of the control circuit of the model. This is based on a force feedback loop. When a desired force is presented by the input command signal, the signal passes through a gain stage, low-pass filter, lag-lead compensator and then a power amplifier driving the motor to the model. The force transducer detects the force acting on the model then compares it with the input command signal. The upper loop shows that the position and velocity of the model are detected by a rotary position encoder and a tachometer, passed through a gain setting and then fed into the conjunction with command signal. By changing the gain setting of the velocity and position signals, the model damping and stiffness forces can be varied.

The whole servo system consists of a DC motor, a power supply, a force transducer, a tacho generator, a rotary position sensor, and control circuit. Short descriptions of these devices are given below.

Motor

A printed armature DC servo motor (type GM12 from Printed Motors Limited), is used to provide driving force for the forced oscillating tests, the damping force for the power absorbing tests and for compensating some unwanted mechanical friction loads. This motor has a very low inertia and provides a torque directly proportional to current even at low speed. Its torque constant is 11.0 Ncm/Amp. The motor shaft is fitted with a roller and with the help of an opposing spring-loaded pinch roller drives the hollow carbon-fibre rod backward and forward. Brush and bearing friction of the motor are quoted as about 3% of rated torque.

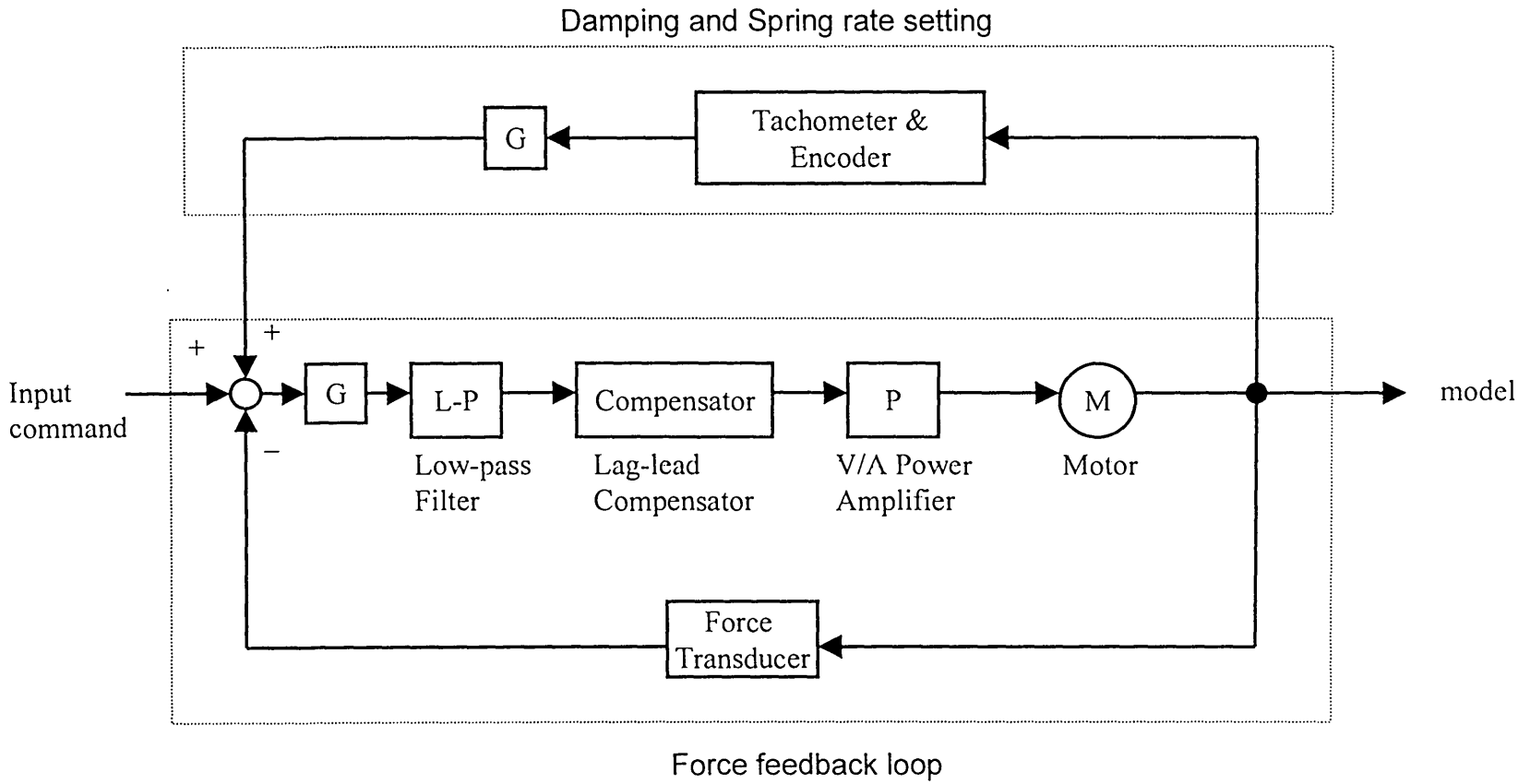

Figure 4.7. Schematic of the model servo system

Voltage to current (V/A) power amplifier

Since we want to control the force rather than the velocity of the model, the motor is used in current mode rather than voltage mode. A power amplifier for driving the motor was required and its circuit is shown in appendix G. It uses an integrated amplifier type LM12 to give current output proportional to its voltage command signal. Thus to a first approximation the force acting on the model can be defined by the voltage input to the power amplifier.

Lag-lead compensator

For an ideal closed loop, a high loop gain is desirable. The reality however is that, at some frequency, sub-components of the mechanical system start to go into oscillation, as stiffness in one part resonates with inertia somewhere else. If the feedback system is still amplifying at these frequencies, energy is fed back into oscillations and the system becomes unstable. The frequency of onset of oscillations depends on the design and construction of the system. The system must be designed to be as stiff and light as possible so that the resonances are well above the range of operational frequencies, which are of interest.

The first stage of the feedback system lets the loop gain be rolled-off with increasing frequency so that oscillations are avoided. Since the experiments were tested in a range of 0.5Hz to 2 Hz, the first stage roll off was given by a first order low-pass filter with a 9.6 Hz roll off frequency. By driving the buoy through a range of frequencies at small amplitudes, the main structure oscillating frequency was found to be at about 45 Hz. Therefore a lag-lead compensation was implemented to alter the frequency response of the feedback control system in order to attain satisfactory system performance (Dorf and Bishop, 1995). Because the phase-lag network first brings the gain down at crossover frequency, the transient response and stability are not impacted too much. The side effect of the phase-lag network is the negative phase that is added to the system between the two corner frequencies. The phase-lead network then adds a positive phase angle. Additional positive phase increases the phase margin and thus increases the stability of the system. Figure 4.8 shows

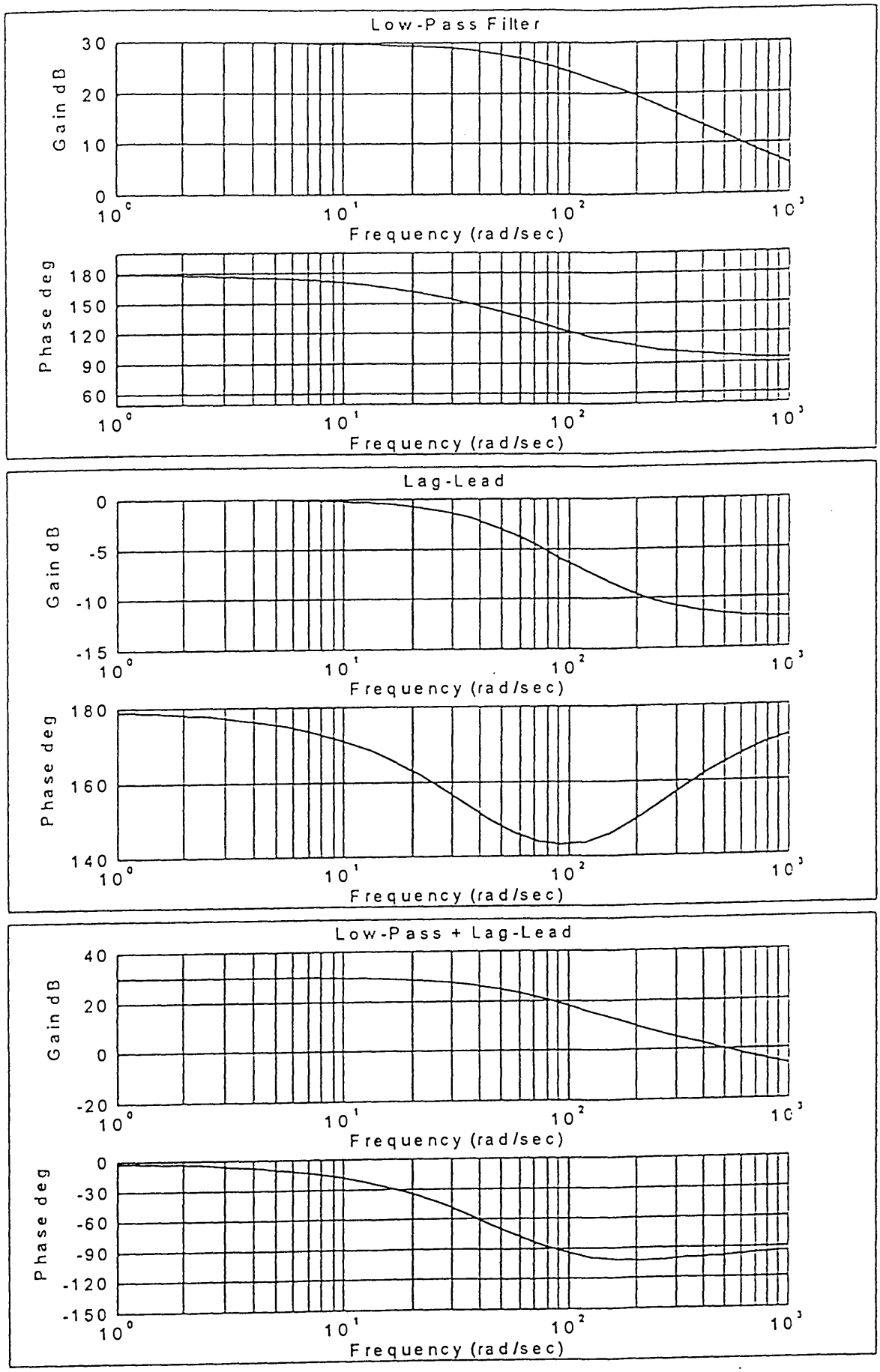

Figure 4.8 Bode diagrams of the servo loop.

MATLAB bode diagrams of the low-pass filter, lag-lead compensator and the combined response of both.

Force sensor

A force sensing transducer (load cell) was required to close the force feedback loop. The load cell should be as close to the model and as rigid as possible to raise the resonant frequency. A piezoelectric crystal-based device was chosen because of its high stiffness. A pair of piezoelectric discs, one inch in diameter and supplied by Vernitron, was constructed into a sandwich structure with a central shim electrode as shown in figure 4.9, and was sealed by self-amalgamating tape for waterproofing. It was fitted inside an aluminum cup with brass bar covered on it. A sharp-nose screw located on the brass bar to give a preload. This screw with sharp- nose was to avoid transmission of moments to load cells. The load cell also formed the physical connection between model and push rod. Piezo load cells produce charge proportional to force. These charges must then be fed into a charge amplifier to give a voltage reading.

Charge amplifier

A piezo-electric load cell gives charge out proportional to change of force across it. It can be helpful to imagine electrons being squeezed into or sucked out of the external circuit as the load cell is compressed and released. A charge amplifier is required to give a voltage proportional to force or, in other words, a voltage proportional the integral of the load cell charge output. As with any electronic integrator there is a drift problem. When the force across the cell is constant, there is no charge movement, and the amplifier is ideally required to hold its output constant. In practical a "drift back to zero" characteristic has to be introduced to prevent unavoidable small offset voltage and currents causing the charge amplifier output voltage to drift toward one or other supply voltage. The drift period sets to lowest frequencies at which the piezo cell can be used, and since it is really an AC device it has to be calibrated dynamically rather than statically, unless the charge amplifier has a very long time constant. A motor with swash plate was used to induce a sinusoidal force on the transducer in series with a calibrated load cell as shown in

figure 4.10. The time constant of the charge amplifier was about twenty seconds. The capacitor was chosen to give a calibration of 10 Newton/Volt. The circuit is shown in Appendix H.

The velocity sensor and position sensor

The velocity of the model was given by a tachogenerator attached to the back of the driving motor. Its output signal passed through a conditioning circuit to cut off noise above 30 Hz and was calibrated as 0.7 (m/s)/V. A rotary position sensor, HEDS-5500 from Hewlett-Packard, was used to detect the model position. This position sensor was fitted to the shaft of an auxiliary roller. This output of the sensor then passes a digital to analogue converter (DAC 877) to give a voltage reading.

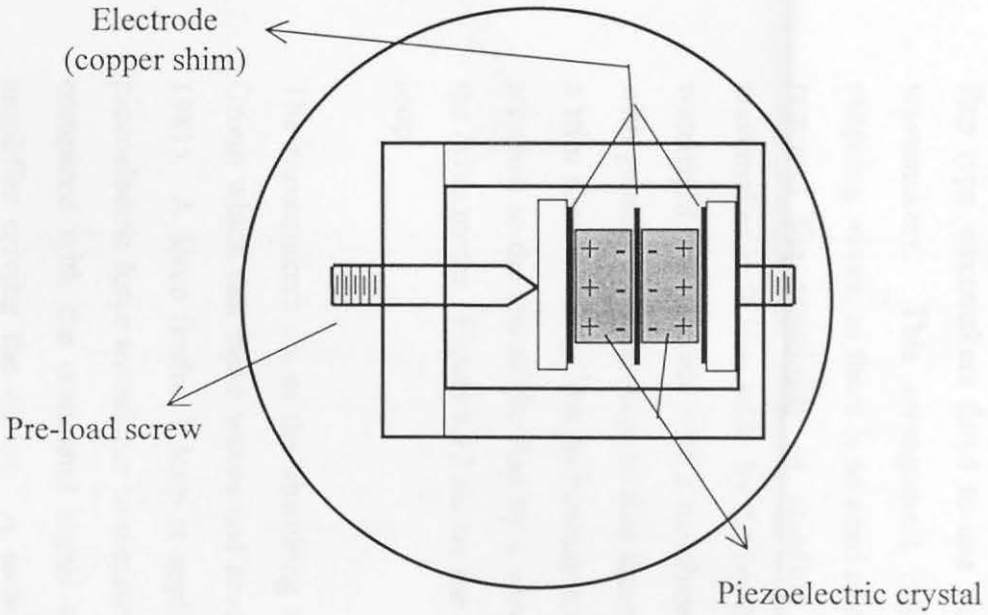

Figure 4.9. Piezoelectric force transducer

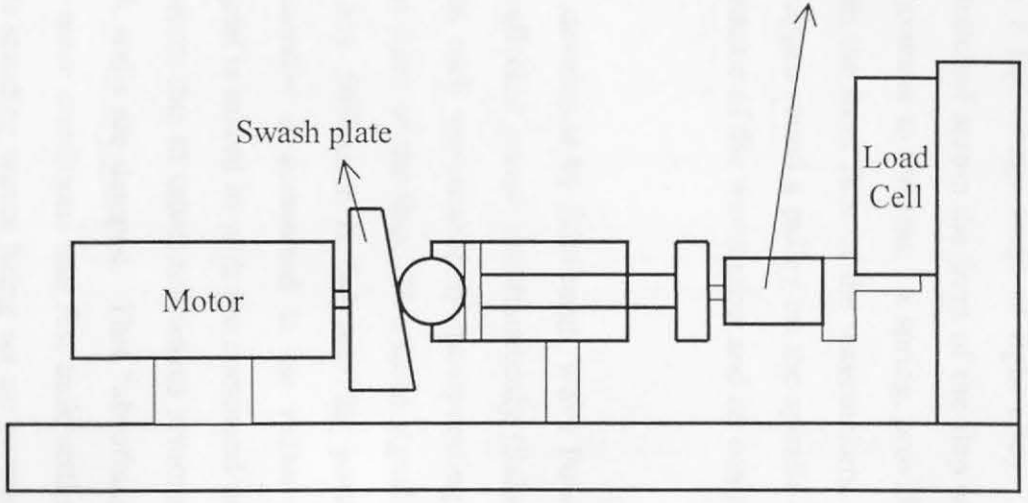

Figure 4.10. Calibration set up for force transducer

4.5 Wave tank and Wave generation

The experimental work was carried out in the "wide" wave tank at the University of Edinburgh. The external dimensions of the tank are 11m in length, 27.5m in width and 1.2m water depth. Figure 4.11 shows the layout of the tank. It has 80 flap type wavemakers fitted to one side of the tank and a dry sump behind the wavemakers. This arrangement minimises the energy required to generate outgoing waves, as there is no need to move water behind the wavemakers. It also removes the possibility of standing waves behind the wavemakers. Each wavemaker is 0.29m wide by 0.61m deep, a flat wedge made of light alloy. A watertight seal is made with a membrane stretched across the front of the flap and with gussets between them so that there is no water to the rear. A spring, provides a trim force to offset the hydrostatic load on the front face of the wavemakers, is attached to the top of the flap by a wire wrapped round a pulley on the spindle of the drive motor. Figure 4.12 shows the schematic of the wavemaker and its control loop.

The wavemakers are of the absorbing type developed by Edinburgh Wave Power Group which can make waves and absorb reflected waves simultaneously (Salter, 1981). A force feedback loop is applied to each wavemaker by incorporating a piezoelectric force transducer to measure the force of the flap. This force signal is compared with the command signal and any difference is fed into the power amplifier driving the motor. A tacho generator is connected to the motor to measure flap velocity. A function of its signal is mixed in with the command and force transducer signals, so that flap movements due to unwanted waves returning as reflections form models or from the tank walls are damped. This "absorbing" characteristic provides exceptionally stable wave conditions and fast tank settling times between experiments. It also prevents standing waves being set up between wavemakers and reflective models.

The opposite and the far side of the tank are lined with absorbing "beaches". These are vertical triangular wedge-shaped cages filled with a metal foil called

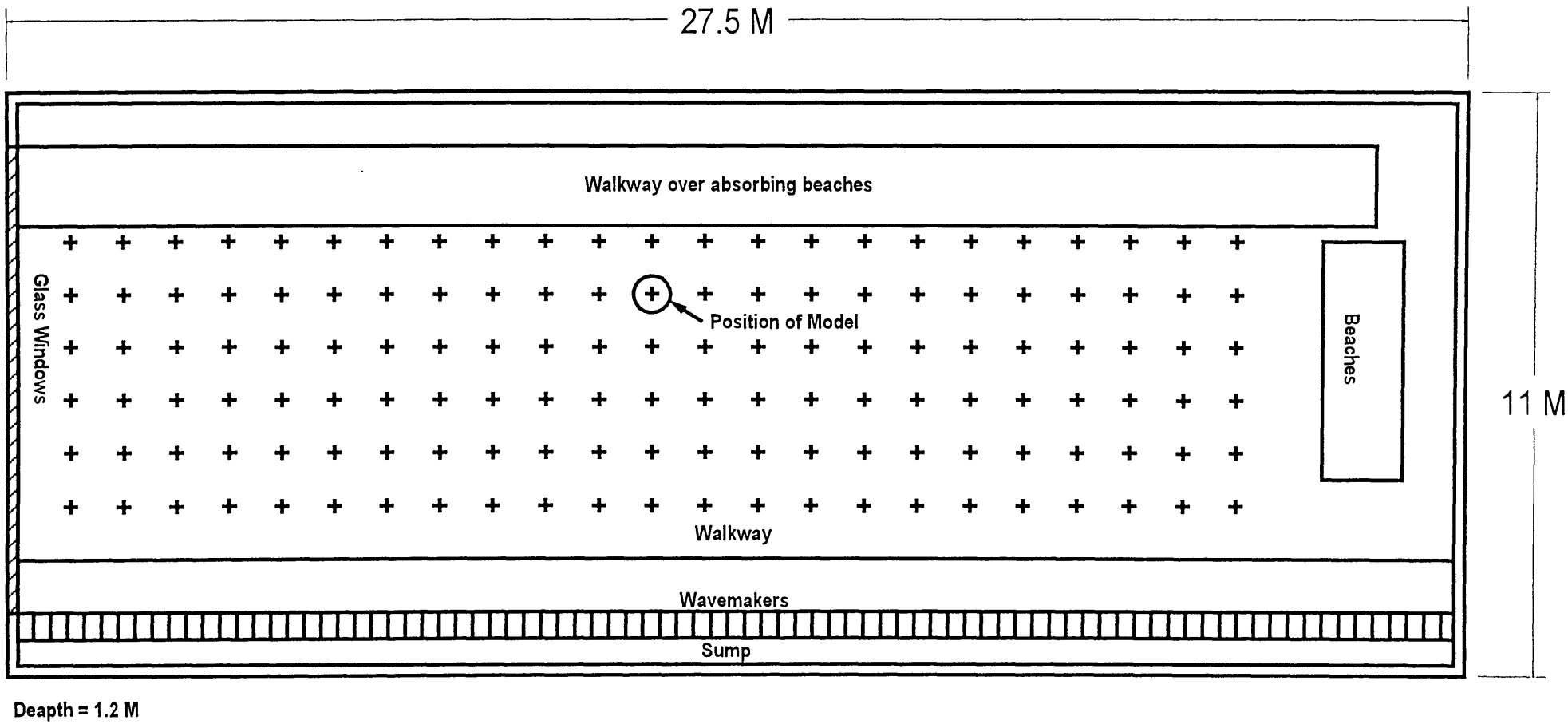

Figure 4.11. The layout of the Edinburgh Wide Tank

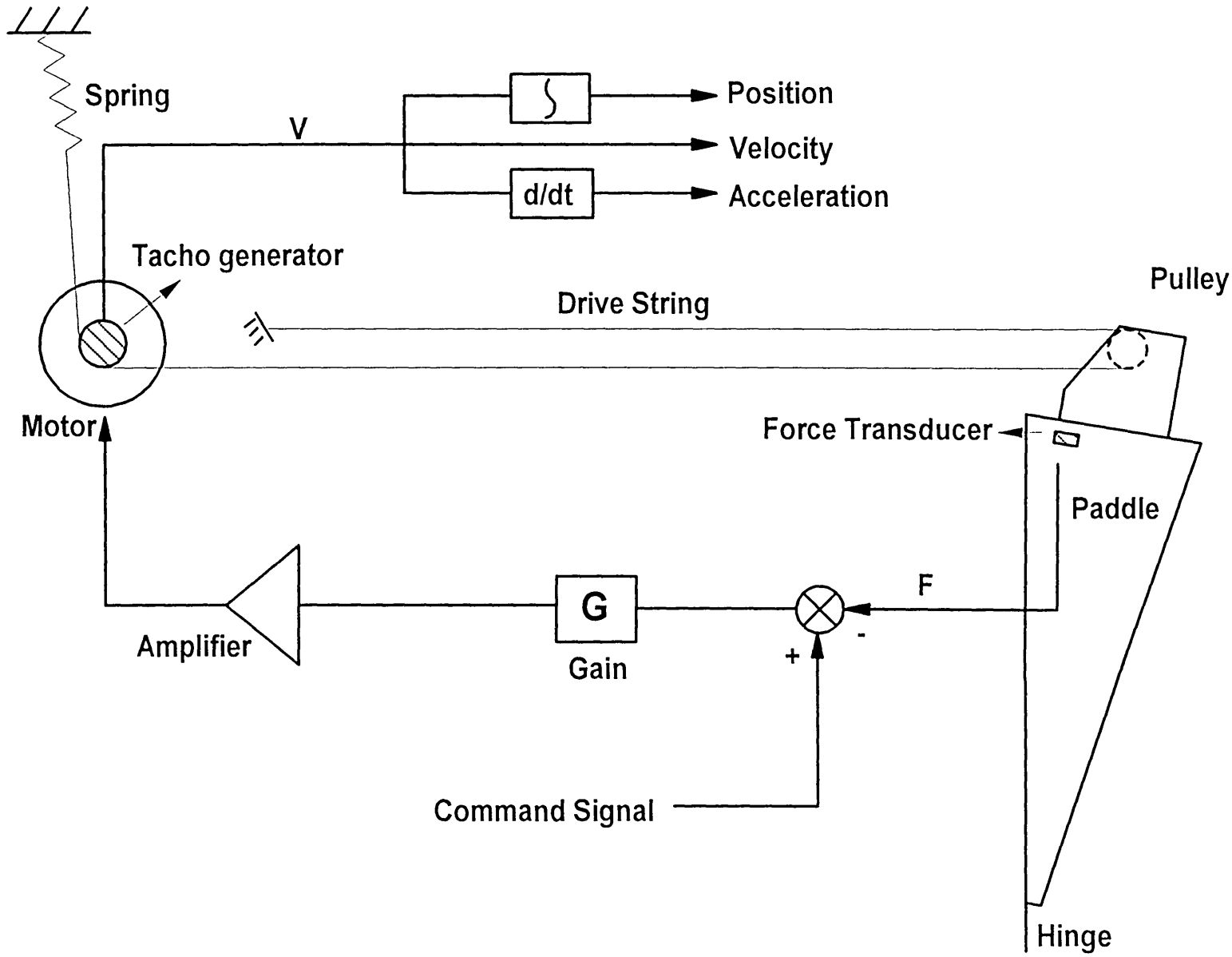

Figure 4.12. Schematic of the wave maker and its control loop.

"Expamet". Expamet has a pattern of slits cut into thin sheet, which is then pulled in such a way as to form a complex punctured three dimensional surface. The front side of the tank is fitted with glass windows, which are used for observation of waves and models under test. A more detailed description can be obtained from Jeffrey *et. al.* (1978).

In order to make three-dimensional (multidirectional) waves in the tank, the wavemakers must be able to be controlled individually. Command distribution is by time-division multiplex. Each wavemaker is addressed by the controlling computer with a command signal 16 times per second. Sea states are generally prepared "off-line" by writing text files in a special "C" like high-level language. These files are then complied in conjunction with the measured tank-transfer function to produce run-time command files (Rogers and King, 1996).

Before the wavemakers can generate accurate waves, it is necessary to calibrate the tank transfer function, which translates output signals to physical wave heights. The tank transfer function used for the experiments is given in Appendix I.

Regular waves and small mixed seas

Wave height variations

Most of the experiments were carried out in single-frequency sinusoidal waves. However, there are variations in the wave heights throughout the tank due to reflections off glass, imperfect beaches and wavemaker absorption. These effects obviously affect experiments, so wave heights need to be regularly checked.

Pierson-Moskowitz spectra

Some experiments were carried out in "mixed seas" using the Pierson-Moskowitz (PM) spectrum. The PM spectrum model describes a fully developed sea determined by one parameter, the wind speed (Pierson, 1964; Pierson and Moskowitz, 1964). This spectrum has been extensively useful in representing the extreme sea conditions for the offshore engineering.

The PM spectrum model of energy density is written as

$$S(\omega) = \frac{\alpha \cdot g^2}{\omega^5} \cdot e^{-\beta(\omega_o/\omega)^4} \qquad (4.1)$$

where $\alpha = 0.0081$ and $\beta = 0.74$.

ω is the angular frequency.

$$\omega_o = \frac{g}{U_o}$$

U_o is the wind speed measured about 19.5 meters above sea surface.

Wave period is an important parameter in the description of a sea state. The most commonly used measure of average period is zero crossing period T_z, which is sensitive to noise and bandwidth of the recording method. Mollison *et. al.* (1976) suggested that to calculate an energy period T_e from a record would be more convenient for wave energy work, provided that there was a way of measuring power. For PM spectra, the wind speed U_o is proportional to period and in particular to energy period T_e, which is closely related to the average energy velocity U_e (Jeffrey *et. al.*, 1976) and this can be expressed as:

$$U_e = \frac{g \cdot T_e}{2} = 0.9773 \cdot U_o \qquad (4.2)$$

Thus

$$T_e = 0.626 \cdot U_o \qquad (4.3)$$

Equation 4.1 can be simplified as

$$S(\omega) = \frac{0.7795}{\omega^5} \cdot e^{(-1052.4587/T_e^4\omega^4)} \qquad (4.4)$$

The detailed description of the PM spectrum and the tank measurements are given in Appendix F.

4.6 Wave gauges and wave measurement

In order to understand the interaction of the device with water, it is essential to accurately measure the wave amplitude. A two-point wave measurement method is described in section 4.6.2.

4.6.1 Three-wire wave-gauge

For measuring the wave heights, resistive type wave probes were employed. The conventional resistive type wave probe consists of two wires. When the two parallel wires are held vertically partly submerged in water, the conductance between them is proportional to the depth of immersion and to the conductivity of the water. The conductance, and hence immersion, can be measured by applying an AC voltage between the wires and measuring the current which flows. The current is proportional to the probe immersion as long as the water conductivity remains constant. The alternative voltage prevented polarisation effects. As the measurement is made using alternating current, the probe circuit must incorporate a demodulator to recover the wave signal.

Since the conductivity of the water changes even over quite short periods, the probe calibration also changes. The Edinburgh Wave Group designed a resistive type wave gauge with a third wire for compensating the change of the water conductivity. The wave gauge consists of two parallel stainless rods and a short rod attached to one side and always fully immersed in the water as shown in figure 4.13. A calibrated current (I_{ref}) is applied to the wire (2), then fed into an operational amplifier to give the rod (1) a reference voltage (V_{ref}).

$$V_{ref} \propto \frac{I_{ref}}{S_w} \tag{4.5}$$

where

S_w is the conductivity of water.

The current between rod (1) and rod (3) is measured. This can be shown as follows:

$$I_{mea} \propto V_{ref} \cdot S_w \cdot D_{im} \qquad (4.6)$$

where

I_{mea} is the current between rod (1) and (3).

D_{im} is the depth of immersion.

Combing equations 4.5 and 4.6 gives

$$I_{mea} \propto I_{ref} \cdot D_{im} \qquad (4.7)$$

The wave height can therefore be calculated form measuring the current I_{mea}.

Because of variation in wave height around the tank, an array or line of wave gauges is usually better than a single one. Therefore, the wave gauges should be put as near to each other as possible. Unfortunately, very small distances between two gauges cause interference between the AC fields. Some tests were done to investigate the distance effect. Figure 4.14 shows the interference with respect to the distance. The results indicated that the interference is worst at distances under 300 mm. This determines the minimum gap spacing. An alternative method is to use gauges energised at different times by using a time division multiplexer.

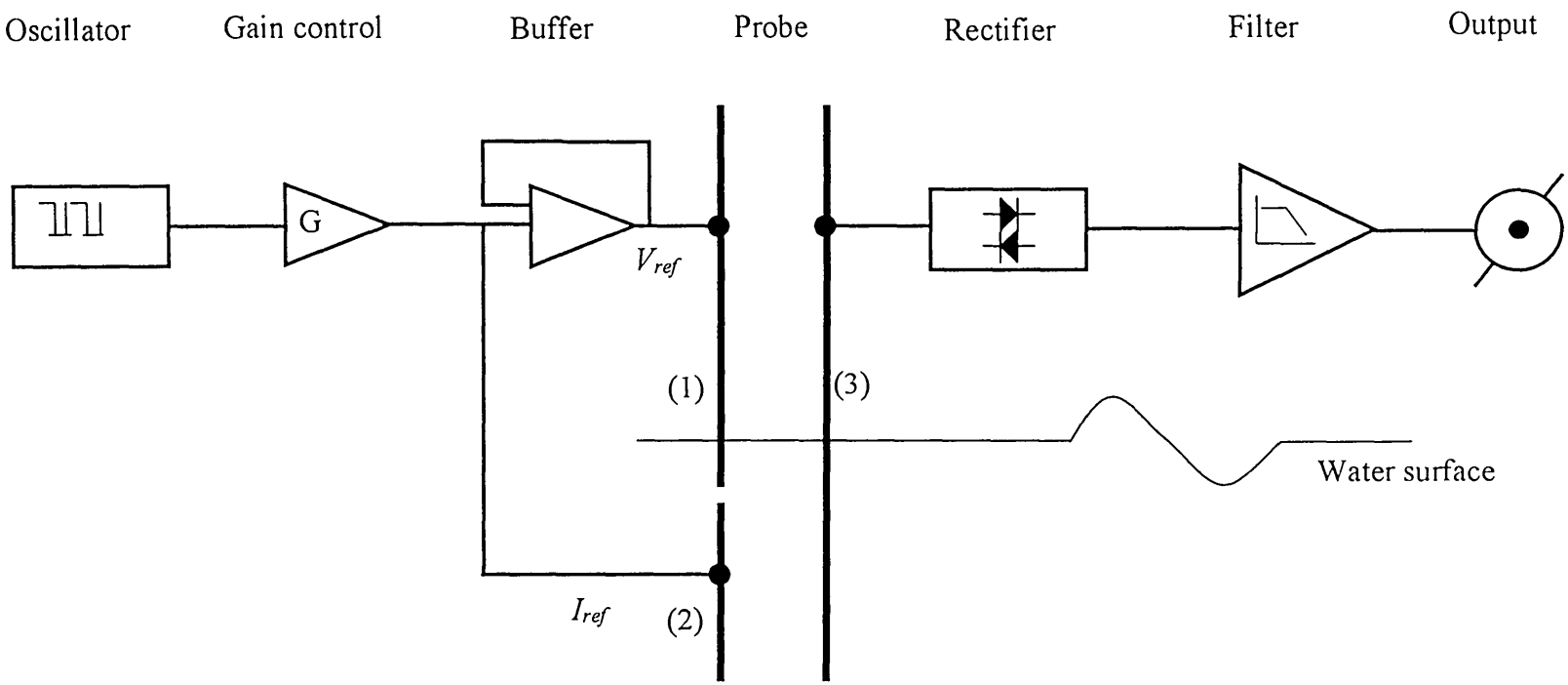

Figure 4.13. Three-wire resistive wave gauge

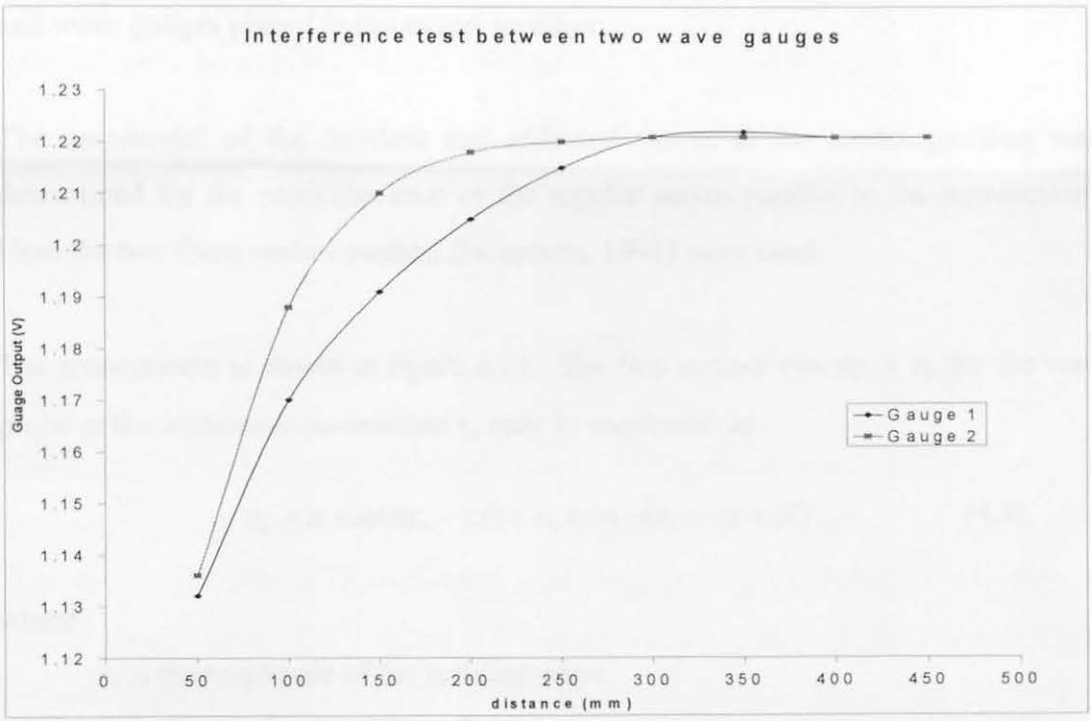

Figure 4.14. Interference test between two compensated wave gauges. When the distance between two gauges is bigger than 300 mm, there is no measurable interference between them.

4.6.2 Incident and reflected waves

In a three-dimensional tank wave measurements particularly in the presence of a model are difficult, because reflecting waves come from many different directions. However as the repeatability of the waves is known to be excellent, in this work the difficulty was reduced by measuring the waves with the model removed from thank and wave gauges placed in the model position.

The amplitudes of the incident and reflected waves at the model position were determined for the particular case of the regular waves parallel to the wavemakers. Here the two fixed probes method (Iscaacson, 1991) were used.

The arrangement is shown in figure 4.15. The free surface elevation η_n for the wave probe at the horizontal co-ordinate x_n may be expressed as:

$$\eta_n = a_i \cos(kx_n - \omega t) + a_r \cos(-kx_n - \omega t + \beta) \qquad (4.8)$$

where

a_i is the amplitude of the incident wave.

a_r is the amplitude of the reflected wave.

k is the wave number ($2\pi/\lambda$).

ω is the angular frequency.

t is the time.

β is the phase angle between incident and reflected wave.

The distance between probes is d, *and* $kx_2 = k(x_1+d)$.

Equation 4.8 in complex notation,

$$\eta_n = a_i e^{i(kx_n+\omega t)} + a_r e^{-i(kx_n+\omega t-\beta)} \qquad (4.9)$$

The recorded elevation at the probes can be written as:

$$\eta_n = A_n e^{i(\phi_n+\delta_n-\omega t)}$$

(4.10)

where

ϕ_n is the theoretical wave phase at the nth probe.

δ_n is the measured phase at the nth probe relative to the phase at first probe.

For two fixed wave probe method, $n = 1, 2$.

The incident and reflected wave amplitudes are derived from equation 4.10.

$$a_i = \frac{1}{2|\sin(kd)|} \cdot (A_1^2 + A_2^2 - 2A_1A_2\cos(kd + \delta_2))^{\frac{1}{2}} \qquad (4.11)$$

$$a_r = \frac{1}{2|\sin(kd)|} \cdot (A_1^2 + A_2^2 - 2A_1A_2\cos(kd - \delta_2))^{\frac{1}{2}} \qquad (4.12)$$

The gauge distance d must avoid $kd \approx n\pi/2$, where n is integral. In the case of the experiments undertaken here, the wave gauge distance was chosen as $\lambda/4$ for each testing wave frequency. Tests were carried out to investigate the beach reflections in the Edinburgh wave tank. Figure 4.16 shows the results of the ratio between beach reflection and incident wave against the wave steepness, which equals to the wave height to the wave wavelength. The results show that the lower wave steepness, the worse beach absorption. When the steepness is above 0.02, the ratio of reflected and incident wave is less than 10%.

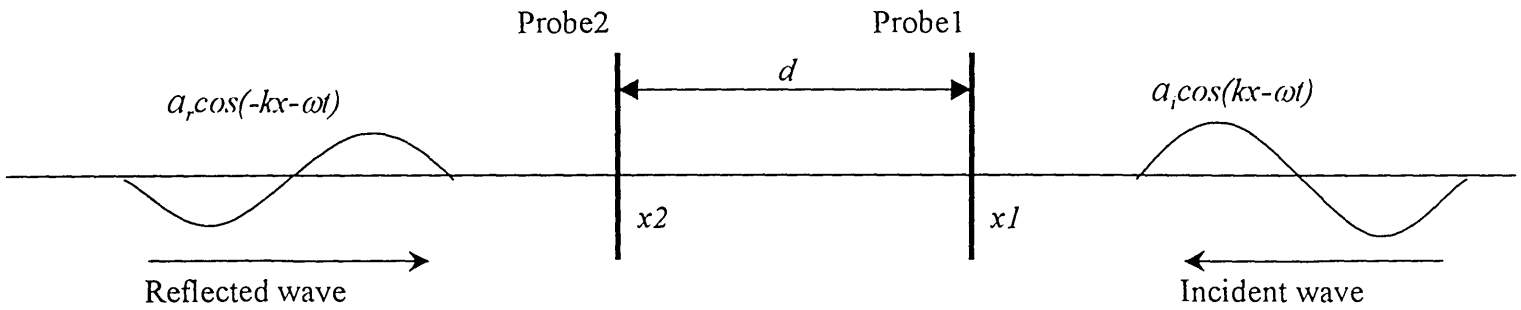

Figure 4.15. Arrangement of wave gauges for measuring the reflected waves.

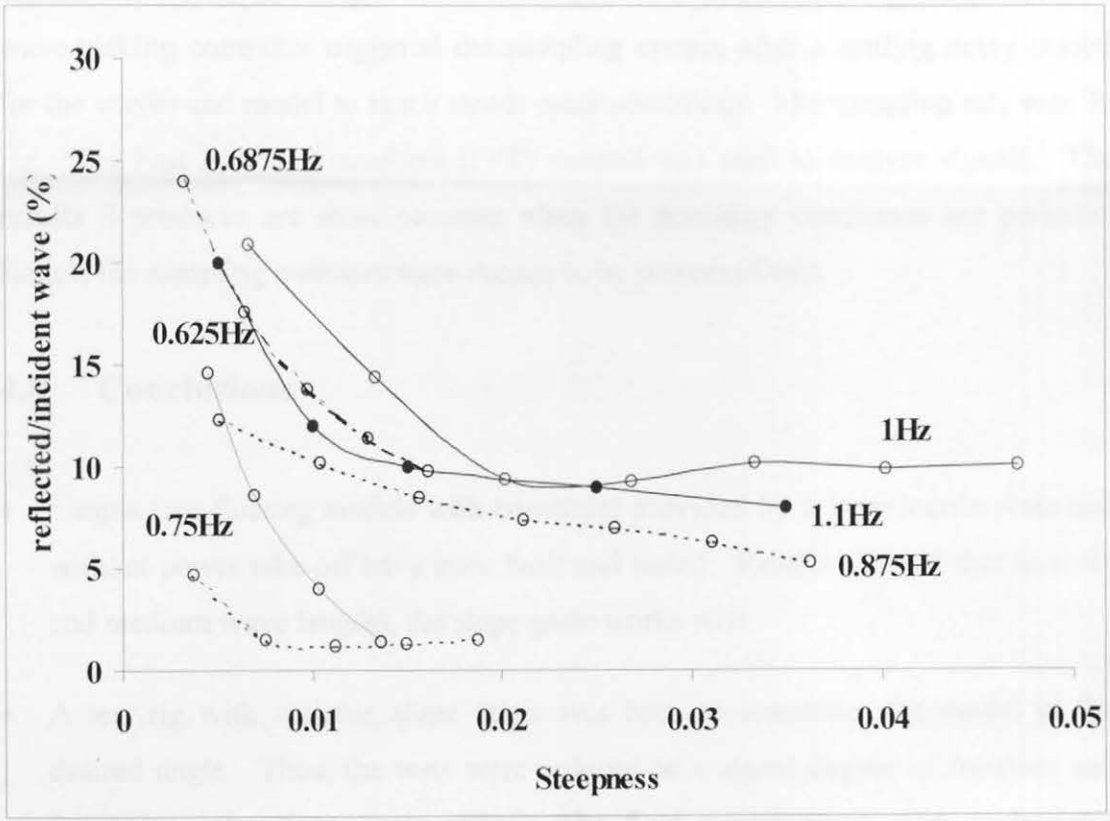

Figure 4.16. Beach reflections in the wave tank. Steepness equals the wave height divided by the wavelength.

4.7 Sampling system

A data sampling system was employed to collect force, velocity and position information for the model. Transducer signals were passed to the sampling computer via an interface (DT-21Ez by Data Translation Ltd.). The interface configures the signals into a form and range, which is compatible with the sampling computer. The wave-making computer triggered the sampling system after a settling delay period for the waves and model to reach steady-state conditions. The sampling rate was 32 Hz. The Fast Fourier Transform (FFT) method was used to analyse signals. The results it produces are most accurate when the boundary conditions are periodic. Hence, the sampling numbers were chosen to be powers of two.

4.8 Conclusions

- Simple free-floating models with constraint provided by a large inertia plate and without power take-off have been built and tested. Results showed that in short and medium wave lengths, the slope-plate works well.

- A test rig with variable slope angle was built to constraint the model at the desired angle. Thus, the tests were reduced to a signal degree of freedom and focused on the slope angle effect. The final model set-up with underwater hydrostatic bearing is described.

- A control system contained a motor and feedback circuit was built to simulate the power take-off system and the control the motion of the model. The components of the control system are described.

- The wave tank layout and apparatus are described. The wave generation including regular and irregular waves are also described.

- Use of three wire wave gauges in the tests is discussed. The measurement method of the incident and reflected waves is described.

Chapter 5

Experimental work in regular waves

5.1 Chapter Summary

In this section the techniques and results of a programme of tank tests in regular waves on the inclined buoy are described and discussed. A simplified sharp cornered buoy was constrained by a fixed guide rod to move at four different angles, of 35, 45, 60 and 90 degrees, of inclination. Two series of tests were conducted. The object of the first tests was to obtain the hydrodynamic coefficients of the model. The object of the second series of tests was to measure power capture in regular waves. Work in mixed seas will be discussed in chapter seven.

The hydrodynamic coefficients are required to solve the equation of motion (equation 3.12) for the model. Two things are needed, the radiation impedance and the wave force coefficient. Both are complex quantities and are functions of wave frequency and wave height. In the radiation impedance tests the model was driven as a wavemaker whilst its velocities and forces were logged. In the wave force coefficient tests the model was locked and the forces induced upon it by incident waves were measured. The natural frequency of the device can also be obtained from the radiation impedance tests. The detail will be discussed in section 5.2.3.
The power capture tests were carried out by measuring the mean value of the power produced by an idealised power take-off system using calculated values of optimal damping set for each period. Corresponding wave conditions were measured and

the power outputs were converted to efficiencies to compare with values calculated by using the measured hydrodynamic coefficients. Figure 5.1 shows an outline of the experimental procedures in regular waves.

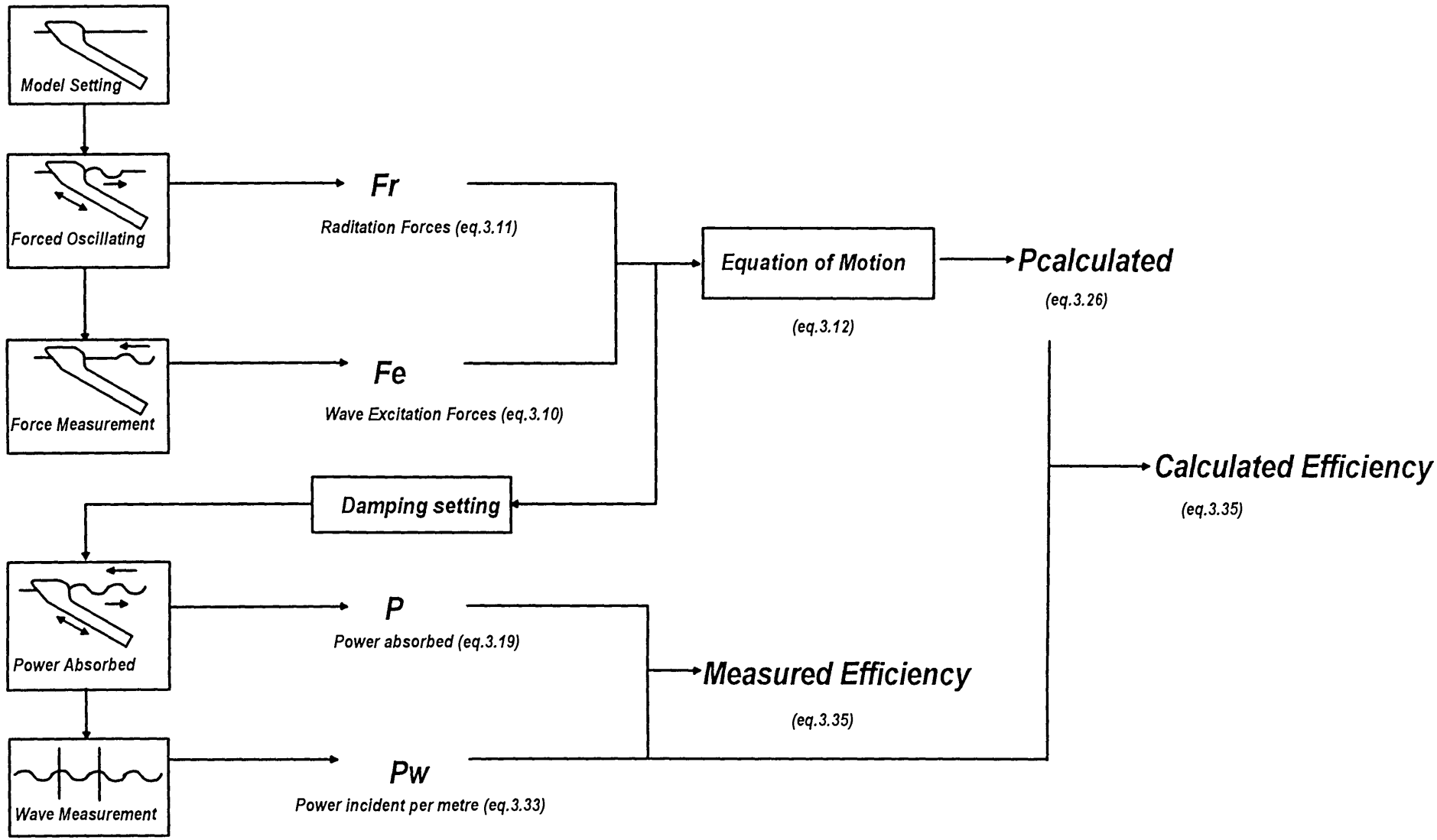

Figure 5.1. Outline of the experimental procedures in regular waves.

5.2 Experimental determination of the hydrodynamic coefficients

A solution of the floating body motion problem at sea requires the determination of the dynamic equilibrium of forces and moments. According to the equation 3.10, the load on the model can be classified into two parts, one is the device radiation force and the other is the wave excitation force. The radiation force is due to a body oscillating near to the free surface experiencing a retarding force proportional to its velocity with this radiation energy generating waves which travel away from the body. The wave excitation force is due to an incident wave train acting on the body when it is held fixed and is a function of the incident wave frequency and height.

For the radiation force measurements, there are two methods that can be used. One is to measure the step response of the model and the other is to use the forced oscillating technique.

The step response is a common tool for obtaining the damping coefficients of a simple dynamic system, which consists of spring, mass and damper, by applying a step force (impulse) and measuring its decay curve of resettling motion. A floating structure can also be treated as a simple oscillating system but with frequency dependent inertia and damping. However, the damping coefficients of a floating structure in calm water are only related to its body geometry and the frequency of the wave excitation force. Therefore, if the geometry and inertia of the buoy are unchanged but vary the spring term by adding external springs, the natural frequency of the model will depend on the setting spring rate only. The frequency-dependent damping-coefficients can then be obtained by measuring each decay curve at a different frequency and the frequency-dependent added-inertia can be obtained from the natural oscillating frequency. This method does not require waiting for the system to achieve steady-state conditions. Therefore, This is good for experiments conducted in a small tank or in a tank with poor beaches or wave absorbers, since the decay curve can be obtained before the reflecting waves come back to the model.

The forced oscillating test is another common tool for measuring the response of a dynamic system. Simple harmonic excitations are applied to the system and the system is assumed to give a steady-state response with the same frequency as the input. By comparing the input and the output of the system, the magnitude and phase can then be achieved. This method has been employed for these experiments since it is less time consuming and potentially has infinite frequency resolution (ie. determined by the drive oscillator). The detail is described below.

5.2.1 Forced oscillating tests

Haskind and Rieman in 1946 developed the forced oscillation experimental method with a ship model at zero forward speed to obtain its hydrodynamic characteristic (Gerritsma, 1991). In this method, a scale model was forced to carry out harmonic oscillation motion with water initially at rest in a range of known amplitudes and frequencies. The required force was split up into a component in phase with the velocity of the body to obtain added damping, whereas the quadrature component was associated with added inertia and restoring force. Their results showed frequency-dependent damping, vanishing at high and low frequencies, and frequency-dependent added inertia. This forced oscillating method is an easily implemented method for ship and offshore researchers to determine the hydrodynamic characteristics.

Recalling the equation of motion 3.12,

$$F(\omega) = W(\omega) \cdot a(\omega) + Z(\omega) \cdot U(\omega)$$

In the absence of incident waves, $Wa=0$, and the equation can be reduced to:

$$F(\omega) = Z(\omega) \cdot U(\omega) \qquad (5.1)$$

The system then can be simplified as a simple dynamic system. The input is a simple harmonic force and the output is the velocity of the model. The transfer function between input and output is the hydrodynamic impedance of the model, which can be shown as:

$$Z(\omega) = \frac{F(\omega)}{U(\omega)}$$

The power take-off system was used to provide the driving force for the oscillating motion. The thrust rod was parallel to the model slide allowing force only in the direction of model motion. A force transducer was connected between thrust rod and model to measure the load acting on it. A dynamic signal analyser HP-35665A generated the driving signal, which swept from 0.5 Hz to 2 Hz in 400 intervals producing the frequency resolution of 1/267 Hz. The signal then fed into the control circuit as a command input. The signals from force and velocity transducers were fed into the signal analyser, allowing the frequency response to be measured.

Results of the frequency response of forced oscillation experiments are normally presented by the Bode chart showing magnitude and phase against frequency. Here, the frequency responses are plotted in complex form, which includes the real and imaginary parts, since it is more convenient for further calculations and useful for understanding the hydrodynamic coefficients.

The results obtained for the 45 degrees slope angle were plotted as real and imaginary components in figure 5.2 and 5.3. The two lines in these figures show the good repeatability of the tests. The lines in the figures, which join up the experimental points, have a 'jagged' or sawtooth appearance. This is common characteristic of frequency domain results from wide tank tests with small frequency increments. It is due to a fraction of the radiated waves being reflected off boundaries of the wave tank and returning to interfere with the motion of the mode (Skyner, 1987). For a given model position the jagged pattern repeats exactly. When the model is moved to different position, the detail of the jagged pattern clearly changes. This is due to the relations between reflected wavelength and the distance of the model to the tank boundaries.

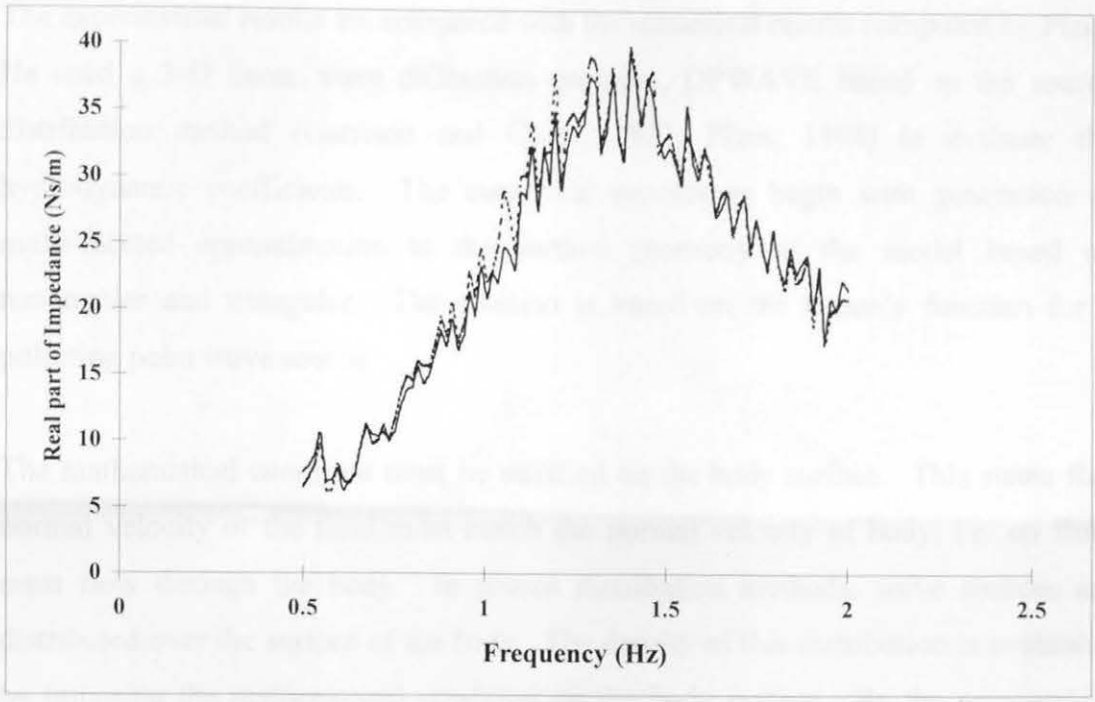

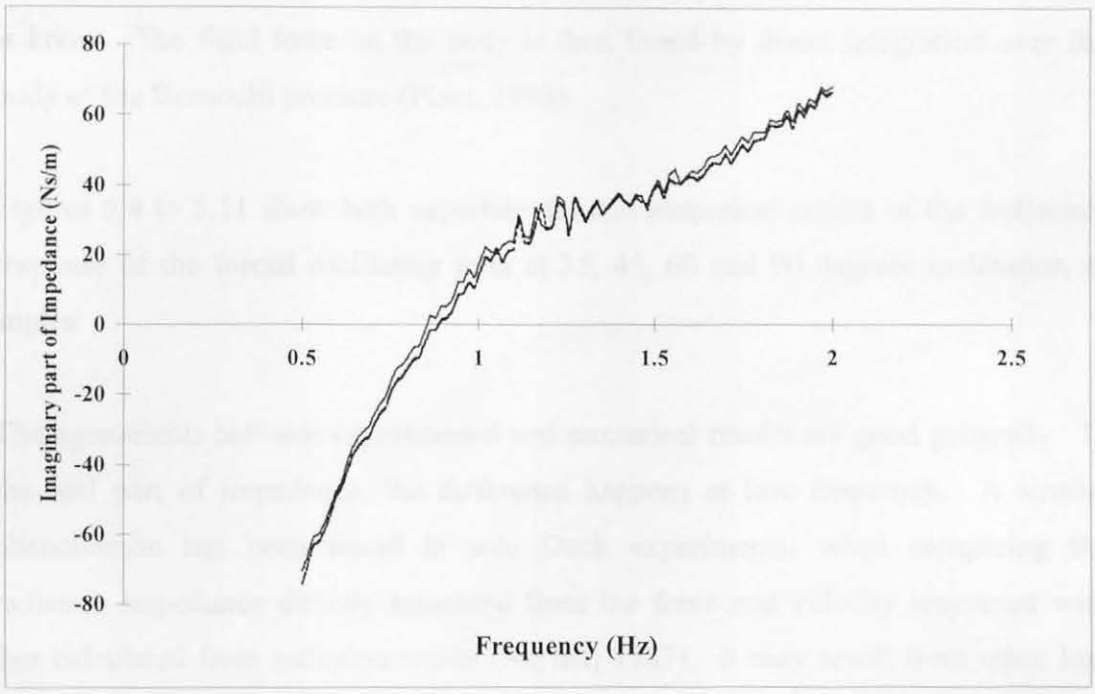

Figure 5.2 and 5.3. The real part (above) and imaginary part (below) of radiation impedance of the model at 45 degrees slope angle. Both results show good repeatability for two separate tests shown superimposed. The natural frequency of the model is about 0.85 Hz.

The experimental results are compared with the numerical results computed by Pizer. He used a 3-D linear wave diffraction program, DPWAVE based on the source distribution method (Garrison and Chow, 1972; Pizer, 1994) to evaluate the hydrodynamic coefficients. The numerical procedures begin with generation of multi-faceted approximation to the surface geometry of the model based on rectangular and triangular. The solution is based on the Green's function for a pulsating point wave source.

The mathematical condition must be satisfied on the body surface. This states that normal velocity of the fluid must match the normal velocity of body, i.e. no fluid must flow through the body. In source distribution methods, wave sources are distributed over the surface of the body. The density of this distribution is evaluated by imposing the mathematical condition on the body surface. By the principal of superposition all the other conditions are automatically satisfied and the fluid motion is know. The fluid force on the body is then found by direct integration over the body of the Bernoulli pressure (Pizer, 1993).

Figures 5.4 to 5.11 show both experimental and numerical results of the frequency response of the forced oscillating tests at 35, 45, 60 and 90 degrees inclination of angles.

The agreements between experimental and numerical results are good generally. In the real part of impedance, the difference happens at low frequency. A similar phenomenon has been found in solo Duck experiments, when comparing the radiation impedance directly measured from the force and velocity responses with that calculated from radiation waves (Skyner, 1987). It may result from other loss terms, perhaps acting in parallel with the hydrostatic spring, which do not produce radiation waves. In the imaginary part, the small discrepancies are at both high and low frequency. At the high frequency the value is presented by the mass of the model and at low frequency the value is presented by the hydrostatic spring of the model.

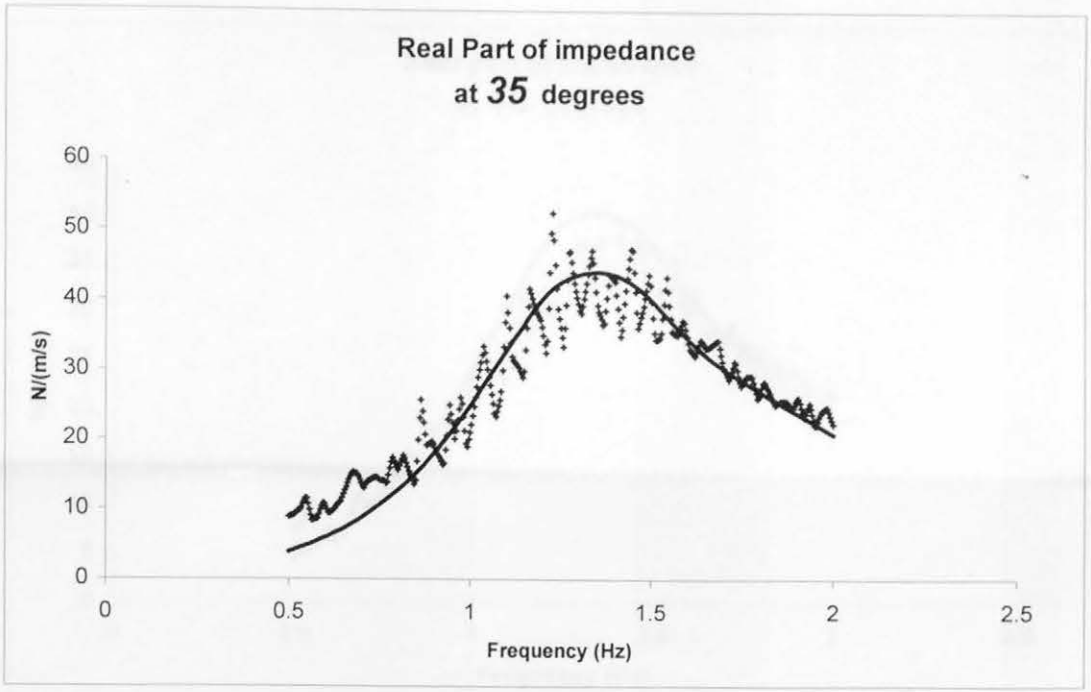

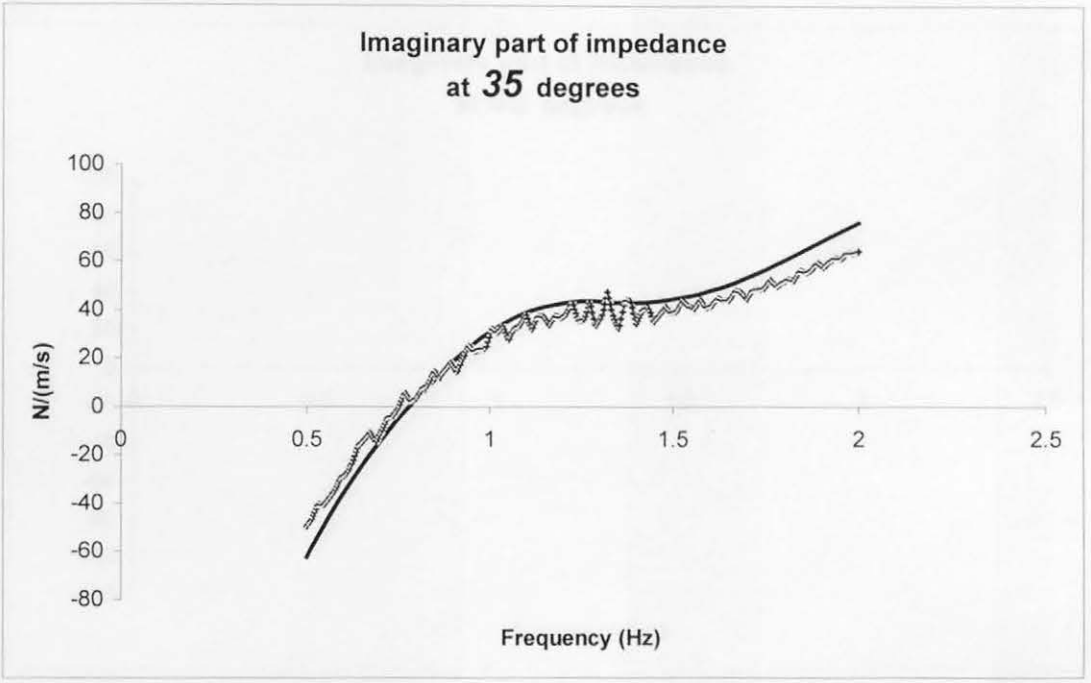

Figure 5.4 and 5.5. The real part (above) and the imaginary part (below) of the radiation impedance of the model at 35 degrees inclined angle. The smooth curve is for the numerical results and the sawtooth line for the experimental results. The natural frequency of the model is about 0.73 Hz.

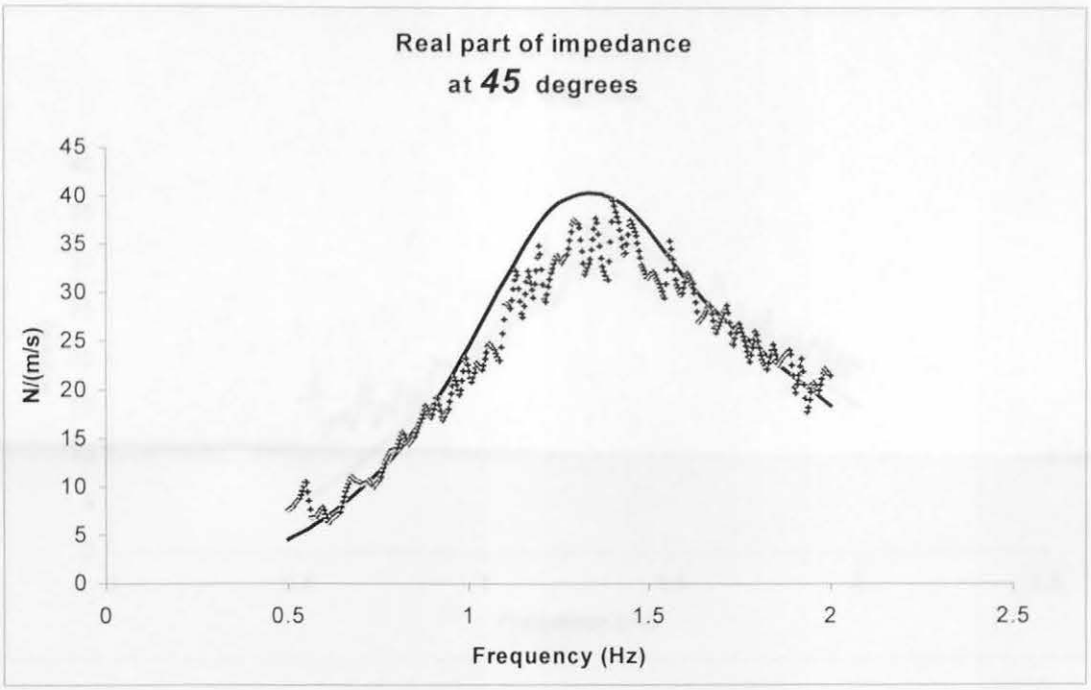

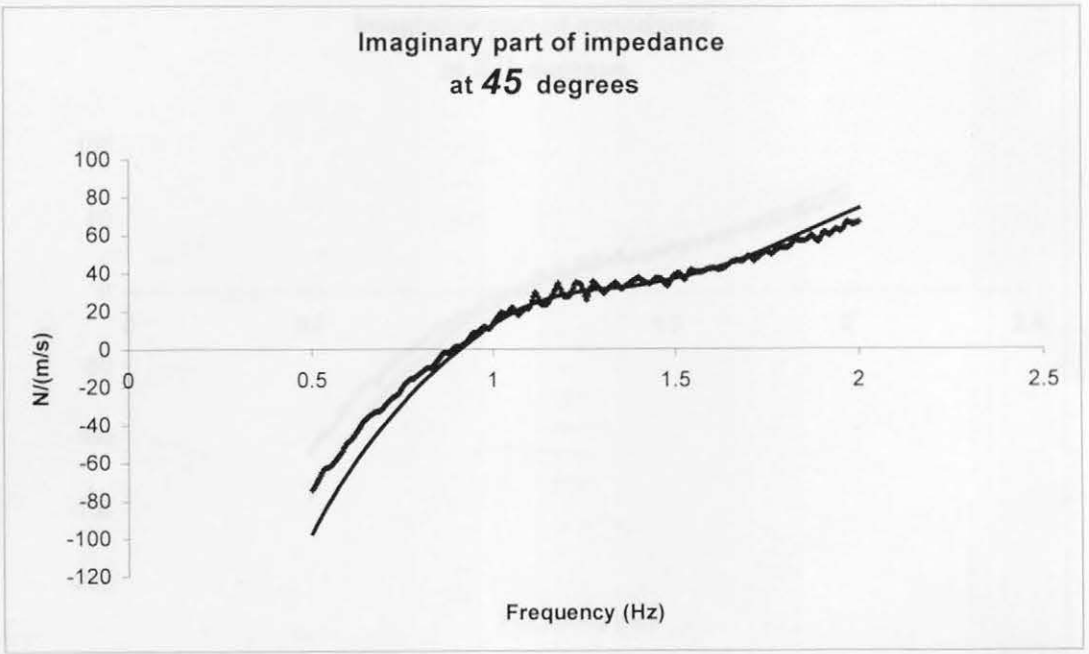

Figure 5.6 and 5.7. The real part (above) and the imaginary part (below) of the radiation impedance of the model at 45 degrees inclined angle. The smooth curve is for the numerical results and the sawtooth line for the experimental results. The natural of the model is about 0.85 Hz.

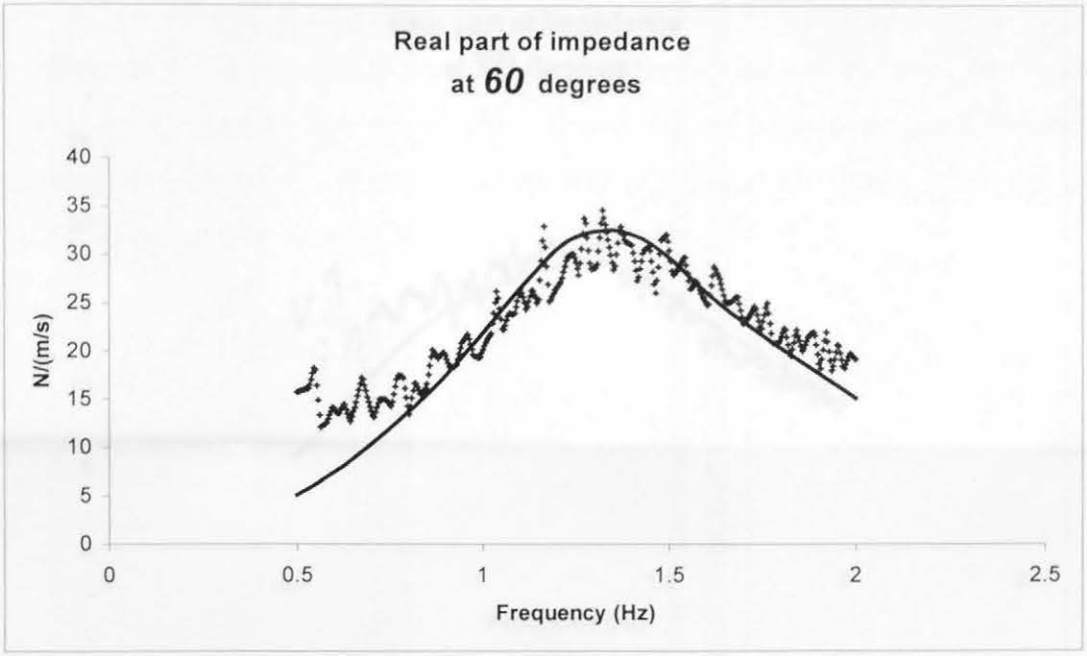

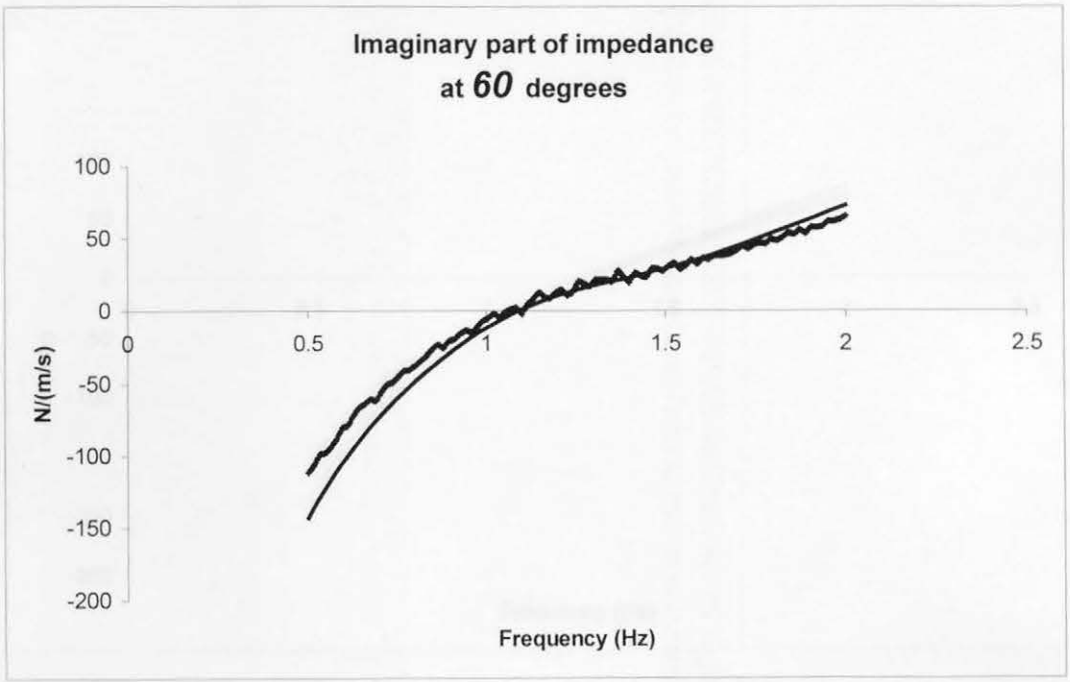

Figure 5.8 and 5.9. The real part (above) and the imaginary part (below) of the radiation impedance of the model at 60 degrees inclined angle. The smooth curve is for the numerical results and sawtooth line for the experimental results. The natural frequency of the model is about 1.07 Hz.

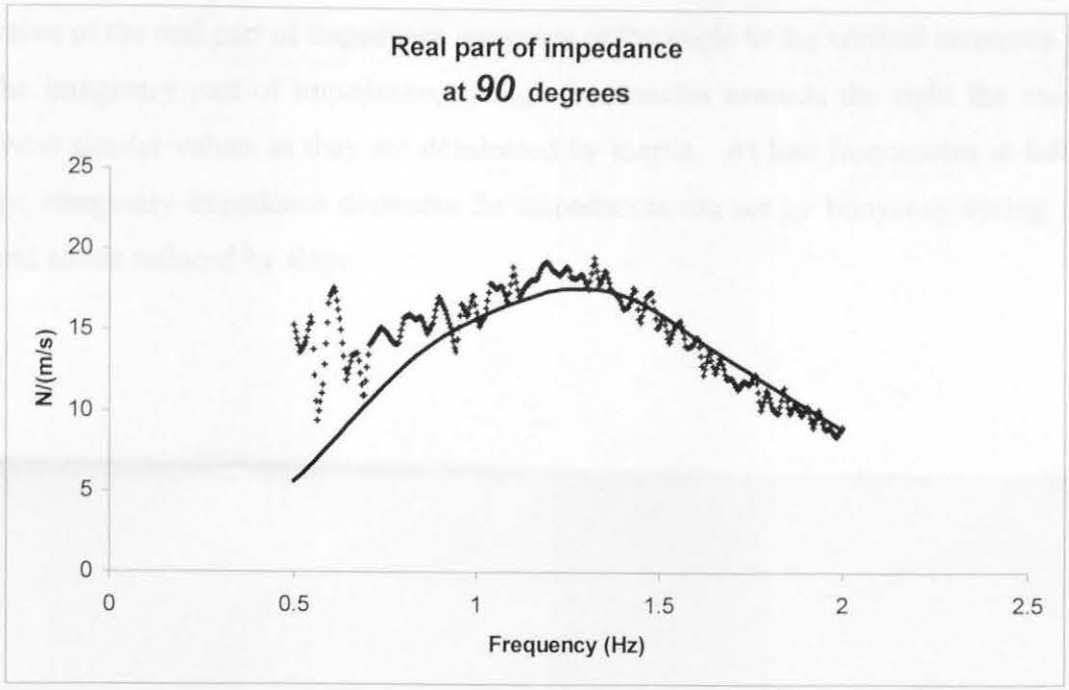

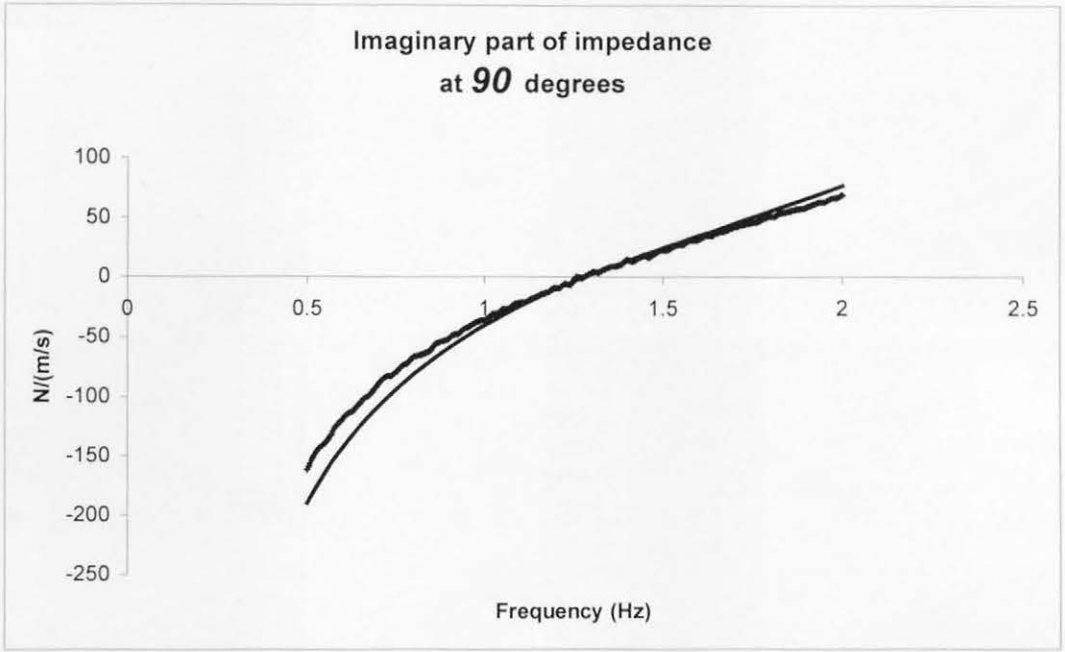

Figure 5.10 and 5.11. The real part (above) and the imaginary part (below) of the radiation impedance of the model at 90 degrees inclined angle. The smooth curve is for the numerical results and the sawtooth line for the experimental results. The natural frequency of the model is about 1.28 Hz.

Figure 5.12 shows the radiation impedance at four slope angles together. The peak value of the real part of impedance increases as the angle to the vertical increases. In the imaginary part of impedance, at high frequencies towards the right the curves show similar values as they are dominated by inertia. At low frequencies at left of the imaginary impedance diagrams the impedances are set by buoyancy spring rate and so are reduced by slope.

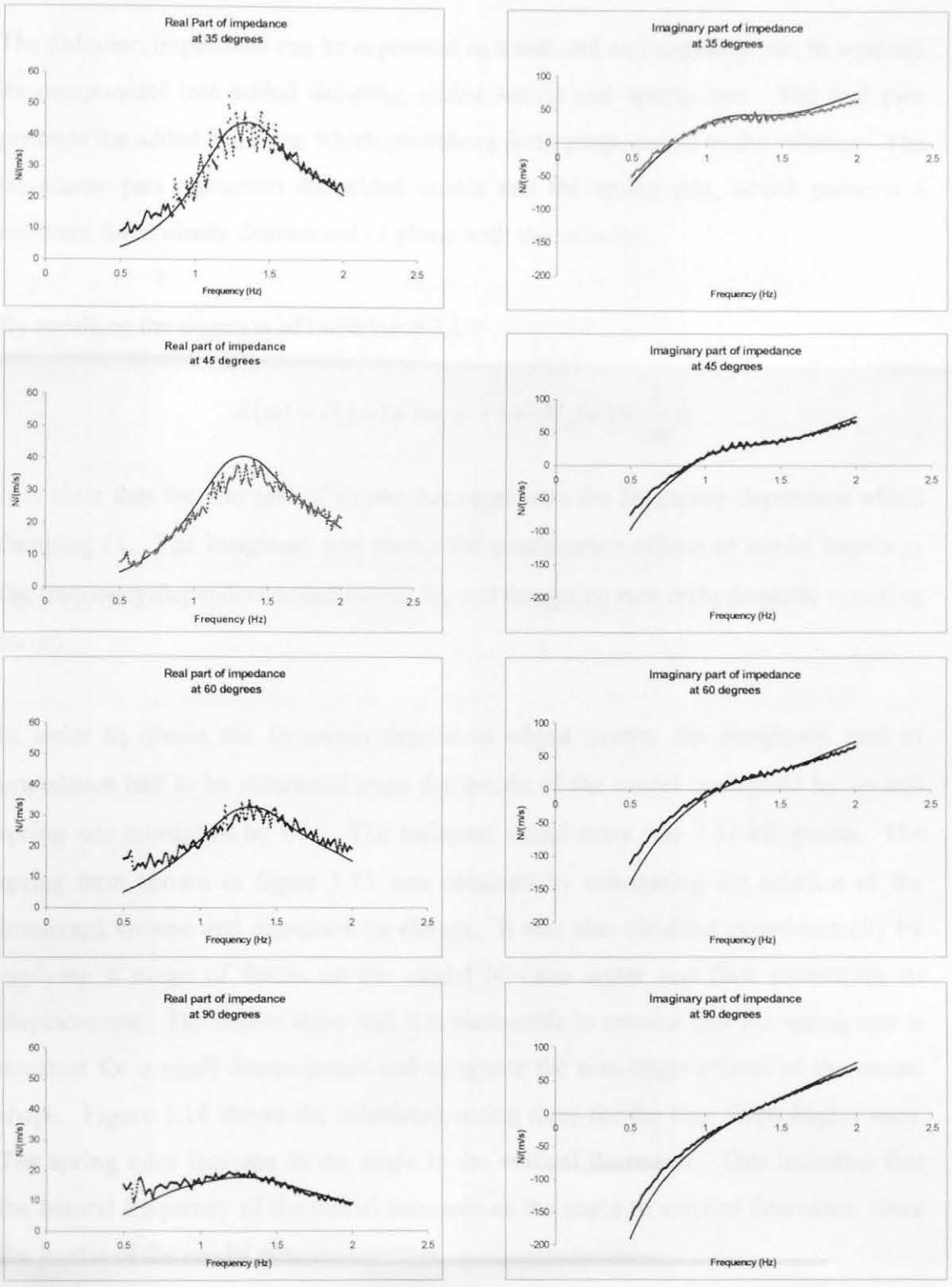

Figure 5.12. Overview of the radiation impedances of the model at 35, 45, 60 and 90 degrees slope angles. All slope angles are plotted to the same scales.

5.2.2 Added damping, added inertia and spring rate

The radiation impedance can be expressed as a real and an imaginary part to separate its components into added damping, added inertia and spring rate. The real part presents the added damping, which provides a force proportional to the velocity. The imaginary part represents the added inertia and the spring rate, which presents a resultant force ninety degrees out of phase with the velocity.

By recalling the equation of impedance 3.13:

$$Z(\omega) = D_a(\omega) + i\omega \cdot \mu + i\omega \cdot M_a(\omega) + \frac{1}{i\omega}\sigma$$

It is clear that the real part of impedance represents the frequency-dependent added damping D_a. The imaginary part shows the combination effects of model inertia μ, the frequency-dependent added inertia M_a and the spring rate σ (hydrostatic restoring force).

In order to obtain the frequency-dependent added inertia, the imaginary part of impedance had to be subtracted from the inertia of the model multiplied by $i\omega$ and spring rate multiplied by $1/i\omega$. The ballasted model mass was 7.31 kilograms. The spring term shown in figure 5.13 was obtained by calculating the relation of the immersed volume and displacement change. It was also obtained experimentally by applying a range of forces on the model in calm water and then measuring its displacement. The results show that it is reasonable to assume that the spring rate is constant for a small displacement and to ignore the non-linear effects of the model shape. Figure 5.14 shows the calculated spring rates for the four slope angles tests. The spring rates increase as the angle to the vertical decreases. This indicates that the natural frequency of the model increases as the angle to vertical decreases, since the inertia of the model remains constant.

In figure 5.15 the components of the imaginary part of impedance at 45 degrees inclined angle are shown. It clearly shows that the value of the added mass gradually

increases with frequency reaching its maximum value at approximately 1 Hz and then decreases to almost zero.

Figure 5.16 shows the model at 35 degrees slope angle. The added mass decreases gradually as the frequency increases and is slightly below than zero at high frequencies.

Figure 5.17 shows that at the 60 degrees slope angle the added mass decreases gradually and retains a positive value at high frequencies.

In figure 5.18 the added mass of 90 degree slope angle continues to increase gently as the frequently increases.

Vugts (1968) did some tests on determination of the hydrodynamic forces acting on the ship's hull forms. He forced the models oscillating in heave, sway, roll and coupling modes between them. The results of 45 degrees slope angle show similar tendency as the rectangular hull in surge mode and 35 degrees is similar to the same hull in coupling surge and roll mode. At 90 degrees slope angle the results are similar to the rectangular hull in heave mode.

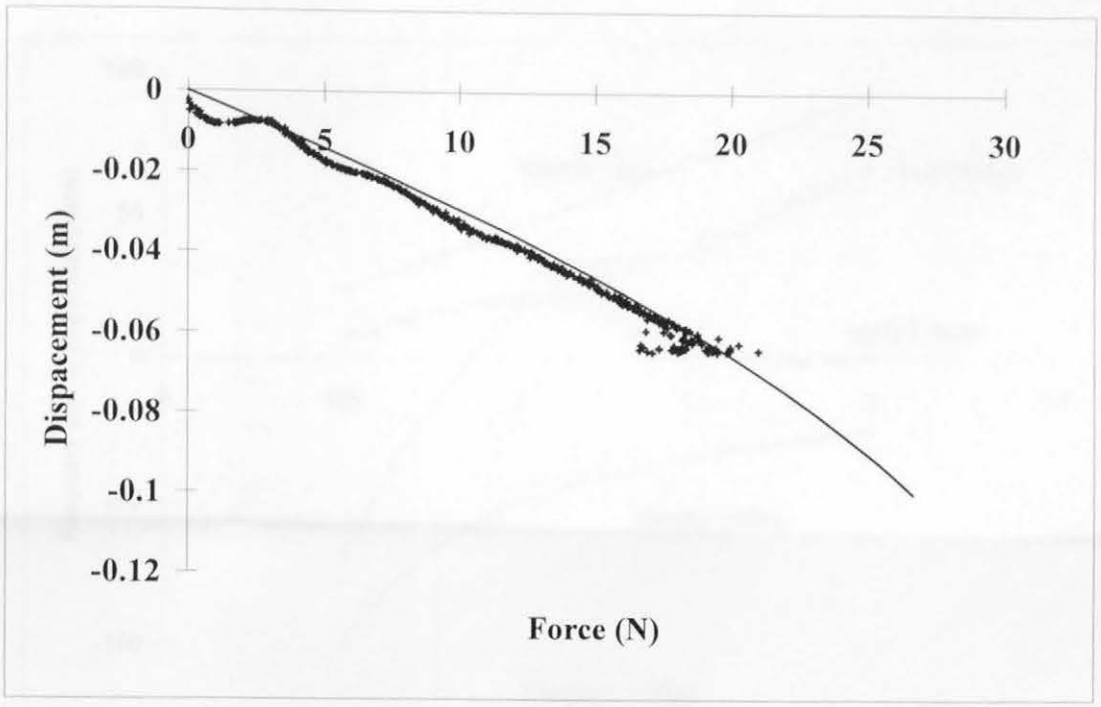

Figure 5.13. The calculated and measured hydrostatic restoring forces of the model at 45 degrees inclined angle. The individual points are measured values and the smooth curve shows the calculated values.

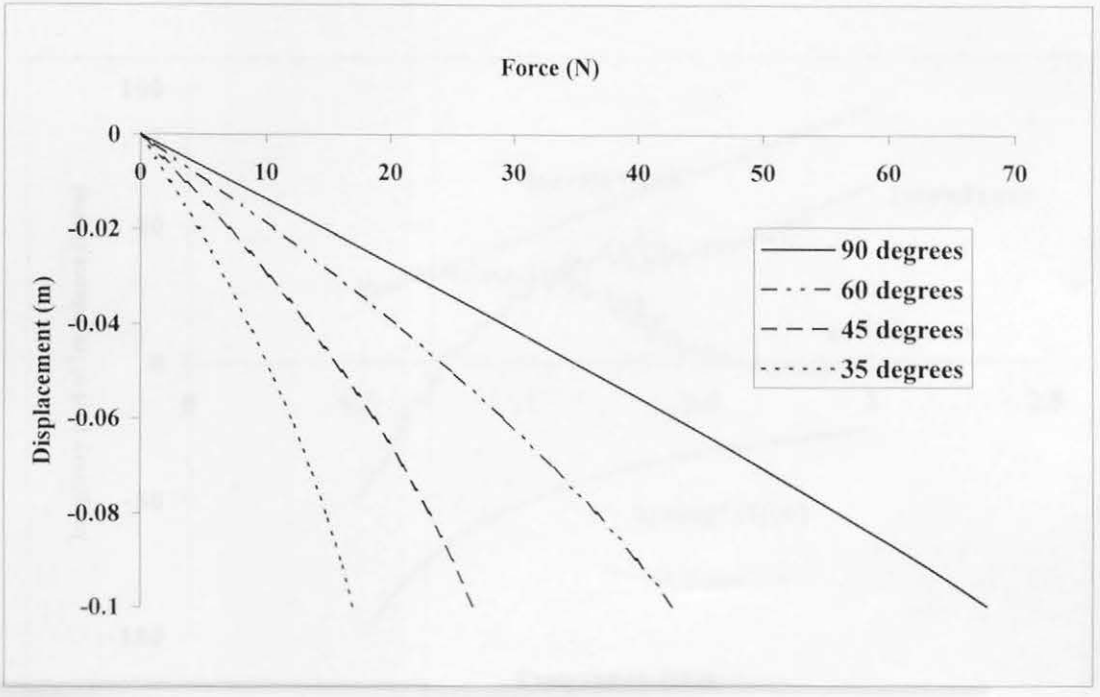

Figure 5.14. The calculated hydrostatic restoring force versus the displacement for various angle of inclination. The spring rate of the model increases as the angle to the vertical decreases.

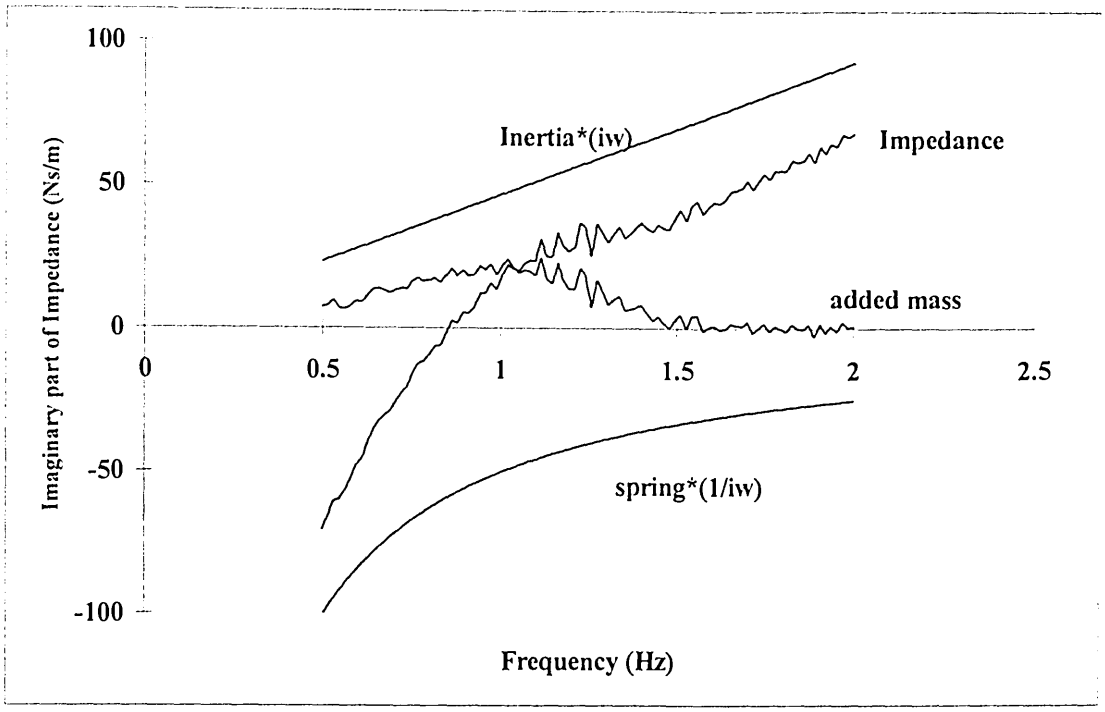

Figure 5.15. The imaginary part of the impedance at 45 degrees inclined angle separated into components

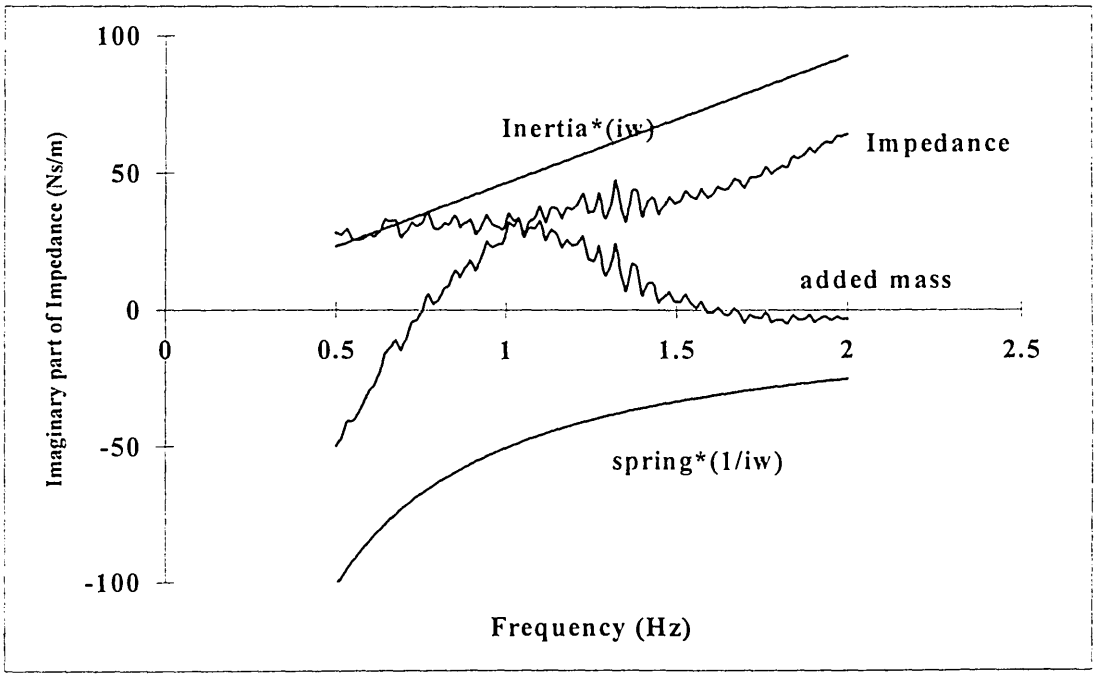

Figure 5.16. The imaginary part of the impedance at 35 degrees inclined angle separated into components

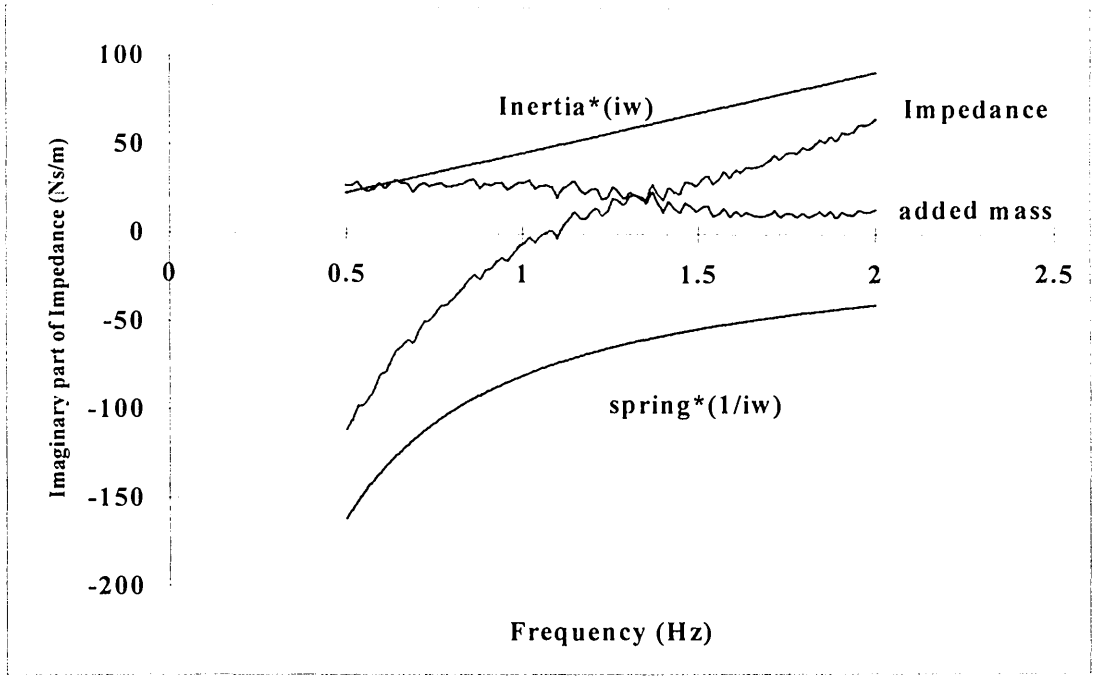

Figure 5.17. The imaginary part of the impedance at 60 degrees inclined angle separated into components.

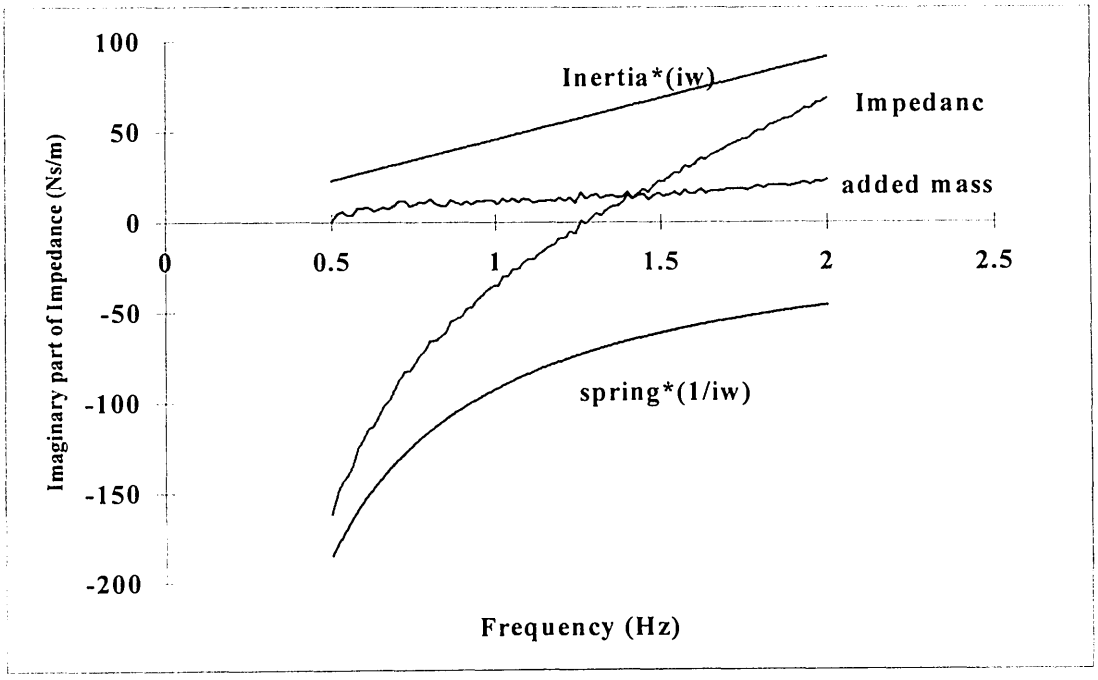

Figure 5.18. The imaginary part of the impedance at 90 degrees inclined angle separated into components.

5.2.3 Natural frequency of the model

For a translating wave energy device to obtain maximum absorption of power from waves two conditions have to be satisfied. Firstly, the velocity must be in phase with the wave excitation force. When the body is resonant this condition is automatically satisfied. Secondly, the damping force applied by the power take-off system must be adjusted to the optimum value. In this condition the power absorbed will be the same as the power that would be radiated in still water by the forced oscillation of the device at the same amplitude. The above two conditions may be referred as the condition for optimum phase and the condition for optimum amplitude. Therefore, when designing a wave device, it is important to design the device to tune to the dominant wave frequency.

An ideal device would be able to vary its natural frequency to always match the incident wave frequency. Furthermore it would have as high as possible absorption efficiency at the low frequency end of the spectrum. This corresponds to being productive in waves that are long compared with the device dimensions. From an economic point of view this implies the minimisation of the size and cost of a sea-going system.

When a system consisting of spring and inertia is oscillating at its natural frequency, the amount of potential energy stored in the spring at maximum deflection is exactly the same as the kinetic energy of inertia when it is at its maximum acceleration. The oscillation involves a transfer of energy between these two forms.

The natural frequency of a system is usually calculated from the square root of the ratio of stiffness to inertia. Thus, it can be expressed as a function of angular frequency:

$$f_n(\omega) = 2\pi\sqrt{\frac{\sigma}{\mu + M_a(\omega)}} \qquad (5.2)$$

Since the total inertia includes the inertia of the device itself and the frequency-dependent added inertia caused by the oscillating fluid, the natural frequency varies with incident wave frequency. However, it is convenient to use the imaginary part of impedance to identify the natural frequency. When this imaginary impedance is equal to zero, all of the energy is presented into the added damping term and the natural frequency is easily obtained. For instance, in the 45 degrees inclination test of figure 5.7, the natural frequency is approximately 0.85 Hz. The natural period for the inclination increases as the angle to the vertical increases, as shown in table 5.1, which summaries the data from figures 5.4 to 5.11.

Inclination angle	Natural frequency/period
35 degrees	0.75 Hz / 1.33 sec
45 degrees	0.85 Hz / 1.17 sec
60 degrees	1.07 Hz / 0.93 sec
90 degrees (heave)	1.28 Hz / 0.78 sec

Table 5.1 Natural frequency of the model at different inclinations.

These results also confirm the possibility of tuning the natural frequency of the device by varying the angle of inclination. For example, by changing the slope angle from 35 degrees to 90 degrees the natural period of the model can be shifted from 1.33 seconds to 0.78 seconds.

5.2.4 Effect of amplitude variation on natural frequency

Forced oscillating tests were conducted with three different drive forces: 5, 10 and 15 Newtons. The tests were carried out over the same frequency range of 0.5 Hz to 2 Hz. Figure 5.19 and 5.20 show that the added damping has no contribution from the added inertia or spring term. The imaginary part of the impedance remains the same shape. The real part of the impedance (added damping) produces little difference at

high frequency and increases slightly with driven force at low frequency. This is possibly due to the large motion of the model making more vortices, the hydrostatic bearing making waves at the lee side of the model and to friction between the bearing and the rig.

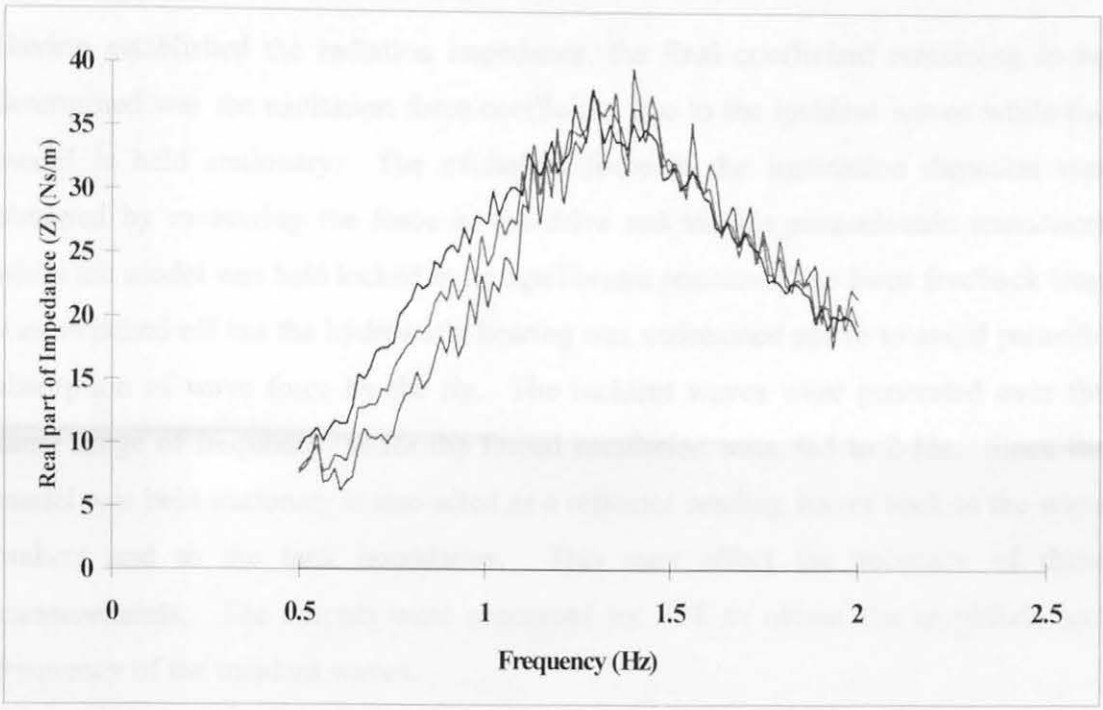

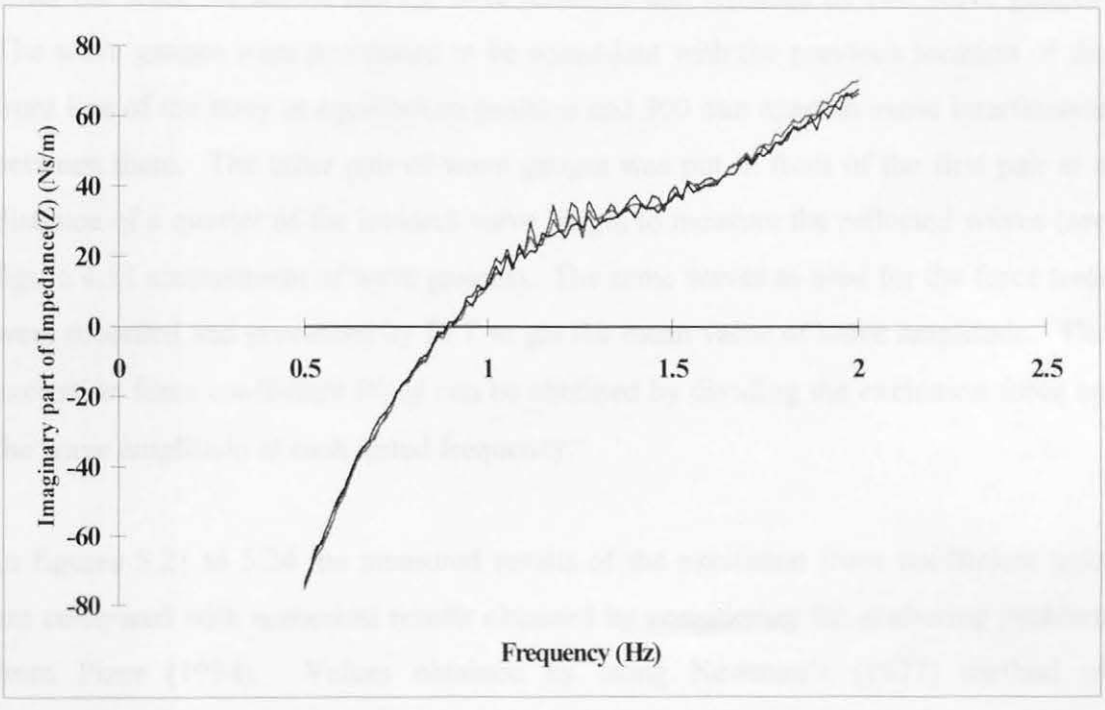

Figure 5.19 and 5.20. The real part (above) and imaginary part (below) of the radiation impedance of the model at 45 degrees slope angle driven by different force amplitudes of 5, 10 and 15 N.

5.2.5 Excitation force coefficient

Having established the radiation impedance, the final coefficient remaining to be determined was the excitation force coefficient due to the incident waves while the model is held stationary. The excitation force in the inclination direction was obtained by measuring the force in the drive rod via the piezoelectric transducer while the model was held locked in its equilibrium position. The force feedback loop was switched off but the hydrostatic bearing was maintained active to avoid parasitic absorption of wave force by the rig. The incident waves were generated over the same range of frequency, as for the forced oscillation tests, 0.5 to 2 Hz. Since the model was held stationary it also acted as a reflector sending waves back to the wave makers and to the tank boundaries. This may affect the accuracy of these measurements. The outputs were processed by FFT to obtain the amplitude and frequency of the incident waves.

After the tests, the model and rig were removed and replaced by two wave gauges. The wave gauges were positioned to be coincident with the previous location of the front line of the buoy at equilibrium position and 300 mm apart to avoid interference between them. The other pair of wave gauges was put in front of the first pair at a distance of a quarter of the incident wave length to measure the reflected waves (see figure 4.11 arrangement of wave gauges). The same waves as used for the force tests were recorded and processed by FFT to get the mean value of wave amplitude. The excitation force coefficient $W(\omega)$ can be obtained by dividing the excitation force by the wave amplitude at each tested frequency.

In figures 5.21 to 5.24 the measured results of the excitation force coefficient tests are compared with numerical results obtained by considering the scattering problem from Pizer (1994). Values obtained by using Newman's (1977) method of calculating the excitation force from added damping coefficients in two dimensions are also plotted.

Newman (1962, 1977) used the Haskind relation and predicted the excitation force from the added damping a vertical axis symmetric body in three dimensions and of a plane ($x=0$) symmetric body in two dimensions. Since the present test model was not symmetric about the vertical axis, using the three-dimensional equation is improper. The model was symmetric to the plane $x=0$ but had a limited width. However, a two-dimensional equation shown below has been used based on the measured added damping coefficients.

$$F_e(\omega) = \left(2\rho g V_g \cdot D_a(\omega)\right)^{0.5} \qquad (5.3)$$

Where V_g is group velocity.

At both high and low frequency the experimental results have lower value than the results of Pizer and Newman. At middle frequencies they have higher values. Both the results of Pizer and Newman have similar tendencies.

Figures 5.21 to 5.24 show the wave excitation force on the model per metre wave amplitude at a 35, 45, 60 and 90 degrees slope angle.

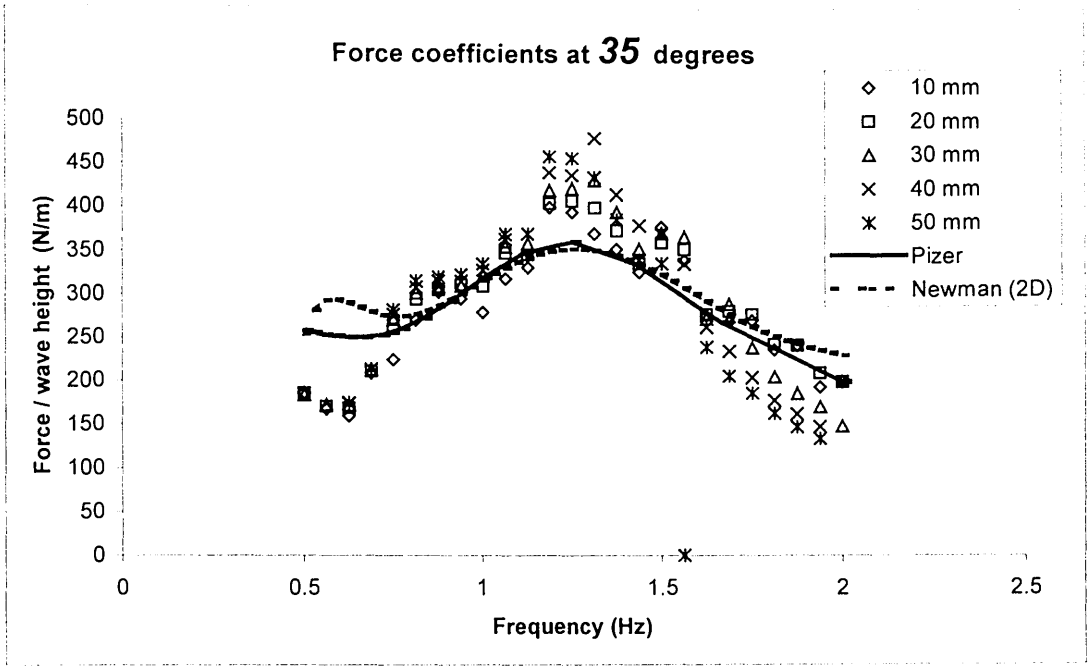

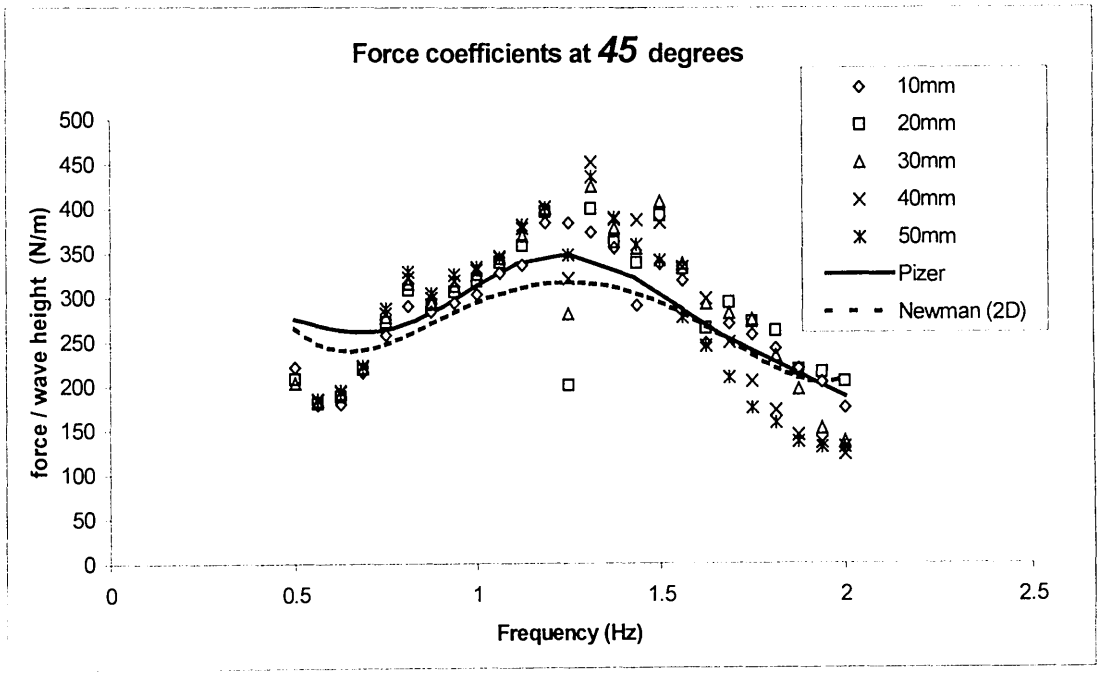

Figure 5.21 and 5.22. The exciting force coefficients for the model at 35 and 45 degrees inclined angle. The tests were conducted at 5 wave heights. Also shown as a solid and a dotted line are numerical results from Pizer and from Newman.

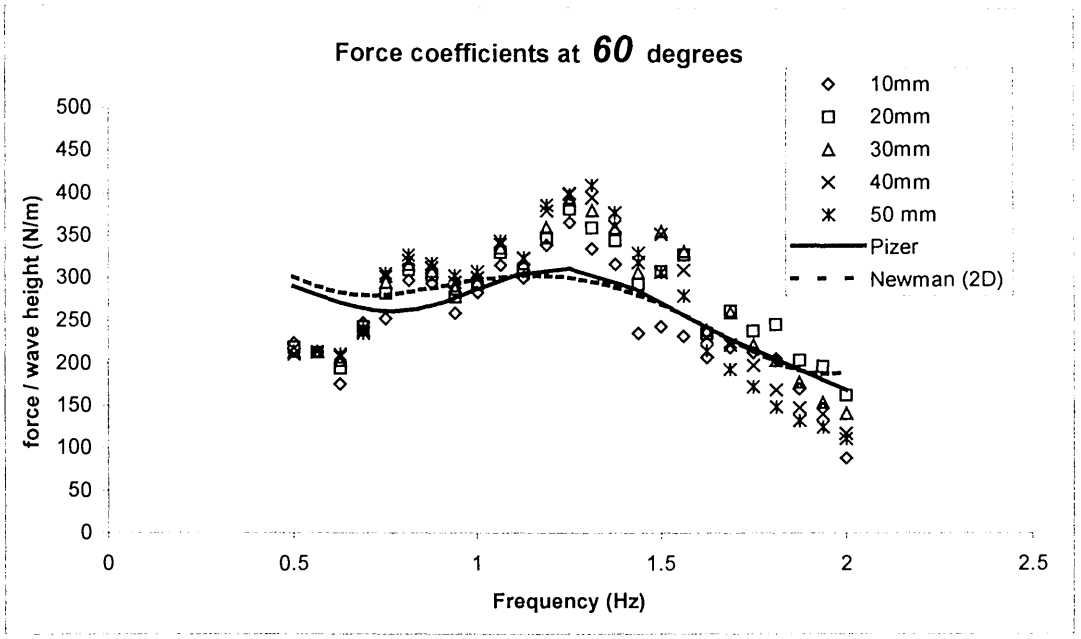

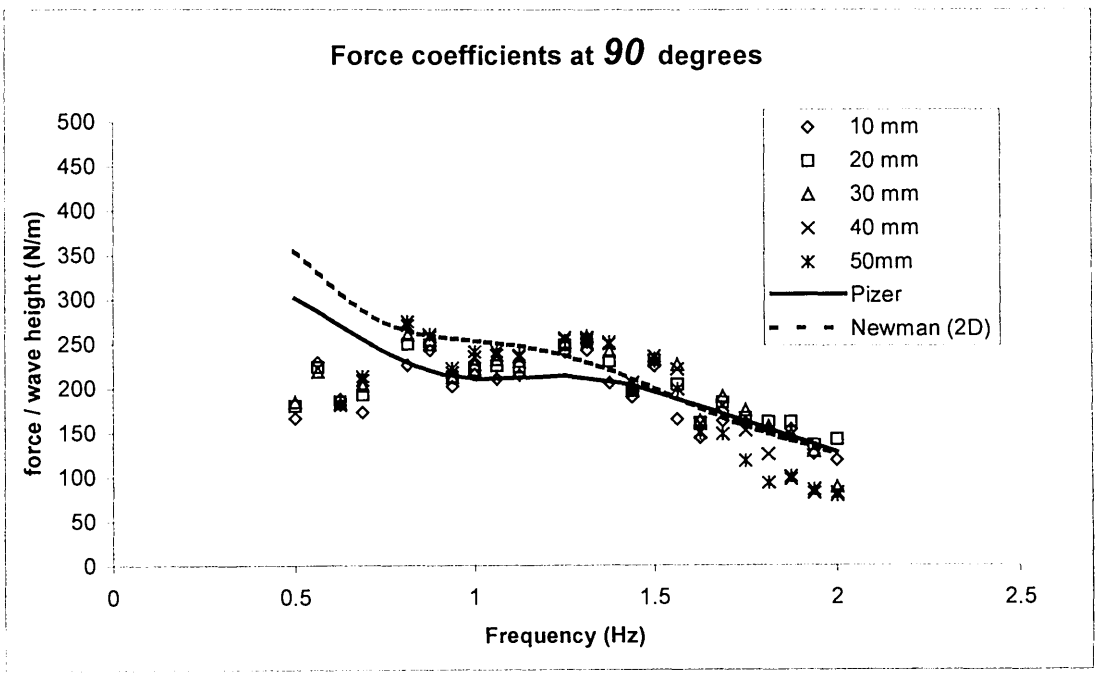

Figure 5.23and 5.24. The exciting force coefficients for the model at 60 and 90 degrees inclined angle. The tests were conducted at 5 wave heights. Also shown as a solid and a dotted line are numerical results from Pizer and from Newman.

5.3 Power capture

The power capture measurement is the main attention of developing a new wave power device. There are different techniques for two-dimensional and three-dimensional tank tests. In a narrow tank (2-D) whose width is marginally greater than that of the model, it is comparatively easy to measure the incident and reflected wave in front of the model and the transmitted wave from its back simultaneously. The power absorbed by the model is equal to the power of the incident wave minus the power of the reflected wave and the transmitted wave. The efficiency then can be obtained by calculating the power ratio between them. The equation can be expressed as:

$$\eta = \frac{1-(a_r{}^2 + a_t{}^2)}{a_i{}^2} \qquad (5.4)$$

where

a_i is the incident wave amplitude.

a_r is the reflected wave amplitude.

a_t is the transmitted wave amplitude.

A dynamometer power take-off system is not necessary if the power take-off system can provide a damping force. In a wide (3-D) tank since the width of the wave tank is much wider than the width of the model, the reflecting waves can come from many directions. It is not possible to use the same technique of measuring power capture as in the narrow tank. Therefore, a precise dynamometer power take-off system, which can obtain the information of power absorbing directly, is required. The power absorbed by the model and the power of the incident waves were measured separately. Since the repeatability of wave making of the tank is known to be good (Bryden, 1983), power of incident waves were measured by replacing the model with wave gauges. This procedure was similar to the measurements of the wave excitation force coefficients.

5.3.1 Power capture tests

Before each test the damping coefficient has to be set properly to achieve the maximum power absorption. The instantaneously absorbed power of the model was calculated from the product of force transducer signal and the model velocity. In the time domain, the mean absorbed power of the model is:

$$P = \frac{1}{T}\int_0^T F(t)\cdot U(t)dt \qquad (5.5)$$

When measurements were carried out by a sampling system, the mean power passing through the model was calculated by an approximating equation of equation 5.5 with a sum:

$$P = \frac{1}{m}\sum_{n=0}^{m-1} F(n)\cdot U(n) \qquad (5.6)$$

where

m is the number of samples.

n is the sample number.

The sample number was chosen to be a multiple of a full wavelength to reduce the error.

Figure 5.25 shows a regular wave power capture test versus wave height with the model set at 45 degrees slope angle and an incident wave frequency of 0.875Hz. The experimental curve drops below the incident power at 30mm wave height. Power capture calculations are also shown. The detail of power calculations will be discussed in the next section.

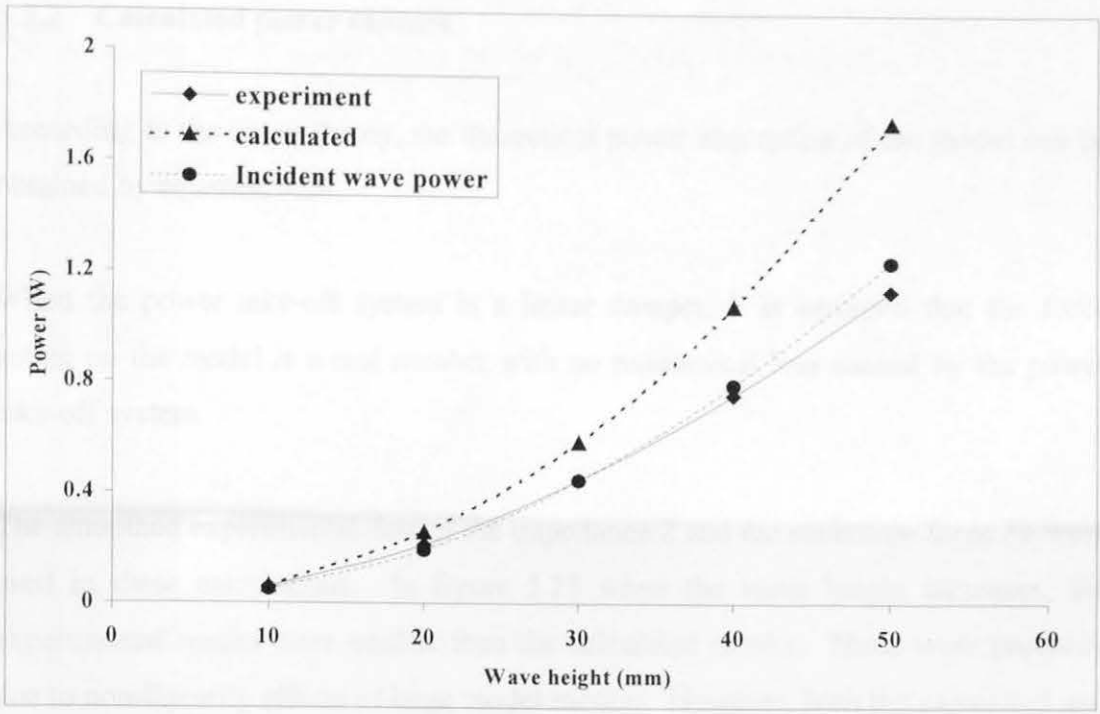

Figure 5.25. The power absorption of model at 45 degrees inclined angle for incident wave frequency 0.875Hz. Wave heights were 10 mm to 50 mm.

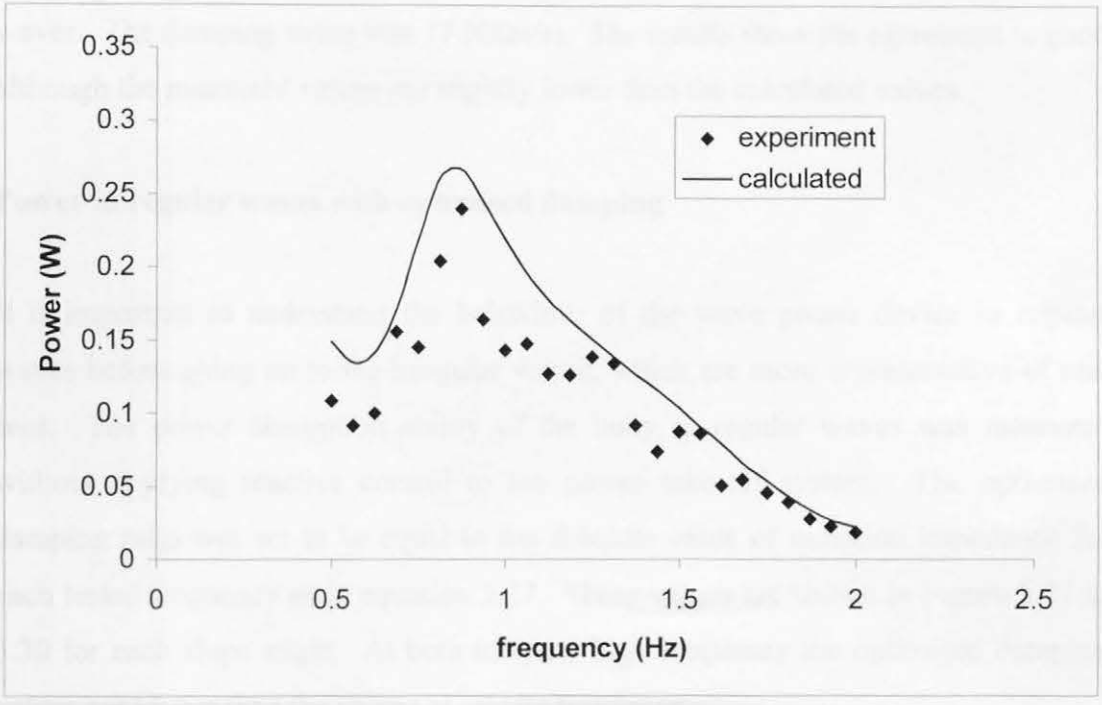

Figure 5.26. The power absorption for 20mm wave height regular waves. The inclined angle of model was 45 degree with constant damping value of 17 N/(m/s).

5.3.2 Calculated power capture

According to the linear theory, the theoretical power absorption of the model can be obtained by equation 3.26.

When the power take-off system is a linear damper, it is assumed that the force acting on the model is a real number with no mechanical loss caused by the power take-off system.

The smoothed experimental data of the impedance Z and the excitation force Fe were used in these calculations. In figure 5.25 when the wave height increases, the experimental results were smaller than the calculated results. These were probably due to non-linearity effects of large model motion. However, both the calculated and measured power at 10mm and 20mm incident wave heights were greater than the power of the incident waves. This is due to the point absorbing effect. Figure 5.26 shows both calculated and measured power absorption in 20mm height regular waves. The damping value was 17 N/(m/s). The results show the agreement is good although the measured values are slightly lower than the calculated values.

Power in regular waves with optimised damping

It is important to understand the behaviour of the wave power device in regular waves before going on to the irregular waves, which are more representative of real seas. The power absorption ability of the buoy in regular waves was measured without applying reactive control to the power take-off system. The optimised damping ratio was set to be equal to the absolute value of radiation impedance for each tested frequency as in equation 3.27. These values are shown in Figure 5.27 to 5.30 for each slope angle. At both low and high frequency the optimised damping values are higher than the values at middle frequency.

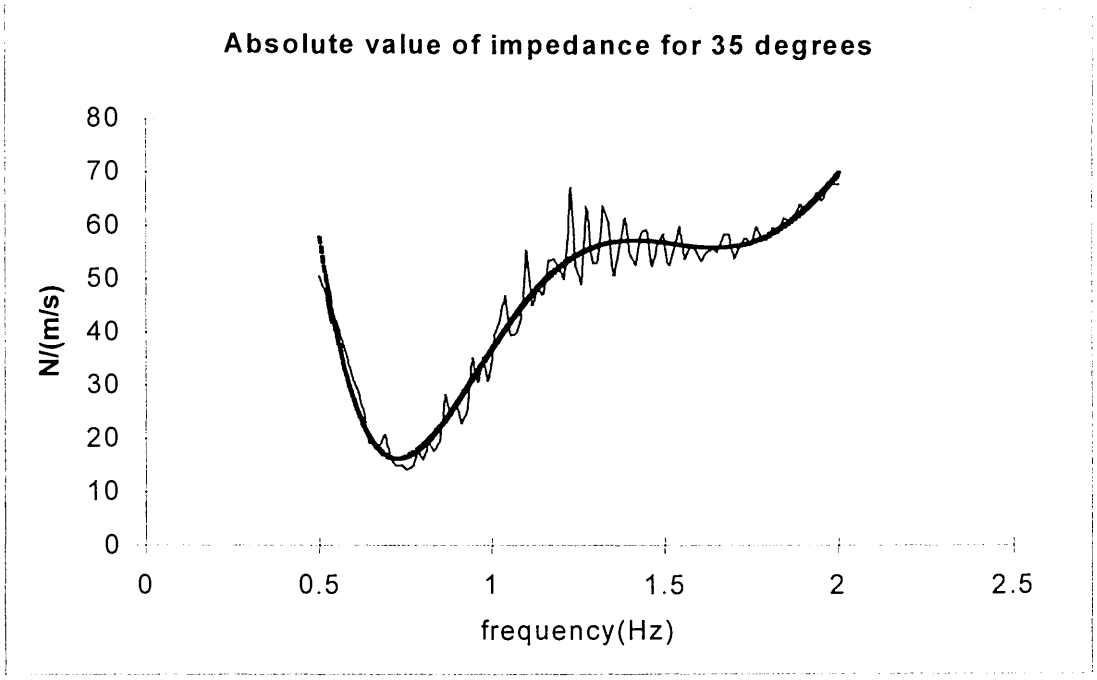

Figure 5.27. The optimised damping value for the model at 35 degrees slope angle. The smoothed curve is used for calculating the power absorption.

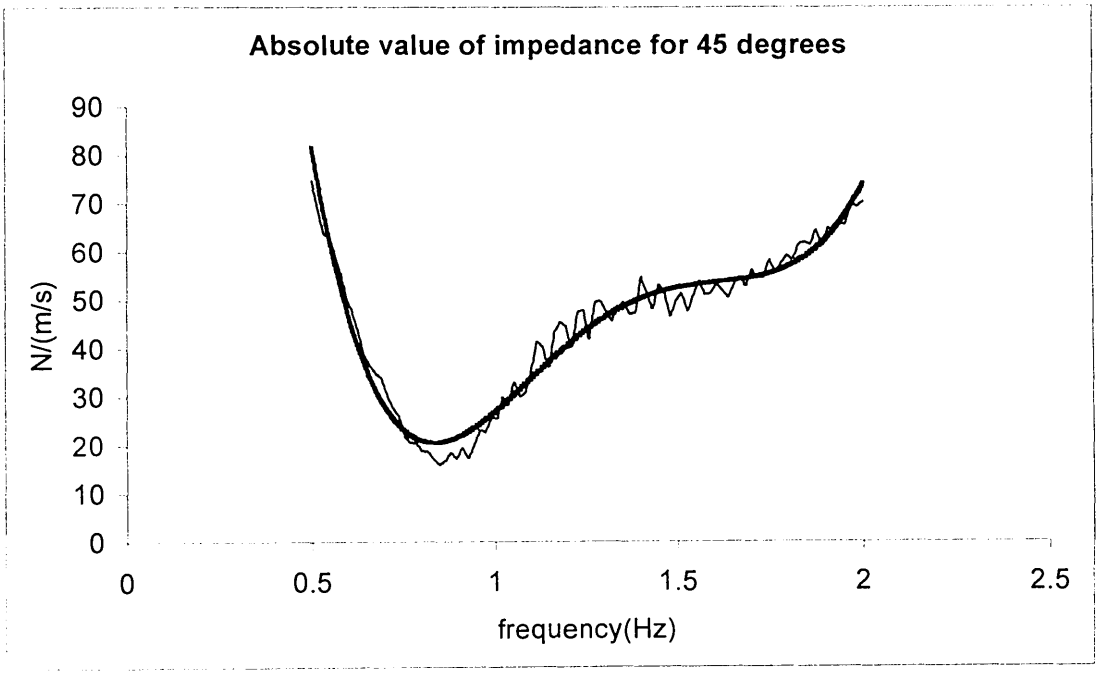

Figure 5.28. The optimised damping value for the model at 45 degrees slope angle. The smoothed curve is used for calculating the power absorption.

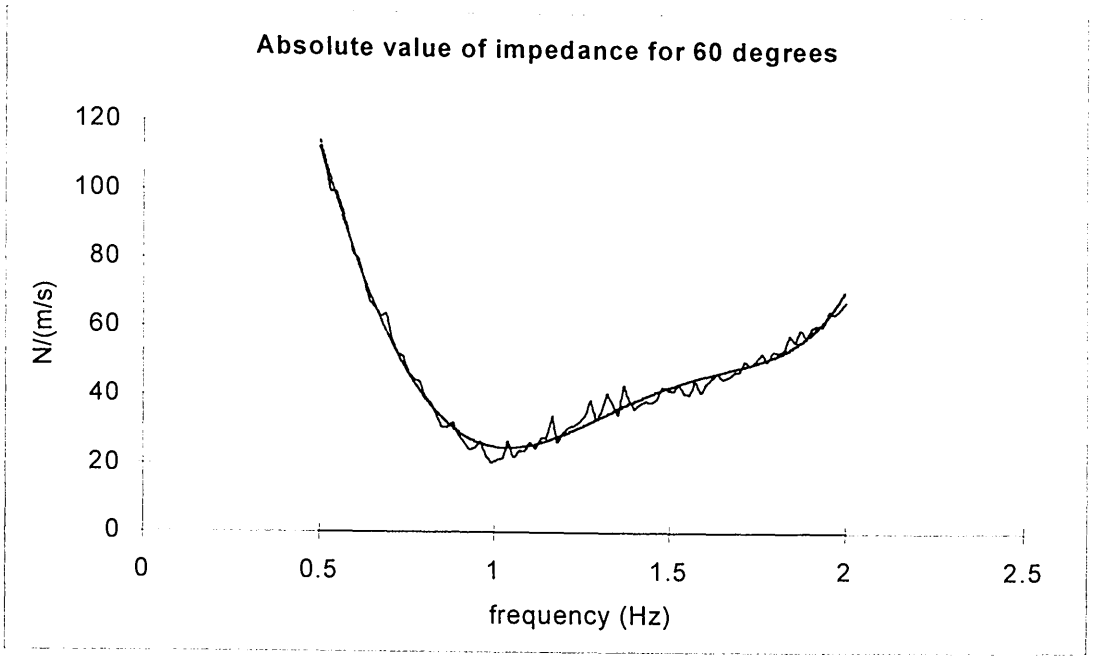

Figure 5.29. The optimised damping value for the model at 60 degrees slope angle. The smoothed curve used for calculating the power absorption.

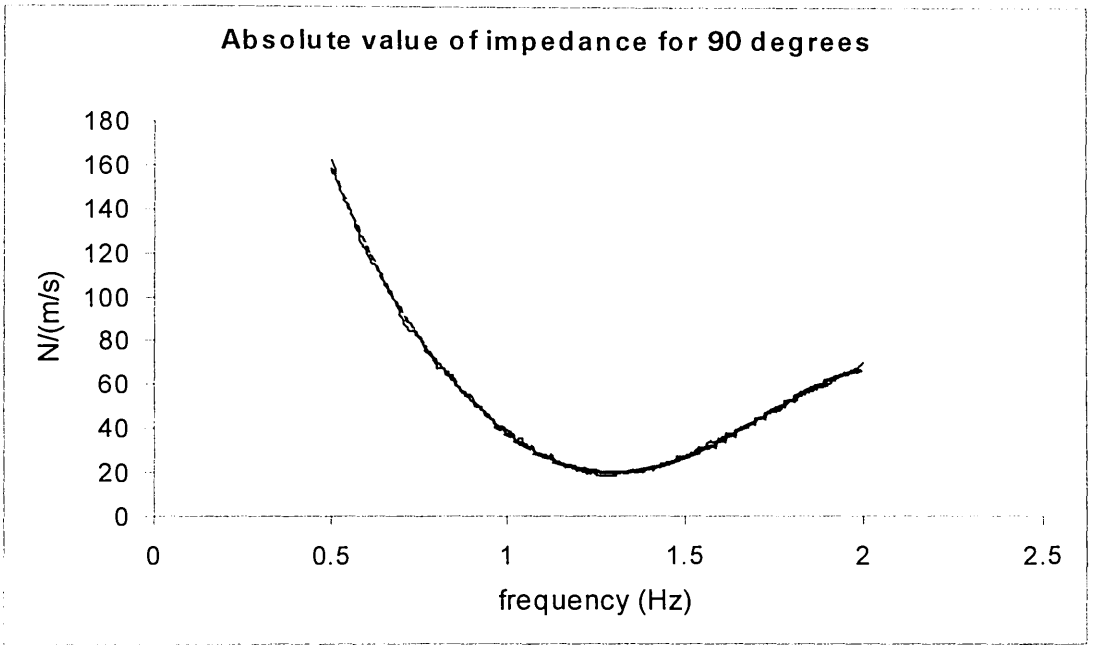

Figure 5.30. The optimised damping value for the model at 90 degrees slope angle. The smoothed curve is used for calculating the power absorption.

Figure 5.31 shows the measured power and the calculated power versus frequency of the model at 45 degrees angle of inclination. Although there are some differences between the measured and calculated results, both curves have a similar tendency.

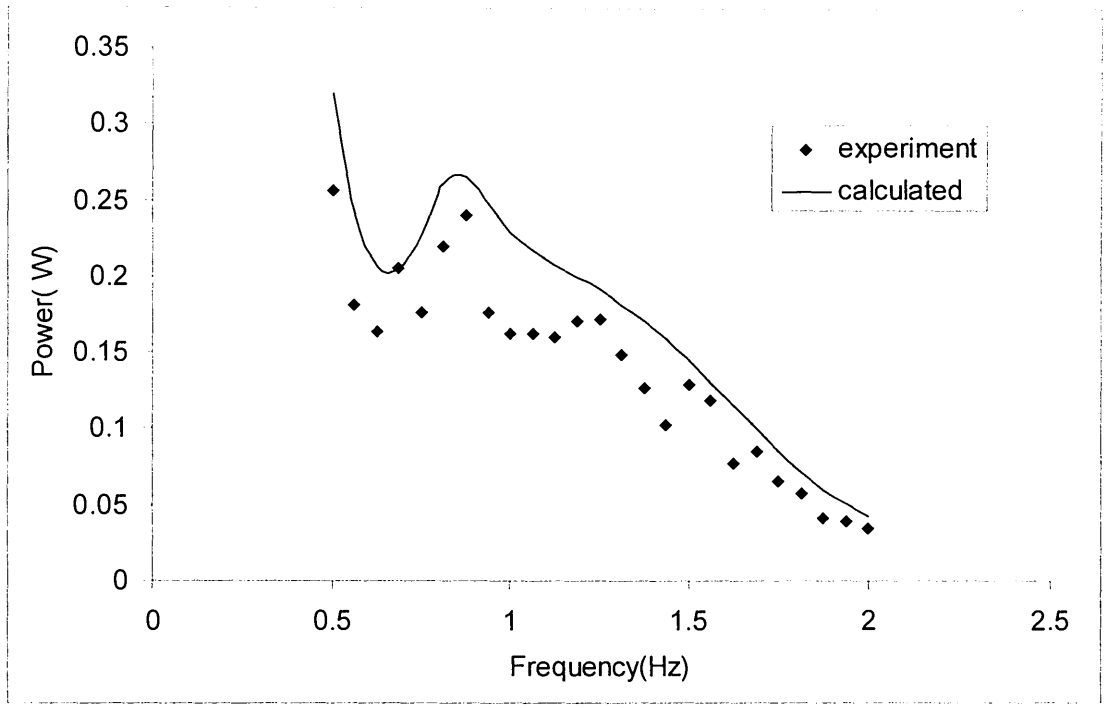

Figure 5.31. The power absorption of the model at 45 degrees slope angle with optimised damping value for each frequency. The wave height was 20mm.

5.4 Efficiency of the device

The efficiency curve gives an overall view of the performance of the device. It can be obtained by applying equations 3.34 and 3.35. Figure 5.32 to 5.35 show both measured and calculated efficiency for the model at the four tested inclinations which are 35,45, 60 and 90 degrees. The damping values of the model were set as optimised values, which are equal to the absolute values of hydrodynamic impedance of the model, at each tested frequency.

The smooth curves present the theoretical efficiency calculated from the impedance and excitation force results based on the wave height of 20 mm. The jagged points are the measured efficiency values calculated from the product of force into the load cell multiplied by the velocity measured by the tacho-generator.

The experimental results are not in exact agreement with the theoretical results and the measured values are generally less than the calculated values. Nevertheless, they have a very similar tendency. The discrepancy between them could be caused by vortex shedding of the model and by small-scale viscous effects.

At the 35 and 45 degrees slope angle, both figures 5.32 and 5.33 show two peaks in the efficiency curves. This "double-peak efficiency effect" is an important factor of the bandwidth of the device. The detail of the effect will be discussed in the next chapter.

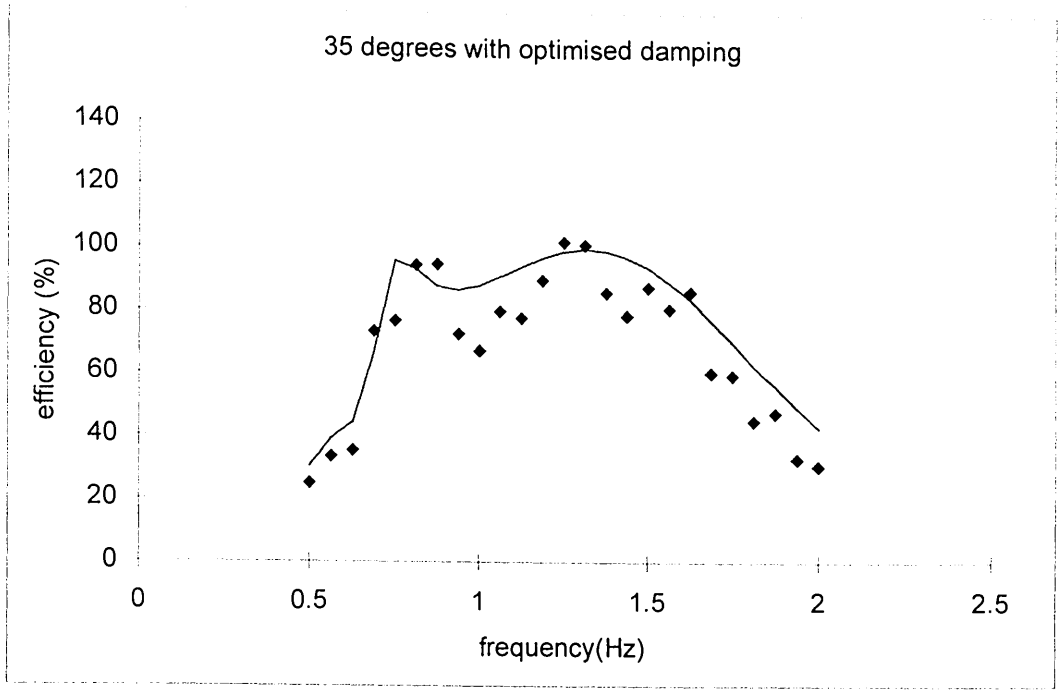

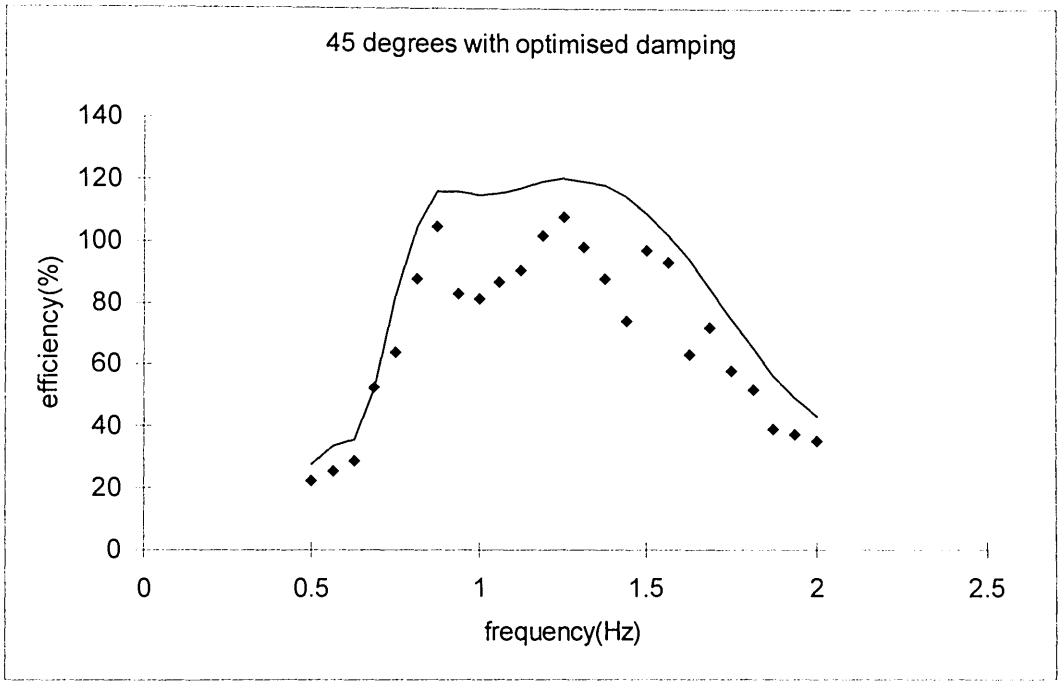

Figure 5.32 and 5.33. The efficiency curve for the model at 35 (above) and 45 (below) degrees slope angle with optimised damping value for each tested frequency. The wave height was 20mm. The smooth curve is the calculated results and dotted points are measured results.

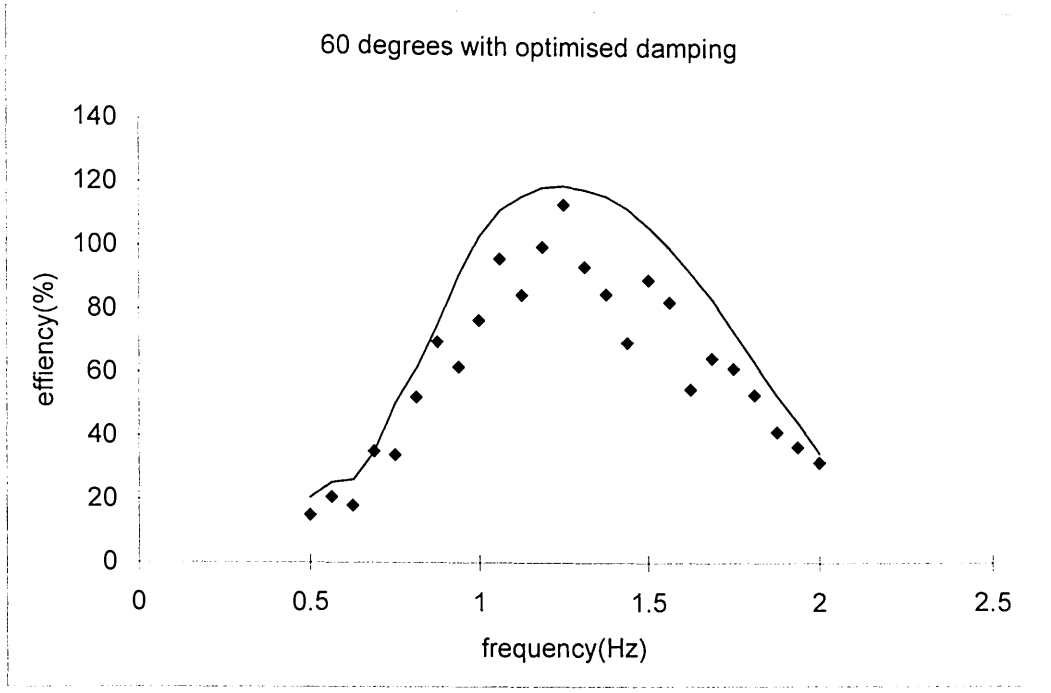

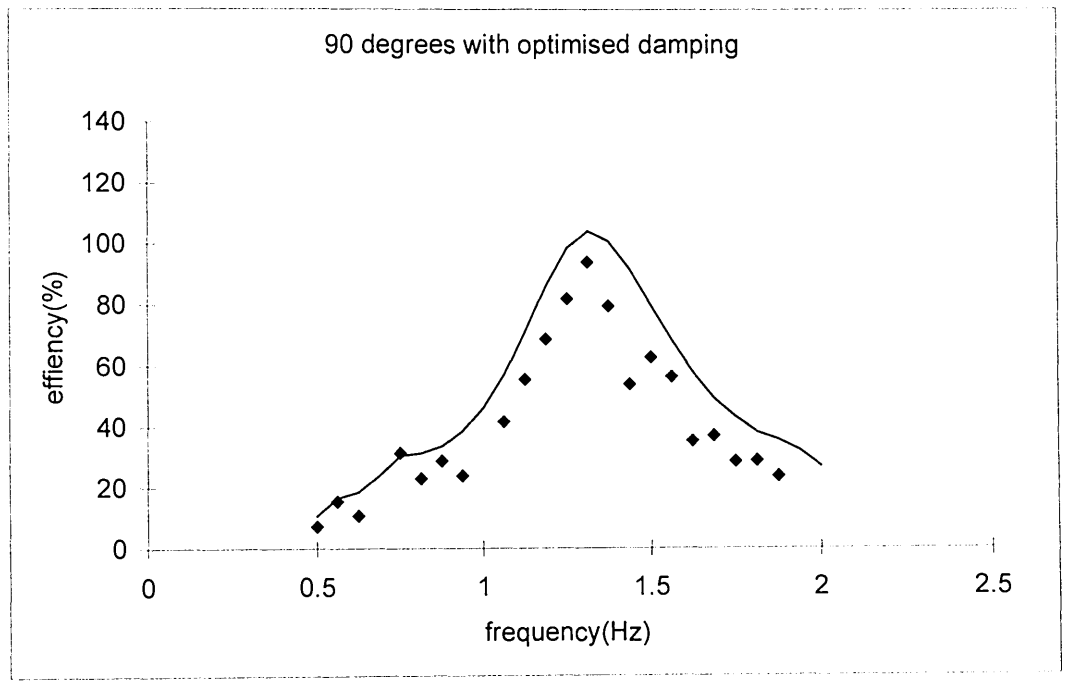

Figure 5.34 and 5.35. The efficiency curve for the model at 60 (above) and 90 (below) degrees slope angle with optimised damping value for each tested frequency. The wave height was 20mm. The smooth curve is the calculated results and dotted points are measured results.

5.5 Conclusions

- An experimental procedure has been established and successfully implemented with the model.

- The hydrodynamic coefficients have been obtained experimentally by using the forced oscillation technique. The results agree well with the numerical results calculated by Pizer, indicating that both measured and numerical coefficients can reasonably be used to describe the system behaviour.

- The hydrodynamic coefficients of added inertia, added damping and restoring terms have also been identified.

- The natural frequency of the device has been measured and validated the important concept of tuning the natural frequency of a device by varying the angle of inclination.

- The wave excitation force has been measured for a range of wave heights and frequencies. The results show that the force increases as the angle to the vertical increases.

- The power absorption ability of the model was obtained by both experiments and calculations. The experimental results generally have good agreement with the calculated results that are based on the measured coefficients in 20 mm incident waves. The optimised damping values have been calculated and used at four slope angles. However, the experimental values are lower than the calculated values.

- The efficiency of the model has been calculated and measured to give an overall view of its performance. The results show that the bandwidth increases as the angle to the vertical increases.

- The model at 45 degrees inclined angle shows a wide bandwidth. If this were a 1/100th scale model the bandwidth would be a very good match to the energetic

parts of Atlantic spectra. It indicates that it may not be necessary to change the slope angle of a full-scale device to suit different wave conditions.

Chapter 6

Practical implications of regular wave tests

6.1 Introduction

In this chapter, we start out by looking in depth the regular wave tests on the Sloped IPS buoy. Then we go on to consider the effect of control system strategies and tube water mass.

In section 6.2 the experimental results in regular waves are shown together to give an overall view of the performance of the model at different slope angles. The point absorber effect apparent in the tank tests is also discussed. The interesting and important "double-peak" efficiency effect is observed in tests at angles smaller than 45 degrees. This effect gives a significant improvement by increasing the bandwidth of the device. The relations between bandwidth of the model and its hydrodynamic impedance are investigated and discussed. The tank tests are compared with published tests on a shallow draught oscillating water column with similar size of reactive part.

In section 6.3 the control of power take-off system is discussed. Although many control methods have been proposed in the last two decades, most of them need advance wave information which is difficult to acquire in real sea conditions, and more complex power take-off systems able to provide reactive forces with variable phase relative to the velocity of the model. In this early stage we have implemented a simple control method by varying the damping value of the power take-off system

at each wave frequency. The reactive mass from the inertia of water inside the tube is also investigated. A simple mathematical model for a finite mass of reaction is derived to evaluate the finite mass effect and predict the movements of the reaction mass. These results produce a reference for designing the tube volume.

6.2 Performance of the model

Since the wave period and wave height vary in a real sea, a desirable property of any wave-absorbing device is to operate at high efficiency over a wide range of wave periods.

Most heave devices such as oscillating water columns and small heaving buoys have a very peaky efficiency curve. Figure 6.1 shows the efficiency curves of our model plotted against period for four slope angles. The damping values were set equal to the absolute value of hydrodynamic impedance to achieve the best performance without applying reactive control. The vertical mode (90 degrees) test has an inherent narrow bandwidth. A useful way to compare performance at different angles is to define the concept of a "80% bandwidth", by taking the ratio of the wave periods at the low and high ends of that part of the efficiency curve. At 90 degrees mode the 80% bandwidth is from 0.65 to 0.85 second, a ratio of 1.31. When the slope angle is changed to 60 degrees, there is a dramatic improvement. The maximum capture width increases to about 1.2 and the 80% bandwidth is increased to 0.55 to 1.1 seconds, a ratio of 2. Thus, the 80% bandwidth of the 60 degrees mode is more than twice that in the vertical mode. In 45 degrees mode the efficiency curve almost overlaps with the 60 degrees mode at low periods but extend to longer periods. The 80% bandwidth is from 0.55 to 1.35 seconds, a ratio of 2.45, and the peak efficiency is 120%.

In 35 degrees mode the 80% bandwidth is slightly wider than the 45 degrees but the maximum efficiency has dropped to 98%.

For the model at 45 and 35 degrees inclined angle, the efficiency curves appear with two peaks and wide bandwidth and high efficiency. This suggests that it may not be necessary to vary the angle to tune the natural frequency. It may be better to keep the device slope angle at 45 degrees, since the 45 degrees mode covers most of the area of the 60 and 90 degrees modes and gives a wide range of high efficiency.

Slope angle (degree)	80% bandwidth (second)	ratio	Peak efficiency (%)
35	0.6 ~1.4	2.33	98
45	0.55 ~ 1.35	2.45	120
60	0.55 ~ 1.10	2	120
90	0.65 ~ 0.85	1.31	105

Table 6.1. The bandwidth of the model for efficiency above 80% at different slope angles.

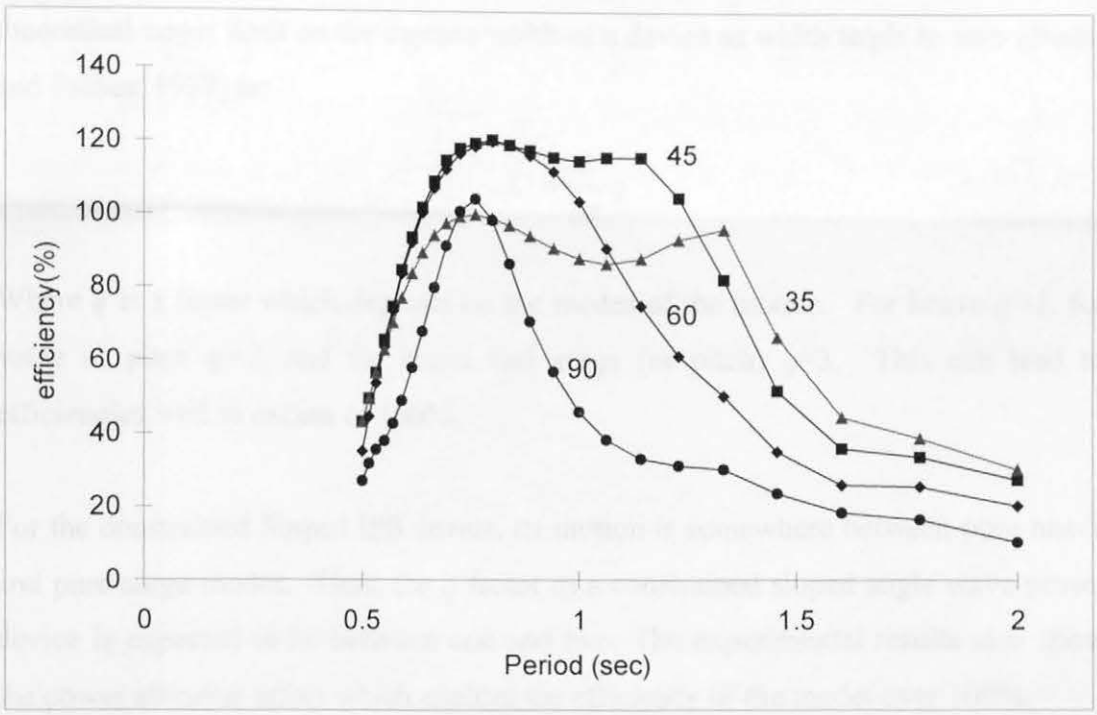

Figure 6.1. Efficiency curves for 35, 45, 60 and 90 degrees slope angle versus period. The 90 degrees slope angle is a pure heave device showing a typical narrow bandwidth. The 45 degrees slope angle shows a very wide bandwidth with high efficiency area.

Point absorber effect

The efficiency of a wave power device is usually defined as the ratio between the power absorbed by the device and the incident power in the device's width. In the three dimensional case, it is possible to absorb energy from a wave front much wider that its physical extension (Newman, 1976; Evans, 1976; Budal, 1977). The theoretical upper limit on the capture width of a device as width tends to zero (Budal and Falnes, 1977) is:

$$C = \frac{\lambda}{2\pi} q$$

Where q is a factor which depends on the modes of the motion. For heave $q=1$, for surge or pitch $q=2$, and for heave and surge (or pitch) q=3. This can lead to efficiencies well in excess of 100%.

For the constrained Sloped IPS device, its motion is somewhere between pure heave and pure surge modes. Thus, the q factor of a constrained sloped angle wave power device is expected to be between one and two. The experimental results also show the power absorber effect which enables the efficiency of the model over 100%.

The double-peak efficiency effect

At both slopes of 35 and 45 degrees the efficiency curve has a double peak. This is a very interesting phenomenon, particularly because the device maintains high efficiency between the peaks. For example, in 45 degrees mode the efficiency has a high plateau between 0.8 and 1.2 seconds and in 35 degrees mode the plateau is between 0.72 and 1.33 seconds.

At 60 and 90 degrees slopes, in figure 6.1 there is only a single peak corresponding to the natural periods. By recalling from section 5.2.3 the natural periods of 90, 60, 45 and 35 degrees which are respectively 0.78, 0.93, 1.17 and 1.33 seconds, the efficiency curves clearly show peaks at the same periods.

Figures 6.2 to 6.5 show the efficiency curve, the real part and the imaginary part of radiation impedance together, in order to observe a clear view of their relations. In figure 6.2 and 6.3, when the model is at 35 or 45 degrees slope angle, it is clear that the left peak of the efficiency curve corresponds to the peak of the real part of the hydrodynamic impedance and the right peak to the zero value of the imaginary part of the hydrodynamic impedance. When the model is at 60 or 90 degrees slope angle, the period differences between the peak of the real part of the impedance and the zero value of the imaginary part of the impedance are small. Thus, the bandwidths are narrow.

In order to understand the relation of power absorption and radiation impedance, equation 3.26 is recalled,

$$P = \frac{|F_e|^2}{4(D_a + |Z|)} \cdot (1 - \frac{(B - |Z|)^2}{|B + Z|^2})$$

When the model is at its resonance, the radiation impedance of the model is equal to the absolute value of added damping ($B = |Z|$). The equation can then be simplified to:

$$P = \frac{|F_e|^2}{4(D_a + |Z|)}$$

From the above equation, the maximum power absorption is dependent on the excitation force $|F_e|$, the damping of the power take-off system D_a and the radiation impedance of the model. The excitation force is directly related to the radiation damping (Newman, 1977). By recognising the peak of the damping curve and resonance period it is possible to identify the bandwidth of a wave energy device.

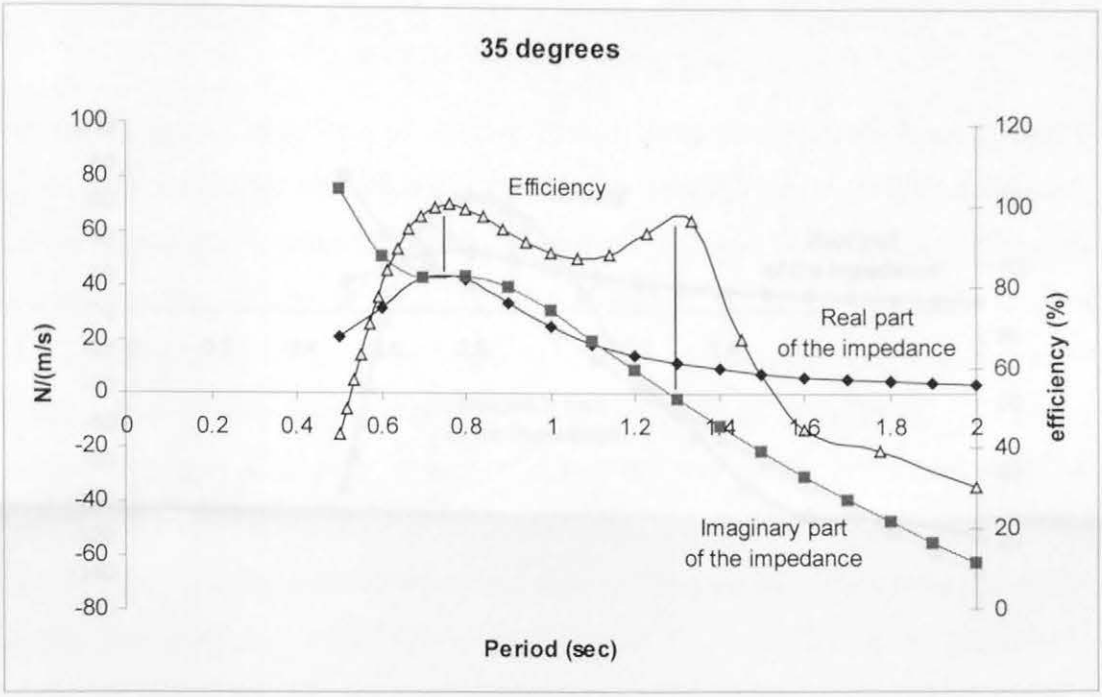

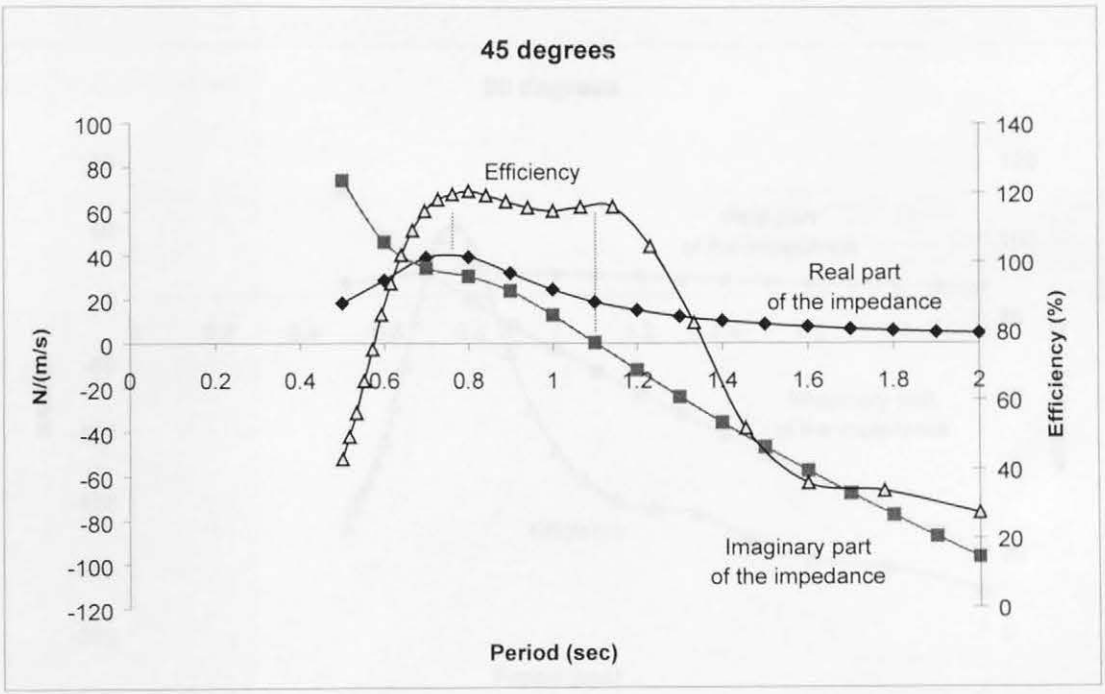

Figure 6.2 and 6.3. The efficiency curve and the hydrodynamic impedance curves are shown together. The model is at 35(above) and 45 (below) degrees slope angle. The left peak corresponds to the peak of the real part of the hydrodynamic coefficients and the right peak corresponds to the zero value of the imaginary part of the hydrodynamic coefficients.

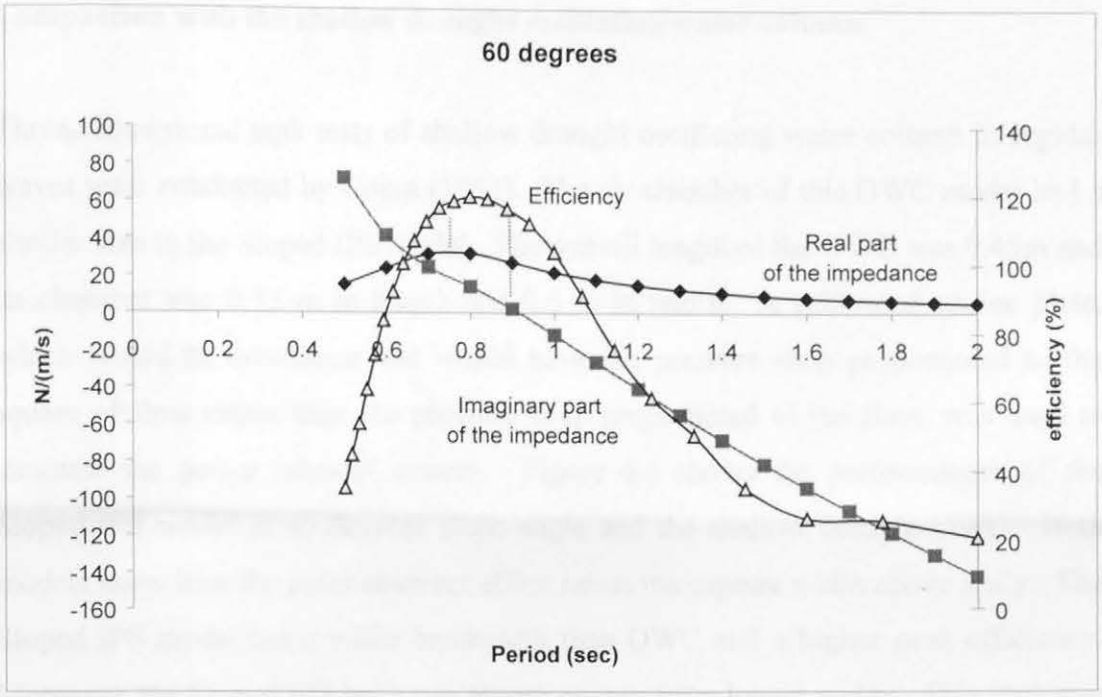

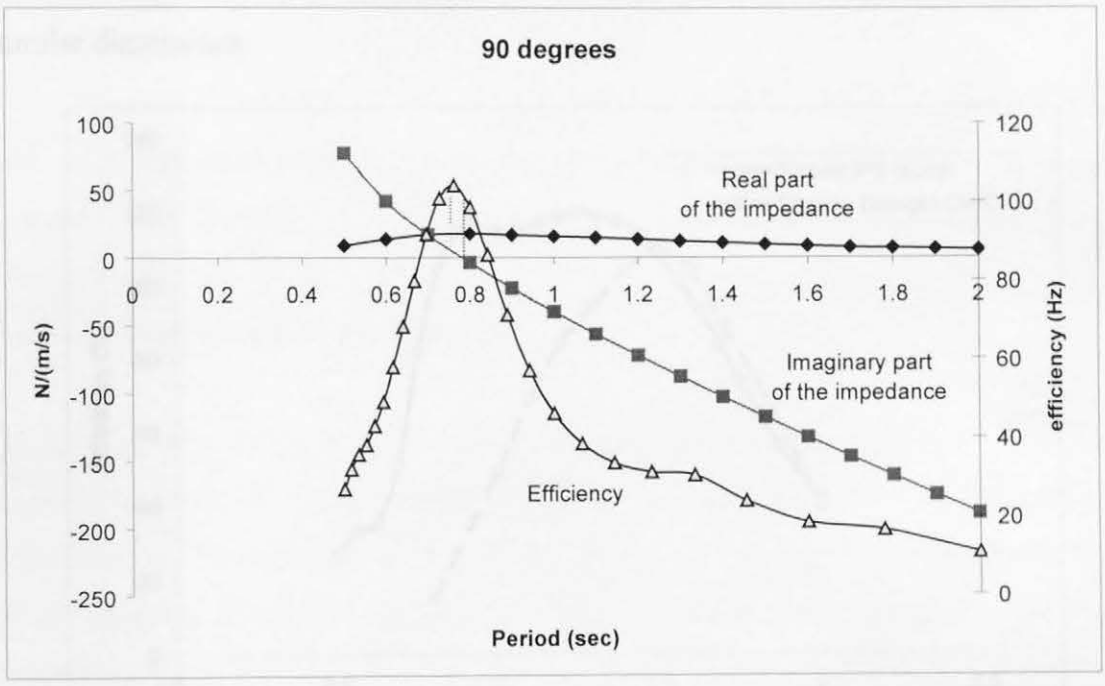

Figure 6.4 and 6.5. The efficiency curve and the hydrodynamic impedance curves are shown together. The model is at 60 (above) and 90 (below) degrees slope angle. The left peak corresponds to the peak of the real part of the hydrodynamic coefficients and the right peak corresponds to the zero value of the imaginary part of the hydrodynamic coefficients.

Comparison with the shallow draught oscillating water column

Three-dimensional tank tests of shallow draught oscillating water column in regular waves were conducted by Count (1982). The air chamber of this OWC model had a similar size to the Sloped IPS model. The overall length of the OWC was 0.45m and its chamber was 0.15 m in length and 0.3 m in width. A calibrated orifice plate, which would be non-linear and would have the pressure drop proportional to the square of flow rather than the pressure drop proportional to the flow, was used to simulate the power take-off system. Figure 6.6 shows the performances of the Sloped IPS model at 45 degrees slope angle and the shallow draught OWC. Both models show how the point absorber effect raises the capture width above unity. The Sloped IPS model has a wider bandwidth than OWC and a higher peak efficiency. Moreover, the Sloped IPS buoy can absorb energy from longer waves. This indicates that the Sloped IPS buoy can absorb more energy than the OWC when they have similar dimensions.

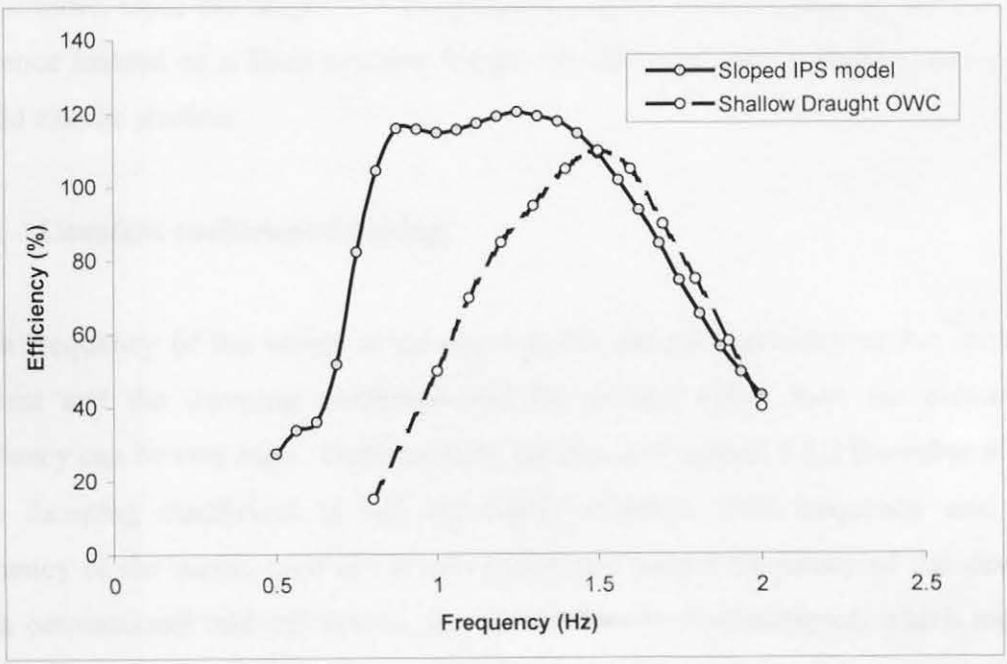

Figure 6.6. The relative performance of the Sloped IPS buoy and the Shallow Draught Oscillating Water Column (Count 1982). The Sloped IPS model is at 45 degrees slope angle and the air chamber of this OWC has similar dimensions to the buoy head.

6.3 Control of the power take-off system

For enhanced net energy conversion, the power take-off of a wave energy device may be bi-directional, not only able to convert mechanical power into electricity but also to convert electrical power back into forces during parts of the wave cycle. Such a capability, sometimes referred to as 'reactive' or 'smart', by allowing some external control over the apparent natural frequency of the system, can cause the device to be better 'tuned' to the prevailing wave periods. It may also be desirable, in principle, to be able to change the power take-off damping constant according to the wave period. However, advance wave information must be needed to perform this control strategy. In the last section, the experiments were conducted with the damping coefficients varied with wave frequency to get maximum power absorption. For the simplest power conversion, the damping coefficients will not vary with frequency. It is worth investigating the effect of such a constant damping coefficient.

Furthermore, since the Sloped IPS buoy uses a massive water inertia as the reacting reference instead of a fixed reaction frame, the effect of such a finite water mass should also be studied.

6.3.1 Constant coefficient damping

If the frequency of the waves is the same as the natural frequency of the moving element and the damping coefficient has the correct value, then the extraction efficiency can be very high. Unfortunately, as shown in section 5.3.2 the value of the ideal damping coefficient is not necessarily constant with frequency and the frequency of the waves does not always match the natural frequency of the device. For a conventional take-off system, the power flow is unidirectional, which means the power will only pass through the buoy body to the power take-off system but not inverse. For a "smart" power take-off system, the power flow is bi-directional, which means the power can pass through the device body to the power take-off system and the power take-off system can also provide power from an external source to correct the buoy motion for achieving better performance. However, in this

early stage of developing a new device we only assumed the power take-off system was a simple linear damper with a preset value.

Figure 6.7 shows the performance of the model at six different constant damping coefficients. The results give a good reference for setting the damping. When the damping coefficients are low, the peak of the capture width tends to be at low frequency. When the damping coefficients are higher, the peaks of the capture width shift to higher frequency. However, since the low frequency (long period) waves have higher energy density, it is important that a wave power device should have a high efficiency at low frequency. When the damping coefficient is set to as low as 5 N/(m/s), the device has a narrow bandwidth and a low overall efficiency. When the damping coefficients is 20 N/(m/s) which is near the absolute value of impedance at resonance frequency, the capture curve has a peak at the resonance frequency. The figure also shows that when the damping coefficient is 30 N/(m/sec) the device has a wide range of high efficiency and only a small reduction at about 0.8 Hz. This suggests that the correct damping coefficient value is not absolutely necessary. When the damping coefficient is set too high, the capture curve shifts to high frequency and the overall performance decreases. This suggests that for a device with a constant coefficient damper, the damping value should be set higher than the value at resonance but not too high.

Figures 6.8 shows the 35 degrees case. The damping value of 30 N/(m/sec) gives a wide bandwidth performance. Figure 6.9 shows the 60 degrees case. The damping value of 40 N/(m/sec) covers most of the area. Figure 6.10 shows the 90 degrees case. Although the damping value of 20 N/(m/sec) has higher peak efficiency, the performance at frequencies below 1.1 Hz is worse than the performance of the device at the damping value of 40 N/(m/sec).

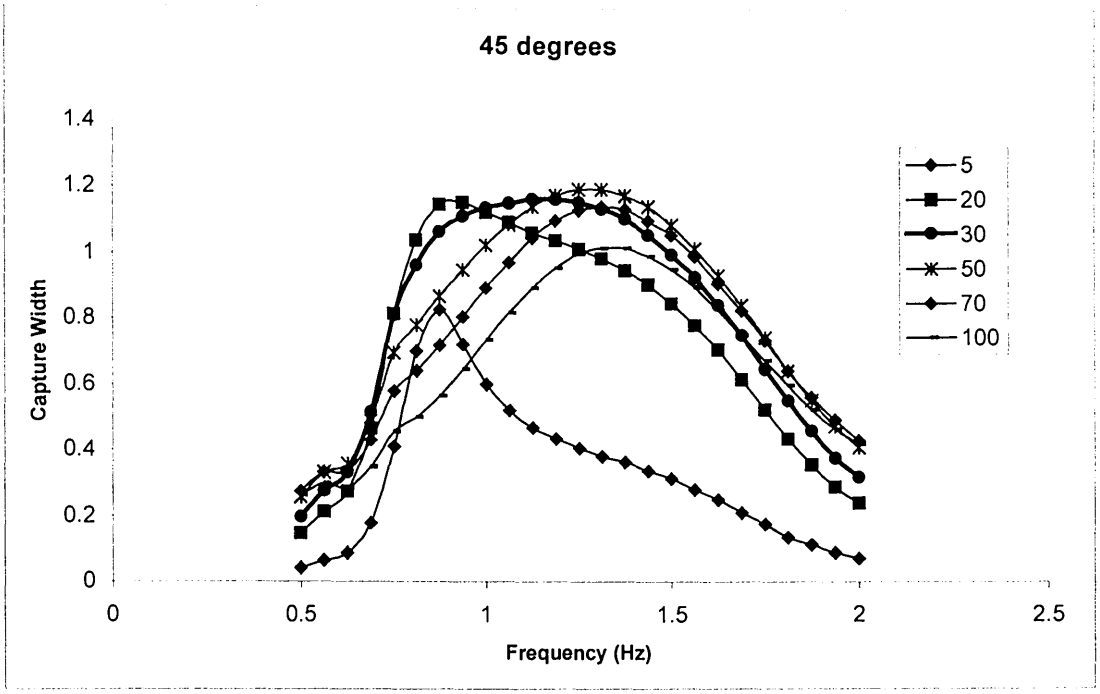

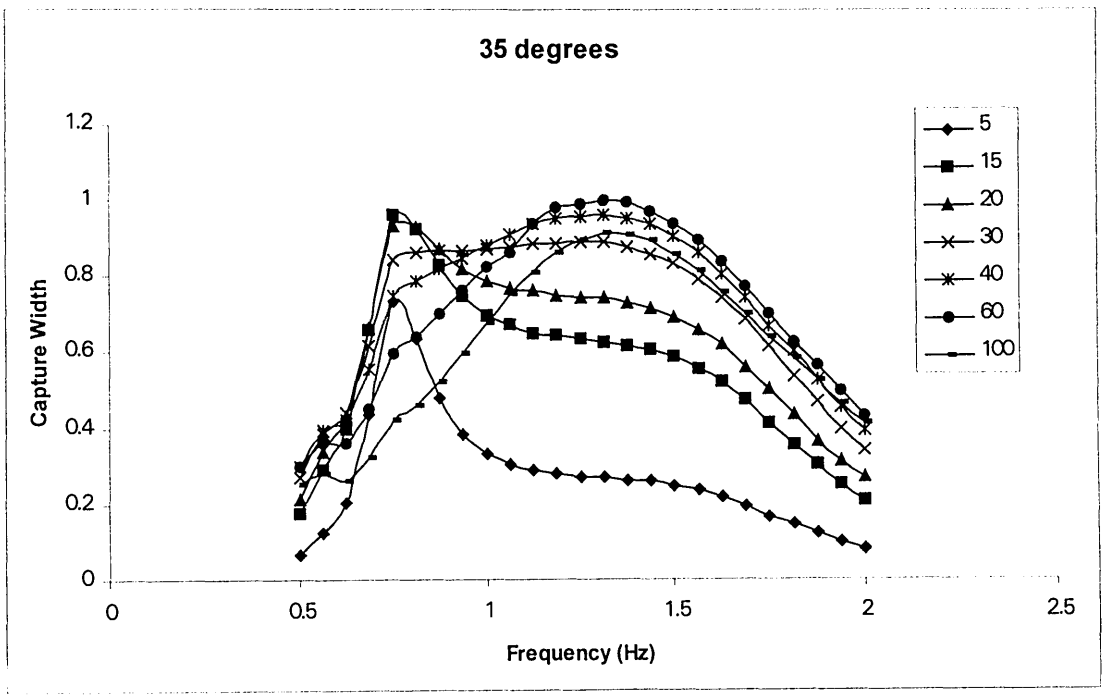

Figure 6.7and 6.8. The capture width of the model at 45 (above) and 35 (below) degrees angle of inclination. The legend shows the preset values of damping coefficient in Nsm^{-1}.

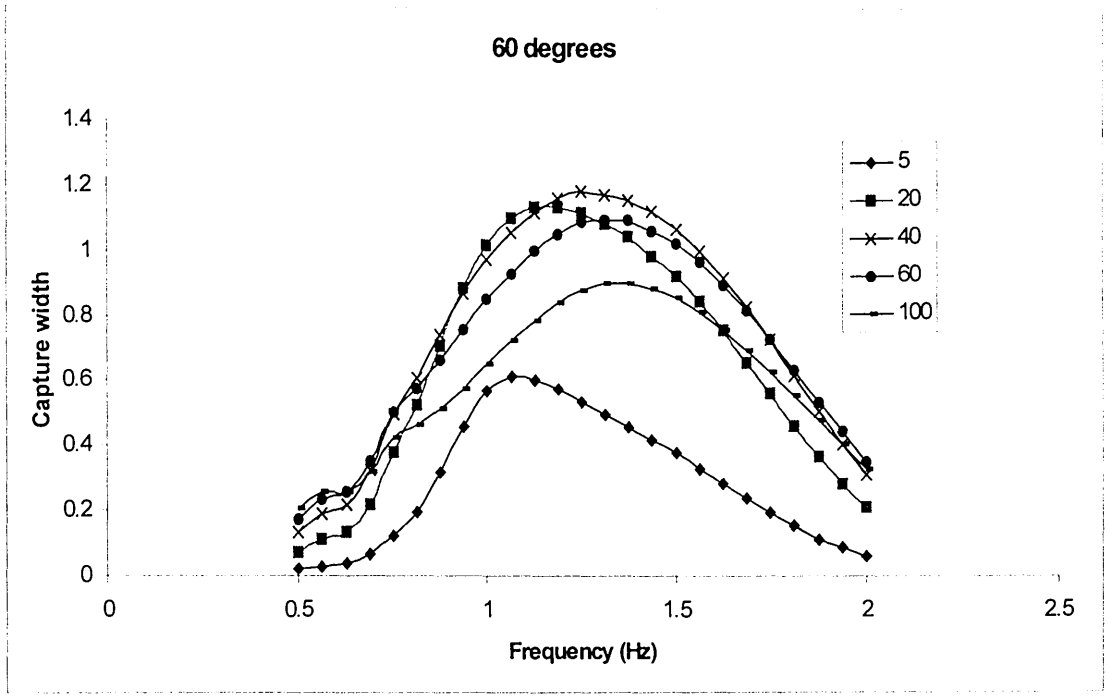

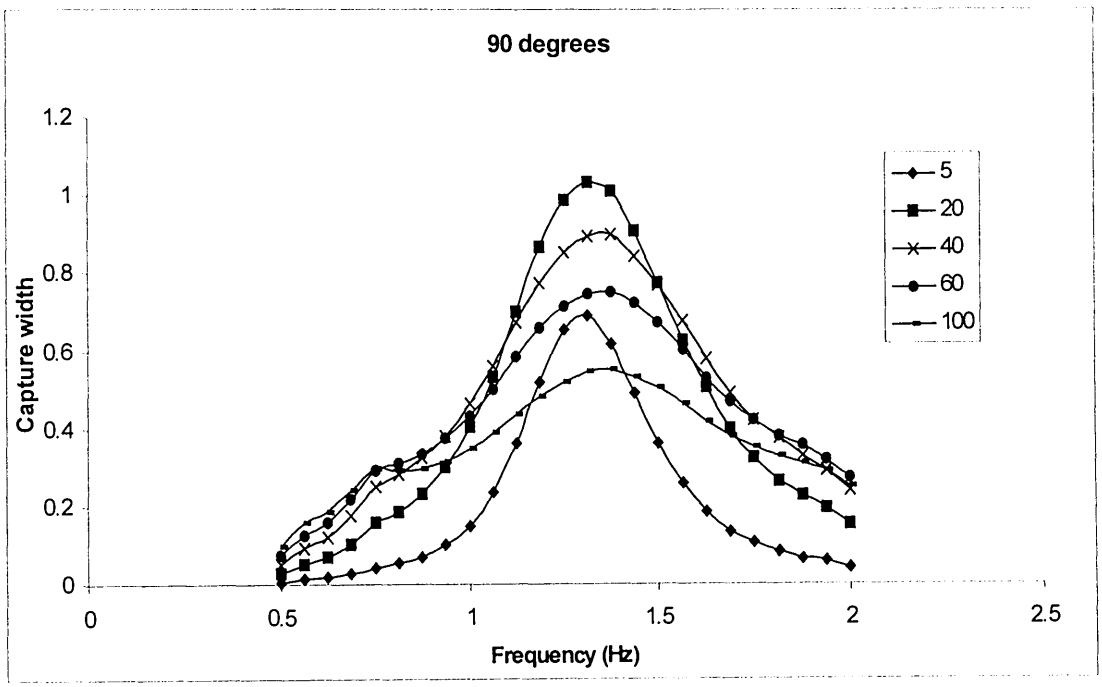

Figure 6.9 and 6.10. The capture width of the model at 60 (above) and 90 (below) degrees angle of inclination. The legend shows the preset values of damping coefficient in Nsm^{-1}.

6.3.2 Damping against a finite mass

It is necessary to provide wave energy converters with a source of reaction for their power take-off system. In these tank tests the simulated power takeoff system was connected to a fixed structure giving an infinite reference mass. However, the power take-off system of the Sloped IPS buoy is designed to connect with a piston inside a tube and react against the water mass. Here a simple model gives some references about the finite mass effect and the design of tube volume.

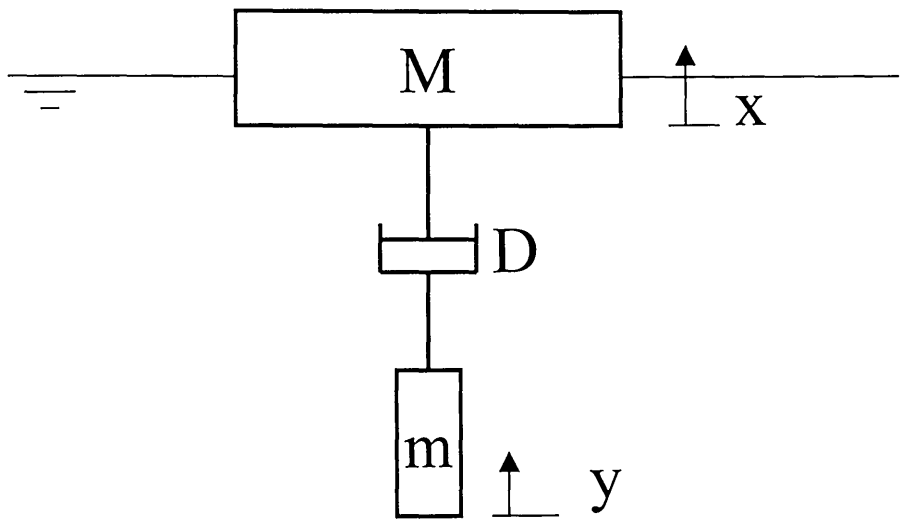

Figure 6.11. Simplified free body diagram of the wave power device

where

M represents the device which includes the added mass, added damping and spring term of wave power device.

m represents the piston mass and tube water mass.

D is the damper for extracting power.

x is the motion of the device.

y is the motion of the piston and water mass.

In a Sloped IPS buoy the water inertia tubes are contained inside the stabilising plate. They do not change the profile of the buoy head, so the hydrodynamic impedances are assumed unchanged. The added mass due to the water piston, the friction loss

between water and tube and the vortex loss at the tube intake are all ignored. We can assume that the device is a simple oscillating system shown as figure 6.11.

The force acting on the damper is equal to the force to accelerate the mass and can be expressed as:

$$-D\cdot(\frac{dx}{dt}-\frac{dy}{dt})=m\cdot\frac{d^2y}{dt^2} \qquad (6.1)$$

Substituting $d/dt = i\omega$, the velocity of mass is:

$$\dot{y}=\frac{-D}{i\omega\cdot m-D}\dot{x} \qquad (6.2)$$

By rearranging the equations 6.1 and 6.2, the force F_B acts on damper can be expressed as a function of the velocity of the device:

$$F_B = DU\cdot(1+\frac{D}{i\omega\cdot m-D}) \qquad (6.3)$$

When the water tube mass m is infinite, the force acting on the damper is equal to DU. When the mass is zero, the force acting on damper is equal to zero.

By recalling the equation 3.12 the equation of motion can be expressed as:

$$F_B = DU\cdot(1+\frac{D}{i\omega\cdot m-D}) = ZU+Wa \qquad (6.4)$$

If the damper can only supply a linear force proportional to the velocity, the damping can be expressed as:

$$D=|Z|$$

The control force coefficient C can be

$$C=|Z|\cdot(1+\frac{|Z|}{i\omega\cdot m-|Z|}) \qquad (6.5)$$

From equation 3.26 the power extracted is:

$$P = \frac{|F_e|^2}{4(D_a + |Z|)} \cdot (1 - \frac{(C - |Z|)^2}{|C + Z|^2})$$

The calculations of the model at four slope angles are based on the measured data of the radiation impedance and the excitation force in section 5.2.1 and 5.2.5. Figures 6.12 to 6.14 show the device capture width against the frequency with different reaction mass. In figure 6.12 the curves slightly shift from high frequency to low frequency when the reactive mass increases. When the reactive mass is 10 kilograms, the peak of capture width increases to 1.4. When the reactive source is fixed, the peak of capture width is only 1.2. This is probably caused by the mass inducing a phase difference between the wave exciting force and the power take-off system and compensated this phase error. When the reactive mass is as small as 3 kilograms, the overall performance drops. The results show that the finite reactive mass can *improve* the peak efficiency of the device and slightly shift the overall efficiency curve to the high frequency side. Similar results show in figure 6.13 and 6.14, when the model is at 35 and 45 degrees slope angle. In figure 6.15 the model is in heave mode (90 degrees), there is no efficiency reduction in the peak of the curve when the reactive mass is small.

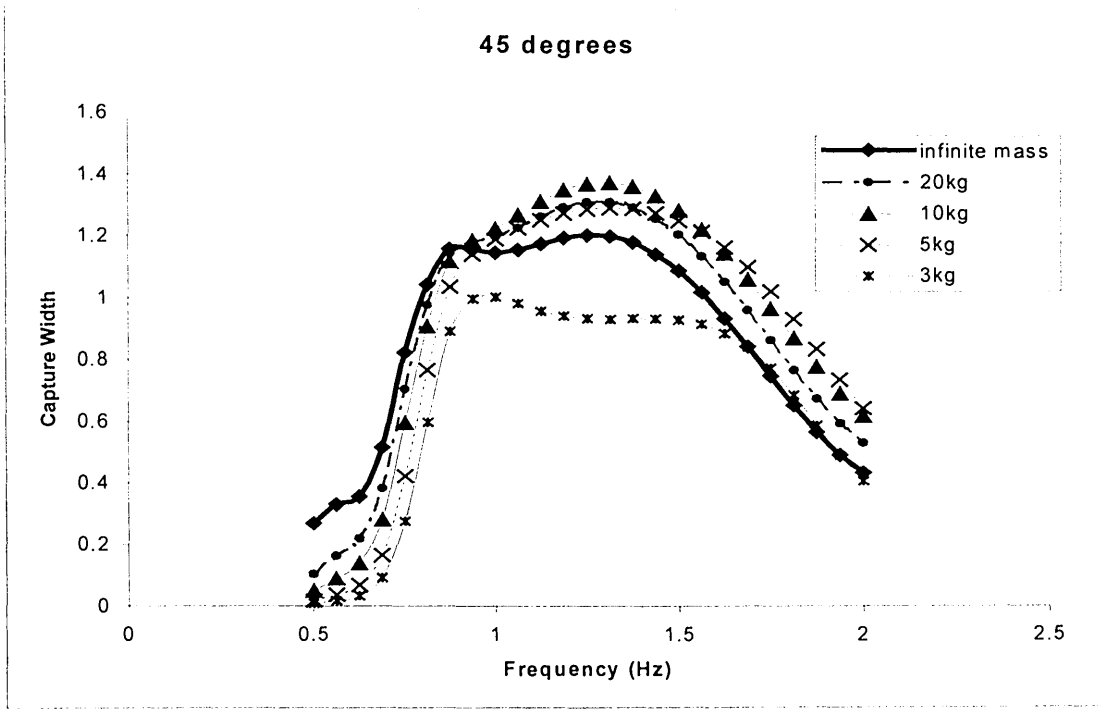

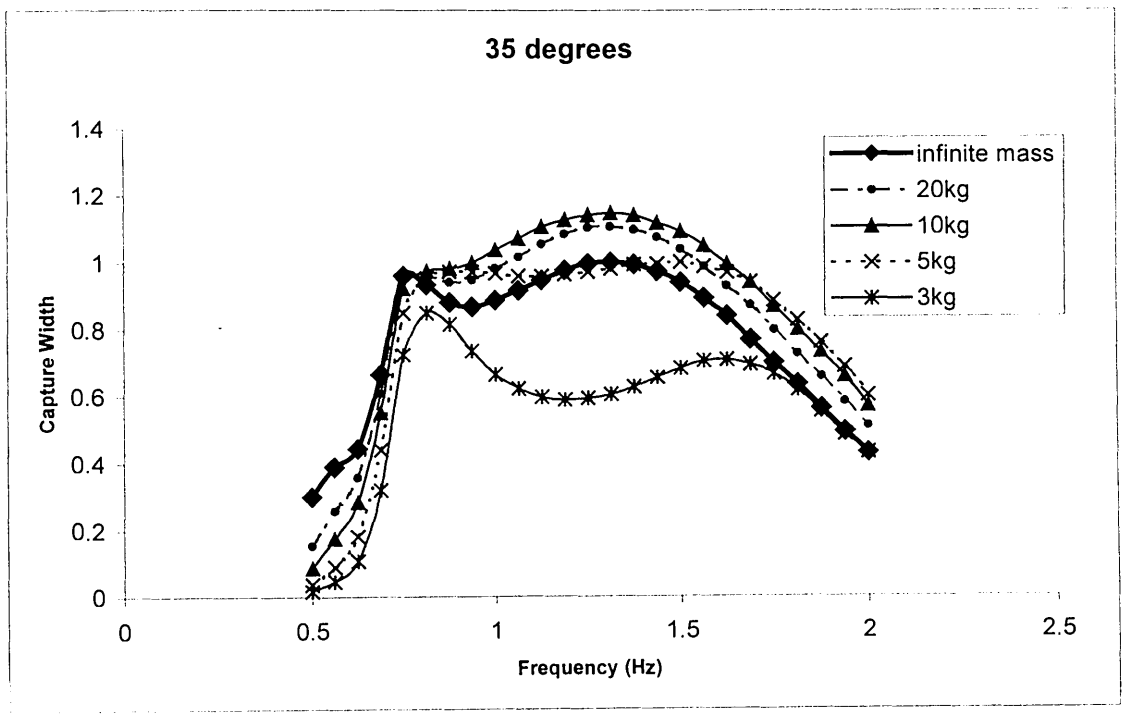

Figure 6.12 and 6.13. Capture width of the model at 45 (above) and 35 (below) degrees slope angle with various masses of reactive water.

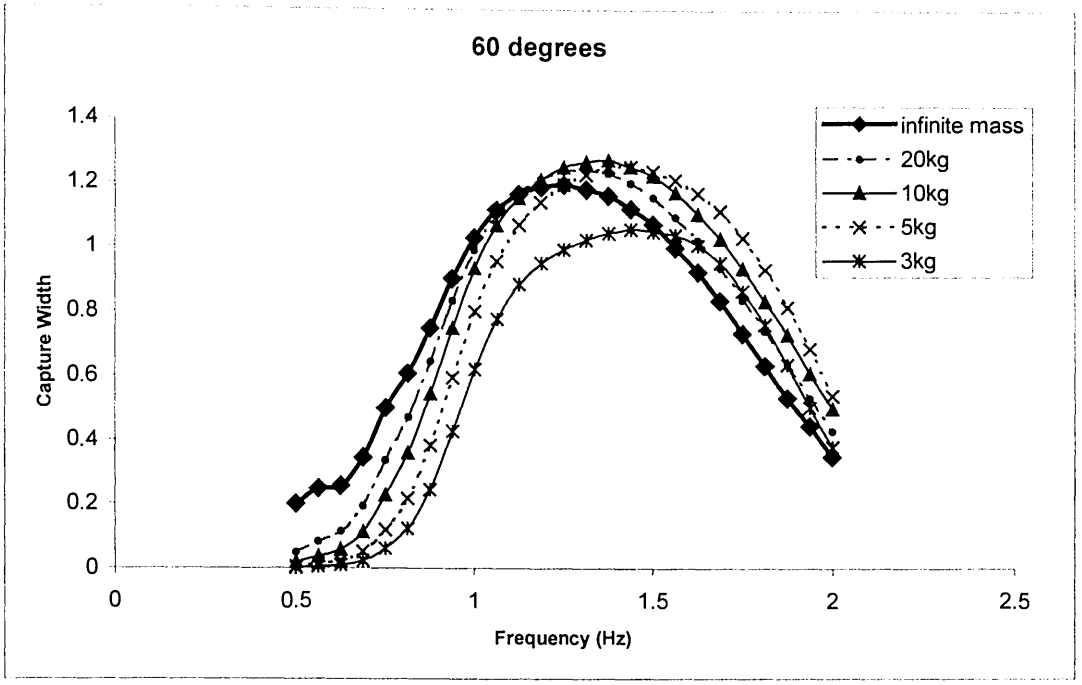

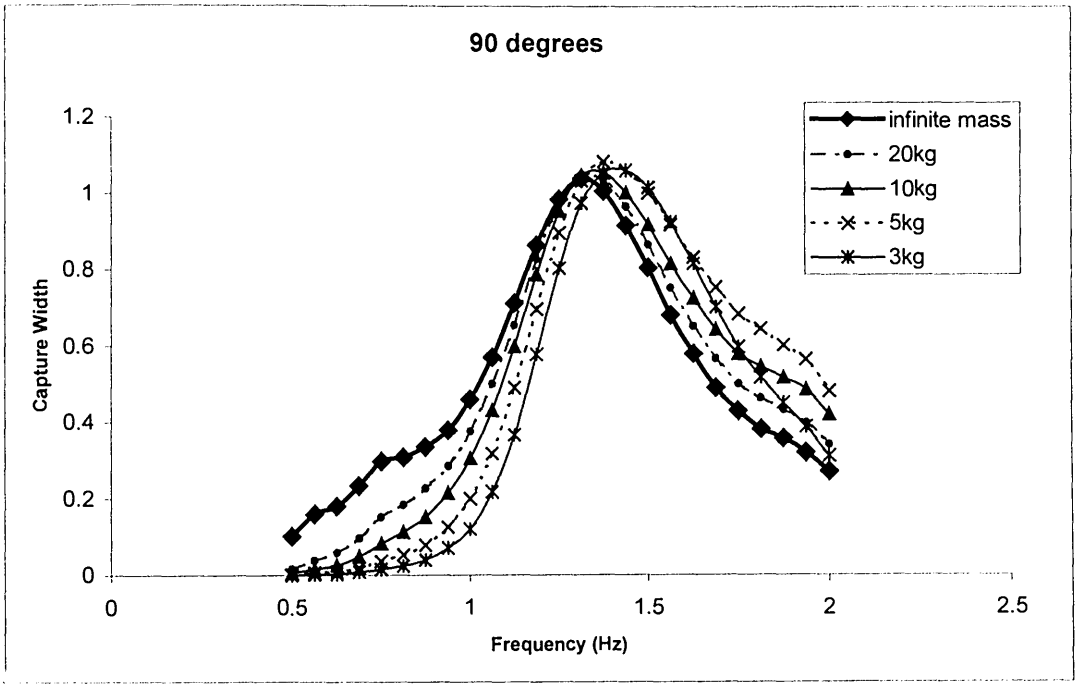

Figure 6.14 and 6.15. Capture width of the model at 60 (above) and 90 (below) degrees slope angle with various masses of reactive water.

6.4 Conclusions

- The performances of the model at different slope angles are compared. The 45 degrees slope angle has much better performance than the vertical (90 degrees) one. Its bandwidth is wider and the efficiency is higher.

- Efficiency values greater than unity are achieved when the sloped angle is 45 and 60 degrees.

- A double-peak effect is found. One of the peaks corresponds to the natural frequency of the model and the other to the peak of the real part of the hydrodynamic impedance, which is also related to the exciting force. This indicates a possible method for identifying the bandwidth from the hydrodynamic impedance.

- The power take-off system has been simulated by a simple linear damper. Various constant damping coefficients have been applied to identify the best value of the damper. The results show that the damping value should be set slightly higher than the value of the model at resonance.

- The Sloped IPS is designed to use water mass as the reacting reference. The effect of finite mass is investigated. The results show the finite mass can improve the peak efficiency but slightly shift the overall efficiency curve to the high frequency side.

Chapter 7

Model tests in irregular waves and full-scale applications

7.1 Introduction

Most of the model tests in this work were carried out in regular waves. The results of these tests identify the basic characteristics of the sloped IPS device. However tests in irregular seas, reasonably representative of the real sea conditions, are also important. Since the results of the regular wave tests suggest that the 45 degrees slope angle produces a particularly wide bandwidth, the model tests in irregular waves were restricted to this angle. The test spectra were based on the Pierson-Moskowitz (PM) definition used with and without directional spreading. Data for power absorption, efficiency and displacement were obtained. The latter is useful for optimising the ram stroke length in the full-scale device. Efficiencies measured in the PM spectra are replotted with "stretched" period axes to give a better feel for the likely net annual productivity in offshore Scottish waters.

7.2 Tests in irregular waves

According to linear theory it is possible to obtain performance data for irregular seas by superposing the results obtained from tests in individual wave components. Therefore it is sufficient from a hydrodynamic point of view to analyse a device in incident regular sinusoidal waves of small wave steepness. As the results of the

encouraging regular wave tests some experiments were undertaken in irregular waves. Two series of waves were used in the experiments. One used the PM spectrum without a spreading function (uni-directional waves) and the other the PM spectrum with a spreading function of $cos^{2n}(\theta/2)$.

7.2.1 Tests in PM waves without spreading function

The irregular wave tests were all conducted at 45 degrees slope angle. The PM spectrum was first used without angular spreading function. The root mean square (rms) wave height of the PM spectra is determined by one parameter, the wind speed. The detail is described in appendix J. In tank tests, it is convenient to define a spectrum by period rather than by wind speed. For wave power, Mollison (1976) suggested that calculation of the "energy period" T_e from a wave record would be more convenient and better defined than "zero crossing period" T_z. The rms wave height H_{rms} can be expressed as:

$$H_{rms} = c \cdot T_e^2 \qquad (6.6)$$

Where c = 0.0136 m/sec^2.

Here the rms wave height is decided by wave energy period only. In order to test the model in different wave amplitudes without varying the wave energy period, a rms wave height multiplier was employed to re-scale the rms wave height (Jeffrey *et. al.*, 1978).

The damping value of the model was set before each test. Figure 7.1 shows a typical time series for velocity and power for the model in a PM spectrum with 1.14 seconds energy period and rms wave height of 6.58 mm. The damping coefficient was set to 18 N/(m/s).

Altogether seven energy periods and six wave heights were chosen for power absorption measurement, 42 tests in total. After 30 seconds from start up data were logged at 32 samples per second for 64 seconds and the mean power value then

calculated. Figure 7.2 shows the power absorption results for the PM spectrum with various wave energy periods and rms wave heights.

The displacement response of the model in two tests of the same wave sequence (T_e=1.14 seconds) but with rms wave heights of 6.6 mm and 13.7 mm is plotted in figure 7.3. Data from the 6.6 mm H_{rms} test have been multiplied by the ratio of 13.7/6.6. The resulting figures show very similar response patterns. The xy plot of the two data sets shows a fairly small amount of scatter either side of the 2.08 slope line.

The experimental efficiency values for the 42 tests are shown together with the calculated efficiency values in figure 7.4. For calculating the efficiency value based on the regular wave tests for a PM spectrum, firstly the power distribution in the PM wave spectrum is divided into 24 discrete units (1/16 Hz) between 0.5 and 2 Hz. Secondly, These incident wave power components at each frequency are multiplied by the model efficiency values from the previous regular wave tests at the corresponding frequency to obtain the prediction. The results show that the efficiency values vary with the wave height even at the same energy frequency and the variation of them could be as big as 20 %. The experimental values are about 20% to 30 % lower than the calculated values.

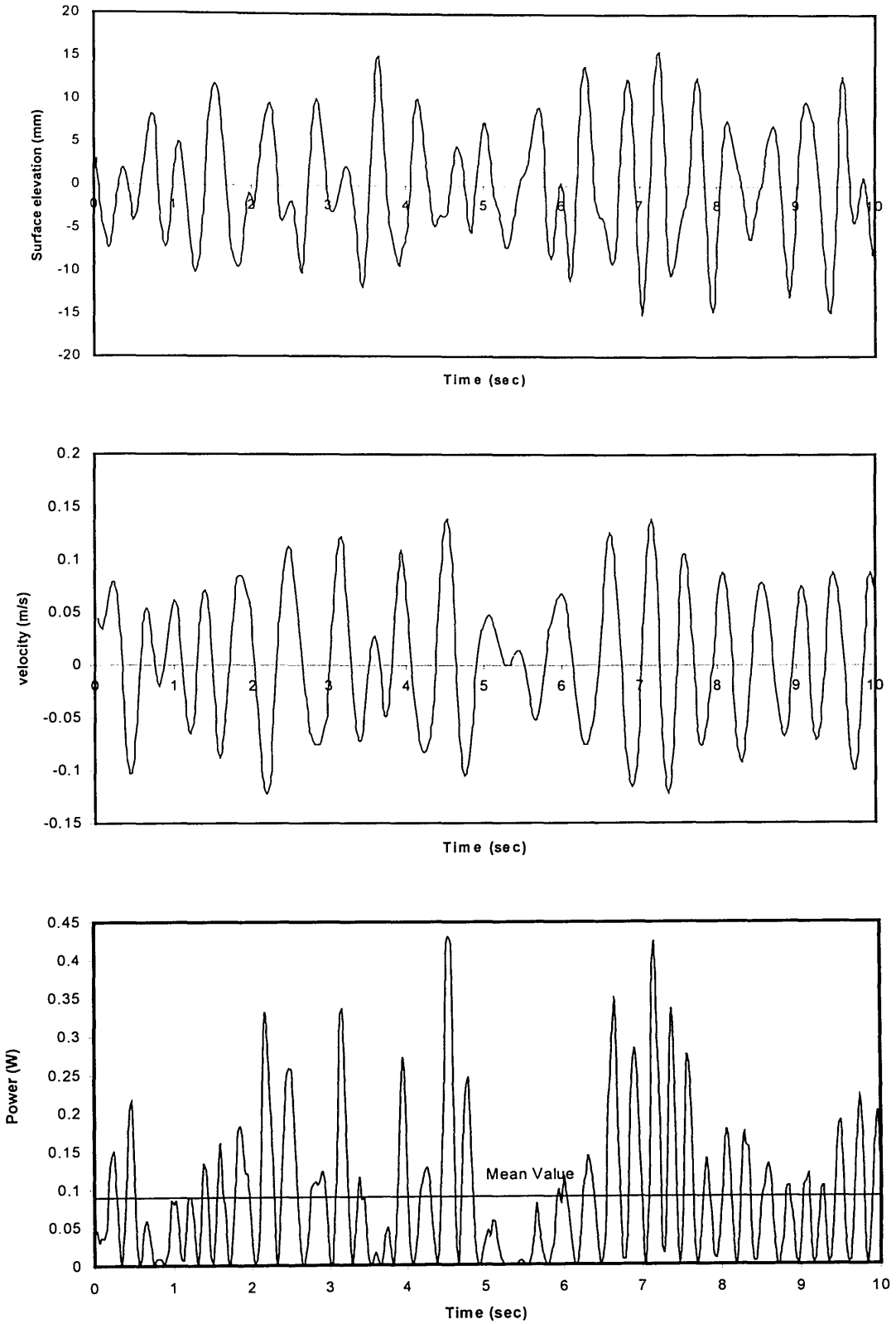

Figure 7.1. A short section (10 seconds) of the time series for a typical irregular wave test. From the top, these show wave elevation, model velocity and power. The sea is a 1.14 second PM spectrum with H_{rms} of 6.58 mm.

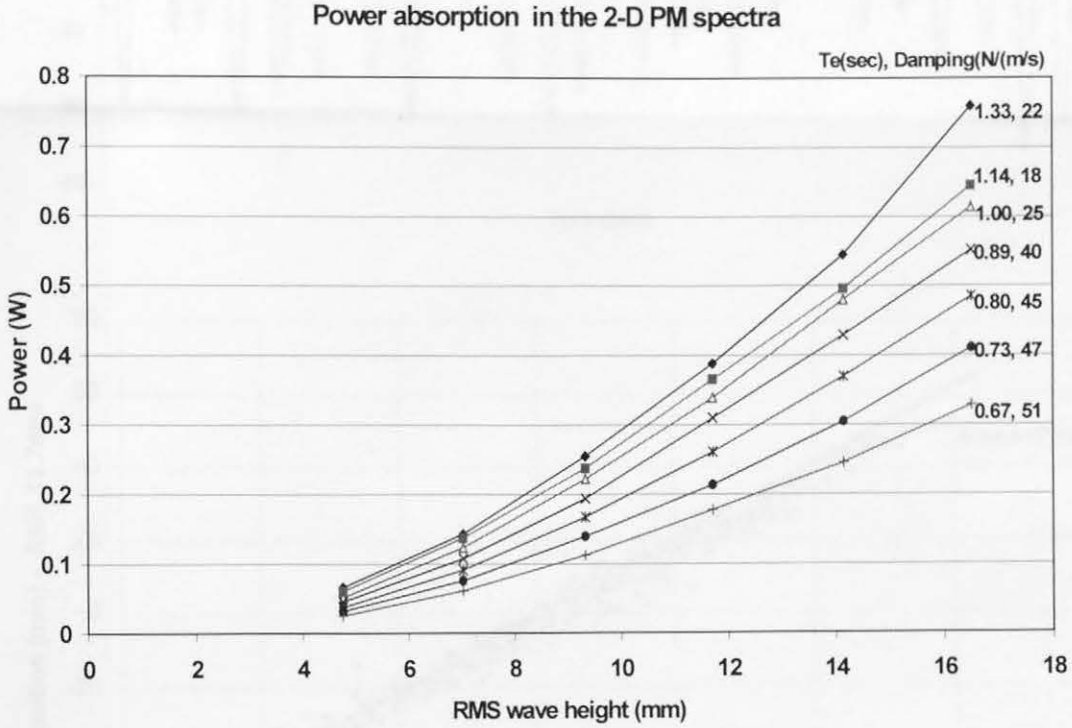

Figure 7.2. Power absorption in the PM spectra, 42 tests at seven periods and six wave heights. The model is at 45 degrees slope angle and its damping is set according to the energy period. The numbers at the right hand side of each curve show the wave energy period and the damping coefficient value.

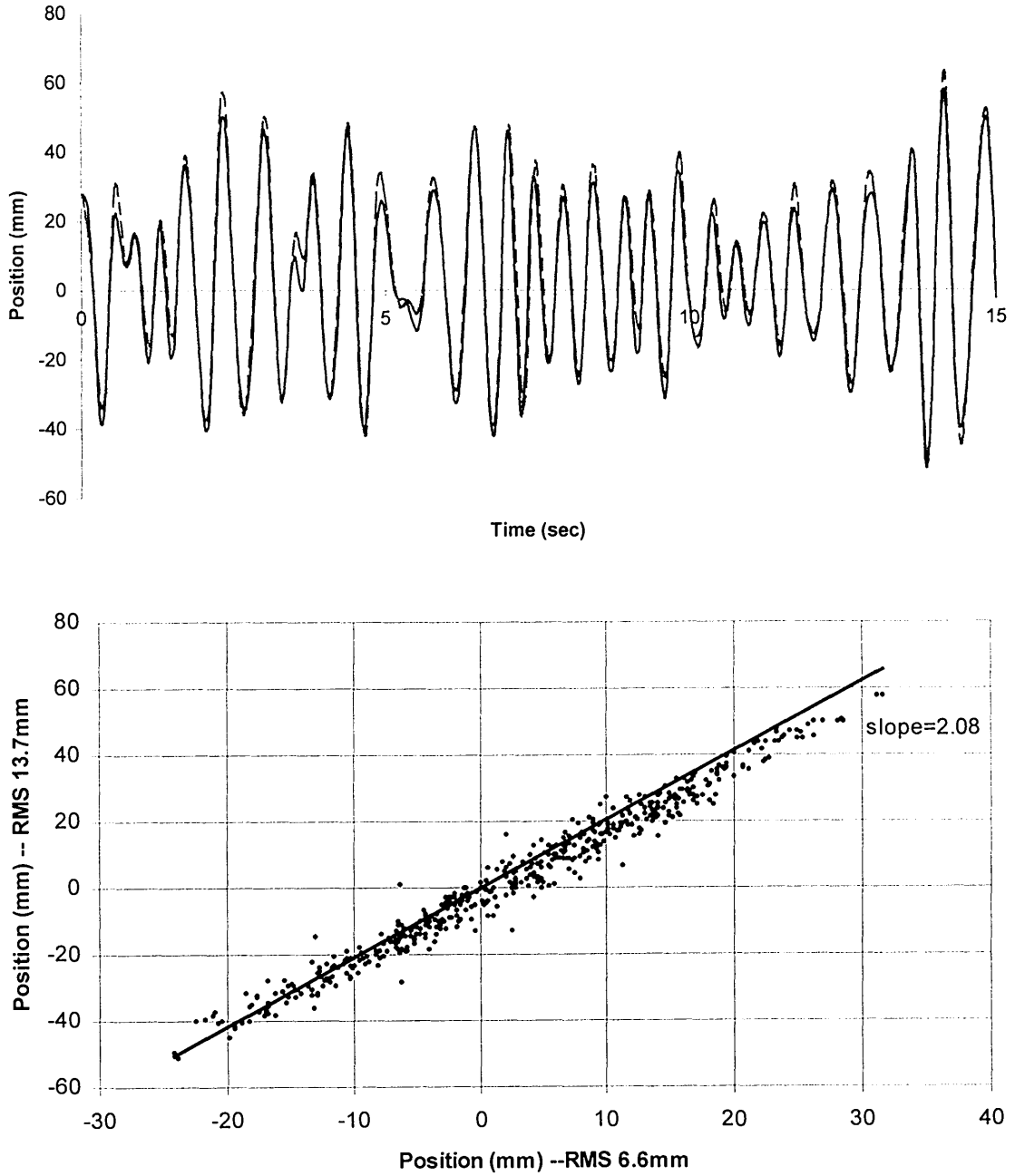

Figure 7.3. Linearity of the model in irregular waves. Top: Two tests at different rms wave heights. The displacement time series for an rms wave height of 6.6 mm has been multiplied by 2.08 (dotted line) and plotted with the time series corresponding to an rms wave height of 13.7 mm. Bottom: xy plot of data points in the 6.6 mm rms wave height, and 13.7 mm RMS wave height tests corresponding to the same time position in the experiments. Clearly the results show very linear behaviour.

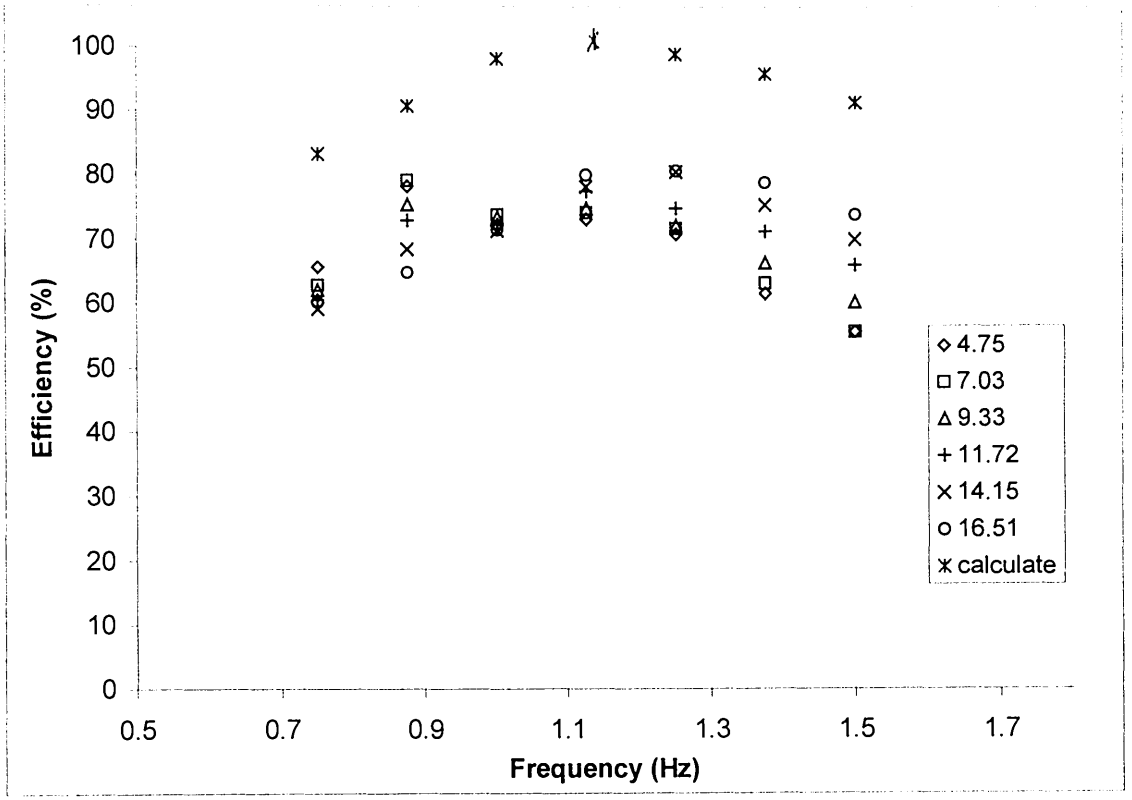

Figure 7.4. Experimental and calculated efficiency values for the PM spectrum without spreading function in various wave heights. The calculated results are based on the measured impedance and excitation forces. The calculated efficiency values are higher than the measured ones. The legends show the rms wave heights in mm.

7.2.2 Tests in PM waves with angular spreading function

A simplified real sea can be best described in terms of a frequency spectrum and a directional spreading function. Some theoretical forms have been suggested for which the distribution of directions is independent of the period. The directional spectra can be expressed as:

$$G(f,\theta) = \frac{S(f)\cdot\cos^n(\theta-\theta_o)}{\int_0^{\pi}\cos^n(\theta-\theta_o)d\theta} \qquad (6.7)$$

Where $S(f)$ is a one dimensional PM spectrum.

θ_o is the principal wave direction and $-{}^1/_2\,\pi \le \theta-\theta_o \le {}^1/_2\,\pi$.

n is the spreading index.

The common use of n value is 2 or 4. Hogben (1970) suggested that the value n = 4 should be used since the corresponding narrower spread of directions would be more accurate.

Mistsuyasu *et al.* (1975) later suggested that the directional spread depends on the period, being narrowest at the period corresponding to the wind speed. The formula is:

$$G(f,\theta) = \frac{S(f)\cdot\cos^{2n}[\frac{1}{2}(\theta-\theta_o)]}{\int_0^{2\pi}\cos^{2n}[\frac{1}{2}(\theta-\theta_o)]d\theta} \qquad (6.8)$$

where $\pi \le \theta-\theta_o \le \pi$.

The spreading index can thus be expressed as a function of frequency:

$$n = 15.85\cdot(\frac{f}{f_o})^5 \qquad for\ f \le f_o$$

$$n = 15.85\cdot(\frac{f}{f_o})^{-2.5} \qquad for\ f \ge f_o \qquad (6.9)$$

The same system was carried out in the PM spectrum with spreading function which was $cos^{2n}(\theta/2)$. Since the wave making software did not support the spreading index n as a function of frequency, we then chose $n=4$ to give the directional distribution of the waves.

Figure 7.5 shows the power absorption for the model in the PM spectrum with spreading function. The damping value was set before tests to suit the best value for the energy period T_e. Results show that the spreading function reduces the power absorbed.

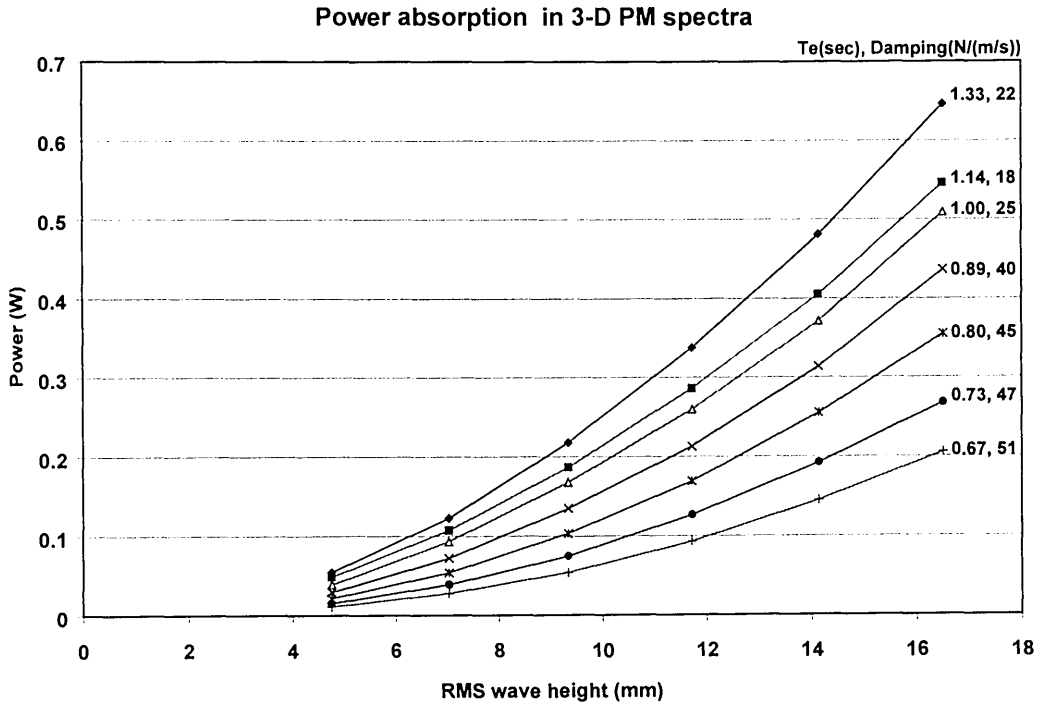

Figure 7.5. Power absorption in the PM spectra with spreading (n=4). The model is at 45 degrees slope angle and its damping is set to suit the energy period. The numbers of the right hand side of each curve show the wave energy period and the damping coefficient value.

7.2.3 Efficiency in PM spectrum with and without spreading function

Since a PM spectra with no spreading could be thought as a PM spectra with very long crests, it is convenient to call it as 2-D PM spectra. The PM spectra with a spreading function will then be called as 3-D PM spectra. Figure 7.6 shows the efficiency curves of tests with both the 2-D and 3-D PM spectrum at 45 degrees slope angle. The performance of the model in the 2-D PM spectrum is better than that in the 3-D PM spectrum. When the model is in a 2-D PM spectrum, the variation in short energy period is bigger than in a long energy period. The average efficiency of the model in the 2-D PM waves is about 75% to 60%. In the 3-D PM waves variation is smaller than in 2-D PM waves. It also shows lower efficiency in short waves and higher efficiency in long waves. This indicates that the model can absorb more energy from long waves which have more energy than short waves. The average efficiency of the model in the 3-D PM sea state is between 35% and 55%.

7.3 The motion of the device

Since it is envisaged that the Sloped IPS buoy will use a linear hydraulic ram as a power take–off device, the stroke of the ram is an important design factor. The motion of the model could give an indication of the stroke length. Figure 7.7 shows the rms and peak-to-peak stroke of the buoy motion when it was at 3-D PM spectrum with optimised damping value. The movement of peak-to-peak is about 5.5 times the rms stroke of the buoy. The rms movement of the buoy is about twice of the rms wave height. Thus, the peak-to-peak motion of the model is about 11 times the rms wave height.

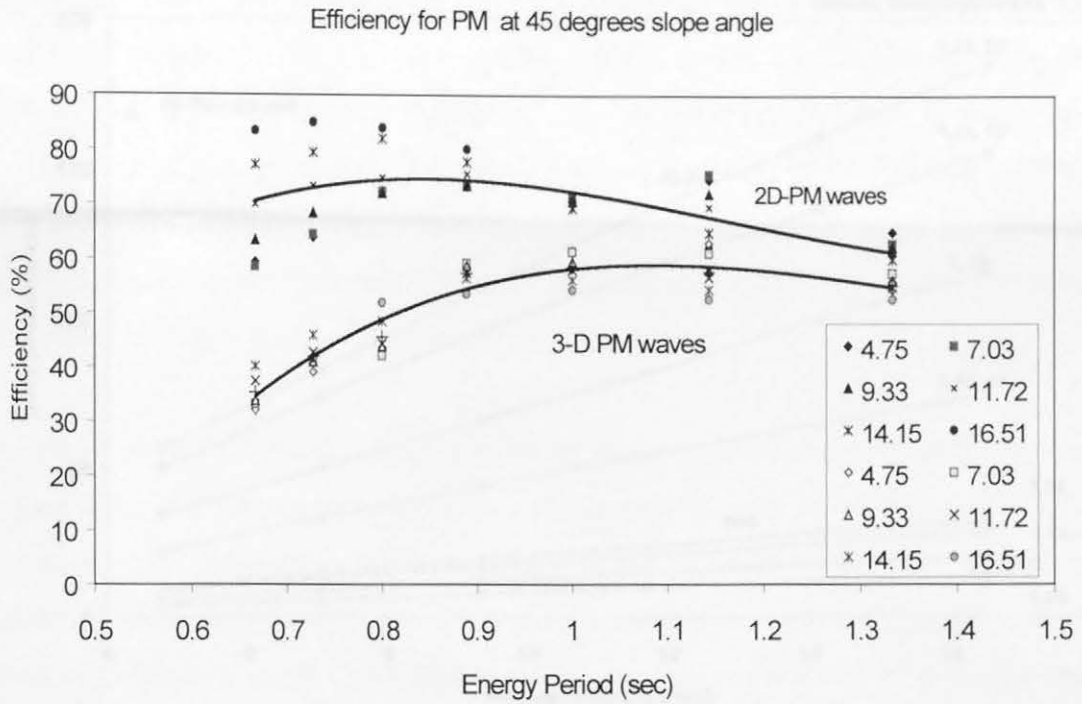

Figure 7.6. Efficiency curves for the model at 45 degrees slope angle in 2-D and 3-D PM waves. The damping values are based on the optimised values for regular waves. The legends show the rms wave heights in mm.

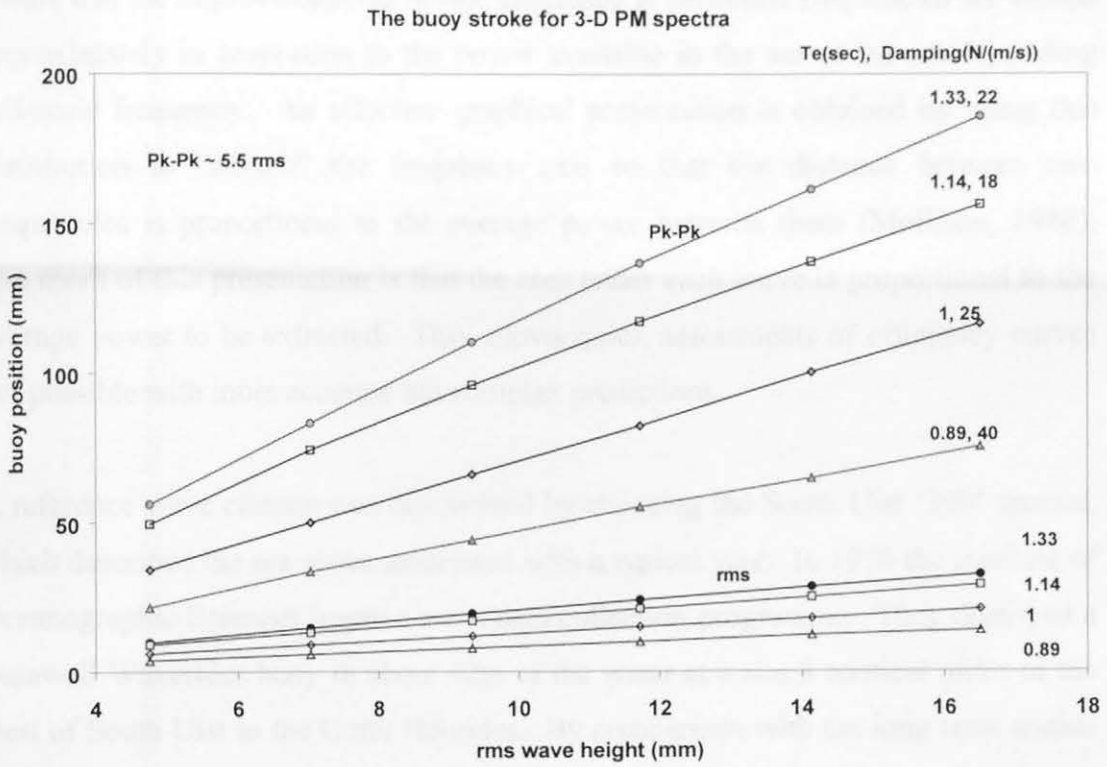

Figure 7.7. Peak-to peak (tope 4 lines) and rms of the buoy motion at 45 degrees slope angle. The peak-to-peak distance is about 5.5 times rms stroke of the buoy and is about 11 times rms wave height.

7.4 Full-scale application

Experiments on a new device usually begin with tank tests in regular waves of moderate wave height. The aim of output predictions at this stage is mainly to ensure that the improvements in device efficiency at particular frequencies are valued approximately in proportion to the power available in the sea at the corresponding full-scale frequency. An effective graphical presentation is obtained by using this distribution to "stretch" the frequency axis so that the distance between two frequencies is proportional to the average power between them (Mollison, 1980). The merit of this presentation is that the area under each curve is proportional to the average power to be extracted. This allows quick assessments of efficiency curves not possible with more accurate but complex predictions.

A reference wave climate was determined by choosing the South Uist '399' spectra, which described the sea states associated with a typical year. In 1976 the institute of Oceanographic Sciences began a wave data collection programme. They deployed a Datawell Waverider buoy in about 42m of the water at a site 8 nautical miles to the west of South Uist in the Outer Hebrides. By comparison with the long term annual wind statistics Crabb (1979) selected 399 wave records to represent a typical year and converted them to frequency distributions. Components in each spectrum were identified as being due to wind conditions, wind conditions just before sampling and distant storms.

The '399' weighted period axis is produced by deforming the period axis so that the distance of points is proportional to the power available in the 399 spectra in that interval. The efficiency curve is re-plotted from the experimental results of regular waves shown in figure 5.32 against full-scale period in figure 7.8 and 7.9. Curves are drawn for three different scales, transformed from model scale after dividing frequency by the square root of scale factor. The area under the curve is proportional to the mean annual efficiency, assuming no power limit, linear behaviour and no change of efficiency with angle.

Table 7.1 gives an idea about the wave power available of the scaled up device. The calculations are based on Skyner's (1987) report for the solo Duck. The mean annual power of 399 spectra is 58 kW/m. The power take-off system is assumed to be 100% in efficiency, the point absorber effect and non-linearity are ignored.

Scale factor	Water line length (m)	Width (m)	Power in width (kW)
50	7.5	25	1450
80	12	40	2320
100	15	50	2900
150	22.5	75	4350
200	30	100	5800

Table 7.1. The power available for different scales

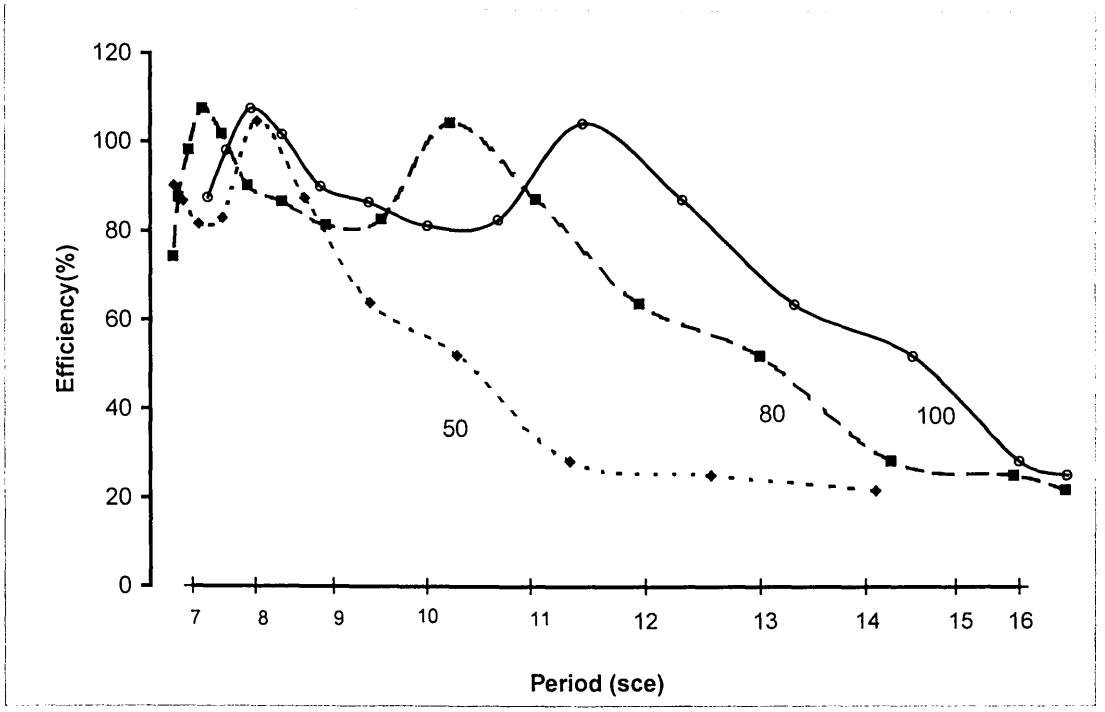

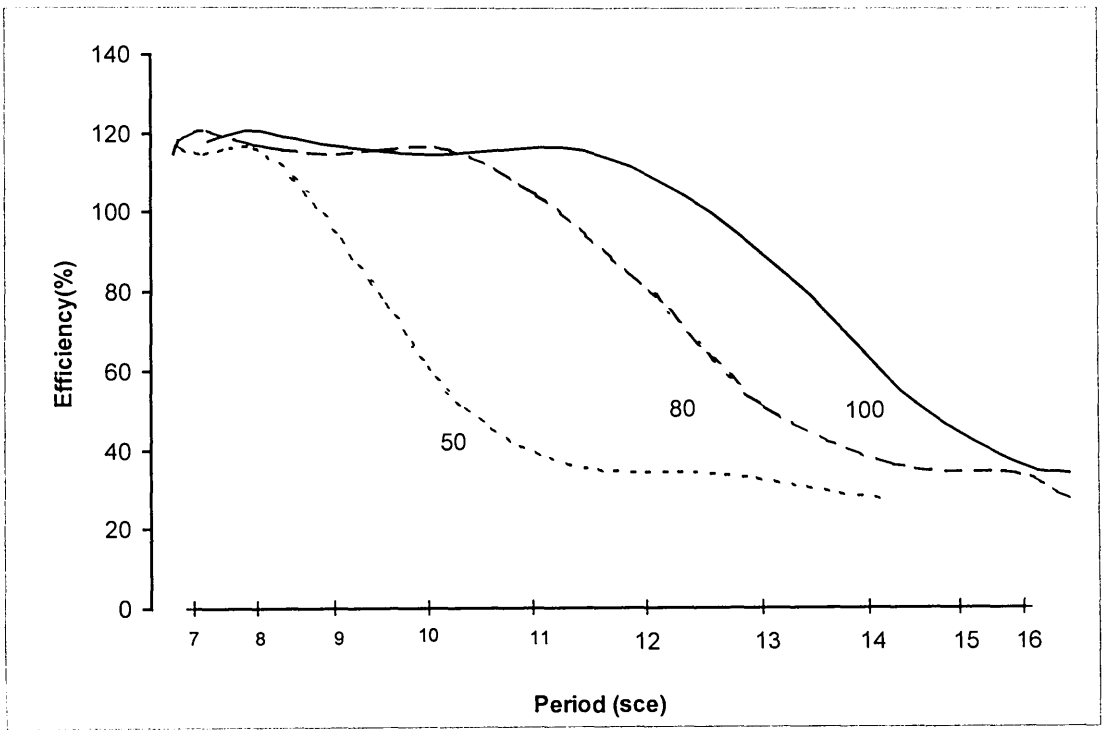

Figure 7.8 and 7.9. Efficiency curves for regular waves from experimental (above) and calculated (below) results, plotted against a period axis stretched so as to represent the distribution of power at South Uist 399. Scale factors are marked.

7.5 conclusions

- Tests in PM spectra with and without angular spreading function were carried out. The experimental results are lower than the calculated results.

- The efficiency of the model in PM spectra without angular spread function is higher than the one with angular spreading function.

- The buoy motion for 45 degrees slope angle was also measured. Its peak-to-peak distance is about 11 times to the rms wave height.

- The power absorption at various scales is shown for design reference. The diagrams are plotted with a stretched frequency axis corresponding South Uist wave climate to indicate the distribution of average energy.

Chapter 8

Discussions and main conclusions

8.1 Disscussions

The study suggests that a Sloped IPS buoy at 45 degrees slope angle exhibits a very wide band of high efficiency energy conversion. It may be worth studying and implementing the slope idea in other devices such as the oscillating water column. In fact, a sloped OWC called LIMPET is under construction in Islay by Queen's University of Belfast and Wavegen, a commercial company (Thorpe, 1998).

The full-scale Sloped IPS buoy is designed to be self constrained by its tail-plate. A small-scale free-floating Sloped IPS model with electronically controlled internal dynamometer should be built to investigate behaviour with six degrees of freedom. Unlike the models in the present study, this would include one or more internal water tubes with reaction piston.

The dynamometer should allow simulation of most conceivable control strategies, so it should be able to present a force between water piston and body as any function of their respective velocity, position and acceleration. Salter (1999) has proposed using a linear eddy current damper. A thin walled copper tube attached to the water piston would translate within the field of a cylindrical stator coil in the body of the model. Instantaneous variation of the current to the coil would allow complete control of the reaction force of the dynamometer.

A non-contact motion measurement system such as Pro-Reflex made by Qualsys (Lin, 1997) would be ideal for capturing the motions of the device and should lend itself to incorporation in the feedback loop of the dynamometer. Pro-Reflex uses a number of special video cameras each with a circular array of high-intensity light-emitting diodes (LED) around the lens. Highly-reflective golf ball sized sphere are attached to various parts of the model and, by analysis and cross-correlation of the various reflected LED video images, the system generates Cartesian time series of the model motions.

Apart from a slack mooring system, such a free-floating Sloped IPS model would be constrained only by electrical wires supplying current to the dynamometer and possibly by a tube supplying pressurised water for internal bearings.

In section 3 it was shown (equation 3.28) that the optimised value of damping, without applying reactive force to compensate the spring and inertia term, is numerically equal to the absolute value of the radiation impedance. However this value is frequency dependent. If the damping coefficients can be spearately controlled for each frequency, the capture curve can be tuned to have wide bandwidth and high efficiency. This suggests that a frequency dependent damper is required. With the power take-off system acting as a pure damper, there is no need to control the phase by applying spring or inertia forces. Therefore, advance information about phase is not required and it might be possible to design a digital filter with zero phase response, which gives the required amplitude response for different frequencies. The damping values could be programmed in advance by calculating the absolute value of radiation impedance.

Although the results of the power absorption tests in regular waves show generally good agreement with the theoretical predictions, the measured results are lower than the predictions. This needs to be investigated. The non-linear effects at various wave amplitudes shown in figure 5.24 must also to be studied.

In order to easily compare with the numerical model, the model used in the work was a simple shape with sharp corners. The sharp concerns may induce vortex shading, and power loss. Further study is required in order to understand such three-dimensional effects and to obtain the optimal geometry.

The mathematical model of the reaction mass used in this thesis is simplified. In further studies of the full-scale device, the added mass caused by the internal water pistons, the viscous effect and the vortex induced by the intake of the inertia tubes should also be considered.

The real sea-going device will face the three dimensional irregular waves. The 3-D irregular wave test results in chapter 7 was disappointing. More effect is needed to investigate the loss between measurement and prediction.

The model tested in this thesis was constrained by a fixed rig. The mooring system of the sea-going device was not simulated. For a free-floating system, the mooring system is very important for both survivability and motion of the model, and needs detailed study.

8.2 Main conclusions

- A free-floating model with no power-take off system has been built and experiments have been conducted in regular waves. Results show that the slope-plate constraint works well in wavelengths between 0.7 and 3 metres, around 1.4 to 6 times of the length of the slope-plate.

- A test rig has been designed and built to measure the hydrodynamic coefficients by using the forced oscillation technique. The results agree well with numerical calculations of the coefficients performed by Pizer. This suggests that both measured and numerical coefficients can reasonably be utilised to describe the model behaviour.

- The inclined angle effect has been investigated. Results show that the natural period of the model for inclinations increases as the angle to the vertical increases. This confirms that tuning the natural period of the device by varying the slope angle is feasible.

- Power absorption tests of the model has been conducted in the Edinburgh 3D wave tank. The results show a good agreement with the calculated results based on 20 mm height incident waves.

- The bandwidth of the model increases as the angle to the vertical increase. In particular, the model at 45 degrees slope angle shows a high efficiency and wide bandwidth characteristic. It suggests that it may not be necessary to continuously adjust the slope angle of a full-scale device to suit different wave.

- A double peak effect has been observed. One of the peaks corresponds to the natural frequency of the model and the other to the peak of the real part of the hydrodynamic impedance.

- Numerical calculations for various constant damping coefficients has been made to identify the best constant coefficient value for the damper. The results show

that the damping coefficient value is better set slightly higher than the value corresponding to the model at resonance.

- The water mass effect of the Sloped IPS buoy has been studied numerically. A mathematic model has been derived. The added mass of the piston, viscous effects, friction and vortex losses are ignored. The results show that finite mass can improve the peak efficiency, but slightly shift the efficiency curve to the high frequency side.

- Irregular wave tests have been conducted. The efficiency results are lower than those of the numerical prediction. This is may be due to vortex losses of the sharp cornered model, faulty power measurement caused by the side load on the model and the signal degree of freedom of the rig.

Bibliography

Barber, N.F. (1969). Water waves. *Wykeham publications (London) Ltd.*, Chapter 2, 1969, 20-35.

Bergdahl, L. (1992). Review of research in Sweden. *Wave energy R&D proceedings of a workshop held at Cork*, October 1992, 129-136.

Bisio, A. and Boots, S. (1995). Encyclopedia of Energy – Technology and the environment. *John Wiley & Sons, Inc.*, vol.4, 1995, 2859-2907.

Boyle G.(1996). Renewable Energy: Power for a sustainable future. *Oxford Express*, Chapter 2, 1996, 27-37.

Bracewell, R.H. (1990). Frog and PS Frog : A study of two reactionless ocean energy converters. *Ph.D. thesis*, Lancaster University, 1990.

Bryden, I.G. (1983). Long floating cylinders in three-dimensional random seas. *Ph.D. thesis*, University of Edinburgh, chapter 3 1983.

Brendmo, A.; Falnes, J. and Lillebekken, P.M. (1995). Conversion of wave energy by twin oscillating-water column. *The second European Wave Power Conference, Lisbon, Portugal*, 1995, 254-259.

Budal, K. (1977). Theory for absorption of wave power by a system of interacting bodies. *Journal Ship Research*, vol. 21, 1977, 248-253.

Budal, K. and Falnes, J. (1977). Optimum operation of improved wave-power converter. *Marine Science Communications*, vol.3, 1977, 133-150.

Budal, K. Falnes, J., and Iversen, L.C. (1981). Model experiment with a phase-controlled point absorber. *The second international symposium on wave & tidal energy*, Cambridge, England, 1981, 191-206.

Cartwright, D.E. and Longuet-Higgins, M.S. (1958). *The statistical distribution of the maximum of a random function.* Proceeding of royal society A., Vol. 237, 1958, 212-232.

Chakravarti, S.K. (1987). *Hydrodynamics of offshore structures. Computational Mechanics Publications*, Southampton Boston, 1987.

Count, B.M. (1978). On the dynamics of wave-power devices. *Proc. R. Soc. Lond.* A. 363, 1978, 559-579.

Count, B. (1980). Power from sea waves. *academic press*, 1980.

Crabb, J.A. (1979). Synthesis of a directional wave climate. Power from sea waves, *academic press*, 1979, 41-74.

Dorf, R.C. and Bishop, R.H. (1995). The design of feedback control systems. *Modern control systems, Addison-Wesley publishing company.*Ch.10, 1995, 527-602.

Edwards, R. (1998). The big break. *New Scientist,* 3 Oct., 1998, 30-34.

Eidsmoen, H. (1995a). On theory and simulation of heaving-buoy wave-energy converters with control. *Ph.D. thesis, The Norwegian institute of technology.* Manuscript section C. 1995.

Eidsmoen, H. (1995b). Simulation of a heaving-buoy wave-energy converter with phase control. *The second European Wave Power Conference*, Lisbon, Portugal, 1995, 281-288.

Elliot, D. (1999). Green power and liberalisation of the UK electricity market. *International journal of Ambient Energy*, Vol. 20, No. 1,1999, 3-13.

Elliot, G. and Caratti, G. (1993). *1993 European wave energy symposium*, Edinburgh, Scotland, July 1993.

Elliot, G. and Diamantaras, K. (1995). *The second European wave power conference*, Lisbon, Portugal, November 1995.

Evans, D.V. (1976). A theory for wave-power absorption by oscillating bodies. *J. Fluid Mech.*, vol.77 part 1, 1976, 1-25.

Evans, D.V. *et. al.* (1979). Submerged cylinder wave-energy device - theory and experiment, *Applied Ocean Research*, vol. 1 No.1, 1979, 3-12.

Evans, D.V. (1980). Some theoretical aspects of three-dimensional wave-energy absorbers. *Power from sea waves*, academic express, 1980, 213-249.

Evans, D.V. (1981). Maximum Wave-Power absorption under motion constraints. *Applied ocean research*, vol.3 no.4, 1981, 200-203.

Evans, D.V. and Falcao, A.F. (1985). Hydrodynamics of ocean wave-energy utilization, *IUTAM symposium Lisbon, Portugal.* Springer-Verlag Press. 1985.

Evans, D.V. and Linton, C.M. (1993). Hydrodynamics of wave-energy devices-Wave energy converters. *Generic technical evaluation study, annex report B1,* JOU2-0003-DK, 1993, 1-33.

Falnes, J. (1980). Radiation impedance matrix and optimum power absorption for interacting oscillators in surface waves. *Applied ocean research*, vol.2 no.2, 1980, 75-80.

Falnes, J. and Badal, K. (1978). Wave power conversion by point absorbers. *Norwegian maritime research*, vol. 6, no. 4, 1978, 2-11.

Falnes, J. and Lρvseth, J. (1991). Ocean Wave Energy. *Energy Policy*, October, 1991.

Fredrikson, G. (1992). *IPS Wave Power Buoy Mark IV*, Wave energy R&D proceedings of a workshop held at Cork, October 1992, 191-194.

French, M.J. and Bracewell, R.H. (1985). Heaving point absorbers reacting against an internal mass. *Proc. IUTAM Int. Symp. on Hydrodynamics of Ocean Wave Energy Utilisation, Lisbon, Portugal*, July 1985.

Garrison, C.J. and Chow, P.Y. (1972). Wave forces on submerged bodies. *J. of Waterways, Harbours and Coastal Eng. Div., Proc. of A.S.C.E.*, August 1972.

Gato, L.M.C. and Falcao, A.F.O. (1988). Aerodynamics of the wells turbine. *International Journal of Mechanical Science*, Vol. 30, No. 6, 1988, 282-395.

Gerritsma, J. (1991). Forced oscillation experiments. *Philosophical Transactions :Physical Science and Engineering, Royal Society, London, Series A,* Vol. 334, 1991, 199-211.

Greenhow, M.J.L. (1980). The hydrodynamic interactions of spherical wave power devices in surface waves. *Power from sea waves*, academic express, 1980, 287-343.

Greenhow, M., Rosen, J.H. and Reed, M. (1984). Control strategy for the Clam wave energy device. *Applied ocean research*, vol. 6, no.4, 1984, 197-206.

Greenhow, M. and Simon, M. (1985). A note on equivalent wavemaker method. *Applied Ocean Research*, vol. 7, no.2, 1985, 107-112.

Haskind, M. D. (1946). The hydrodynamical theory of the oscillation of a ship in waves. *Prikladnaya Matematika I Mekhanika*, vol. 10, no.1, 1946, 33-66

Hogben, N. (1995). Increases in wave heights over the North Atlantic: a review of the evidence and some implication for the naval architect. *The Royal Institute of Naval Architect.* Vol.137, Pt. 1, 1995, 93-115.

Inoue, M. *et. al.* (1988). Studies on the wells turbine for wave power generator. *JSME International Journal*, series II, vol. 31, No.4, 1988, 676-682.

Iscaacson, M. (1991). Measurement of Regular Wave Reflection. *Journal of Waterway, Port, Coastal, and Ocean Engineering,* Vol.117, No.6, 1991, 553-569.

Jeffrey, D.C. *et. al.*,(1978) Study on mechanisms for extracting power from sea waves. *Four year report on Edinburgh wave power project*, 1978.

Jefferys, E.R. (1979). Modelling and optimisation of a wave energy converter. *Ph.D. thesis, The University of Cambridge,* 1979.

Kato, M. and Miyazaki, T. (1991). Model experiments on waves and nearshore currents around floating wave power-plant in coastal waters in comparison with detached breakwater. *Oceanis 91*, vols 1-3, ch. 337, 1991, 207-214

Lin, C. (1997). Roll and Capsize tests of the tank models in beam sea (LCU Model tests Phase I). *Report no. PN5170, Ship Safety Agency*, 1997.

Masuda, Y. (1971). Wave-activated generator. *International coll. on the exploitation of the oceans*, (Trans), Bordeaux, French, 1971.

Masuda, Y. *et. al.* (1993). High performance of cylinder float Backward Bent Duct Buoy (BBDB) and its use in European seas. *Proceedings of an international symposium (1993 European wave energy symposium)*, Edinburgh, Scotland, July, 1993, 323-338.

McCormick, M. *et. al.* (1975). An experimental study of a wave-energy conversion buoy. *MTS Journal*, vol. 9, no. 3, March 1975, 39-42.

Mehlum, E. (1985). TAPCHAN, *Hydrodynamics of Ocean Wave-Energy Utilization, IUTAM symposium, Lisbon, Portugal*, 1985.

Mei, C.C. (1987). The applied dynamics of ocean surface waves. *World Scientific Publishing*, chapter 7, 1989.

Mei, C.C. (1976). Power extraction from water waves. *Journal of ship research*, vol. 20, no.2, 1976, 63-66.

Miyazaki, T. and Masuda, Y. (1978). Research and development of wave power electricity generation system. *Oceanology International*, 1978, 45-49.

Mollison, D. (1985). Wave climate and the wave power resource. *Hydrodynamics of Ocean Wave-Energy Utilization, IUTAM symposium, Lisbon, Portugal*, 1985, 133-156

Mollison, D. et. al.(1976). Wave power availability in the N.E. Atlantic. Nature, vol. 263, 1976, 223-226.

Nebel, P. (1992). Maximizing the efficiency of wave-energy plant using complex-conjugate control. *Proc Instn Mech Engrs*, vol.206, *Journal of systems and control engineering*, 1992, 225-236.

Nebel, P. (1994). Synthesis of optimal control of a wave energy converter, *Ph.D. thesis, Edinburgh University*, 1994.

Newman, J.N. (1962). The exciting forces on fixed bodies in waves. *Journal of ship research*, vol. 6, no. 3, 1962, 10-17.

Newman, J.N. (1976). The interaction of stationary vessels with regular waves. *Proceeding 11th symposium, Naval hydrodynamics, London*, 1976, 491-501.

Newman, J.N. (1977). Marine Hydrodynamics, *The MIT Press*, Chapter 6, 1977, 237-327.

Norman, W.B. (1982). Development of the sea clam wave energy converter. *The second international symposium on wave energy utilization.* Trondheim, Norway, June 1982, 175-190.

Patel, M.H. and Ionnaou, P.A. (1980). Comparative performance study of paddle and wedge-type wave generators. *Journal of Hydronautics*, vol. 14, no. 1, 1980, 5-9.

Pierson, W.J. (1964). The interpretation of wave spectrums in terms of the wind profile instead of the wind measured at a constant height. *Journal of geophysical research*, Vol. 69 No.24, 1964, 5191-5203.

Pierson, W.J. and Moskowitz, L. (1964). *A proposed spectral form for fully developed wind seas based on the similarity theory of S.A. Kitagorodakill.* Journal of geophysical research, Vol. 69 No.24, 1964, 5181-5190.

Pizer, D.J. (1993). Numerical prediction of the performance of a solo duck. *proc. Int. Symp. on wave energy, Edinburgh,* 1993, 129-137.

Pizer, D.J. (1994). Numerical modelling of wave energy absorbers, *Edinburgh wave power project report*, 1994. (DTI contract number V/03/00172/00/00).

Pontes, M.T. (1998). Assessing the European wave energy resource. *Journal of Offshore Mechanics and Artic Engineering*, vol. 120, November 1998, 226-231.

Raghunathan, S. and Ombaka, O.O. (1985). Effect of frequency of air flow on the performance of the Wells turbine. *Int. J. heat and Fluid Flow*, vol. 6, no. 2, June 1985, 127-132.

Randlov, P. (1993). Wave Energy Converters generic technical evaluation study. *Commission of the European Communities*, August 1993.

Rogers, D. and King, G.B. (1996). Wave generation using ocean and wave. *Edinburgh design Ltd.,* 1996.

Russell, A. and Diamantaras, K (1995). The European Commission wave energy R&D programme. *The second European wave power conference, Lisbon Portugal,* 1995, 8-11.

Sarmento, A.J.N.A; Gato, L.M.C. and Falcao A.F. de O. (1987). Wave energy absorption by an OWC device with blade-pitch controlled air turbine. *The Proceedings of the 6th International offshore Mech. and Arctic Engineering Symposium on wave and tidal energy*, BHRA, Bedford, England, vol. 1, 1987, B85-B92.

Salter, S.H. (1974). Wave Power. *Nature*, vol. 249, no. 5459, June 1974, 720-724.

Salter, S.H. (1975)*. Study of mechanisms for extracting power from sea waves. *The first year interim report on Edinburgh wave power project*, 1975.

Salter, S.H. (1980). Recent progress on Ducks. *IEE Proceeding*, vol. 127, Pt. A, No. 5, June 1980, 308-319.

Salter, S.H. (1981). Absorbing wave-makers and wide tanks. *Conference on directional wave spectrum applications*, Berkeley, California, ASCE, 1981.

Salter, S.H. (1986). Wave powered desalination. *Energy for rural and island communities IV*, Ch45, 1986, 235-241.

Salter, S.H. (1992a). Wave energy power-conversion studies, *Wave energy R&D Proceedings of a workshop held at Cork*, October 1992, 59-99.

Salter, S.H. (1992b). The swinging Mace. *Wave energy R&D proceedings of a workshop held at Cork*, October 1992, 197-206.

Salter, S.H. (1999). *Private communication.*

Salter, S.H. *et. al.* (1978)*. *Fourth Year report* Volume 3, Edinburgh wave power project, July 1978.

Salter, S.H., Jeffrey, D. C. and Taylor, J.R.M. (1976). The architecture if nodding duck wave power generators. *The Naval Architect*, January 1976, 21-24.

Salter, S.H. and Lin, C. (1995). The Sloped IPS Wave Energy Converter. *The second European wave power conference*, Lisbon, Portugal 1995, 337-344.

Salter, S.H. and Lin, C. (1998). Wide tank efficiency measurements on a Model of the Sloped IPS buoy. *The third European wave power conference*, Patras, Greece, 1998.

Salter, S.H. and Taylor, J. (1995). The design of high speed stop value for oscillating water columns, *The second European Wave Power Conference, Lisbon, Portugal*, 1995, 195-202.

Shaw, R. (1982). Wave Energy - a design challenge. *Ellis Horwood Ltd.*, 1982.

Skyner, D.J. (1987)*. Solo duck linear analysis. *Edinburgh University Wave Power Project report*, 1987.

Taylor, J.R.M. (1984)*. Bending moments in long spines. *Edinburgh wave power project*, 1984.

Taylor, J.R.M. and Salter, S.H.(1995). Design and testing of a plano-convex bearing for a variable pitch turbine. *The second European Wave Power Conference, Lisbon, Portugal*, 1995, 240-247.

Taylor, S.J. (1998). Sustainable development in the use of energy for electricity generation. *Proc. Instn. Civil Engineering*, 1998, 126 Aug. 126-132.

Thorpe, T.W. (1992). A review of wave energy. *DTI report*, vol.1 ETSU-R-72, December 1992.

Thrope, T.W. (1998). An overview of wave energy technologies. *AEA report. AEAT-3615.* May 1998.

Ursell, F. (1949). On the heaving motion of a circular cylinder on the surface of a fluid. *Quart. Journ. Mech. and Applied Math,* vol. II, Pt.2, 1949, 218-225.

Vugts, J.H. (1968). The hydrodynamic coefficients for swaying, heaving and rolling cylinders in a free surface. *Int. Shipbuilding Progress*, vol.15, 1968, 251-276.

Watabe, T. *et. al.* (1986). Wave Power extraction at coastal structures by means of Pendulor system. *JSME papers (B),* vol. 4, May 1986. (in Japanese).

Whittaker, T.J.T. and McPeake, F.A. (1985). Design optimization of axis-symmetric tail tube buoys. *Hydrodynamics of Ocean Wave-Energy Utilization, IUTAM symposium, Lisbon, Portugal*, 1985, 103-111.

Whittaker, T.J.T. *et. al.* (1985a). The development and testing of a wave-activated navigation buoy with a Wells turbine. *Journal of energy resources technology, transactions of the ASME,* vol.107, June 1985, 268-273.

Whittaker, T.J.T. *et. al.* (1985b). The Q.U.B. axisymmetric and multi-resonant wave energy convertors. *Journal of energy resources technology, transactions of the ASME,* vol.107, March 1985, 74-86.

Whittaker, T.J.T. (1987). Recent developments in wave energy systems. *The institution of electrical engineerings 5th international conference on energy options-the role of alternatives in the world energy scene*, Reading, UK, April, 1987.

Whittaker, T.J.T. (1991). Shoreline wave power on the Isle of Islay. *Journal of the society for underwater technology,* vol. 17, No. 2, 1991, 9-15.

Yemm, R., Pizer, D. and Retzler, C. (1998). The WPT-375 - A near shore wave energy converter submitted for Scottish Renewables Obligation 3. *The third European wave power conference*, Patras, Greece, 1998.

Yu, Z., Jiang, N. and You, Y. (1993). Power output of an offshore OWC wave power station at Danwanshan island. *Proceedings of an international symposium (1993 European wave energy symposium)*, Edinburgh, Scotland, July, 1993, 271-276.

*: *the internal reports of the Edinburgh Wave Power Group.*

Appendix A

Conversion of the power equation from the time domain to the frequency domain

$$P = \frac{1}{T}\int_0^T F(t)\cdot U(t)\cdot dt$$

$$= \frac{1}{T}\int_0^T \frac{1}{2}\sum_{n=-\infty}^{\infty} F(\omega_n)e^{i\omega_n t}\cdot\frac{1}{2}\sum_{m=-\infty}^{\infty} U(\omega_m)e^{i\omega_m t}dt$$

$$= \frac{1}{4}\sum_{n=1}^{\infty}\sum_{m=1}^{\infty}\frac{1}{T}\int_0^T (F(\omega_n)e^{i\omega_n t} + F^*(\omega_n)e^{-i\omega_n t})\cdot(U(\omega_m)e^{i\omega_m t} + U^*(\omega_m)e^{-i\omega_m t})\cdot dt$$

$$= \frac{1}{4}\sum_{n=1}^{\infty}\sum_{m=1}^{\infty}\frac{1}{T}\int_0^T (F(\omega_n)U(\omega_m)e^{i(\omega_n+\omega_m)t} + F^*(\omega_n)U^*(\omega_m)e^{-i(\omega_n+\omega_m)t}$$

$$+ F(\omega_n)U^*(\omega_m)e^{i(\omega_n-\omega_m)t} + F^*(\omega_n)U(\omega_m)e^{-i(\omega_n-\omega_m)t})dt$$

$$= \frac{1}{4}\sum_{n=1}^{\infty}\sum_{m=1}^{\infty}(0+0+F(\omega_n)\cdot U^*(\omega_m) + F^*(\omega_n)\cdot U(\omega_m))\delta_{nm}$$

$$= \frac{1}{4}\{\sum_{n=1}^{\infty} F(\omega_n)\cdot U^*(\omega_n) + \sum_{n=1}^{\infty} F^*(\omega_n)\cdot U(\omega_n)\}$$

Appendix B

Rearrange the equation 3.16 and 3.22

Equation 3.16 :

$$U = -(B+Z)^{-1} \cdot W \cdot a$$

Equation 3.22:

$$P = \frac{1}{4}(B+B^*) \cdot |U|^2$$

Substituting equation 3.16 to equation 3.22:

$$P = \frac{1}{4}(B+B^*) \cdot \left|\frac{F_e}{B+Z}\right|^2$$

$$= \frac{|F_e|^2}{4} \cdot \frac{(B+B^*)}{|B+Z|^2}$$

$$= \frac{|F_e|^2}{4} \cdot \frac{(B+B^*)}{(B+Z)\cdot(B^*+Z^*)}$$

$$= \frac{|F_e|^2}{4} \cdot \frac{1}{(Z+Z^*)} \cdot \frac{(Z+Z^*)\cdot(B+B^*)}{(B+Z)\cdot(B^*+Z^*)}$$

$$= \frac{|F_e|^2}{4} \cdot \frac{1}{2D_a} \cdot \left(\frac{ZB+ZB^*+Z^*B+Z^*B^*}{(B+Z)\cdot(B^*+Z^*)}\right)$$

$$= \frac{|F_e|^2}{8D_a} \cdot \left(1-\frac{(B-Z^*)\cdot(B^*-Z)}{(B+Z)\cdot(B^*+Z^*)}\right)$$

$$= \frac{|F_e|^2}{8D_a} \cdot \left(1-\frac{|B-Z^*|^2}{|B+Z|^2}\right)$$

Appendix C

The schematic diagram of free floating model I.

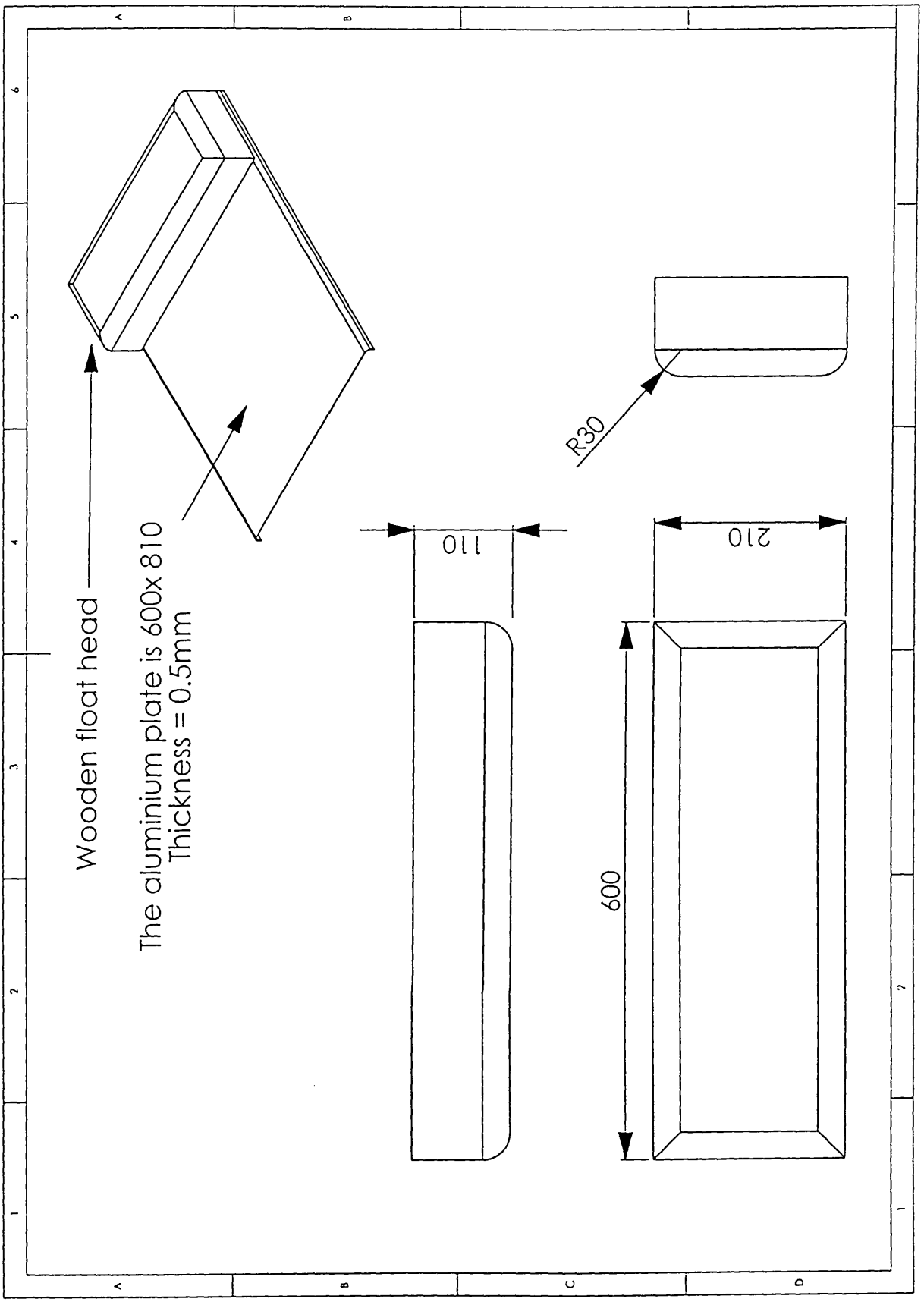

Appendix D

The schematic diagram of free floating model II.

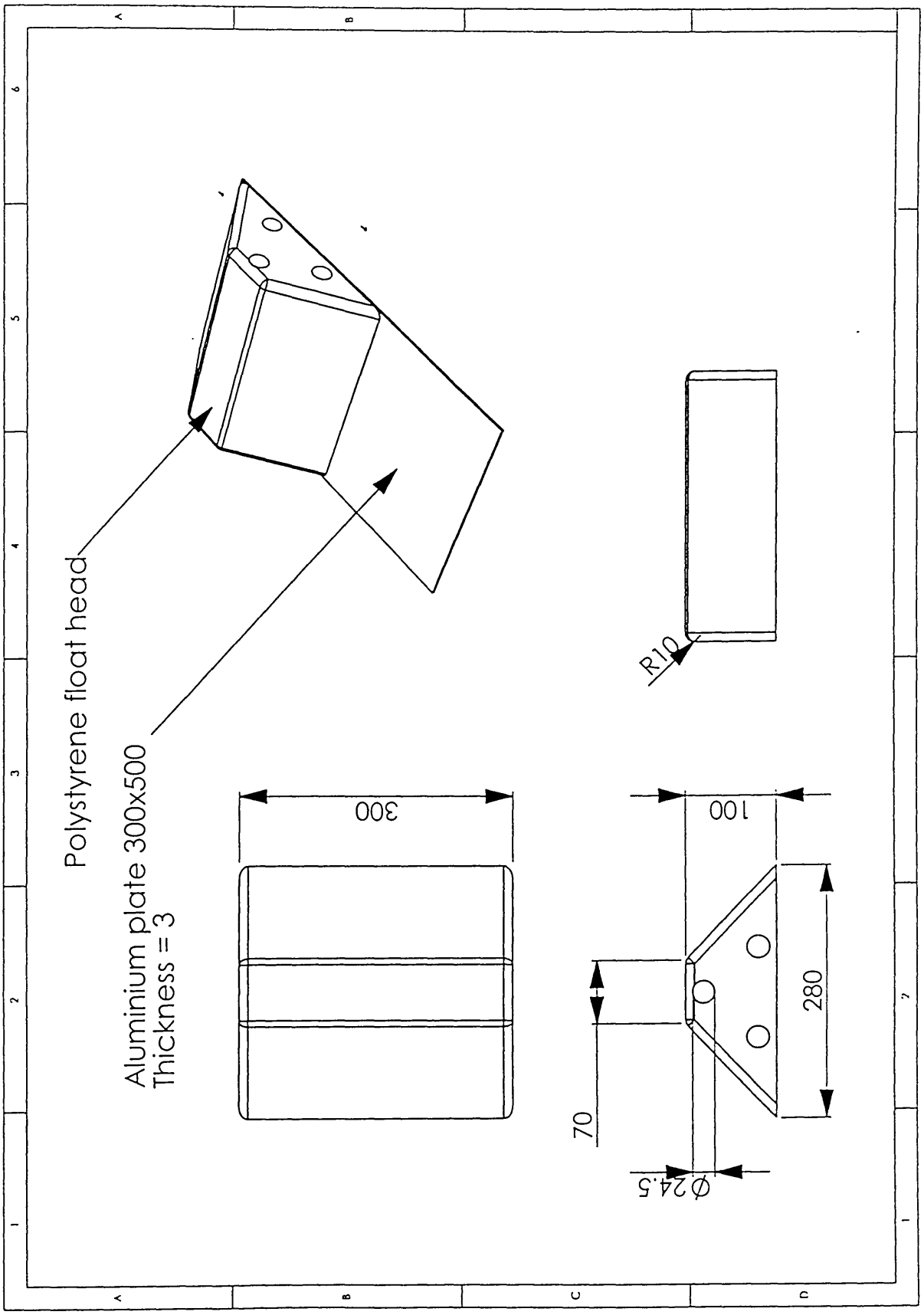

Appendix E. The schematic diagram of the first rig.

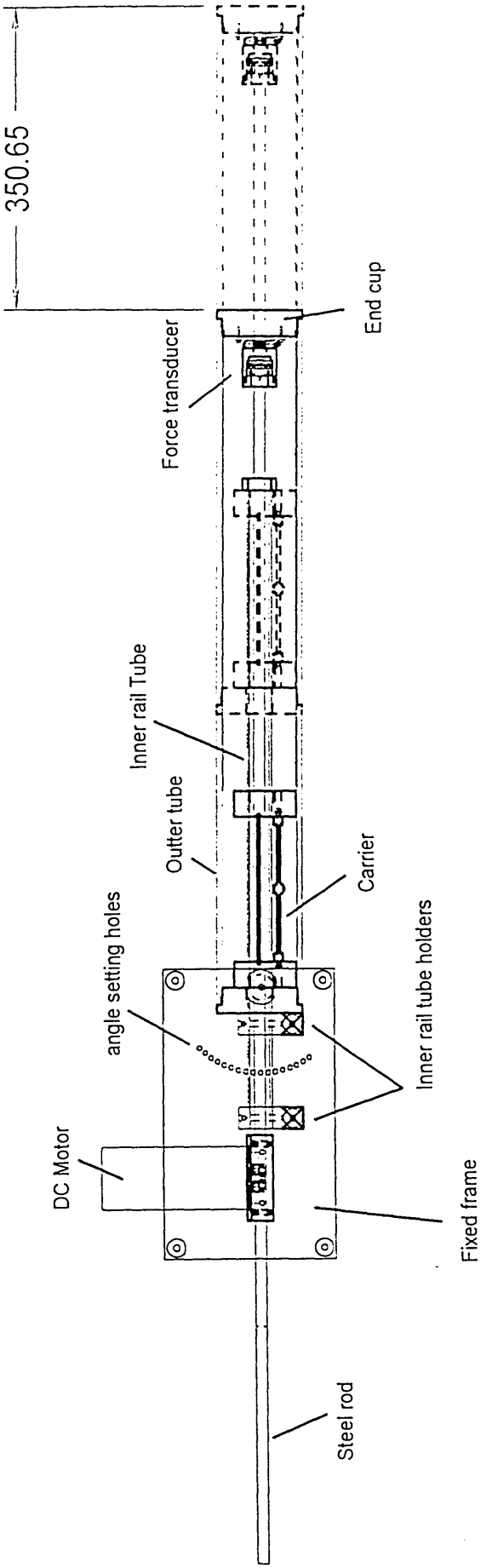

The schematic diagram of the first rig

Appendix F

The schematic diagram of the simulated power take-off system.

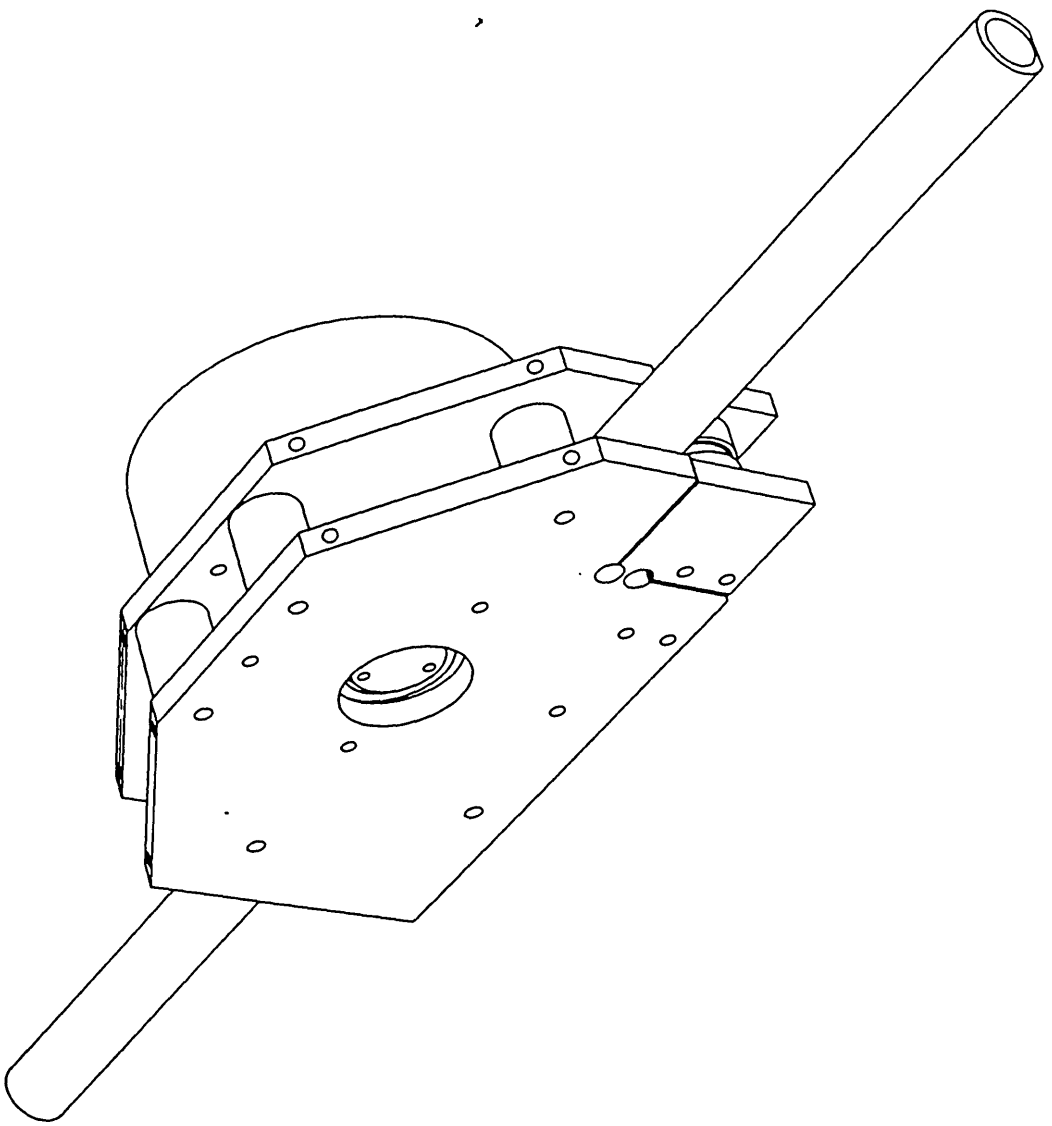

Appendix G

Circuit schematic of power amplifier

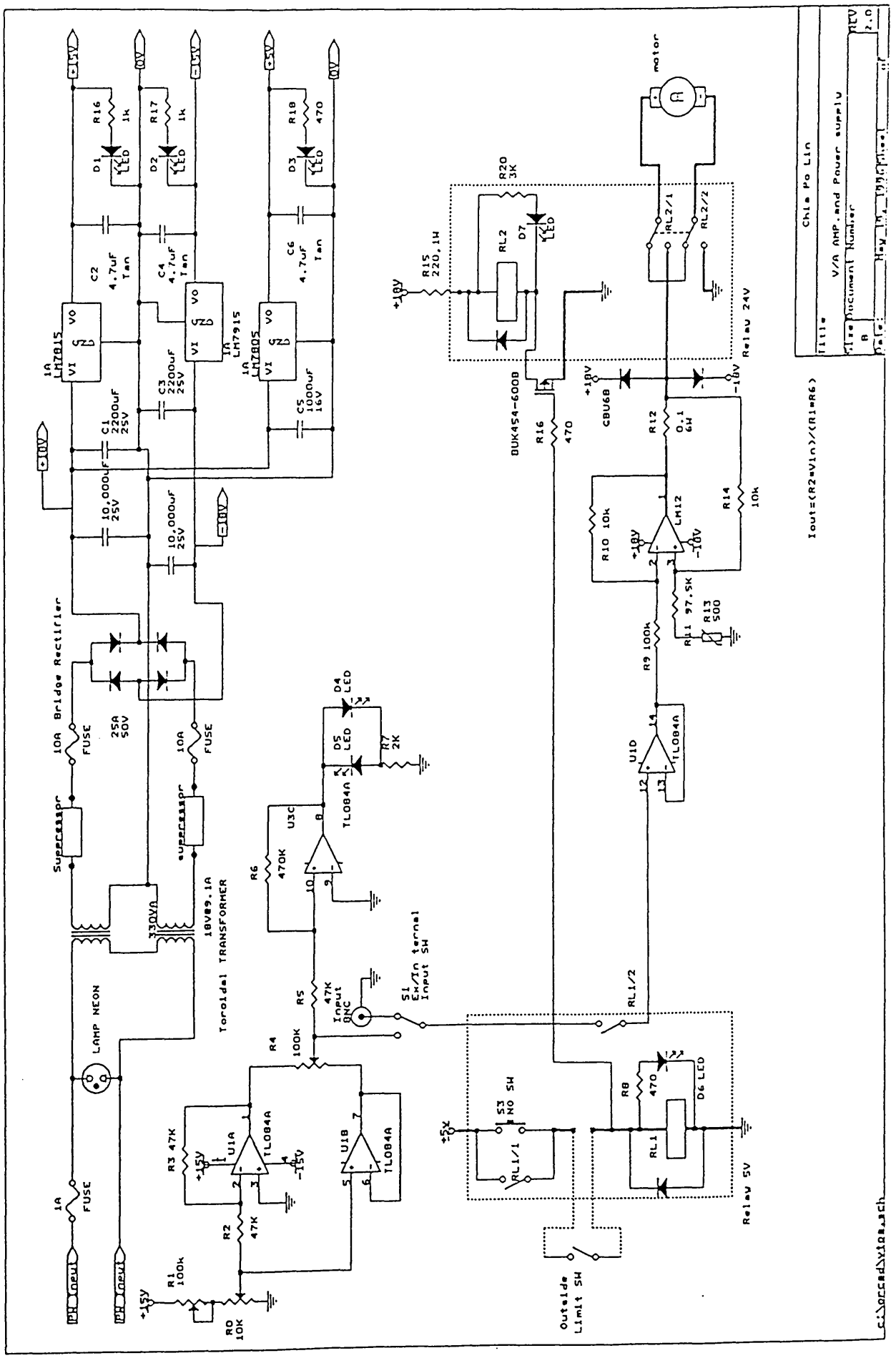

Appendix H

Circuit schematic of charge amplifier

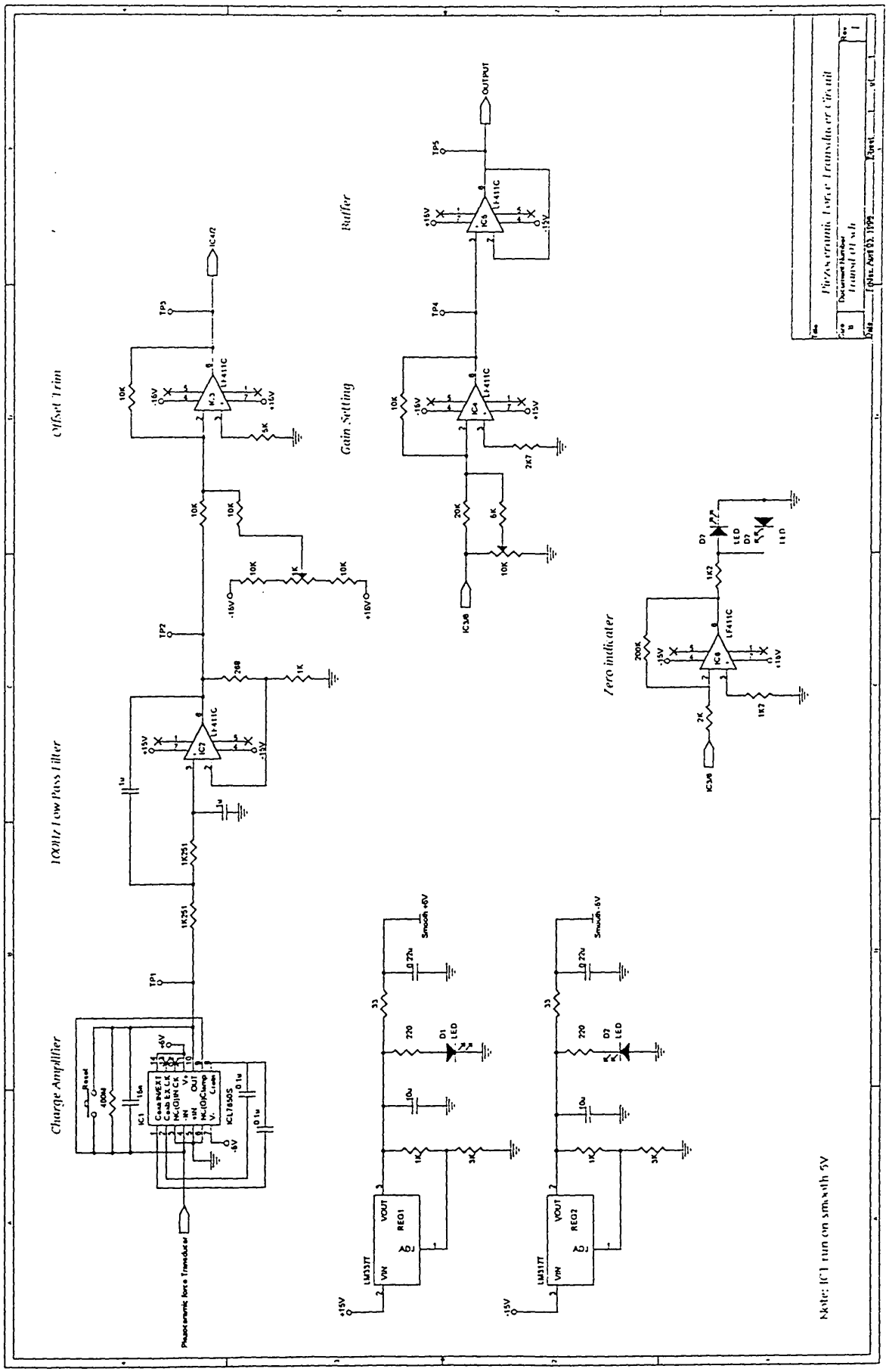

Appendix I
Tank transfer function

The wave making sorftware use a tank transfer function to translate output signals to physical wave height.
The frequency is equal to the n/64 Hz.

Frequency(n)	angle(rad)	gain	phase	angle(rad)	gain	phase	angle(rad)	gain	phase
20	-0.7854,	83.6,	0	-0.6981,	83.6,	0	-0.5236,	83.6,	0\
	-0.3491,	83.6,	0	-0.1745,	83.6,	0	0,	83.6,	0\
	0.1745,	83.6,	0	0.3491,	83.6,	0	0.5236,	83.6,	0\
	0.6981,	83.6,	0	0.7854,	83.6,	0			
46	-0.7854,	36.8,	0	-0.6981,	34.4,	0	-0.5236,	37,	0\
	-0.3491,	39.7,	0	-0.1745,	40.2,	0	0,	40.6,	0\
	0.1745,	38.9,	0	0.3491,	41.5,	0	0.5236,	35.7,	0\
	0.6981,	33.5,	0	0.7854,	37.4,	0			
47	-0.7854,	34,	0	-0.6981,	32.1,	0	-0.5236,	35.6,	0\
	-0.3491,	37.1,	0	-0.1745,	37.6,	0	0,	38.3,	0\
	0.1745,	36.5,	0	0.3491,	39.4,	0	0.5236,	35.4,	0\
	0.6981,	32.3,	0	0.7854,	34.8,	0			
48	-0.7854,	33.6,	0	-0.6981,	32.3,	0	-0.5236,	37.1,	0\
	-0.3491,	37.9,	0	-0.1745,	38.7,	0	0,	38.9,	0\
	0.1745,	37.7,	0	0.3491,	39.4,	0	0.5236,	37.7,	0\
	0.6981,	33.2,	0	0.7854,	33.9,	0			
49	-0.7854,	33.4,	0	-0.6981,	32.6,	0	-0.5236,	38.1,	0\
	-0.3491,	38.3,	0	-0.1745,	39.4,	0	0,	39.3,	0\
	0.1745,	37.4,	0	0.3491,	39.4,	0	0.5236,	38.5,	0\
	0.6981,	33.3,	0	0.7854,	33.3,	0			
50	-0.7854,	32.3,	0	-0.6981,	31.3,	0	-0.5236,	36.4,	0\
	-0.3491,	36.3,	0	-0.1745,	38.8,	0	0,	38.9,	0\
	0.1745,	36.1,	0	0.3491,	38.3,	0	0.5236,	36,	0\
	0.6981,	32,	0	0.7854,	34.2,	0			
51	-0.7854,	33,	0	-0.6981,	31.8,	0	-0.5236,	36.2,	0\
	-0.3491,	36.6,	0	-0.1745,	39.7,	0	0,	39.9,	0\
	0.1745,	38,	0	0.3491,	38.8,	0	0.5236,	36,	0\
	0.6981,	31.7,	0	0.7854,	34.8,	0			
52	-0.7854,	33.4,	0	-0.6981,	32.9,	0	-0.5236,	37.2,	0\
	-0.3491,	36.9,	0	-0.1745,	38.9,	0	0,	39.3,	0\
	0.1745,	38.4,	0	0.3491,	38.4,	0	0.5236,	37.6,	0\
	0.6981,	32.3,	0	0.7854,	32.4,	0			
53	-0.7854,	31.7,	0	-0.6981,	31.7,	0	-0.5236,	36.9,	0\
	-0.3491,	35.2,	0	-0.1745,	37.2,	0	0,	37.8,	0\
	0.1745,	36.2,	0	0.3491,	36.3,	0	0.5236,	37.4,	0\
	0.6981,	31.5,	0	0.7854,	31,	0			
54	-0.7854,	31.2,	0	-0.6981,	31.3,	0	-0.5236,	36.3,	0\
	-0.3491,	35.6,	0	-0.1745,	38.4,	0	0,	38.5,	0\
	0.1745,	36.6,	0	0.3491,	36.1,	0	0.5236,	36.9,	0\
	0.6981,	30.6,	0	0.7854,	33.4,	0			
55	-0.7854,	31.6,	0	-0.6981,	32,	0	-0.5236,	36.2,	0\
	-0.3491,	37.5,	0	-0.1745,	39.2,	0	0,	39.5,	0\
	0.1745,	38.1,	0	0.3491,	37.4,	0	0.5236,	37.1,	0\
	0.6981,	31.2,	0	0.7854,	32.9,	0			
56	-0.7854,	31.1,	0	-0.6981,	31.6,	0	-0.5236,	35.7,	0\
	-0.3491,	36.8,	0	-0.1745,	37.7,	0	0,	38.6,	0\
	0.1745,	37.3,	0	0.3491,	37.1,	0	0.5236,	36.8,	0\
	0.6981,	32.7,	0	0.7854,	29.7,	0			
57	-0.7854,	30.7,	0	-0.6981,	31.2,	0	-0.5236,	35.7,	0\
	-0.3491,	36.2,	0	-0.1745,	37.9,	0	0,	38.1,	0\
	0.1745,	37.1,	0	0.3491,	36.8,	0	0.5236,	36.8,	0\
	0.6981,	32.1,	0	0.7854,	31.2,	0			
58	-0.7854,	30.3,	0	-0.6981,	31.7,	0	-0.5236,	36.2,	0\
	-0.3491,	37.2,	0	-0.1745,	38.1,	0	0,	37.3,	0\
	0.1745,	37.2,	0	0.3491,	37.1,	0	0.5236,	36.9,	0\
	0.6981,	30,	0	0.7854,	33.7,	0			
59	-0.7854,	29.6,	0	-0.6981,	31.7,	0	-0.5236,	36.4,	0\
	-0.3491,	36.8,	0	-0.1745,	36.5,	0	0,	35.8,	0\
	0.1745,	35.6,	0	0.3491,	36.9,	0	0.5236,	36.8,	0\

```
      0.6981,  30.8,  0   0.7854,  30,    0
60    -0.7854, 29.8,  0   -0.6981, 31.5,  0   -0.5236, 36.5,  0\
      -0.3491, 35.6,  0   -0.1745, 36.7,  0   0,      36.4,  0\
      0.1745,  35.1,  0   0.3491,  36.2,  0   0.5236,  38.4,  0\
      0.6981,  32.9,  0   0.7854,  28.4,  0
61    -0.7854, 30.1,  0   -0.6981, 31.8,  0   -0.5236, 36.5,  0\
      -0.3491, 35.2,  0   -0.1745, 37.9,  0   0,      38.1,  0\
      0.1745,  36.1,  0   0.3491,  34.7,  0   0.5236,  39.4,  0\
      0.6981,  31.5,  0   0.7854,  31.5,  0
62    -0.7854, 29.5,  0   -0.6981, 32.3,  0   -0.5236, 36,    0\
      -0.3491, 35.3,  0   -0.1745, 36.8,  0   0,      37.6,  0\
      0.1745,  36,    0   0.3491,  34.4,  0   0.5236,  37.1,  0\
      0.6981,  30.5,  0   0.7854,  31,    0
63    -0.7854, 29.6,  0   -0.6981, 32.6,  0   -0.5236, 35.3,  0\
      -0.3491, 35.5,  0   -0.1745, 36,    0   0,      36.7,  0\
      0.1745,  36,    0   0.3491,  35.8,  0   0.5236,  35.3,  0\
      0.6981,  32.6,  0   0.7854,  29,    0
64    -0.7854, 29.9,  0   -0.6981, 33.1,  0   -0.5236, 34.8,  0\
      -0.3491, 35.5,  0   -0.1745, 36.7,  0   0,      36.6,  0\
      0.1745,  36.9,  0   0.3491,  35.5,  0   0.5236,  36.4,  0\
      0.6981,  32.6,  0   0.7854,  31.4,  0
65    -0.7854, 29.2,  0   -0.6981, 33.5,  0   -0.5236, 34,    0\
      -0.3491, 35.3,  0   -0.1745, 36.5,  0   0,      35.9,  0\
      0.1745,  36.1,  0   0.3491,  34,    0   0.5236,  36.8,  0\
      0.6981,  30.8,  0   0.7854,  31.9,  0
66    -0.7854, 29.5,  0   -0.6981, 33.4,  0   -0.5236, 33.4,  0\
      -0.3491, 35.9,  0   -0.1745, 36.4,  0   0,      35.6,  0\
      0.1745,  35.1,  0   0.3491,  35.2,  0   0.5236,  34.8,  0\
      0.6981,  32.7,  0   0.7854,  29.1,  0
67    -0.7854, 31.1,  0   -0.6981, 32.7,  0   -0.5236, 33.4,  0\
      -0.3491, 36,    0   -0.1745, 36.9,  0   0,      35.6,  0\
      0.1745,  35.3,  0   0.3491,  36.5,  0   0.5236,  34.6,  0\
      0.6981,  34.5,  0   0.7854,  29.9,  0
68    -0.7854, 30.8,  0   -0.6981, 32.9,  0   -0.5236, 34,    0\
      -0.3491, 34.7,  0   -0.1745, 35.9,  0   0,      35.3,  0\
      0.1745,  35.2,  0   0.3491,  35,    0   0.5236,  36.4,  0\
      0.6981,  32.8,  0   0.7854,  31.4,  0
69    -0.7854, 29.4,  0   -0.6981, 33.7,  0   -0.5236, 34.2,  0\
      -0.3491, 34.5,  0   -0.1745, 35.1,  0   0,      35.3,  0\
      0.1745,  34.3,  0   0.3491,  34.5,  0   0.5236,  36,    0\
      0.6981,  32.7,  0   0.7854,  29.9,  0
70    -0.7854, 29.3,  0   -0.6981, 33.6,  0   -0.5236, 34,    0\
      -0.3491, 35.4,  0   -0.1745, 35.7,  0   0,      35.9,  0\
      0.1745,  34.6,  0   0.3491,  34.8,  0   0.5236,  34.5,  0\
      0.6981,  33.5,  0   0.7854,  29.9,  0
71    -0.7854, 29.8,  0   -0.6981, 32.3,  0   -0.5236, 34.2,  0\
      -0.3491, 35,    0   -0.1745, 35.7,  0   0,      35.6,  0\
      0.1745,  35.5,  0   0.3491,  33.3,  0   0.5236,  34.8,  0\
      0.6981,  32.2,  0   0.7854,  30.5,  0
72    -0.7854, 29.5,  0   -0.6981, 32.2,  0   -0.5236, 34.1,  0\
      -0.3491, 34.2,  0   -0.1745, 35.2,  0   0,      35,    0\
      0.1745,  35.2,  0   0.3491,  32.5,  0   0.5236,  35,    0\
      0.6981,  32.3,  0   0.7854,  29.2,  0
73    -0.7854, 29.5,  0   -0.6981, 32.7,  0   -0.5236, 32.9,  0\
      -0.3491, 34.4,  0   -0.1745, 35.6,  0   0,      35.4,  0\
      0.1745,  34.4,  0   0.3491,  33.3,  0   0.5236,  34,    0\
      0.6981,  33.5,  0   0.7854,  29.2,  0
74    -0.7854, 30.1,  0   -0.6981, 32.6,  0   -0.5236, 32.1,  0\
      -0.3491, 34.4,  0   -0.1745, 35.8,  0   0,      35.7,  0\
      0.1745,  34.5,  0   0.3491,  33.7,  0   0.5236,  33.8,  0\
      0.6981,  32.4,  0   0.7854,  30.8,  0
75    -0.7854, 29.8,  0   -0.6981, 32.6,  0   -0.5236, 32.5,  0\
      -0.3491, 33.7,  0   -0.1745, 35,    0   0,      34.9,  0\
      0.1745,  34.7,  0   0.3491,  34.1,  0   0.5236,  34.1,  0\
      0.6981,  31.6,  0   0.7854,  30.1,  0
76    -0.7854, 28.8,  0   -0.6981, 32.8,  0   -0.5236, 33,    0\
      -0.3491, 33.5,  0   -0.1745, 34.6,  0   0,      34.1,  0\
      0.1745,  34.2,  0   0.3491,  35,    0   0.5236,  32.7,  0\
      0.6981,  32.2,  0   0.7854,  29.3,  0
77    -0.7854, 28.6,  0   -0.6981, 32.6,  0   -0.5236, 32.8,  0\
      -0.3491, 34,    0   -0.1745, 34.4,  0   0,      33.8,  0\
      0.1745,  33.9,  0   0.3491,  35.1,  0   0.5236,  31.5,  0\
```

	0.6981,	33.2,	0	0.7854,	29.4,	0			
78	-0.7854,	28.7,	0	-0.6981,	32.4,	0	-0.5236,	32.6,	0\
	-0.3491,	34.4,	0	-0.1745,	33.6,	0	0,	33.6,	0\
	0.1745,	33.5,	0	0.3491,	34.6,	0	0.5236,	32.4,	0\
	0.6981,	33.6,	0	0.7854,	29.2,	0			
79	-0.7854,	28.6,	0	-0.6981,	32.4,	0	-0.5236,	32.3,	0\
	-0.3491,	33.8,	0	-0.1745,	33.3,	0	0,	33.4,	0\
	0.1745,	33.5,	0	0.3491,	33.5,	0	0.5236,	34.3,	0\
	0.6981,	33.1,	0	0.7854,	29.4,	0			
80	-0.7854,	29.1,	0	-0.6981,	31.6,	0	-0.5236,	32,	0\
	-0.3491,	33.2,	0	-0.1745,	33.6,	0	0,	33.3,	0\
	0.1745,	33.5,	0	0.3491,	32.1,	0	0.5236,	35.2,	0\
	0.6981,	32.1,	0	0.7854,	29.3,	0			
81	-0.7854,	29.7,	0	-0.6981,	30.6,	0	-0.5236,	32.6,	0\
	-0.3491,	33.2,	0	-0.1745,	34,	0	0,	33.2,	0\
	0.1745,	32.7,	0	0.3491,	32,	0	0.5236,	34.8,	0\
	0.6981,	32.1,	0	0.7854,	28.9,	0			
82	-0.7854,	29.2,	0	-0.6981,	30.1,	0	-0.5236,	32.6,	0\
	-0.3491,	33.2,	0	-0.1745,	33.9,	0	0,	33.4,	0\
	0.1745,	32.3,	0	0.3491,	32,	0	0.5236,	33.9,	0\
	0.6981,	31.6,	0	0.7854,	29.2,	0			
83	-0.7854,	28.8,	0	-0.6981,	29.5,	0	-0.5236,	31.4,	0\
	-0.3491,	33.1,	0	-0.1745,	33.7,	0	0,	33.3,	0\
	0.1745,	33.6,	0	0.3491,	31.8,	0	0.5236,	33.1,	0\
	0.6981,	31.2,	0	0.7854,	29.1,	0			
84	-0.7854,	29.1,	0	-0.6981,	29.3,	0	-0.5236,	30.8,	0\
	-0.3491,	33.2,	0	-0.1745,	33,	0	0,	32.6,	0\
	0.1745,	33.1,	0	0.3491,	32.6,	0	0.5236,	31.9,	0\
	0.6981,	31.5,	0	0.7854,	28.6,	0			
85	-0.7854,	28.9,	0	-0.6981,	29.9,	0	-0.5236,	30.8,	0\
	-0.3491,	32.7,	0	-0.1745,	32.4,	0	0,	32,	0\
	0.1745,	30.8,	0	0.3491,	32.1,	0	0.5236,	30.9,	0\
	0.6981,	31.4,	0	0.7854,	29.3,	0			
86	-0.7854,	28.9,	0	-0.6981,	30.6,	0	-0.5236,	30.6,	0\
	-0.3491,	31.9,	0	-0.1745,	32.2,	0	0,	31.9,	0\
	0.1745,	31.1,	0	0.3491,	29.8,	0	0.5236,	30.4,	0\
	0.6981,	31.9,	0	0.7854,	29.4,	0			
87	-0.7854,	29.6,	0	-0.6981,	30.5,	0	-0.5236,	30.3,	0\
	-0.3491,	31,	0	-0.1745,	32.1,	0	0,	31.2,	0\
	0.1745,	31.9,	0	0.3491,	29.7,	0	0.5236,	30,	0\
	0.6981,	32.9,	0	0.7854,	28.8,	0			
88	-0.7854,	29.3,	0	-0.6981,	30.2,	0	-0.5236,	30.5,	0\
	-0.3491,	30,	0	-0.1745,	31.7,	0	0,	30.9,	0\
	0.1745,	31.5,	0	0.3491,	29.8,	0	0.5236,	30.4,	0\
	0.6981,	32.4,	0	0.7854,	28.9,	0			
89	-0.7854,	29,	0	-0.6981,	30,	0	-0.5236,	30.5,	0\
	-0.3491,	30.1,	0	-0.1745,	31.1,	0	0,	30.3,	0\
	0.1745,	31.3,	0	0.3491,	28.9,	0	0.5236,	31.1,	0\
	0.6981,	31.4,	0	0.7854,	29.5,	0			
90	-0.7854,	29.4,	0	-0.6981,	29.6,	0	-0.5236,	30.4,	0\
	-0.3491,	31.1,	0	-0.1745,	30.3,	0	0,	28.9,	0\
	0.1745,	30.2,	0	0.3491,	29.6,	0	0.5236,	30.4,	0\
	0.6981,	31.8,	0	0.7854,	29.7,	0			
91	-0.7854,	29.5,	0	-0.6981,	29.3,	0	-0.5236,	30.8,	0\
	-0.3491,	31.7,	0	-0.1745,	30.1,	0	0,	28.2,	0\
	0.1745,	28.7,	0	0.3491,	31.5,	0	0.5236,	29.9,	0\
	0.6981,	31.7,	0	0.7854,	29.2,	0			
92	-0.7854,	29.2,	0	-0.6981,	29.3,	0	-0.5236,	31.6,	0\
	-0.3491,	32.1,	0	-0.1745,	30.3,	0	0,	28.3,	0\
	0.1745,	28,	0	0.3491,	31,	0	0.5236,	30.7,	0\
	0.6981,	30.9,	0	0.7854,	28.8,	0			
93	-0.7854,	29,	0	-0.6981,	29.5,	0	-0.5236,	31.1,	0\
	-0.3491,	33,	0	-0.1745,	29.9,	0	0,	28.3,	0\
	0.1745,	28.7,	0	0.3491,	30.6,	0	0.5236,	31.6,	0\
	0.6981,	31.7,	0	0.7854,	28,	0			
94	-0.7854,	28.6,	0	-0.6981,	29.5,	0	-0.5236,	30.5,	0\
	-0.3491,	32,	0	-0.1745,	29.7,	0	0,	29.2,	0\
	0.1745,	29.8,	0	0.3491,	31.9,	0	0.5236,	32,	0\
	0.6981,	32.6,	0	0.7854,	29.4,	0			
95	-0.7854,	27.9,	0	-0.6981,	29.4,	0	-0.5236,	31.2,	0\
	-0.3491,	30.5,	0	-0.1745,	31.4,	0	0,	30.9,	0\
	0.1745,	30.9,	0	0.3491,	32,	0	0.5236,	32.2,	0\

```
                0.6981,   32.4,    0     0.7854,   29.4,    0
96              -0.7854,  27.9,    0     -0.6981,  29.9,    0     -0.5236,  30.5,    0\
                -0.3491,  30.4,    0     -0.1745,  33.2,    0     0,        31.7,    0\
                0.1745,   31,      0     0.3491,   30.6,    0     0.5236,   31.2,    0\
                0.6981,   31.8,    0     0.7854,   28.2,    0
97              -0.7854,  28.6,    0     -0.6981,  30.5,    0     -0.5236,  28.6,    0\
                -0.3491,  30.9,    0     -0.1745,  32.6,    0     0,        32.3,    0\
                0.1745,   32.9,    0     0.3491,   30,      0     0.5236,   30.1,    0\
                0.6981,   32.7,    0     0.7854,   29,      0
98              -0.7854,  28.1,    0     -0.6981,  29.4,    0     -0.5236,  27.1,    0\
                -0.3491,  29.9,    0     -0.1745,  30.6,    0     0,        32,      0\
                0.1745,   34,      0     0.3491,   29.8,    0     0.5236,   29.6,    0\
                0.6981,   34.3,    0     0.7854,   30.2,    0
99              -0.7854,  27.7,    0     -0.6981,  28.8,    0     -0.5236,  28.3,    0\
                -0.3491,  29.9,    0     -0.1745,  30,      0     0,        31.7,    0\
                0.1745,   31,      0     0.3491,   30,      0     0.5236,   29.4,    0\
                0.6981,   34.2,    0     0.7854,   30.8,    0
100             -0.7854,  28.2,    0     -0.6981,  29.7,    0     -0.5236,  30.6,    0\
                -0.3491,  29.8,    0     -0.1745,  29.5,    0     0,        31,      0\
                0.1745,   28.7,    0     0.3491,   29.2,    0     0.5236,   28.9,    0\
                0.6981,   33,      0     0.7854,   30.3,    0
101             -0.7854,  29.6,    0     -0.6981,  30.3,    0     -0.5236,  30.2,    0\
                -0.3491,  28.3,    0     -0.1745,  27.8,    0     0,        29.1,    0\
                0.1745,   27.6,    0     0.3491,   27,      0     0.5236,   28.4,    0\
                0.6981,   31,      0     0.7854,   29.8,    0
102             -0.7854,  30.3,    0     -0.6981,  30.3,    0     -0.5236,  30,      0\
                -0.3491,  28.2,    0     -0.1745,  27.2,    0     0,        27.4,    0\
                0.1745,   26.9,    0     0.3491,   26.8,    0     0.5236,   28.4,    0\
                0.6981,   31,      0     0.7854,   30,      0
103             -0.7854,  30.4,    0     -0.6981,  31,      0     -0.5236,  31.2,    0\
                -0.3491,  29.3,    0     -0.1745,  28.2,    0     0,        27.4,    0\
                0.1745,   27.5,    0     0.3491,   28.6,    0     0.5236,   28.3,    0\
                0.6981,   32,      0     0.7854,   30.1,    0
104             -0.7854,  31.6,    0     -0.6981,  31,      0     -0.5236,  31.3,    0\
                -0.3491,  28.6,    0     -0.1745,  27.5,    0     0,        26,      0\
                0.1745,   27.2,    0     0.3491,   28.5,    0     0.5236,   27.8,    0\
                0.6981,   33.3,    0     0.7854,   30.3,    0
105             -0.7854,  31.2,    0     -0.6981,  29.6,    0     -0.5236,  30.3,    0\
                -0.3491,  28.8,    0     -0.1745,  26.4,    0     0,        26,      0\
                0.1745,   26,      0     0.3491,   27.5,    0     0.5236,   28.8,    0\
                0.6981,   33.8,    0     0.7854,   32.1,    0
106             -0.7854,  30.6,    0     -0.6981,  30,      0     -0.5236,  29.9,    0\
                -0.3491,  31.3,    0     -0.1745,  27.1,    0     0,        28.1,    0\
                0.1745,   26.9,    0     0.3491,   28.9,    0     0.5236,   32.1,    0\
                0.6981,   31.6,    0     0.7854,   33.8,    0

Ttf             module    originallygeneraton       Mon  Apr      29   13:45:40   1996
```

Appendix J

The Pierson-Moskowitz (PM) spectrum

In 1964 Pierson and Moskowitz (Pierson, 1964; Pierson and Moskowitz, 1964; Chakravarti, 1987) proposed a new formula for the energy spectrum distribution of wind generated sea states. Their model describes a fully developed sea determined by wind speed alone. This spectrum has been commonly used in the design of offshore structures.

The PM spectrum model is written as

$$S(\omega) = \frac{\alpha \cdot g^2}{\omega^5} \exp\left[-\beta \left(\frac{g}{U_w \cdot \omega} \right)^4 \right] \quad \text{(J.1)}$$

Where $\alpha = 0.0081$, $\beta = 0.74$

U_w is wind speed in m/sec.

ω is angular frequency in rad/sec.

The frequency of maximum spectral energy, based on Neuman and Pierson, and the measured wind speed at 19.5m above sea surface is given by

$$\omega_o = 0.877 \cdot \frac{g}{U_w} \quad \text{(J.2)}$$

Alternatively, substituting ω_o for U_w, in terms of the angular frequency of the spectral peak

$$S(\omega) = \frac{\alpha \cdot g^2}{\omega^5} \exp\left[-\gamma \left(\frac{\omega_o}{\omega} \right)^4 \right] \quad \text{(J.3)}$$

Where γ = 1.2509. Figure A-1 shows an example of a PM spectrum at ω_o = 4.71 rad/sec (= 0.75 Hz).

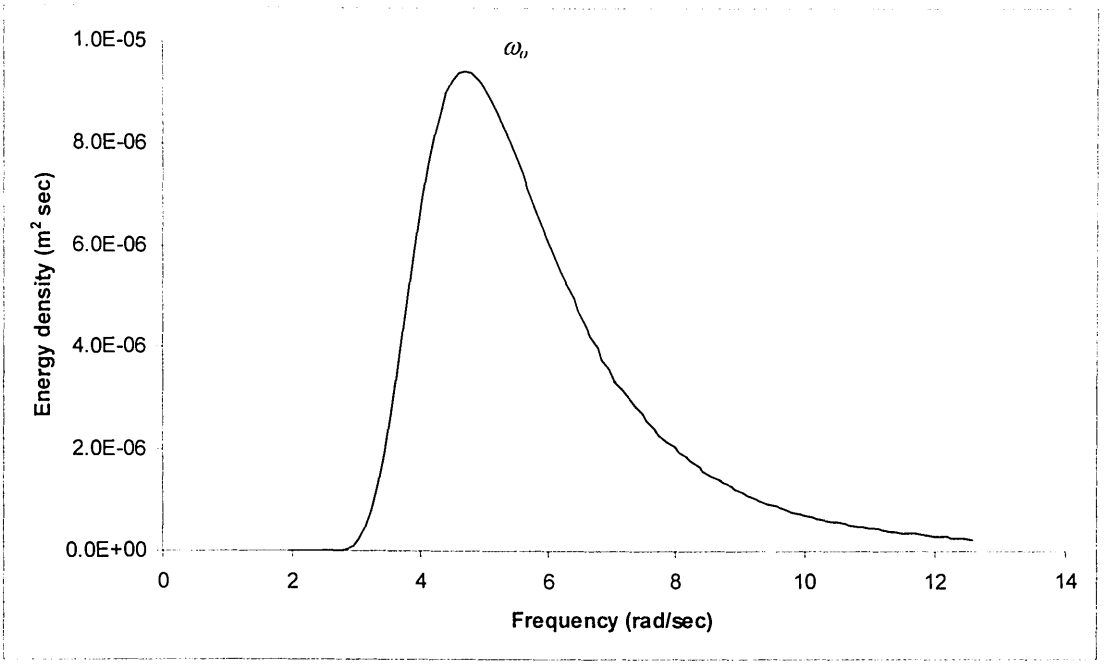

Figure J-1. An example of the energy density of a PM spectrum defined by the spectral peak frequency ω_o = 4.71 rad/sec.

In the wave tank, the cyclic frequency f in Hz is more convenient than the angular frequency ω in rad/sec. $\omega = 2\pi f$.

The zero moment, m_o, represents the area under the energy density spectrum curve, and is equal to the square of the root mean square wave height.

$$m_o = H_{rms}^{\ 2} = \int_0^\infty S(\omega)d\omega = \int_0^\infty S(f)df \qquad \text{(J.4)}$$

$$S(f) = 2\pi \cdot S(\omega) \qquad \text{(J.5)}$$

$$S(f) = \frac{\alpha \cdot g^2}{(2\pi)^4 \cdot f^5} \exp\left[-\gamma\left(\frac{f_o}{f}\right)^4\right] \qquad \text{(J.6)}$$

Where $d\omega = 2\pi\, df$, thus, $S(f) = 2\pi\, S(\omega)$.

Therefore, the PM spectrum model in cyclic frequency (Hz) becomes
Where $f_o = \omega_o / 2\pi$.

In the PM model, the relation of significant wave height H_s and wind speed U_w is

$$H_s = 0.0214 \cdot U_w^{\ 2} \quad \text{(J.7)}$$

$$H_s = 4 \cdot H_{rms} \quad \text{(J.8)}$$

$$H_{rms} = 0.0041 \cdot (\frac{g}{2\pi \cdot f_o})^2 \quad \text{(J.9)}$$

The significant wave height H_s is now defined as being four times the root mean square of wave height H_{rms} (Cartwright and Longuet-Higgins, 1958). The relation between H_{rms} and f_o be can be obtained from *(J.2), (J.7)* and *(J.8)*.

In wave tank, it is convenient to simulate PM and other wave spectra by generating a finite number of discrete regular wave components or wave fronts. The amplitude and frequencies at the wave fronts are chosen to give the closet possible match to the spectral energy distribution of the normal sea states.

Normally frequencies are chosen such that an integer number of cycles at that frequency will occur during the command signal time series. The minimum spacing in the frequency domain, Δf, between wave fronts is the determined as the reciprocal of the period, T, of the command signal time series, ie $\Delta f = 1/T$.

The period of the command signal time series is given by the number of samples, n, divided by the command sampling rate, f_c. i.e. $T = n/f_c$.

In the Edinburgh wave tank, f_c is usually set to 16 Hz, because the command time series is performed by reverse fouries transfer of the command spectra, the number of samples is always an integer power of 2. i.e. $n = 2^r$.

The export r is referred to the "repeat number"(Roger and King, 1996), the most commonly used value is 10, giving 1024 samples.

So in the Edinburgh wave tank, the resolution of frequency $\Delta f = 1024/16 = 64$ *Hz.* The wave height is the only parameter can be measured. The root mean square wave

$$h_{rms} = [\int_{f}^{f+\Delta f} S(f)df]^{1/2} \qquad \text{(J.10)}$$

height h_{rms} for each frequency division can be obtained by
The amplitude a for each frequency division is

$$a = \frac{h_{rms}}{\sqrt{2}} \qquad \text{(J.11)}$$

An example of wave amplitude for PM spectrum is shown in figure J-2. The resolution of frequency is 1/64 Hz and the maximum amplitude is at 0.75 Hz.

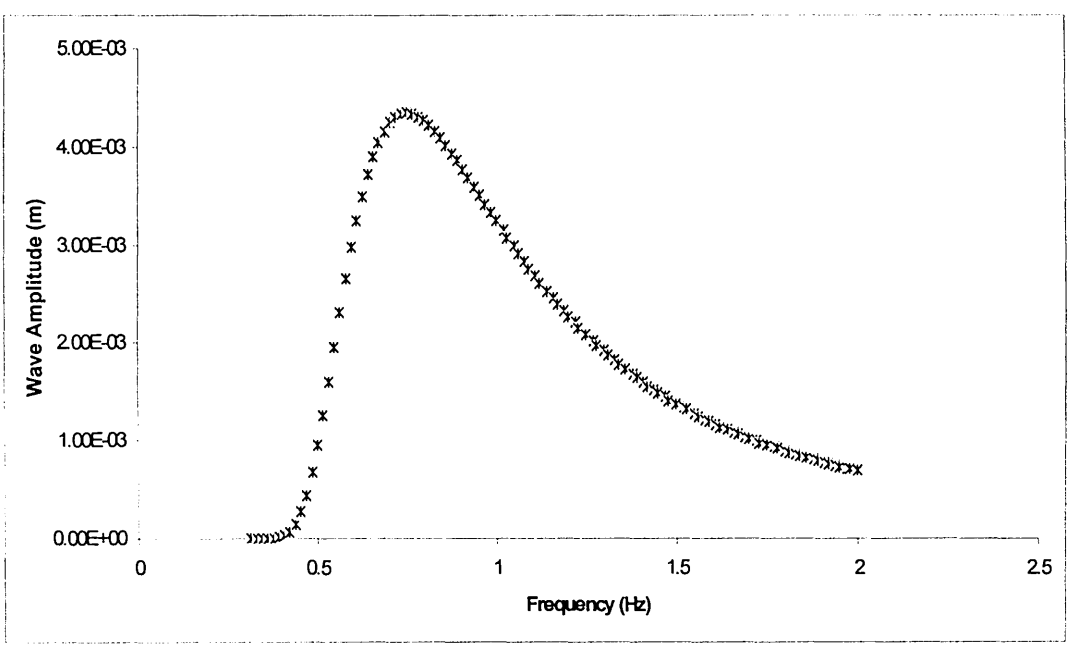

Figure J-2. The wave amplitude of PM spectrum with maximum amplitude at 0.75 Hz.

The power density of PM spectrum

$$P = \frac{\rho g^2}{4\pi} \cdot h_{rms}{}^2 \cdot \frac{1}{f} \qquad \text{(J.12)}$$

Where ρ is the water density.

g is acceleration of gravity.

The following figure J-3 is the power density of the above example.

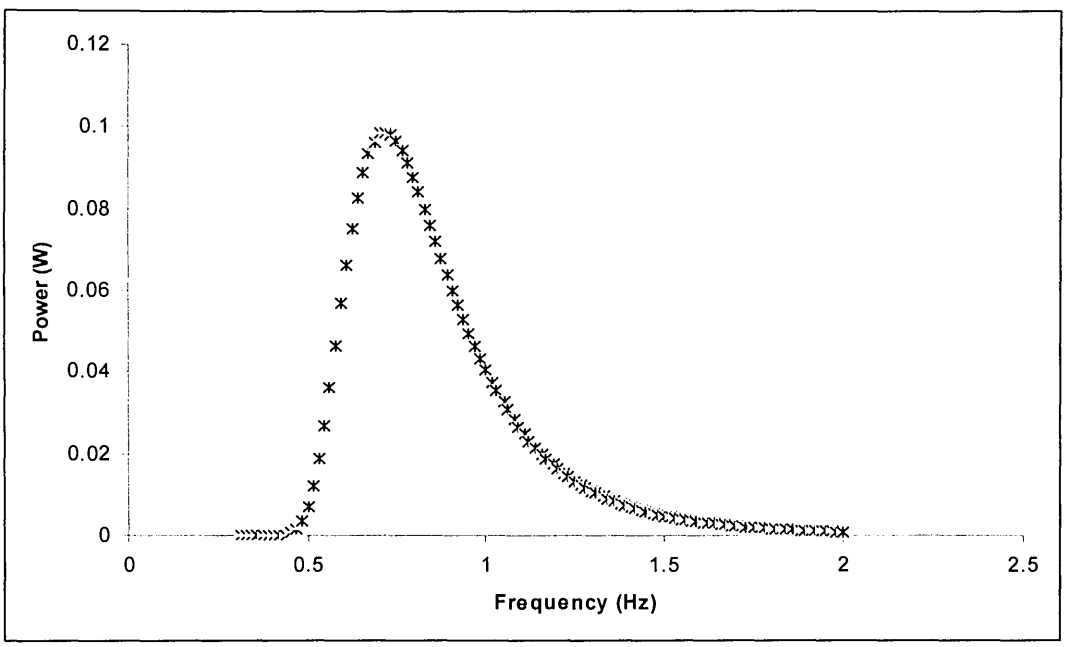

Figure J-3. The power density of PM spectrum with maximum power at 0.75 Hz.

The following figures J-4 and J-5 show the tank measurements and the theoretical curves at the same condition as above example.

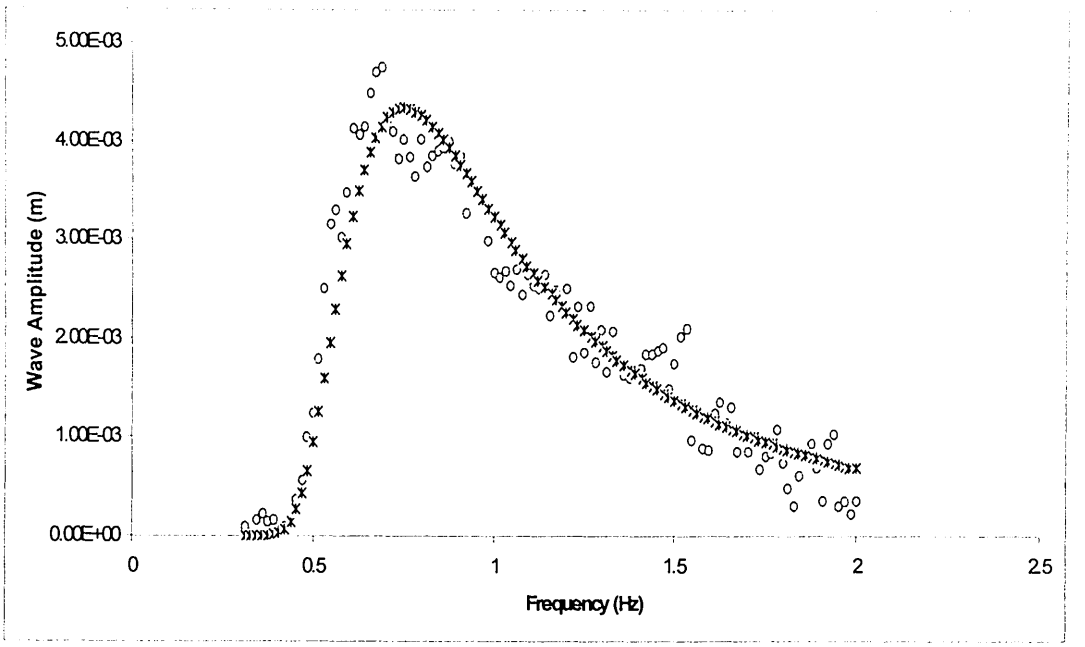

Figure J-4. Measured (o) and calculated (*) wave amplitudes for a PM spectrum.

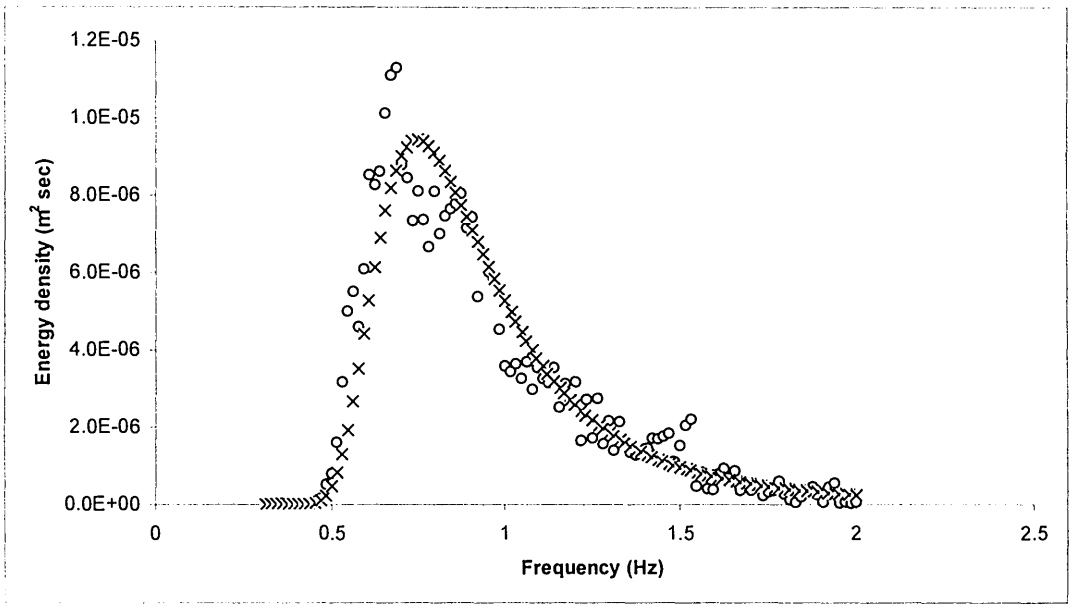

Figure J-5. Measured (o) and calculated (x) wave power density for a PM spectrum.

Appendix K

Notation

		Unit
λ *(alpha)*	Wave length	m
β *(beta)*	Phase angle between incident and reflected wave	rad
δ_n *(delta)*	Measured phase	rad
η *(eta)*	Efficiency	%
η_n	Water surface elevation	m
θ *(theta)*	Direction of incident wave	rad
μ *(mu)*	The device inertia	Kg
ρ *(rho)*	Water density	Kg/m^3
σ *(sigma)*	Hydrostatic spring	N/m
ϕ *(phi)*	Time independent potential	
ϕ_n	Theoretical wave phase	rad
ω *(omega)*	Angular frequency	rad
a	Wave amplitude	m
a_i	Amplitude of incident wave	m
a_r	Amplitude of reflected wave	m
a_t	Transmitted wave amplitude	m
B	The complex damping coefficient of the power take-off system	Ns/m
C	Point absorber factor	
D_a	Added damping	Ns/m
D_{im}	The depth of immersion	m
E	energy	Nm
F_e	The force acting in the device	N

f_n	Natural frequency	Hz
F_r	The force due to the oscillation of the body	N
g	Gravitational acceleration	m/sec^2
G	Directional spectra	
h	Tank depth	m
H_{rms}	Root mean square wave height	m
I	Current	Amp
k	Wave number	
l	Capture width	
m	Number of samples	
M_a	Added mass	Kg
n	The ratio of group to phase velocity	
n	The sample number	
P	power	W
P_w	Power of incident wave in unit width	W
q	Motion mode factor	
S	Energy density	
S_w	Conductivity of water	1/Ω
T	period	sec
T_e	Energy period	sec
T_z	Zero crossing period	sec
U	Velocity of the device	m/sec
U	Wind speed	m/sec
V	Voltage	V
V_g	Group velocity	m/sec
W	Excitation force coefficient	N/m
W	Device width	m
Z	Radiation impedance	Ns/m